

**INNOVATIVE CONTROL ALGORITHMS AND  
SOCIOECONOMIC BENEFITS OF ENERGY STORAGE  
SYSTEM FOR PEAK REDUCTION**

**CHUA KEIN HUAT**

**DOCTOR OF PHILOSOPHY IN ENGINEERING**

**LEE KONG CHIAN FACULTY OF ENGINEERING AND  
SCIENCE  
UNIVERSITI TUNKU ABDUL RAHMAN  
SEPTEMBER 2016**

**INNOVATIVE CONTROL ALGORITHMS AND SOCIOECONOMIC  
BENEFITS OF ENERGY STORAGE SYSTEM FOR PEAK  
REDUCTION**

By

**CHUA KEIN HUAT**

A thesis submitted to the Department of Electrical and Electronic Engineering,  
Lee Kong Chian Faculty of Engineering and Science,  
Universiti Tunku Abdul Rahman,  
in partial fulfilment of the requirements for the degree of  
Doctor of Philosophy in Engineering  
September 2016



## **ABSTRACT**

### **INNOVATIVE CONTROL ALGORITHMS AND SOCIOECONOMIC BENEFITS OF ENERGY STORAGE SYSTEM FOR PEAK REDUCTION**

**Chua Kein Huat**

Under the existing commercial framework of electricity in Malaysia, commercial and industrial customers are required to pay for the peak power demand charge every month. Usually, the peak demand charge contributes up to 30 % to their electricity bills due to the use of peak power plants that deliver expensive electricity to the customers. Therefore, alternative means are sought after in order to reduce the peak demand for the customers. Distributed small-scaled energy storage offers a good option to reduce the peak demand. However, the main challenge associated with energy storage is that the cost of the batteries is very high. It is not financially viable to install batteries of large capacity for the peak reduction. In this thesis, three control algorithms have been developed and implemented into the energy storage system. The control algorithms are known as fixed-threshold, adaptive-threshold control and fuzzy-based control algorithms. The overall experimental results show that the fuzzy-based control algorithm is the most effective strategy among the three controllers without over discharging the batteries. The energy storage can be used for load shifting to reduce high cost peak energy for utility. For the energy storage system installed near the customer-ends, the reinforcement of transmission and distribution infrastructure can be deferred since the energy storage can supply peaking



power to a feeder on rare occasions when the local load is beyond its operational limits. This helps to reduce or defer the need for a costly transmission and distribution upgrade. Apart from that, the cost-benefit of the energy storage system for utility companies and customers has been evaluated. An energy dispatch model is developed in HOMER to calculate the cost of electricity. The model considers the heat rates of power plants in calculating the costs of electricity under different regulatory frameworks of natural gas with various prices of battery components. The cost-benefit for the customers under various electric tariff structures is evaluated. The simulation results show that the storage system with lead acid batteries is more cost-effective than other battery technologies. The electricity cost savings using lead acid battery storage system to reduce the maximum demand charge is economically viable for commercial and industrial customers. The customers can reduce their electricity bills with a payback period of 2.8 years. The generation cost for the power system with energy storage is lower than that without energy storage. Besides, the system with energy storage has lower greenhouse gas emissions than that without energy storage.

## ACKNOWLEDGEMENTS

I would like to extend my gratitude to my supervisor, Prof. Ir. Dr. Lim Yun Seng, for not only giving me the opportunity to test my abilities in academic research but also being a great mentor. He teaches me not only academic skills but also help me to develop self-discipline, responsibility, and honesty. This thesis could not have been completed without his generous and professional assistance. I would also like to thank him for introducing me a great teacher of my life, Master Jing Kong. I am impressed with his wisdom and contributions to the world. I picked up his lessons on how to become a better one to add value to the world. I would like to thank my co-supervisor, Dr. Stella Morris, for her patient guidance, encouragement and constructive suggestions to complete my research work. I would like to show my special thanks to Prof. Phil Taylor from the University of Newcastle for giving me the opportunity to work in his laboratories and his hospitality during my wonderful visit to the United Kingdom. I would also like to thank my colleagues, particularly Dr. Wong Jianhui, Alvey Hau, Tang Jun Huat and Lim Khim Yan who have worked together in setting up the experimental laboratory.

I would like to express my gratitude to my parents for their love and support in pursuing my dream. Dad and mom, thank you for making me realize that I'm worth everything in this world. I must express my gratitude to Wong Pei Yin, my wife, for her tireless efforts on my behalf and on the behalf of our children. Thank you for taking good care of our children so that I can focus on my research work.

Finally, I would also like to thank the faculty and staffs for their support throughout my graduate career.

## APPROVAL SHEET

This dissertation/thesis entitled **“INNOVATIVE CONTROL ALGORITHMS AND SOCIOECONOMIC BENEFITS OF ENERGY STORAGE SYSTEM FOR PEAK REDUCTION”** was prepared by CHUA KEIN HUAT and submitted as partial fulfillment of the requirements for the degree of Doctor of Philosophy in Engineering at Universiti Tunku Abdul Rahman.

Approved by:

\_\_\_\_\_  
(Prof. Ir. Dr. LIM YUN SENG)

Supervisor

Department of Electrical and Electronic Engineering  
Lee Kong Chian Faculty of Engineering and Science  
Universiti Tunku Abdul Rahman

Date:.....

\_\_\_\_\_  
(Assoc. Prof. Dr. STELLA MORRIS)

Co-supervisor

Department of Electrical and Electronic Engineering  
Lee Kong Chian Faculty of Engineering and Science  
Universiti Tunku Abdul Rahman

Date:.....

**LEE KONG CHIAN FACULTY OF ENGINEERING AND SCIENCE**  
**UNIVERSITI TUNKU ABDUL RAHMAN**

Date: \_\_\_\_\_

**SUBMISSION OF THESIS**

It is hereby certified that **CHUA KEIN HUAT** (ID No: **10UED07325** ) has completed this thesis entitled “Innovative Control Algorithms and Socioeconomic Benefits of Energy Storage System for Peak Reduction” under the supervision of Prof. Ir. Dr. Lim Yun Seng (Supervisor) from the Department of Electrical and Electronic Engineering, Lee Kong Chian Faculty of Engineering and Science, and Assoc. Prof. Dr. Stella Morris (Co-Supervisor) from the Department of Electrical and Electronic Engineering, Lee Kong Chian Faculty of Engineering and Science.

I understand that University will upload softcopy of my thesis in pdf format into UTAR Institutional Repository, which may be made accessible to UTAR community and public.

Yours truly,

\_\_\_\_\_  
(*Chua Kein Huat*)

## DECLARATION

I (CHUA KEIN HUAT) hereby declare that the dissertation is based on my original work except for quotations and citations which have been duly acknowledged. I also declare that it has not been previously or concurrently submitted for any other degree at UTAR or other institutions.

\_\_\_\_\_  
(CHUA KEIN HUAT)

Date:

## TABLE OF CONTENTS

	<b>Page</b>
<b>ABSTRACT</b>	<b>iv</b>
<b>ACKNOWLEDGEMENTS</b>	<b>vi</b>
<b>APPROVAL SHEET</b>	<b>vii</b>
<b>SUBMISSION SHEET</b>	<b>viii</b>
<b>DECLARATION</b>	<b>ix</b>
<b>LIST OF TABLES</b>	<b>xvi</b>
<b>LIST OF FIGURES</b>	<b>xviii</b>
<b>LIST OF ABBREVIATIONS/NOTATION</b>	<b>xxv</b>

### **CHAPTER**

<b>1.0</b>	<b>INTRODUCTION</b>	<b>1</b>
1.1	Research Background	1
1.2	Research Objectives	5
1.3	Research Methodology	5
1.4	Thesis Organization	8
1.5	List of Publications	11
<b>2.0</b>	<b>LITERATURE REVIEW</b>	<b>13</b>
2.1	Introduction	13
2.2	Review of the Power Dispatch and Generation of Existing Power Grid	13
2.3	Challenges of High Peak Demands	16
2.3.1	High Power Production Cost	16
2.3.2	Reinforcement of Transmission and Distribution (T&D) Network	17

2.4	Existing Solutions for Confronting High Peak Demands	18
2.5	Various Energy Storage Technologies	24
2.5.1	Pumped Hydro Energy Storage	25
2.5.2	Compressed Air Energy Storage	26
2.5.3	Flywheel Energy Storage	27
2.5.4	Superconducting Magnetic Coil Energy Storage	27
2.5.5	Supercapacitors	28
2.5.6	Thermal Energy Storage	28
2.5.7	Electrochemical Energy storage	29
2.6	Battery Technologies	30
2.6.1	Flooded Lead-acid Batteries	30
2.6.2	Valve Regulated Lead-acid Batteries	31
2.6.3	Nickel-cadmium Batteries	32
2.6.4	Nickel-metal Hydrate Batteries	32
2.6.5	Lithium-ion Batteries	33
2.6.6	Sodium-sulphur Batteries	34
2.6.7	Flow Batteries	35
2.6.8	Summary of the Capital Cost and Technical Characteristics of the Battery Storage Technologies	36
2.7	General Principles and Terminologies Used for Batteries	37
2.7.1	General Principles	37
2.7.2	State-of-charge	37
2.7.3	State-of-health	40
2.7.4	Self-discharge	40
2.7.5	Depth-of-discharge	41
2.7.6	Battery Capacity	41
2.7.7	Cycle Life	41
2.7.8	Specific Energy, Energy Density, Specific Power, and Power Density	42
2.8	Summary	43

<b>3.0</b>	<b>ARCHITECTURE OF THE EXPERIMENTAL ENERGY STORAGE SYSTEM</b>	<b>44</b>
3.1	Introduction	44
3.2	Low-voltage Distribution Network	44
3.3	Low-voltage Network Connection Panel	48
3.4	Load Bank	52
3.5	Bi-directional Power Flow Converter	56
3.6	Battery Bank Configuration	59
3.7	Configuration of Sunny Island 5048	61
3.8	External Communication of Sunny Island 5048	64
3.9	Configuration of Sunny Island 5048 Communication System	66
3.10	Data Acquisition System	67
3.11	Installation of the Data Acquisition System	70
3.12	Summary	76
<b>4.0</b>	<b>CONTROL ALGORITHMS IN ENERGY STORAGE FOR PEAK REDUCTION</b>	<b>78</b>
4.1	Introduction	78
4.2	Challenges in Reducing the Peak Demands	78
4.3	Load Prediction	80
4.3.1	Load Prediction for KA Block at Sungai Long campus	81
4.3.2	Load Prediction for SE Block in Setapak campus	83
4.4	Fixed-threshold Control Algorithm	87
4.5	Adaptive-threshold Control Algorithm	91
4.6	Software Implementation	92
4.6.1	Introduction to LabVIEW	93
4.6.2	Project Explorer for the energy storage system in SE Block	95
4.6.3	Data Acquisition Programs	97
4.6.4	Implementation of the Control Algorithms	105



4.6.5	Project Explorer of the energy storage system for KA Block	124
4.7	Summary	127
<b>5.0</b>	<b>EVALUATION OF THE FIXED-THRESHOLD AND ADAPTIVE-THRESHOLD CONTROL ALGORITHMS FOR PEAK REDUCTION</b>	<b>128</b>
5.1	Introduction	128
5.2	Single-phase Energy Storage with Fixed-threshold Control Strategy	128
5.3	Evaluation of Fixed-Threshold and Adaptive-Threshold Control Algorithms in Three-Phase Energy Storage	131
5.3.1	Performance Evaluation of the Fixed-Threshold Control Algorithm	131
5.3.2	Performance Evaluation of the Adaptive- Threshold Control Algorithm	135
5.4	Summary	141
<b>6.0</b>	<b>FUZZY-BASED CONTROL ALGORITHM AND EXPERIMENTAL EVALUATION</b>	<b>143</b>
6.1	Introduction	143
6.2	Overview of Fuzzy Logic and Its Applications in Energy Storage systems	144
6.3	Fuzzy Inference system	147
6.4	Fuzzy-based Control Algorithm	149
6.4.1	Fuzzy Sets and Membership Functions for the Energy Storage System	149
6.4.2	Fuzzy Inference Rules for the Energy Storage System	151
6.5	Experimental Results	155
6.5.1	Case Study 1: Predicted Peak Demand is Close to Actual Value	155

6.5.2	Case Study 2: Peak Demand is Unexpectedly High	156
6.5.3	Case Study 3: Actual Peak Demand Occurs for a Much Longer Duration	157
6.5.4	Case Studies 4 & 5: Peak Demand Occurs Much Earlier Than the Predicted Time of Occurrence	158
6.6	Performance Comparisons of the Three Control Algorithms	161
6.7	Summary	162
<b>7.0</b>	<b>COST-BENEFIT ASSESSMENT OF ENERGY STORAGE FOR UTILITY AND CUSTOMERS</b>	<b>163</b>
7.1	Introduction	163
7.2	Power Demand and Generation in Malaysia	164
7.3	Methodology	167
7.3.1	Introduction to HOMER	167
7.3.2	Electrical System Configuration	169
7.3.3	Electrical Load Profile	174
7.3.4	System without ESS	174
7.3.5	System with ESS	181
7.3.6	Carbon Dioxide Emissions	184
7.3.7	Deferral of Transmission and Distribution Reinforcement	184
7.3.8	Cost-benefit to Industrial and Commercial Customers	186
7.4	Results and Discussion	190
7.4.1	System without ESS	191
7.4.2	System with ESS	195
7.4.3	Reduction in Carbon Dioxide Emissions	200
7.4.4	Deferral of T&D Reinforcement	200
7.4.5	Cost-benefit Analysis of Peak Shaving for Commercial and Industrial Customers	201
7.5	Summary	203

<b>8.0</b>	<b>CONCLUSIONS AND FUTURE WORKS</b>	<b>205</b>
8.1	Conclusions	205
8.2	Limitations and Opportunities for Future Improvement	210
	<b>LIST OF REFERENCES</b>	<b>212</b>
	<b>APPENDICES</b>	

## LIST OF TABLES

Table		Page
1.1	Potential benefits of energy storage in various aspects	4
1.2	List of publications	11
2.1	Costs for base-load, intermediate-load and peak-load power plants	17
2.2	Worldwide large-scale battery storage systems for peak shaving application	20
2.3	Advantages and disadvantages of flooded lead-acid batteries	30
2.4	Advantages and disadvantages of VRLA batteries	31
2.5	Advantages and disadvantages of NiCd batteries	32
2.6	Advantages and disadvantages of the NiMH batteries	33
2.7	Advantages and disadvantages of the Li-ion batteries	33
2.8	Advantages and disadvantages of the NaS batteries	34
2.9	Capital cost and technical characteristics of the battery storage technologies	36
3.1	Technical data of the Sunny Island 5048	56
3.2	Technical data of the voltage and current modules	69
3.3	Specification of the sbRIO-9632	73
4.1	Power consumption of each venue according to the power consumption of the electrical appliances	85
5.1	Summary of the electricity bill saving	140
6.1	Definition of the fuzzy sets of the SOC, $t_{op}$ and $P_{ES}$ in linguistic variables	149
6.2	The fuzzificated SOC, $t_{op}$ and the corresponding $P_{ES}$ of the fuzzy controller	153

6.3	Summary of the electricity bill saving using fuzzy-based control algorithm	160
6.4	Performances summary of the fixed-threshold, adaptive-threshold and fuzzy-based control algorithms	161
7.1	Comparison of periodical average growth rates of GDP with electricity sales, generation, and peak demand during the period between 2012 and 2030	164
7.2	Key parameters of CCGT and OCGT	178
7.3	Key parameters for LA, VRB, ZnBr and Li-ion.	182
7.4	Tariff rates for different categories of commercial and industrial customers	186
7.5	Key assumptions for the lead acid-based ESS	189
7.6	The operating parameters of the system without ESS	194
7.7	Comparison of cost components for the system without ESS for cases of with and without subsidy	194
7.8	Cost of energy for the four battery technologies with subsidy	195
7.9	Cost of energy for the four battery technologies without subsidy	196
7.10	Summary of the reduction of CO <sub>2</sub> emissions cost for the system with ESS	200
7.11	Monthly electricity bill for the system with and without ESS	202

## LIST OF FIGURES

<b>Figures</b>		<b>Page</b>
1.1	Research methodology and research goals	8
2.1	Generic daily generation in Peninsular Malaysia	16
2.2	Classification of the Energy Storage Systems	25
3.1	TT grounding system	45
3.2	Single-line diagram of the experimental low-voltage distribution network	46
3.3	(a) 3-phase synchronous generator coupled with induction motor and (b) variable speed drive	47
3.4	Topology of the network emulator	47
3.5	The overall experimental setup of the experimental low-voltage distribution network with energy storage	48
3.6	Low-voltage network connection panel	49
3.7	STAR3 3-phase energy analyser and its connection to the network	50
3.8	Interior design of the low-voltage network connection panel	51
3.9	Electrical layout of the low-voltage network panel	51
3.10	Power resistor and SSR	52
3.11	Per-phase electrical circuit of the load bank	53
3.12	Load bank encased in the net	53
3.13	Configuration of the SSRs	54
3.14	NI 9403 32-channel digital I/O module	55
3.15	NI cDAQ-9174 4-slot chassis	55
3.16	Overview of all control elements and connections	58

	of the Sunny Island 5048	
3.17	Batteries connected to the Sunny Island 5048	59
3.18	Physical 3-phase ESS setup	60
3.19	Number of cycle life of the batteries with respect to its depth of discharge	61
3.20	(a) Single unit connection and (b) dual unit connection	62
3.21	The interior master-slave configuration of the Sunny Island converters	63
3.22	Configuration of Sunny Island 5048 in a 3-phase system	64
3.23	Ports for external interface at Sunny Island 5048	65
3.24	Interface of the RS485/USB converter with the Sunny Island 5048	66
3.25	Topology of the communication system between Sunny Island 5048 and the supervisory computer	66
3.26	Path of an analogue signal in a LabVIEW DAQ application	68
3.27	Logical organization of NI-DAQmx applications	69
3.28	Location of the DAQ systems installed in the switch room and the ESS	70
3.29	DAQ system installed at the research laboratory for ESS	71
3.30	Ring-type current transformer	72
3.31	The DAQ system for measuring the power consumption of the whole building	72
3.32	Split-core current transformer	74
3.33	Front view and back view of the portable DAQ system	75
3.34	DAQ system installed at the switch room	75

3.35	Installation of STAR3 Energy Analyser on the riser of the KA building	76
4.1	Single-line diagram of the electrical network for the KA block	81
4.2	Historical load profiles of KA block from Monday to Friday and its average load profile	83
4.3	Single-line diagram of the electrical network for the SE block	84
4.4	Historical load profiles of SE block from Monday to Friday and its average load profile	84
4.5	Actual daily load profile and predicted load profile on 16th October 2014	86
4.6	APE for the actual and forecasted load demand	87
4.7	Daily load profile and the desired response of the energy storage system	88
4.8	Flow chart of the fixed-threshold control algorithm	90
4.9	Flow chart of the adaptive-threshold control algorithm	92
4.10	Front panel, block diagram, icon and connector pane in a VI	94
4.11	Organization of project explorer for the energy storage system at SE block	97
4.12	'1.1- DA- sbRIO.vi' (a) Front panel (b) part 1 (c) part 2 (d) part 3 and part 4 of the block diagram	99
4.13	'1.2- DA- Power measurement.vi' (a) Front panel (b) initialization (c) acquisition of fundamental power parameters (part 2A), and (d) acquisition of fundamental power parameters (part 2B)	103
4.14	Block diagram of '1.3-DA- Data Logging.vi'	105
4.15	Front panel of '2.1-Control- Peak Reduction.vi' (a) Real-time data tab and (b) control tab	106
4.16	Block diagram of '2.1-Control- Peak Reduction.vi'	107



4.17	Connection of '2.3-Control-SubVI(Algorithm).vi'	108
4.18	'2.3-Control- SubVI (Algorithm).vi' (a) Front panel and (b) block diagram	109
4.19	Block diagram of Check 1, Check 2, and Check 3	110
4.20	Block diagram of Case A and Case A-transition	111
4.21	Block diagram of Case B	112
4.22	Block diagram of Case C	112
4.23	Block diagram of Case C-T2	113
4.24	Block diagram of Case C-T3	114
4.25	Block diagram of Case C-T4	114
4.26	Block diagram of Case C-T5	115
4.27	Block diagram of the adaptive threshold control strategy	116
4.28	Front panel of '2.2-Control SubVI (SOC).vi'	116
4.29	Block diagram of the Check SOC case	117
4.30	Block diagram of the Charge case	118
4.31	Block diagram of the Check SOC(t-1) case	119
4.32	Block diagram of the Charge case	120
4.33	Block diagram of the Discharge case	121
4.34	Front panel of '2.6-Control- Sunny Island.vi'	122
4.35	Upper portion of block diagram of '2.2-Control-Peak reduction.vi'	123
4.36	Lower portion of the block diagram of '2.2-Control- Peak reduction.vi'	123
4.37	Organization of project explorer for the ESS in KA block	124
4.38	Front panel and block diagram of '1.1-DA-STAR3 meter.vi'	125

4.39	Block diagram of '1.2-DA- Database.vi'	126
4.40	'subVI-ORG.vi' (a) Front panel and (b) block diagram	127
5.1	Experimental setup of the single-phase energy storage system	129
5.2	Reduction of the grid demand with the threshold setting of 1 kW	130
5.3	The peak reduction using the fixed-threshold control algorithm for case study 1	132
5.4	The peak reduction using the fixed-threshold control algorithm for the case study 2	133
5.5	The peak reduction using the fixed-threshold control algorithm for the case study 3	134
5.6	The peak reduction using the fixed-threshold control algorithm for the case study 4	135
5.7	The peak reduction using the fixed-threshold control algorithm for the case study 5	136
5.8	The peak reduction using the adaptive-threshold control algorithm for the case study 6	137
5.9	The peak reduction using the adaptive-threshold control algorithm for the case study 7	138
5.10	The peak reduction using the adaptive-threshold control algorithm for the case study 8	139
5.11	The peak reduction using the adaptive-threshold control algorithm for the case study 9	140
6.1	General fuzzy inference system	148
6.2	Membership functions of (a) SOC, (b) $t_{op}$ and (c) $P_{ES}$	151
6.3	Flow chart of the algorithm developed to optimize the $P_{ES}$ of the energy storage system	152
6.4	Fuzzy inference rules in the Fuzzy System Designer Toolbox	154

6.5	Surface chart of the SOC, $t_{op}$ and $P_{ES}$ plotted using the surface viewer in the LabVIEW Fuzzy System Designer toolbox	154
6.6	The peak reduction using the fuzzy-based control algorithm for the case study 1	156
6.7	The peak reduction using the fuzzy-based control algorithm for the case study 2	157
6.8	The peak reduction using the fuzzy-based control algorithm for the case study 3	158
6.9	The peak reduction using the fuzzy-based control algorithm for the case study 4	159
6.10	The peak reduction using the fuzzy-based control algorithm for the case study 5	160
7.1	Generation profile of Malaysia on 1 July 2013	165
7.2	Electricity generation portfolios of Malaysia in 2013	166
7.3	User interface of the HOMER software	169
7.4	Schematic of electrical system in HOMER for (a) System without ESS and (b) System with ESS	170
7.5	Parameters under the economics tab	171
7.6	Parameters under the system control tab	172
7.7	Parameters in the emissions tab	173
7.8	Parameters in the constraints tab	173
7.9	Daily electrical load profile	174
7.10	The scaled down generation profile of the CCGT and OCGT	175
7.11	(a) Heat rate and (b) Electrical efficiency curve of CCGT and OCGT with respect to its loading conditions	177
7.12	User interface of the CCGT setup in HOMER	179
7.13	Fuel flow and fuel efficiency of the CCGT	180

7.14	Fuel flow and fuel efficiency of the OCGT	181
7.15	User interface for batteries in HOMER	183
7.16	Lead acid capacity curve under the storage tab	183
7.17	Growth projection of the peak demand and ESS from 1990 till 2030	185
7.18	Typical daily load profile for one of the buildings at UTAR	188
7.19	Results in ascending order of COE	192
7.20	Cost summary of the system without ESS	192
7.21	Annual electricity production of CCGT and OCGT and consumption of electricity	193
7.22	Annual fuel consumption of the system without ESS	193
7.23	Range of COE for the highest and lowest battery cost	197
7.24	Break-even price of (a) Lead acid (b) VRB (c) ZnBr and (d) Li-ion	199
7.25	Projection of T&D upgrade deferral from 2015 to 2030	201
7.26	Electricity bill and the cost of the ESS	202

## LIST OF SYMBOLS/ ABBREVIATIONS

CAES	Compressed air energy storage
CCGT	Combined-cycle gas turbine
CO <sub>2</sub>	Carbon dioxide
COE	Cost of Electricity
DOD	Depth-of-discharge
ESS	Energy storage system
FiT	Feed-in tariff
GDP	Gross domestic product
HOMER	Hybrid Optimization of Multiple Energy Resources
Li-ion	Lithium-ion
LV	Low voltage
MAPE	Mean average percentage error
NaS	Sodium sulphur
NiCd	Nickel-cadmium
NiMH	Nickel-metal hydrate
OCGT	Open-cycle gas turbine
PID	Proportional-integral-derivative
PV	Photovoltaic
SMES	Superconducting magnetic energy storage
SOC	State-of-charge
SOH	State-of-health
SNG	Synthetic natural gas
SRP	Subsidy Rationalization Program

T&D	Transmission and distribuion
TNB	Tenaga Nasional Berhad
VI	Virtual instrument file format
VRLA	Valve regulated lead-acid
VUF	Voltage unbalance factor

## CHAPTER 1

### INTRODUCTION

#### 1.1 Research Background

Today, nearly 80% of the world's electricity production comes from fossil and nuclear fuels. The burning of fossil fuels has raised many environmental issues such as water pollution, toxic waste, greenhouse gas emissions and climate change. The increased environmental concerns in the last decade or so have led to a historical agreement to combat climate change and unleash actions as well as the investment towards a low carbon, resilient and sustainable mother earth at Paris Climate Change Conference in 2015. The Paris Agreement that is agreed by 195 nations aims at keeping the global temperature rise below 2 degrees Celsius (United Nations, 2015). In line with the agreement, the Malaysian government has agreed to reduce its emissions up to 40 % based on 2005 levels by 2020.

In tandem with the growth of the economy in Malaysia, the peak demand for electricity has increased from 15,826 MW in 2012 to 16,562 MW in 2013. The maximum daily energy demand has also registered a new record from 328.72 GWh in 2012 to 344.42 GWh in 2013 (Energy Commission, 2014). The high energy demand has urged the utility companies to build more power plants and

reinforce the existing transmission and distribution networks when the peak demand approaches the system's load-carrying capacity.

Commercial and industrial electricity consumers usually need a large amount of electricity for a short duration. Therefore, meeting these customers' needs requires investment in infrastructures such as generators, transmission lines, and distribution system. A heterogeneous mix of generation technologies is indispensable for modern power systems in providing flexible power output to the grid. Hence, the electricity charge for the commercial and industrial electricity customers are more expensive than that for the residential users (Johnson et al., 2011). In many countries, the monthly electricity bills of the commercial and industrial electricity customers are usually calculated based on two charging schemes by the utility companies, namely the amount of energy in kWh being consumed and the highest power demand required during the billing period, typically a 15 or 30 minutes interval during the billing cycle (Berg and Savvides, 1983). The peak demand charge levied on industrial and commercial customers can contribute up to 30 % of the total monthly electricity bills (Sun et al., 2013).

Malaysia aspires to become a fully developed nation to achieve a self-sufficient industrialized nation by the year 2020. The vision encompasses the economic prosperity, social and political stability, world class education, and psychological balance. However, the recent price hikes of electricity may alleviate the industrialization process. In January 2014, the average electricity tariff in Malaysia hiked up 15% from an average rate of RM 0.3354 /kWh to



RM 0.3853 /kWh. The hike of electricity price is part of the government's strategy towards rationalization and gradual trimming of gas subsidies. However, this has increased the burden of customers as they need to pay higher electricity bills.

Nowadays energy storage plays an important role in grid modernization to provide a number of services, such as peak shaving (Leadbetter and Swan, 2012a; Levron and Shmilovitz, 2012; Wu and Wang, 2014; Chua et al., 2015), providing spinning reserves (Castillo and Gayme, 2014; Reddy et al., 2013), frequency control (Serban and Marinescu, 2014), load levelling (Papic, 2006), transmission and distribution upgrade deferral (Walawalkar et al., 2007), power quality control (Chua et al., 2012), and voltage regulations (Kashem and Ledwich, 2007). The energy storage units can provide peak reduction by acting as an "energy buffer" to decouple the power generating units and their loads by delivering or absorbing power in response to the customer demand. Large energy storage allows the coal-fired units to produce their optimal output even when the system load varies to achieve highest plant efficiency. The large energy storage stores excess electricity produced during periods of low price and low load demand and delivers power back to the grid during peak periods to reduce the curtailment of the coal-fired units. This practice reduces the need for expensive peak power plants to maintain the supply-demand balance.

The potential benefits of energy storage in various aspects are summarized in Table 1.1.

**Table 1.1: Potential benefits of energy storage in various aspects**

Aspect	Potential benefits
Bulk energy services	<ul style="list-style-type: none"> <li>- Improve the power supply security and reliability</li> <li>- Reduce the need of building new peak power plants</li> <li>- Provide load-shifting to balance the supply-demand chain during off-peak and on-peak periods</li> </ul>
Ancillary services	<ul style="list-style-type: none"> <li>- Provide voltage and frequency support</li> <li>- Provide spinning, non-spinning and supplemental reserves</li> <li>- Provide black start services</li> </ul>
Transmission and distribution infrastructure	<ul style="list-style-type: none"> <li>- Defer the reinforcement of transmission and distribution network</li> <li>- Relieve the congestion of the network during peak periods</li> <li>- Reduce the transmission and distribution losses incurred during peak periods</li> </ul>
Integration of renewable energy sources	<ul style="list-style-type: none"> <li>- Allow more renewable energy sources to be connected to the grid</li> <li>- Solve the intermittency issues arisen from renewable energy sources</li> <li>- Resolve the power quality issues raised by renewable energy sources</li> </ul>

Environmental and social	<ul style="list-style-type: none"> <li>- Reduce carbon dioxide emissions</li> <li>- Reduce land occupation for new power plant</li> <li>- Create job opportunities in energy storage related industries</li> <li>- Increase public support for renewable energy</li> </ul>
--------------------------	--

## 1.2 Research Objectives

The objectives of this research work are as follows:

1. To design and develop a laboratory-scale low-voltage distribution network with renewable energy sources and energy storage system.
2. To develop suitable control algorithms for energy storage system to cut down the peak demand of a commercial building.
3. To evaluate the performance of the proposed energy storage system and control algorithms in mitigating the peak demand of the commercial building.
4. To investigate the socioeconomic benefits of using the energy storage in peak reduction for utility companies and customers.

## 1.3 Research Methodology

This research aims to assess the socioeconomic benefits of the energy storage systems in peak reduction for both the utility companies and customers. The

cost-benefit analysis was carried out using a software that is capable of investigating feasibility study, optimization, and sensitivity analysis for various system configurations. Besides, this research also aims to develop control algorithms for the energy storage system to mitigate the peak demand of a building. Experiments have been carried out to evaluate the performance of the control algorithms. The research methodology is divided into 5 steps as follows:

*Step 1: Literature review*

Review of the power dispatch and generation of existing power grid, as well as the challenges associated with high peak demands, are carried out thoroughly. An overview of the existing state-of-the-arts to solve the problems of high peak demand is reviewed thoroughly. Various energy storage technologies, as well as their characteristics, are investigated. General principles and terminology used for energy storage are also presented in this chapter.

*Step 2: Design and development of experimental low-voltage distribution network and energy storage system*

Establish the experimental low-voltage distribution network and energy storage system to investigate the peak reduction of a commercial building using energy storage system.

*Step 3: Problem formulation and development of control algorithms*

The problem of peak reduction is formulated. The load profiles of the building under investigation are obtained from load prediction. Three control algorithms have been developed to cut down the peak demand of the building. The three

control algorithms are fixed-threshold, adaptive-threshold and fuzzy-based control algorithms.

*Step 4: Evaluation of control algorithms*

A single-phase energy storage system is set up to describe the operation of the energy storage system on the single-phase distribution network before it is extended to the three-phase distribution network. Experiments are then carried out at the three-phase distribution network to evaluate the performance of the control algorithms. Three control algorithms are developed to reduce the peak demand of a building. The performance of the three algorithms is evaluated at two buildings, namely UTAR Setapak campus and Sungai Long campus. Several case studies are carried out at these buildings under various load characteristics.

*Step 5: Cost-benefit Assessment*

An energy dispatch model is developed in HOMER to investigate the social-economic benefits of energy storage system in peak reduction. The model considers the heat rates of power plants in calculating the costs of electricity under different regulatory frameworks of natural gas with various prices of battery components. The cost-benefit for the customers under various electric tariff structures is evaluated. Figure 1.1 shows the research methodology and research goals.

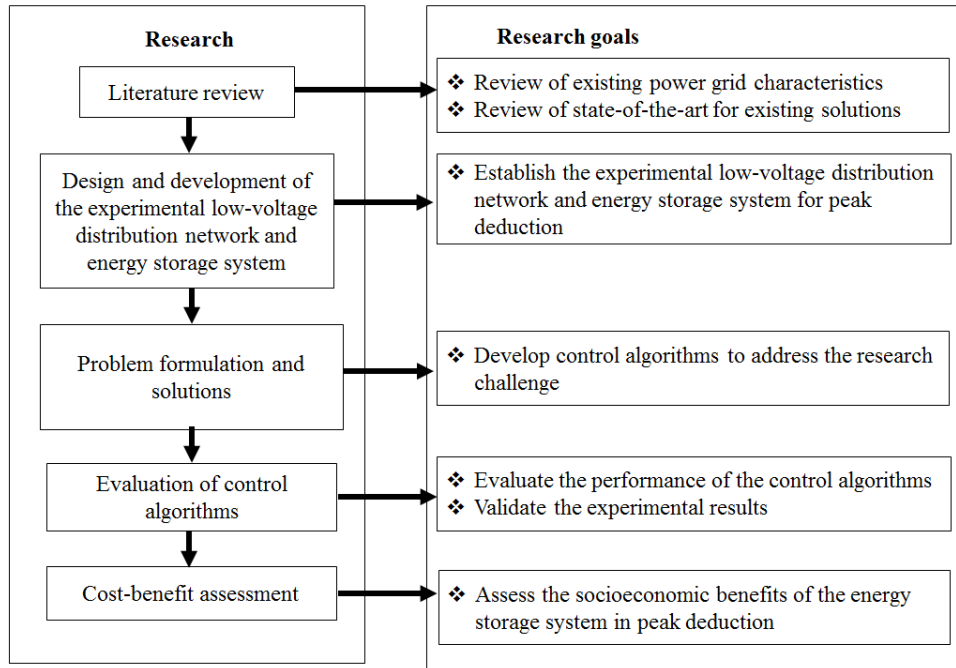


**Figure 1.1: Research methodology and research goals**

## 1.4 Thesis Organization

The structure of the thesis is organized as follows:

Chapter 2 of this thesis summarizes the literature review with regard to existing power generation system and dispatch strategies. The challenges associated with high peak demand and high renewable energy source penetration are investigated. It is followed by the literature review on existing approaches to address high peak demand for utility companies and customers. Various energy storage technologies and their pros-and-cons are described in detail. Terminologies that are frequently used for energy storage are elaborated to ease the understanding of the rest of the content in this thesis.

Chapter 3 describes the design and development of the experimental low-voltage distribution network. Low-voltage network connection panel, load bank, photovoltaic system, wind emulator, bi-directional power converter, battery bank, and data acquisition system are described clearly.

Chapter 4 describes the challenges in reducing the peak demand of a building. The problem is formulated based on the building power consumption characteristics as well as power flow between the grid and energy storage. Load prediction is carried out to predict the load characteristics of the building under investigation and formulate a suitable strategy to reduce the peak demand. Three control algorithms have been developed to mitigate the peak demand of the building. This chapter highlights the fixed-threshold and adaptive-threshold control algorithms. The control algorithms are developed in LabVIEW software.

Chapter 5 illustrates the evaluation of fixed-threshold and adaptive-threshold control algorithms in reducing the peak demand. A preliminary investigation is carried out to affirm the operation of the ESS for a single-phase distribution network. Experiments are carried out at a three-phase distribution network to evaluate the performance of the fixed-threshold and adaptive-threshold control algorithms. Several case studies are carried out at designated buildings for the purpose of evaluating the performance of these two control algorithms under various load characteristics. The advantages and limitations of fixed-threshold and adaptive-threshold control algorithms are explained clearly.

Chapter 6 describes a novel fuzzy-based control algorithm to reduce the peak demand under irregular load conditions and improve the effectiveness of peak reduction. A fuzzy-based control algorithm is developed based on the load characteristic of the building and takes into account the usable energy from the batteries during the operation of the ESS based on their state-of-charge (SOC). Experiments are carried out to evaluate the performance of the fuzzy-based control algorithms. The performance of the fuzzy-based control algorithm is compared with the performance of the fixed-threshold and adaptive-threshold control algorithms using the performance evaluation index, namely power shaving factor.

Chapter 7 assesses the socioeconomic benefits of energy storage in peak reduction. An energy dispatch model has been developed in Hybrid Optimization Model for Electric Renewables (HOMER) software to determine the cost of electricity for the system with- and without energy storage. Sensitivity analyses have been carried out for various prices of battery components and its cycle life. The cost-benefits for the customers are evaluated based on the current tariffs applied to the commercial and industrial sectors. The cost of electricity is calculated for the cases with gas subsidy and without gas subsidy are compared. The deferral cost of reinforcement of the T&D infrastructure and the reduction of CO<sub>2</sub> emission cost are also evaluated.

Finally, conclusions are drawn in Chapter 8. The key findings of the research and their implications are summarized. The limitations and opportunities for future improvement of the energy storage system are also elaborated.



## 1.5 List of Publications

The research findings have been published in peer review journals and international conferences as listed in Table 1.2.

**Table 1.2: List of publications**

No	Authors/ Title/ Status/ Link	Journal (J)/ Proceeding (P)/ Conference (C)	Index/ Impact factor
1	Kein Huat Chua, Yun Seng Lim, Jianhui Wong, Philip Taylor, Ezra Morris, and Stella Morris. Voltage Unbalance Mitigation in Low Voltage Distribution Network with Photovoltaic Systems (published) <a href="http://www.ccs.asia.edu.tw/ezfiles/2/1002/img/374/1201-1.pdf">http://www.ccs.asia.edu.tw/ezfiles/2/1002/img/374/1201-1.pdf</a>	(J):Journal of Electronic Science and Technology	SCOPUS
2	Chua, K.H., Lim, Y.S., Taylor, P., Morris, S., Wong, J., 2012. Energy Storage System for Mitigating Voltage Unbalance on Low-Voltage Networks With Photovoltaic Systems. IEEE Trans. Power Deliv. 27, 1783–1790. <a href="http://dx.doi.org.libezp.utar.edu.my/10.1109/TPWRD.2012.2195035">http://dx.doi.org.libezp.utar.edu.my/10.1109/TPWRD.2012.2195035</a>	(J):IEEE Transactions on Power Delivery	ISI/ 1.733
3	Chua, K.H., Lim, Y.S., Morris, S., 2015. Cost-benefit assessment of energy storage for utility and customers: A case study in Malaysia. Energy Convers. Manag. 106, 1071–1081. <a href="http://dx.doi.org/10.1016/j.enconman.2015.10.041">http://dx.doi.org/10.1016/j.enconman.2015.10.041</a>	(J):Energy Conversion and Management	ISI/ 4.38
4	Kein Huat, C., Yun Seng, L., Stella, M., 2016. Energy Storage System for Peak Shaving. Int. J. Energy Sect. Manag. 10, 3–18. <a href="http://dx.doi.org.libezp.utar.edu.my/10.1108/IJESM-01-2015-0003">http://dx.doi.org.libezp.utar.edu.my/10.1108/IJESM-01-2015-0003</a>	(J):International Journal of Energy Sector Management	SCOPUS

5	Chua, K.H., Wong, J., Lim, Y.S., Taylor, P., Morris, E., Morris, S., 2011. Mitigation of Voltage Unbalance in Low Voltage Distribution Network with High Level of Photovoltaic System. Energy Procedia, The Proceedings of International Conference on Smart Grid and Clean Energy Technologies <a href="http://dx.doi.org/10.1016/j.egypro.2011.10.066">http://dx.doi.org/10.1016/j.egypro.2011.10.066</a>	(P):Energy Procedia	SCOPUS
6	Chua, K.H., Lim, Y.S., Taylor, P., Morris, S., 2012. Specific power capacity for estimating the allowable load and PVs installation, in: 2012 IEEE International Conference on Power System Technology (POWERCON). Presented at the 2012 IEEE International Conference on Power System Technology (POWERCON), pp. 1–6. <a href="http://dx.doi.org.libezp.utar.edu.my/10.1109/PowerCon.2012.6401334">http://dx.doi.org.libezp.utar.edu.my/10.1109/PowerCon.2012.6401334</a>	(C):Int. Conf. on Power System Technology	IEEE
7	Kein Huat Chua, Yun Seng Lim, and Stella Morris. Battery Energy Storage System for Peak Shaving and Voltage Unbalance Mitigation <a href="http://www.ijsgce.com/uploadfile/2013/1016/20131016114948861.pdf">http://www.ijsgce.com/uploadfile/2013/1016/20131016114948861.pdf</a>	(C):Int. Conf. on Smart Grid and Clean Energy Technologies	SCOPUS
8	Kein Huat Chua, Yun Seng Lim, and Stella Morris. Building Peak Reduction using Energy Storage System	Symposium: Kuala Lumpur Symposium on ASEAN University Network (AUN) Kyoto University (KU)	Not applicable

## **CHAPTER 2**

### **LITERATURE REVIEW**

#### **2.1 Introduction**

This chapter presents the review of the power dispatch and generation of existing power grid as well as the challenges associated with high peak demands. An overview of the existing state-of-the-arts to solve the problems of high peak demands are reviewed thoroughly. Energy storage is found to be a promising solution for solving the issues associated with high peak demands. Various energy storage technologies as well as their advantages and disadvantages are illustrated. General principles and terminologies used for batteries are also presented in this chapter.

#### **2.2 Review of the Power Dispatch and Generation of Existing Power Grid**

In the electrical supply industry, the power generated by power plants is instantly used by the loads connected to the network. Hence it is described as “just-in-time” supply-demand system. The operation of the electricity supply grid is a complex task because there is tremendous variation in daily demand in accordance with consumers’ activities. Unlike other energy carriers, electricity

can only be stored in other energy forms such as chemical, thermal, and potential energy. Hence, the power generation must meet the constantly changing demand from time to time. Consequently, the electricity supply and demand must be balanced throughout the day. Any imbalance between supply and demand could lead to instability of frequency and voltage (Kundur et al., 2004).

Generally, there are three types of power plants being built for balancing the supply-demand, namely the base-load power plants, intermediate-load power plants and peak-load power plants. The base-load power plants are operated in such a way to supply power to the grid consistently near to the plants' capacities. These power plants are made to operate at all times except for scheduled maintenance or repairs. The base-load power plants are typically large generating units and have low energy production cost. In Malaysia, coal-fired power plants are typically chosen as the base-load plants. The intermediate and peak-load power plants are designated to meet the rest of the demand that is not covered by the base-load power plants. These plants usually serve as the load-following plants that adjust their output power as demand fluctuates throughout the day. Intermediate-load power plants can quickly change their output power to match with the change in load demands. Typically, combined cycle gas-fired (CCGT) power plants are used as the intermediate-load power plants. Peak-load power plants are used to cope with the high demands during peak demand hours. They are required to supply electricity for 8 to 12 hours a day. Peak-load power plants must be able to start up within 5 to 10 minutes and must be highly responsive to the changes in the load demands. Due to this fast response

requirement, open-cycle gas turbine (OCGT) power plants are the right choice for the peak-load power plants (IRENA, 2015). Figure 2.1 shows a generic daily generation in Peninsular Malaysia. The generation varies from time to time following the load demands. The load demand begins to increase in the morning as customers begin their activities. Peak demand occurs in the afternoon due to the increases of ambient temperature and then the load demand decreases in the late evening as well as early morning. The base-load power plants provide consistent output power throughout the day while the intermediate-load power plants and peak-load power plants have inconsistent output power to cope with the variation of the load demands. It is noticed that the peak-load power plants are operated for a shorter period of time as compared to the base-load and intermediate-load power plants.

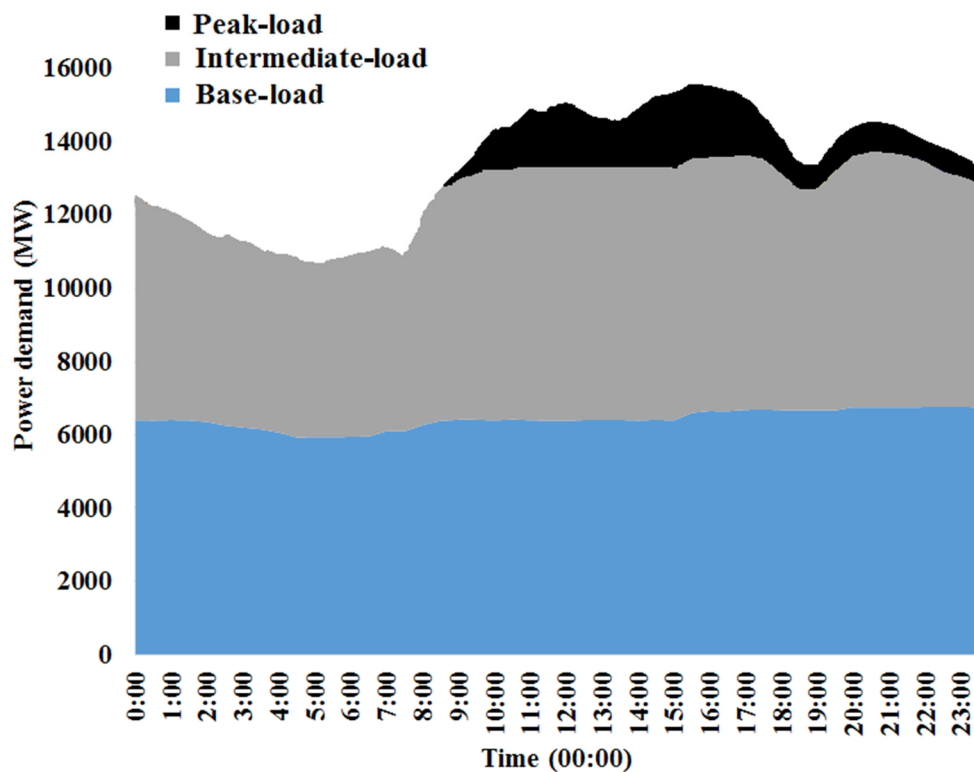


**Figure 2.1: Generic daily generation in Peninsular Malaysia**

## 2.3 Challenges of High Peak Demands

### 2.3.1 High Power Production Cost

Table 2.1 shows the costs for base-load, intermediate-load and peak-load power plants. It can be seen that the levelized cost of electricity (COE) for intermediate-load power plants is the lowest while the levelized COE for peak-load plants is the highest among the power plants. The factors influencing the cost of electricity are the plant's capacity factor, capital cost, fixed operation and maintenance (O&M) cost, variable O&M, fuel cost, and efficiency of the plants. Capacity factor is the ratio of the amount of energy generated by the generator in a year to the maximum amount of energy the generator could generate if it is operated at full-load (Stan, 2008). It can be seen that the capacity factor of the peak-load power plants is only 30 % while the base-load and intermediate-load power plants have relatively high capacity factor. The capacity factor of the peak-load power plants is low because the plants are operated for only a few hours per day. Therefore, the electricity price (RM/kWh) of the peak-load power plants has to be higher than that of other power plants in order to recover the capital cost as well as the O&M costs within their life spans (Van den Bergh and Delarue, 2015).

**Table 2.1: Costs for base-load, intermediate-load and peak-load power plants**

<b>Power Plant</b>	<b>Base-load</b>	<b>Intermediate-load</b>	<b>Peak-load</b>
<b>Levelized COE (USD/MWh)</b>	95.1 <sup>a</sup>	75.2 <sup>a</sup>	141.5 <sup>a</sup>
<b>Capacity factor (%)</b>	85 <sup>a</sup>	87 <sup>a</sup>	30 <sup>a</sup>
<b>Capital cost (USD/kW)</b>	4,724 <sup>b</sup>	2,095 <sup>b</sup>	973 <sup>b</sup>

<b>Fixed O&amp;M (USD/kW-year)</b>	66.43 <sup>b</sup>	31.8 <sup>b</sup>	7.34 <sup>b</sup>
<b>Variable O&amp;M (USD/MW-year)</b>	9.51 <sup>b</sup>	6.78 <sup>b</sup>	15.45 <sup>b</sup>
<b>Fuel cost (USD/MWh)</b>	0.0703 <sup>b</sup>	0.08547 <sup>b</sup>	0.13431 <sup>b</sup>
<b>Heat rate (BTU/kWh)</b>	12,000 <sup>b</sup>	7,525 <sup>b</sup>	10,850 <sup>b</sup>
<b>Efficiency (%)</b>	33 – 47 <sup>c</sup>	52 – 60 <sup>c</sup>	35 – 42 <sup>c</sup>
<b>Plant life (year)</b>	30 <sup>c</sup>	20 <sup>c</sup>	20 <sup>c</sup>

a- Data collected from (EIA, 2015)

b- Data collected from (EIA, 2013)

c- Data collected from (European Commission, 2012)

Utility companies often charge the commercial and industrial customers at a higher electricity price than the residential customers based upon their maximum demand during the billing cycle, in addition to the energy consumption charges. The maximum demand is calculated by multiplying the demand over the successive time period of 30 minutes and then multiplied by 2 (Tenaga Nasional Berhad, 2016). For instance, if the demand over the successive time period of 30 minutes is 100 kWh, then the maximum demand recorded will be 200 kW.

### **2.3.2 Reinforcement of Transmission and Distribution (T&D) Networks**

Utility companies are required to enhance the T&D facility when the electricity demand approaches its carrying capacity. Heavily-loaded lines can increase the T&D losses and shorten the life span of the T&D circuits. Therefore, the utility companies have to reinforce the T&D infrastructures when it reaches their technical limits as well as their current ratings (Imre, 2003). The cost of T&D

network reinforcement is passed on to the customers through the appropriate adjustment to the electricity price.

#### **2.4 Existing Solutions for Confronting High Peak Demands**

A number of methods have been proposed in the literature to reduce the peak demands. Demand response is a common program in the US and European countries to reduce the peak demands (Bradley et al., 2013; Cappers et al., 2013). With the rewarding incentives offered by this program, the customers are more willing to shift some of their peak period activities to off-peak periods. However, there are still many technical, legal and commercial issues to be resolved before the demand response program can be successfully implemented. For instance, the advanced metering infrastructure which involves a multi-million dollar investment needs to be ready before the implementation of the demand response program. Rules and regulations are mandatory to prevent the misuse of information for commercial purposes and violation of privacy. Furthermore, conflicts may arise from the existing contract and the incentive mechanism provided by the demand response (Cappers et al., 2013).

Photovoltaic systems can offer an alternative solution to the reduction of the peak demand because it can supply power to the customers during peak hours (Li and Hedman, 2015; R  ther et al., 2008). However, the output of the photovoltaic systems is highly intermittent due to its cloudy weather conditions in Malaysia. Hence, additional spinning reserves may be required from the



utility to regulate network frequency, hence increasing the operating cost for the utility.

In the recent years, energy storage has emerged as a promising technology in reducing the peak demand. Large-scale energy storage such as thermal storage, pumped hydro storage, fuel cell storage, compressed air storage, batteries, flywheel, ultra capacitor, and super conducting magnetic energy offer the similar functionality of the peaking power plants (Amodeo et al., 2009; Castillo and Gayme, 2014; Ngamroo, 2011; Sharma and Bhatti, 2010; Zhang and Xiang, 2014; Zhao et al., 2015). Many large-scale battery storage systems have been installed for the purposes of peak shaving worldwide. Table 2.2 shows the worldwide large-scale battery storage systems for peak shaving application.

**Table 2.2: Worldwide large-scale battery storage systems for peak shaving application**

Project	Operational dates	Location	Battery type	System size	
				MW	MWh
Crescent Electric Membership Cooperative BESS <sup>a</sup>	1987 to 2002	Carolina, USA	Flooded cell, lead acid	0.5	0.5
Sumitomo Densetsu Office Battery System <sup>a</sup>	2000 to present	Japan	Vanadium redox flow	3	0.8
New York Bus Terminal Energy Storage Systems <sup>a</sup>	2008 to present	New York, USA	Sodium-sulphur	1.2	6.5
ZBB Energy Corporation Battery Storage Systems <sup>b</sup>	2005 to present	California, USA	Zinc-bromine	2	2
Zurich Battery Energy Storage System <sup>c</sup>	2012 to present	Dietikon, Switzerland	Li-ion	1	0.5

Footnotes:

a- Data collected from (Poullikkas, 2013)

b- Data collected from (Peter, 2012)

c- Data collected from (Koller et al., 2015)

One of the earliest large-scale battery-based energy storage systems (ESS) developed for peak shaving is the 500 kW, 500 kWh, lead-acid storage system constructed by the Crescent Electric Membership Cooperation (now Energy United) in the United States in 1987 (Joseph and Shahidehpour, 2006). The system is designed to perform either a 500 kW constant power discharge for one hour, or a 200 kW constant discharge for three hours, depending on the load demands for the specific day. This system is able to significantly reduce the peak demand during the peak periods. A recent large-scale battery-based ESS for peak shaving has been installed at the Sumitomo Densetsu Office, Osaka, Japan in 2000 (Gareth et al., 2011). The system is formed by vanadium-redox flow batteries with a capacity of 3MW and 800 kWh. These studies show that the large-scale ESS is feasible and reliable to be used for peak reduction.

Distributed small-scale energy storage is a good option for the customers to reduce their peak demands. The benefits of the distributed small-scaled energy storage are high portability, short setup time, simple installation and commission, low capital cost investment, minimal space occupation and low maintenance and operating cost (Masoum et al., 2011; Nair and Garimella, 2010). The distributed small-scale energy storage is widely adopted to absorb and moderate the fluctuations of the power from renewable energy resources (Taylor et al., 2013) while providing voltage regulation and peak shaving for the networks (Yang et al., 2014). Various approaches have been proposed to optimize the peak shaving by eliminating the peaks from the load profile. In addition, the distributed energy storage located downstream from transmission

lines can reduce the loading on the transmission system during peak periods, hence deferring the upgrade of the T&D and extending the T&D equipment life (Yan et al., 2014).

Sigrist et al. (2013) carried out an assessment to investigate the economic benefits of the ESS in providing primary reserves and peak shaving in small isolated power systems with the renewable energy sources. Also, Pudjianto et al. (2014) proposed an approach to evaluate the possible contribution of the grid-connected energy storage to the operation cost, generation investment, transmission investment, interconnection investment, and distribution investment. Oudalov et al. (2007a) has achieved 8 % of peak reduction using a dynamic programming method to optimize the operation of the energy storage system. Purvins et al. (2013) showed the feasibility of using ESS for reducing the peak demand of distribution grid using a demand tracking management model. The peak reductions is 27 - 45 %.

The appropriate size of the ESS is important because it enables the customers to achieve the successful reduction in the peak demands. Leadbetter and Swan (2012b) have developed a sizing algorithm for the storage devices used in the residential buildings based on the storage capacity, power capability, and a grid demand limit. Venu et al. (2009) has proposed another sizing strategy for the energy storage in the residential power distribution feeders with the PV systems to reduce peak demand. The size of the energy storage system is derived from the feeder load characteristics and PV penetration.

A heuristic and competitive approach has been proposed by Johnson et al. (2011) for the peak reduction with the batteries. The algorithms were evaluated by simulations based on the actual datasets collected from customers. A simple method has been proposed by Rahimi et al. (2013) for peak-load shaving using battery ESS. The study compares the aggregated load profile with its average value during a specific period and operates the energy storage devices based on the proposed weighting factors. The average load reduction is 0.35 - 1 %.

Lu et al. has proposed an optimal sizing and control of battery-based storage system for peak shaving at the utility side (Lu et al., 2014). The study has diminished the difference between the peak load and the valley load via the optimal control of the energy storage system and the peak reduction is 4.5 - 6.6 %.

Thermal energy and water storage system can also be used to reduce the peak load contributed by the residential air conditioning systems (Upshaw et al., 2015). An integrated thermal energy and water storage system has been modeled and the analysis suggested that the system can reduce the peak demand by approximately 29 – 53 % as compared to traditional air conditioning with an air-cooled condenser.

A hybrid energy systems with renewable energy resources have also been investigated widely to reduce volatility in demand. Wang et al. have proposed a methodology for the application of receding horizon optimization techniques to manage the energy flows in the chlor-alkali plant with a hybrid renewable

energy generation (Wang et al., 2014). The study showed that the energy production cost for the wind-solar-fuel cell hybrid system can be reduced significantly by applying the optimization approach to the chlor-alkali synthesis process. A hybrid energy system with nuclear energy has been investigated by (Garcia et al., 2016) to meet both electrical and thermal energy needs. This study has investigated the challenges and opportunities that may arise from accommodating the high penetration of renewable energy resources. An economic optimization of operations for hybrid energy systems has been proposed by (Chen and Garcia, 2016) to maximize the system economics based on renewable and market information. The study have proposed a multi-environment computation platform to manage the energy balance of the supply and demand.

Although there are many studies carried out for peak reduction using the energy storage, most of the research work is simulation-based (Chen and Garcia, 2016; Garcia et al., 2016; Johnson et al., 2011; Leadbetter and Swan, 2012a; Levron and Shmilovitz, 2012; Lu et al., 2014; Oudalov et al., 2007b; Upshaw et al., 2015; Wang et al., 2014; Yang et al., 2014). The simulation-based ESS was controlled to supply power over a specified peak hour which was determined from the historical load data. The capacity (kWh) and the rating (kW) of the ESS were then determined based on the historical load data. However, the real-time peak reduction is challenging because the actual peak demand can be quite different from the forecasted load profiles. When the actual peak demand is unexpectedly high, the ESS may fail to reduce the peak due to the limited capacity of the converter. Also, the actual peak can happen much earlier or later

than the forecasted one. The ESS may fail to cut down the peak if it supplies the power at the wrong time. Another possibility is that the actual peak can happen for an extended period of time. The ESS may not have enough energy to sustain the supply of power. Considering the possible variation in the actual load profiles, any control strategies used for the ESS has to be evaluated empirically through experiments. Since the cost of the batteries is still high at present, the capacity of the energy storage system has to be limited or reduced in order to justify the financial viability of the system.

## **2.5 Various Energy Storage Technologies**

Energy storage provides multifaceted functionality that can solve the problems associated with the high peak demands, high penetration of renewable energy sources, power quality, and power systems reliability. The load demands can be handled efficiently if energy storage is incorporated into the electrical network. The operating principle of the energy storage is to move energy through time in which the energy generated at one time can be used at another time through storage. Operational changes to the modern grid system caused by the integration of renewable energy sources have created an opportunity for the energy storage to provide solutions to the problems arisen. Energy storage systems can be classified into thermal, electrochemical, chemical, electrical and mechanical energy storage systems as illustrated in Figure 2.2.

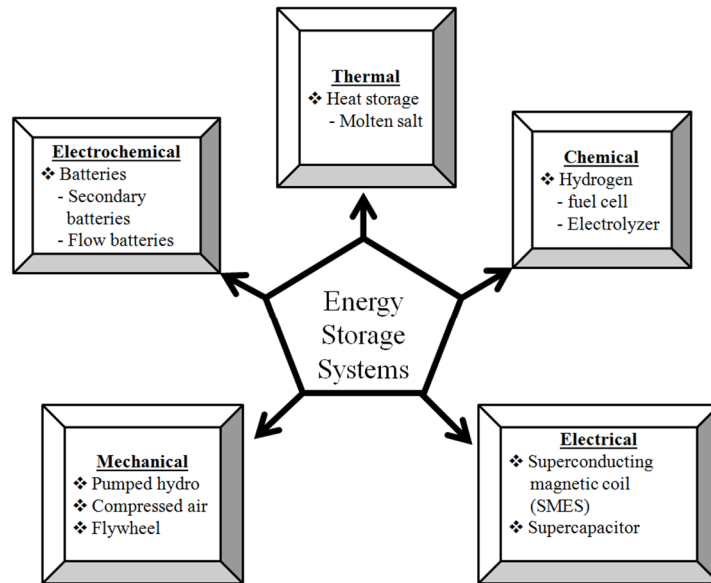


**Figure 2.2: Classification of the Energy Storage Systems**

### 2.5.1 Pumped Hydro Energy Storage

A pumped hydro energy storage technology has more than 85 year's old history in power systems. The hydro pumped energy storage plant pumps the water from a lower reservoir to an upper reservoir during the off-peak periods to store energy in the form of hydraulic potential energy (Ardizzon et al., 2014). Pumped hydro system installations are considered a mature technology and cost-effective technology for the large-scale of energy storage with typical capacity of more than 100 MW. Currently, there are about 104,000 MW of pumped hydro storage capacity installed worldwide (Energy Information Administration, 2008). Pumped hydro energy storage play a role as a buffer between the constantly changing demand by absorbing the excess generation

capacity from the grid during the off-peak periods, and discharging the stored energy to the grid during the peak periods (Thomas, 2010a).

### **2.5.2 Compressed Air Energy Storage**

Compressed air energy storage (CAES) technology emerged in 1970s to provide cushion to the transition of power demand during the peak and off-peak periods. CAES converts electrical energy into the compressed air potential energy in an underground reservoir or an aboveground piping or vessel system during the off-peak periods. During the peak periods, it will release the compressed air from the storage reservoir by preheating the cool and high pressure air and then directing the air into high efficiency turbines that is driving electric generators (Imre, 2003). CAES has a fast response time and start up time where it can output power to the grid within 10 minutes.

### **2.5.3 Flywheel Energy Storage**

Flywheel energy storage is one of the earliest mechanical energy storage mechanisms discovered in the early year of the Industrial Revolution. Flywheels store energy in the form of the angular momentum of a spinning mass. A flywheel system transfers kinetic energy into electrical power through power conversions systems. Modern flywheel systems consist of a huge rotating cylinder that is substantially supported on a stator by magnetically levitated



bearings that are able to minimize bearing wear-and-tear. Usually the rotating cylinder is encapsulated in a vacuum environment to reduce air friction (Liu and Jiang, 2007). Flywheel energy storage system can be charged relatively fast as compared to other storage systems and it exhibits excellent cycle life in comparison with other energy storage systems. (Nasiri, 2011).

#### **2.5.4 Superconducting Magnetic Coil Energy Storage**

Superconducting magnetic energy storage (SMES) systems stores energy in the field of a large magnetic coil with direct current (DC) and convert back to alternative current (AC) as needed. A DC current is supplied to a closed coil of superconducting wire which is kept below its superconducting critical temperature (Andreas, 2012). SMES systems can absorb and deliver power in milliseconds. This fast response characteristic makes the SMES systems suitable for power quality control in manufacturing plants. It can also provide very high power output for a short duration of time (Chen and Jin, 2013).

#### **2.5.5 Supercapacitors**

Supercapacitor is one of the latest innovations in the field of electrical energy storage. Although it has lower energy density compared to lead-acid batteries, supercapacitors have very high charging and discharging capability with tens of thousands cycle life (Rufer and Barrade, 2002). Supercapacitors are

maintenance free, high reliability and durability, and can be operated over a wide range of temperatures without any degradation. The round-trip efficiency is around 90% (Yang and Zhang, 2013).

### **2.5.6 Thermal Energy Storage**

Thermal energy storage systems are deployed to balance the supply and demand of thermal energy. Thermal storage can be subdivided into three different categories, namely storage of sensible heat, storage of latent heat, absorption storage and thermo-chemical. The storage of sensible heat is the most popular thermal energy storage system that provides domestic hot water by absorbing heat from the solar radiation. Currently, thermal energy storage systems have been widely used in dessert and rural area to harness solar energy (IEC, 2011).

### **2.5.7 Electrochemical Energy Storage**

A battery is a device that converts the chemical energy into electric energy via electrochemical oxidation-reduction (redox) reaction. Batteries are a convenient source of power for portable devices such as mobile phones, tablets, automotive applications, watches, toys, and music players. Generally there are two categories of batteries, namely the primary batteries and secondary batteries. The primary battery is a portable voltaic cell that is not rechargeable while the secondary battery is a portable voltaic cell that is rechargeable. Examples of

primary batteries include carbon-zinc, alkaline-manganese, mercury-zinc, silver-zinc, lithium-manganese dioxide, lithium-sulphur dioxide, and lithium-thionyl chloride. Examples of secondary batteries include lead-acid, lithium-ion, sodium-sulphur, zinc-bromine, nickel-metal hydride, nickel-cadmium, nickel-iron, silver-zinc, silver-cadmium, and alkaline dioxide. The energy densities of the secondary batteries are usually lower than that of the primary batteries. Besides, their charge retention is also poorer than those of the primary batteries (Thomas, 2010a).

One of the important characteristics of the secondary batteries is their transformation between electric energy and chemical energy. The charging and discharging of the batteries should proceed nearly reversibly and with minimal physical changes to prolong the cycle life of the batteries. It is required that the cell should have low resistance with high specific energy and can be operated over a wide temperature range without deteriorating their performance (Thomas, 2010a).

In the following subsections, 6 secondary battery technologies are selected for discussions, namely flooded lead-acid (FLA), valve regulated lead-acid (VRLA), nickel-cadmium (NiCd), nickel-metal hydride (NiMH), lithium-ion (Li-ion), sodium-sulphur (SF), and flow battery.

## 2.6 Battery Technologies

### 2.6.1 Flooded Lead-acid Batteries

Flooded lead-acid batteries are the oldest type of electrochemical energy storage that have been commercially deployed since 1890. Flooded lead-acid batteries are used extensively in automotive applications, lighting systems, power tools, stand-alone systems with PV, and communication devices due to its low price and the ease of manufacture. Flooded lead-acid batteries have strong growth in the global battery market due to the improvement in their cycle life and depth-of-discharge. The cycle life of flooded lead-acid batteries ranges from 50 to 2000 at 80 % depth-of-discharge, depending on the design of the batteries. Table 2.3 shows the advantages and disadvantages of flooded lead-acid batteries (Thomas, 2010a).

**Table 2.3: Advantages and disadvantages of flooded lead-acid batteries**

<b>Advantages</b>	<b>Disadvantages</b>
Low cost	Low cycle life
Ease of manufacturing	Low energy density
Available in variety of sizes and designs from mili-Ah to several thousand Ah	Long-term storage in a discharged condition can lead to irreversible polarization of electrodes
High cell voltage	Thermal runaway
Good float service	Acid is extremely corrosive
Good charge retention	Harmful effects to environment
Cell components are easily recycled	Health hazard

### 2.6.2 Valve Regulated Lead-acid Batteries

A valve regulated lead-acid (VRLA) battery is commonly known as sealed or maintenance battery. A one-way, pressure-relief valve is designed to seal the

cell in order to prevent build-up of excessive pressure in the cell and prevents entry of outside air into the cell. The VRLA battery is maintenance free and more reliable as compared to the flooded lead-acid batteries. The electrolyte of the VRLA is immobilized in two ways, namely the gelled electrolyte and absorptive glass mat (AGM). The immobilization of the electrolyte allows batteries to operate in different orientations without leakage. Although the design and the construction of the VRLA battery are different from the flooded batteries, its electrochemical reactions are the same as the traditional lead-acid battery. The advantages and disadvantages of VRLA batteries are shown in Table 2.4 (Thomas, 2011).

**Table 2.4: Advantages and disadvantages of VRLA batteries**

<b>Advantages</b>	<b>Disadvantages</b>
Maintenance-free	Low energy density
Moderate life on float service	Low cycle life
Immobilized electrolyte	Thermal runaway can occur with incorrect charging
State of charge can usually be determined by its voltage	Should not be stored in discharged condition
Available from small 2V single-cell units to large 48V batteries	More sensitive to higher temperature environment

### **2.6.3 Nickel-cadmium Batteries**

Nickel-cadmium (NiCd) batteries are a type of alkaline storage battery where its electrolyte is alkaline. NiCd batteries are well-known for its reliability, sturdiness, long cycle life, ability to be operated effectively at relatively high discharge rates and over a wide temperature ranges, and ability to withstand electrical and physical abuses. It has excellent charge retention properties and

can be stored in a fully discharged condition without any detrimental effects. NiCd batteries are widely used in heavy-duty industrial and aerospace applications. Table 2.5 shows the advantages and disadvantages of NiCd batteries.

**Table 2.5: Advantages and disadvantages of NiCd batteries**

<b>Advantages</b>	<b>Disadvantages</b>
Long cycle life	Low energy density
Rugged and reliable	Higher cost than lead-acid battery
Good charge retention	Caustic alkaline electrolyte
Excellent long-term storage	Memory effect
Low maintenance	Contains cadmium which is toxic
Flat discharge profile	
Excellent performance at low temperature	

#### **2.6.4 Nickel-metal Hydrate Batteries**

Nickel-metal hydrate (NiMH) batteries are an extension of the NiCd battery technology with the substitution of a hydrogen-absorbing negative electrode for the cadmium-based electrode. The key motivations for the NiMH battery were the environmental advantages associated with higher energy, lower pressure, and lower cost of NiMH compared to NiCd. NiMH batteries have the same basic structure to that of NiCd batteries. Indeed, NiMH batteries have all the positive properties of NiCd batteries. Table 2.6 shows the advantages and disadvantages of the NiMH batteries.

**Table 2.6: Advantages and disadvantages of the NiMH batteries**

<b>Advantages</b>	<b>Disadvantages</b>
Higher energy density compared to NiCd and lead-acid batteries	Lower specific energy and specific power compared to Li-ion batteries
Long cycle life	Higher cost than lead-acid
Long shelf life	High rate of self-discharge

Rapid recharge capability	
Sealed maintenance-free design	
Excellent thermal properties	

### 2.6.5 Lithium-ion Batteries

Lithium-ion (Li-ion) batteries have conquered almost 75% of the secondary consumer market since its emergence in 1991. Li-ion batteries have become the most important storage technology in the areas of portable and mobile applications such as laptop computers, cell phones, electric vehicles, and many other electronic gadgets. Due to the fact that Lithium is the lightest of all metals as well as has the greatest electrochemical potential, Li-ion batteries have remarkable high energy density and specific energy. Besides, Li-ion batteries also have much longer cycle life as compared to the lead-acid batteries. Table 2.7 shows the advantages and disadvantages of the Li-ion batteries.

**Table 2.7: Advantages and disadvantages of the Li-ion batteries**

<b>Advantages</b>	<b>Disadvantages</b>
High energy density and specific energy	High cost
High nominal cell voltage	Possible venting when crushed
High-rate and high-power discharge capability	Potential thermal runaway when overcharged
Long cycle life	Degrades at high temperature
High coulomb and energy efficiency	Need for protective circuitry
No memory effect	Capacity loss when overcharged
Long cycle life and shelf life	Electrodes are thermally unstable
Maintenance free	May become unsafe if rapidly charged at low temperature
Rapid charge capability	
Low self-discharge rate	
Flat discharge voltage	

### 2.6.6 Sodium-sulphur Batteries

Sodium-sulphur (NaS) batteries were introduced in the mid-1970s. NaS batteries offer attractive solutions for many large-scale, electric utility energy storage applications to provide load levelling, power quality, peak shaving, and renewable energy management and integration. The main reason that make NaS battery technology a potential candidate for use in grid services is its long discharge period, approximately 6 hours (Abbas et al., 2013). However, NaS batteries are not suitable for portable and mobile applications due to its high operating temperature during charging and discharging cycles. NaS batteries have very high cycle life, approximately 4500 cycles and have fast response during charging and discharging process. The advantages and disadvantages of the NaS batteries are shown in Table 2.8.

**Table 2.8: Advantages and disadvantages of the NaS batteries**

<b>Advantages</b>	<b>Disadvantages</b>
High cycle life	Operation safety concern
High energy and good power density	Requires thermal management
High energy efficiency	Requires protection circuitry
Low maintenance	Reaction with molten active materials must be controlled
Inexpensive raw materials	Corrosion of the insulators
Insensitivity to ambient conditions	
Simple state-of-charge identification	

### 2.6.7 Flow Batteries

A flow battery is a type of rechargeable battery where their recharge ability is provided by two chemical components dissolved in liquids and separated by a membrane. Electrolyte is stored externally in tanks and pumped through the cell



of the reactor. There are two categories of flow batteries, namely redox flow batteries and hybrid flow batteries. If one or more electro-active components are deposited as a solid layer, the system is known as a hybrid flow battery. Redox flow batteries have long cycle life because there are no solid-solid phase changes. It can be recharged rapidly by replacing the electrolyte from the storage tanks. Redox flow batteries can also be discharged fully without causing permanent defects on the batteries. It has rapid response time and hence it is well suited to uninterruptible power applications. However, it has relatively lower energy density as compared to other battery technologies. Vanadium redox batteries are the most commonly found redox flow batteries in the market. Vanadium redox flow batteries have an important advantage among flow batteries, where its two electrolytes are identical when fully discharged. This advantage makes shipment and storage of these batteries simple and cheap. Hybrid flow batteries have 100% depth-of-discharge capability and can be left fully discharged without causing a permanent damage on batteries. It also has long cycle life and is scalable from 10kWh to over 500kWh. One of the most commonly found hybrid flow battery is the zinc-bromine (ZnBr) flow battery. The lifetime of the ZnBr flow battery is not strongly dependent on the number of cycles and the depth-of-discharge, but it is highly affected by the number of hours that the batteries have been operated (Poullikkas, 2013).

## 2.6.8 Summary of the Capital Cost and Technical Characteristics of the Battery Storage Technologies

Table 2. 9 summarize the capital cost and technical characteristics of the battery-based storage technologies.

**Table 2. 9 Capital cost and technical characteristics of the battery storage technologies**

<b>Technology</b>	<b>Capital cost (USD/kW)</b>	<b>Discharge duration</b>	<b>Efficiency (%)</b>	<b>Cycle life</b>
Lead-acid <sup>a</sup>	50-310	< 8 hours	85	500-2800
Nickel-cadmium <sup>a</sup>	400-2400	< 8 hours	60-70	500-2000
Sodium-sulphur <sup>a</sup>	180-500	< 8 hours	75-86	4500
Vanadium redox flow <sup>a</sup>	175-1000	< 10 hours	85	13000
Zinc-bromine flow <sup>a</sup>	200-600	< 4 hours	75	2000
Lithium-ion <sup>b</sup>	600-2500	< 4 hours	90	10000
Nickel-metal hydride <sup>b</sup>	400-2400	< 1 hour	60-71	500-2000

Footnotes:

a- Data collected from (Poullikkas, 2013)

b- Data collected from (Abbas et al., 2015)

By considering the technical characteristics of the battery technologies and their capital costs, it is found that the lead-acid batteries are the most suitable candidate for peak reduction in this research.

## **2.7 General Principles and Terminologies Used for Batteries**

This section explains the general principles of electrochemical reactions that occur in batteries and the technical terms used to describe the specifications of the battery.

### **2.7.1 General Principles**

A battery consists of three major components, namely the negative electrode, the positive electrode, and the electrolyte. The negative electrode or anode is the reducing electrode that gives up electrons to the external circuit and is oxidized during the electrochemical reaction. The positive electrode or cathode is the oxidizing electrode that accepts electrons from the external circuit and is reduced during the electrochemical reaction (Thomas, 2010b).

### **2.7.2 State-of-charge**

State-of-charge (SOC) of a battery is the most commonly used terminology to describe the residual capacity state of the battery. SOC is the percentage of its capacity available relative to the capacity when it is fully charged. A good-condition battery has a SOC of 100% when it is fully charged. The SOC can be expressed by the following equation:

$$SOC = \frac{Q_{res}}{Q_{rated}} \times 100\% \quad (2.1)$$

where  $Q_{res}$  is the ampere-hour remaining in a battery at a given rate, and  $Q_{rated}$  is the battery rated capacity. An ampere-hour is the unit used to describe the amount of energy that the battery can store in.

The SOC cannot be measured directly from the battery and can only be estimated with various degrees of accuracy. There are four typical ways to measure the SOC of batteries, namely open-circuit voltage measurements, specific gravity measurement, coulomb counting method, and internal impedance measurement (Piller et al., 2001). The simplest method is to measure the open-circuit voltage of the battery. However, this method is not accurate due to diffusion time constants and acid stratification effects. Furthermore, the accuracy of the measurement is affected by the battery temperature. If the battery temperature is high, the chemical compositions that deliver voltage will give the high open-circuit voltage, and vice versa. Moreover, if the SOC of the battery is measured after it is being charged or discharged, the error of measurement will be higher. In order to get accurate measurements, the battery needs to be put down to rest for at least four hours so that the chemical reactions can attain an equilibrium state. During the measurement of the SOC by open-circuit voltage method, the battery must be disconnected from the load. This method is not practical for the applications where the battery power must be continuously supplied to the devices (Piller et al., 2001).

For the specific gravity measurement method, the hydrometer is used to measure the specific gravity of the electrolyte. When the battery receives a

charge, the sulphuric acid gains weight causing the specific gravity to increase. During the discharge of the batteries, the chemical reactions of the sulphuric acid produces lead sulphate and results in the reduction of the specific gravity. However, this method of estimating the SOC of the batteries is only applicable for the flooded lead-acid and flooded nickel-cadmium batteries.

In Coulomb counting method, the current that flows in and out of the battery is measured continuously to estimate the SOC of the batteries. For example, if the battery is charged for one hour at one ampere, the same amount of energy should be available during the discharge of batteries. However, the efficiency of the charging and discharging processes in the batteries are different and may result in inaccuracy of the SOC measurement. In fact, the available energy is always less than the energy that has been delivered to the battery. Nevertheless, the Coulomb counting works reasonably well with lithium-ion batteries. Hence, this method of estimating the SOC is widely used for mobile phones and laptops.

Electrochemical impedance spectroscopy has been recognized as a fast, non-destructive and reliable method to estimate the SOC. Many electrical parameters are varied monotonously as a function of the SOC from the impedance spectra. The impedance of the battery is measured by high precision device at frequencies from 6 kHz down to few micro-Hz. Impedance measurements down to the micro-Hz region may take a long period of time (12 hours). Nevertheless, the electrochemical impedance measurement has high accuracy in estimating the SOC of the batteries (Blanke et al., 2005). The development of

Electrochemical Impedance Spectroscopy (EIS) in the recent years have shortened the measurement time to 15 seconds with high accuracy.

### **2.7.3 State-of-health**

State-of-health (SOH) of a battery is a measure of the battery's ability to store and deliver electrical energy. SOH is the percentage of its capacity available when fully charged relative to its rated capacity. For instance, a 100 Ah battery that can only deliver 70 Ah when fully charged is said to have 70% of SOH. The SOH of battery tends to deteriorate gradually due to chemical and physical changes of the battery during charging and discharging processes. Hence, the knowledge of the battery SOH is crucial to estimate the exact aging conditions and maximum available capacity in a battery (Coleman et al., 2008).

### **2.7.4 Self-discharge**

Self-discharge is a phenomenon in batteries in which internal chemical reactions reduce the stored charge of the battery without any connection between the electrodes. Thermodynamically, the discharged state is more stable because the equilibria of the electrode reactions are normally in the discharge direction. The rate of self-discharge depends on ambient temperature and humidity. Typically the lead-acid and nickel-cadmium batteries have very high self-discharge rate while Li-ion batteries illustrate a much lower self-discharge rate.

### **2.7.5 Depth-of-discharge**

Depth-of-discharge (DOD) is defined as the percentage of battery capacity that has been discharged. DOD is used to describe how deeply the battery is discharged. DOD is the complement of SOC and can be expressed by the following equation:

$$DOD = 1 - SOC \quad (2.2)$$

### **2.7.6 Battery Capacity**

The battery capacity is a measure of the amount of energy stored in the battery. The most commonly used unit for battery capacity is ampere-hour (Ah). The energy storage capacity of the battery can be estimated by multiplying the Ah capacity of the battery with its nominal battery voltage.

### **2.7.7 Cycle Life**

The cycle life of a battery is the number of discharge-charge cycles the battery can undergo before it fails to meet the specific performance criteria. Typically, when the battery's nominal capacity falls below 80 % of its initial rated capacity, the battery can be considered as unusable. The aging process of the batteries results in a gradual reduction in capacity over time. The cycle life of the battery is affected by many factors such as the DOD, humidity, and

operating temperature. Temperature can affect the chemical reactions in the battery. High humidity can increase the corrosion rate while high temperature can increase the chemical reactions of the battery and could result in passivation of the electrodes, corrosion and gassing that can reduce the cycle life of the battery.

### **2.7.8 Specific Energy, Energy Density, Specific Power, and Power Density**

The specific energy of a battery is the nominal battery energy per unit mass (Wh/kg). Specific energy is used to relate the energy content of a given battery to its weight. A higher specific energy implies lighter weight. For example, a typical value for the specific energy of a Li-ion and lead-acid batteries are 125 Wh/ kg and 25 Wh/ kg, respectively (H. A., 2003). In other words, the lead-acid battery is 5 times heavier than Li-ion battery for the same amount of energy. The energy density of a battery is the nominal battery energy per unit volume (Wh/L). Similar to specific energy, higher energy density implies smaller physical size. The specific power of a battery is the maximum available power per unit mass (W/kg). On the other hand, the power density of a battery is the maximum available power per unit volume (W/L). The specific power and power density indicate the loading capability of the battery or the amount of current that the battery can provide.



## **2.8 Summary**

The pumped hydro energy storage is the cheapest and the most established technology for large-scale peak shaving among all energy storage system. However, this storage technology is limited by the resource distribution and suitable terrains for reservoirs and tailwaters. In the recent years, the battery storage system has emerged to be a competitive candidate for peak shaving due to the advancement of its technology as well as the fall of the prices. Energy can be stored in the batteries during the off-peak periods and can be delivered to the grid during the peak periods. Currently, the lead-acid battery technology is the most promising candidate for peak shaving due to its low-priced, maturity, stability, and availability as compared to other battery technologies.

## **CHAPTER 3**

### **ARCHITECTURE OF THE EXPERIMENTAL ENERGY STORAGE SYSTEM**

#### **3.1 Introduction**

An experimental energy storage system (ESS) has been developed to investigate the peak reduction on the low-voltage distribution network. In this chapter, the design of the experimental ESS and details of the individual components and systems are presented in this chapter. The ESS is installed at two different buildings of Universiti Tunku Abdul Rahman (UTAR) to reduce the peak demand over a period of time.

#### **3.2 Low-voltage Distribution Network**

A low-voltage distribution network has been established based on the Malaysian low-voltage distribution network. The Malaysian low-voltage distribution network has a Terre-Terre (TT) grounding system where only the neutral point at the secondary side of the transformer is grounded. The TT grounding system is defined as an electrical system whose exposed conductive parts are connected to the earth independently of the ground electrodes of the local utility as shown in Figure 3.1.

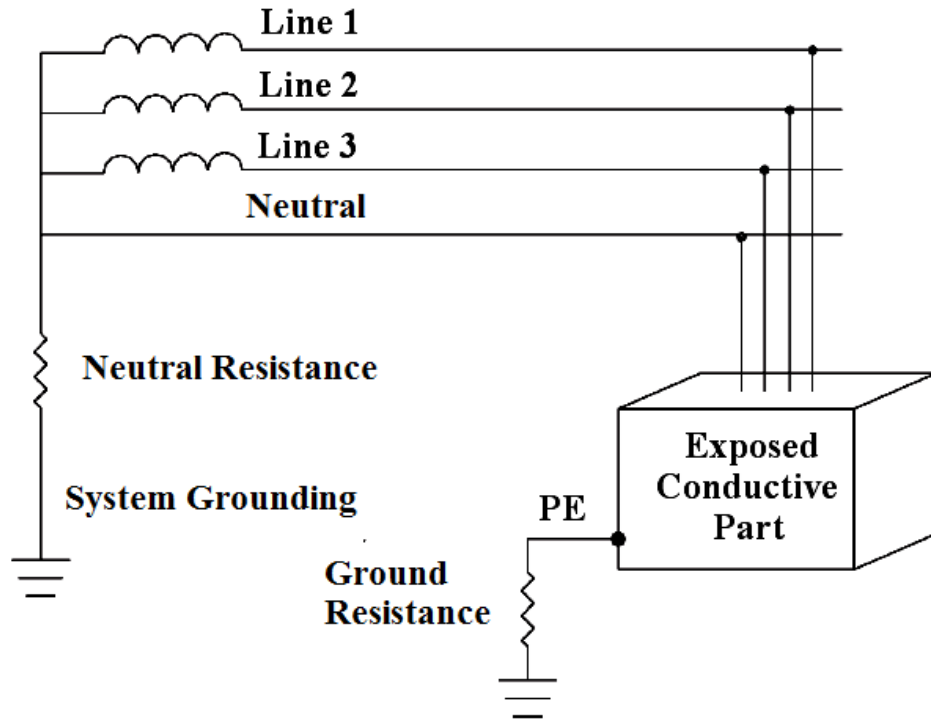


**Figure 3.1: TT grounding system**

The experimental low-voltage distribution network is designed in a radial 3-phase, 415V, 50Hz, four wire network with TT grounding system. Figure 3.2 shows the single-line diagram of the experimental low-voltage distribution network. The low-voltage distribution network consists of a photovoltaic (PV) system, a wind turbine emulator, a load bank, and an energy storage system. The network can be configured in either a stand-alone network or a grid-connected network using the LV network selector switch.

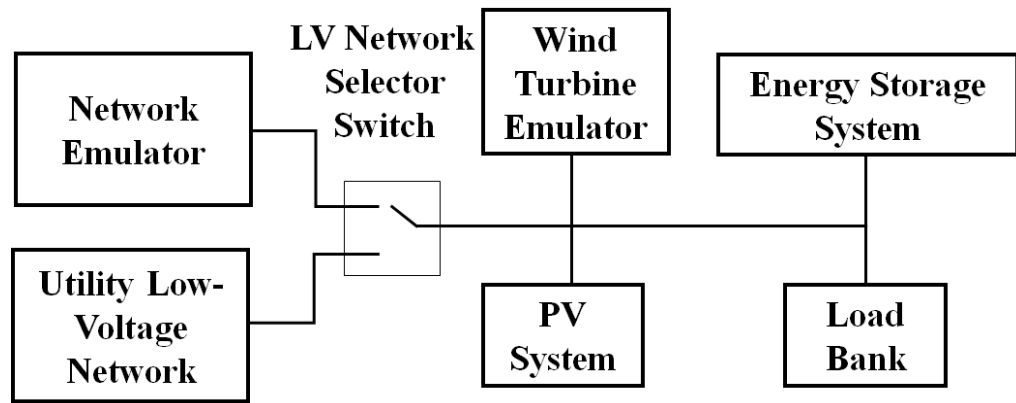
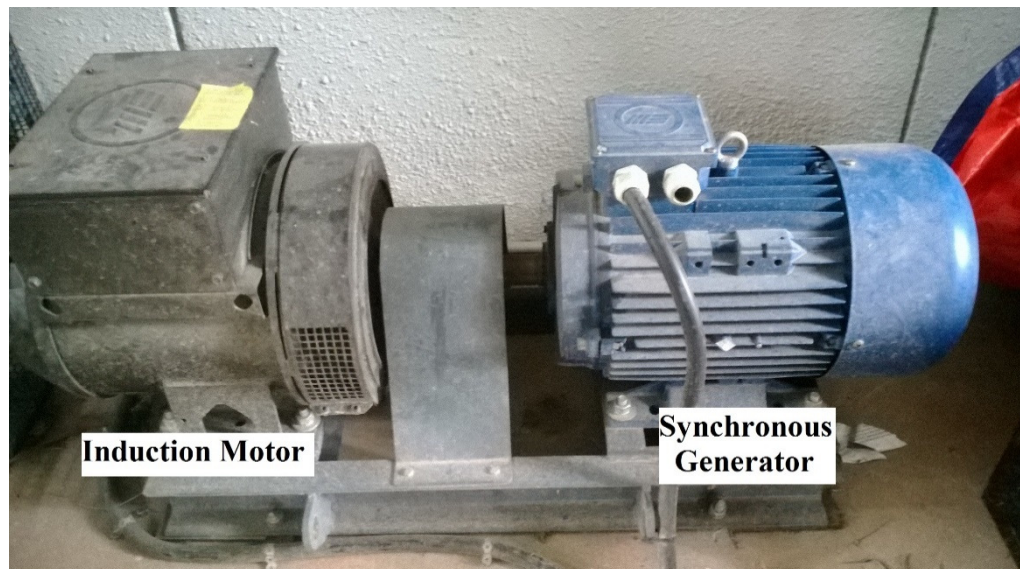


**Figure 3.2: Single-line diagram of the experimental low-voltage distribution network**

A 15 kVA, 3-phase synchronous generator is used to form a 415 V, 50 Hz low-voltage network emulator. The generator is coupled to a 3-phase induction motor as shown in Figure 3.3 (a). The 3-phase induction motor is driven by a variable speed drive (VSD) as shown in Figure 3.3 (b).



**(a)**



(b)

**Figure 3.3: (a) 3-phase synchronous generator coupled with induction motor and (b) variable speed drive**

Figure 3.4 shows the topology of the network emulator. The VSD motor control is based on the Direct Torque Control (DTC) method. DTC is used in VSD to control the torque of a 3-phase induction motor by estimating the motor's magnetic flux and torque using the measured voltage and current. The 3-phase induction motor acts as a prime mover for the 3-phase synchronous generator so that the synchronous generator can supply a consistent 3-phase, 415 V, 50 Hz power under various load conditions.

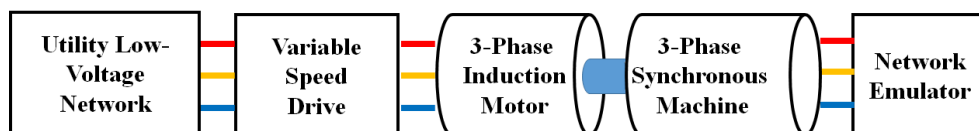


**Figure 3.4: Topology of the network emulator**

The overall experimental setup of the low-voltage distribution network with energy storage is illustrated in Figure 3.5. The ESS consists of bi-directional

converters and lead-acid batteries. There is a total of 6 bi-directional converters as shown in the figure. However, only three of them are used in the experiments due to the limitation of the battery capacity.

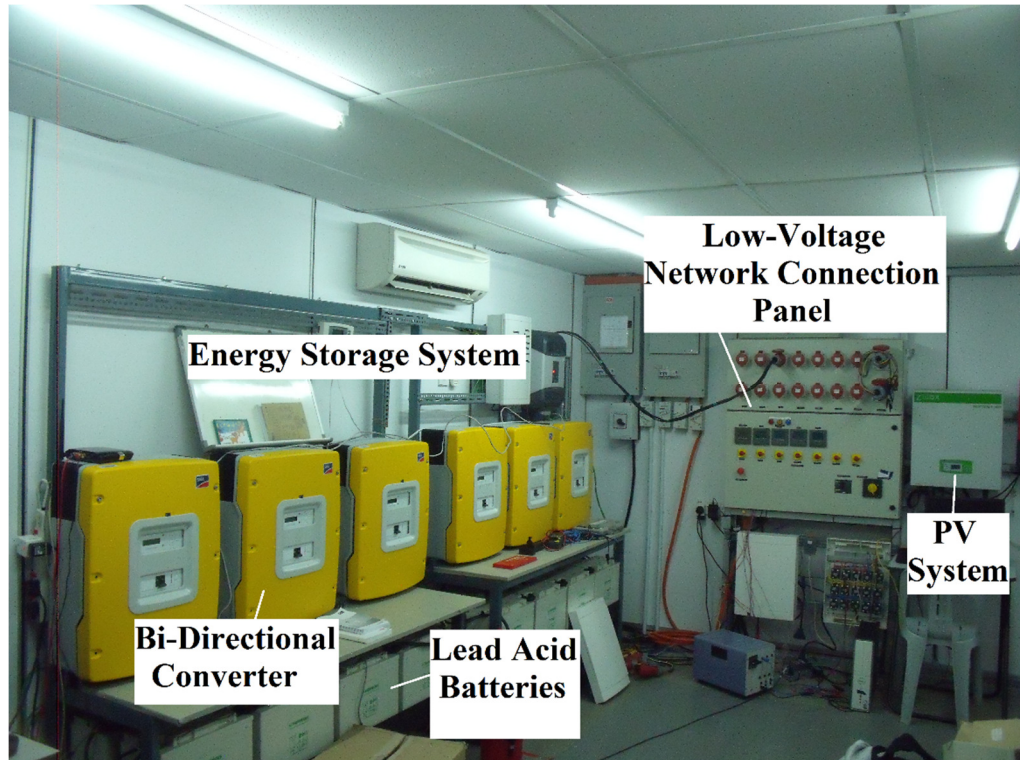


**Figure 3.5: The overall experimental setup of the experimental low-voltage distribution network with energy storage**

### **3.3 Low-voltage Network Connection Panel**

Figure 3.6 shows the low-voltage network connection panel. The panel comprises three main parts, namely the measurement system, busbar connecting terminals, and switches. There are 7 busbar connecting terminals that enable users to connect to the designated renewable energy sources such as PV systems and wind turbine emulators. Seven phase selector switches are used to connect

the busbar connecting terminals to the designated phase in the network. The LV network selector switch allows users to select either the utility low-voltage network or the network emulator. A moulded case circuit breaker (MCCB) rated at 100 A is used to protect the panel from any overcurrent and short-circuits faults. The load bank connecting terminals allow the users to connect or isolate the load bank from the panel. The emergency switch is installed to cut-off the panel from the supply immediately during any emergency or faulty conditions.

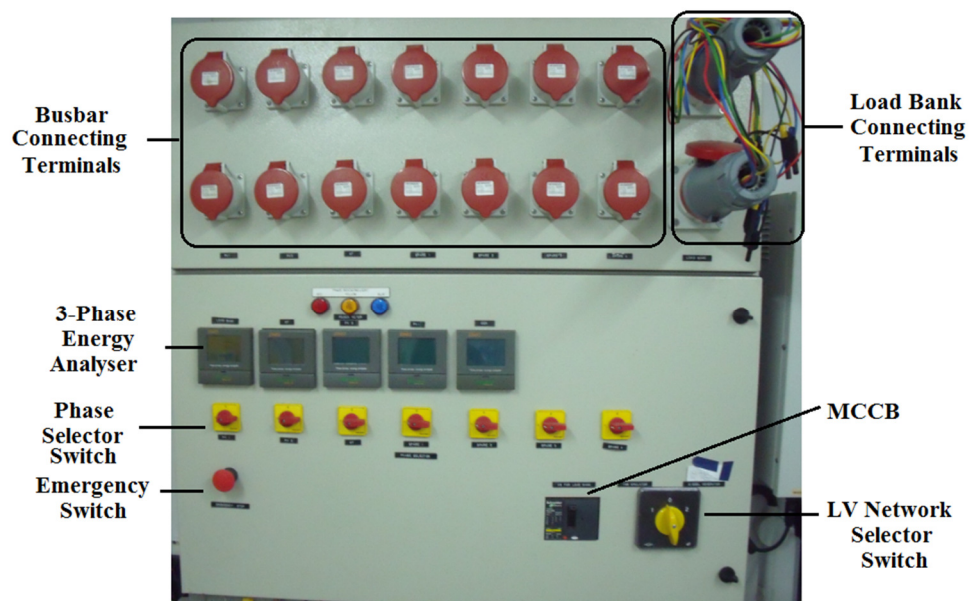


**Figure 3.6: Low-voltage network connection panel**

Five units of STAR3 3-phase energy analysers are used to measure the power flows of the PV system, wind turbine emulator, load bank and energy storage system in the low-voltage network connection panel. These analysers provide a real-time reading on the LCD screen and send the measurements to a computer for recording, via RS485 port. STAR3 energy analysers can also provide voltage, current, frequency, power, and total harmonic distortion (THD) measurements. It is capable of measuring up to 350 V phase-to-neutral and 600 V phase-to-phase voltages. The voltmeter impedance is 2 M $\Omega$ . The maximum



input current is 5 A and its burden is 1 VA. The measuring range of the current is from 0 to 120 % of its nominal value. In order for the energy analyser to measure high currents, a current transformer is used. The sensitivity for the voltage and current measurement are 10 V and 20 mA, respectively. Figure 3.7 shows the STAR3 3-phase energy analyser and its connection to the low-voltage distribution network.

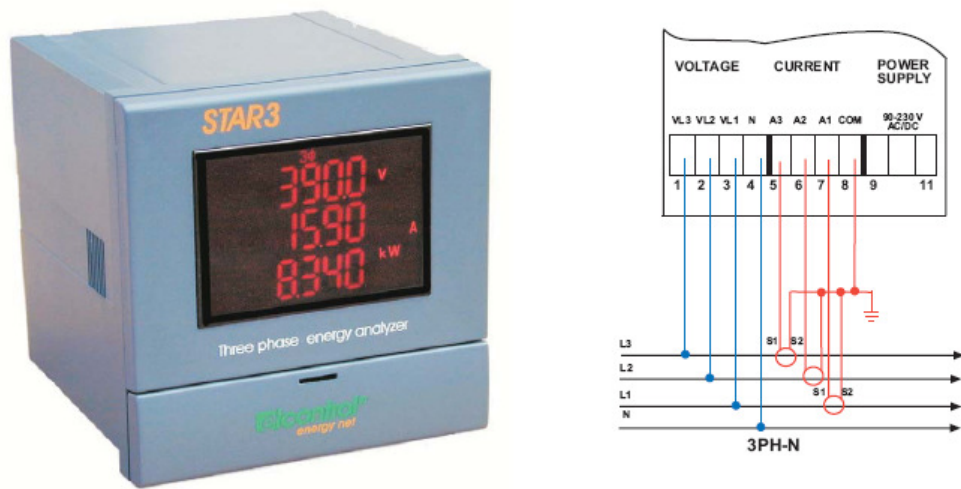


**Figure 3.7: STAR3 3-phase energy analyser and its connection to the low-voltage distribution network**

The interior of the low-voltage network connection panel consists of miniature circuit breakers (MCB), a data logger, connecting terminals to the utility low-voltage network, and a contactor. The MCBs are used to prevent overcurrent that flows through the devices that are connected to the panel. The data logger collects data from the STAR3 3-phase energy analysers and transmits the data to a supervisory computer for monitoring and recording purposes. The contactor is used to connect and isolate the low-voltage distribution network with the panel. The contactor is actuated by the LV network selector switch. Figure 3.8 shows the interior design of the low-voltage network connection panel.



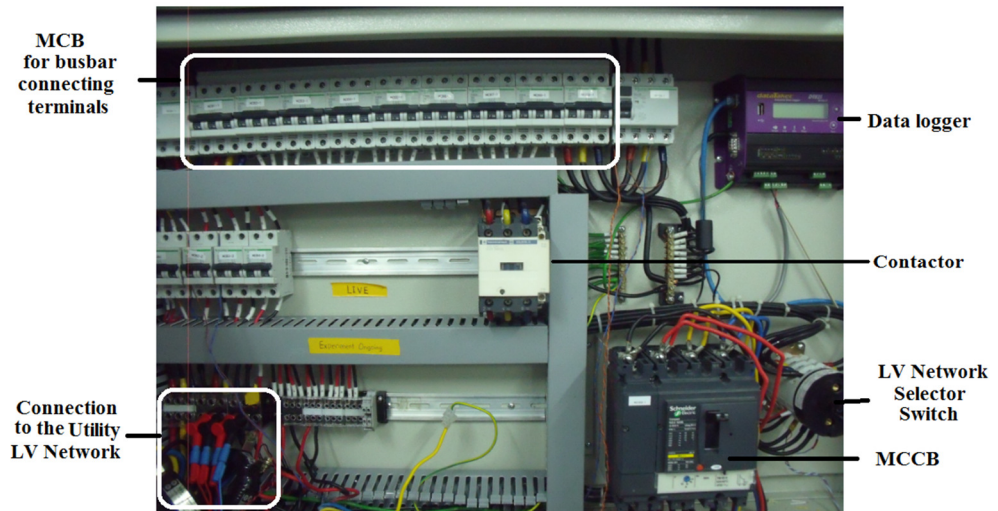


**Figure 3.8: Interior design of the low-voltage network connection panel**

The electrical layout of the low-voltage network connection panel is illustrated in Figure 3.9. There are four spare connecting points to allow interconnection of additional systems to the network for expansion in the future.

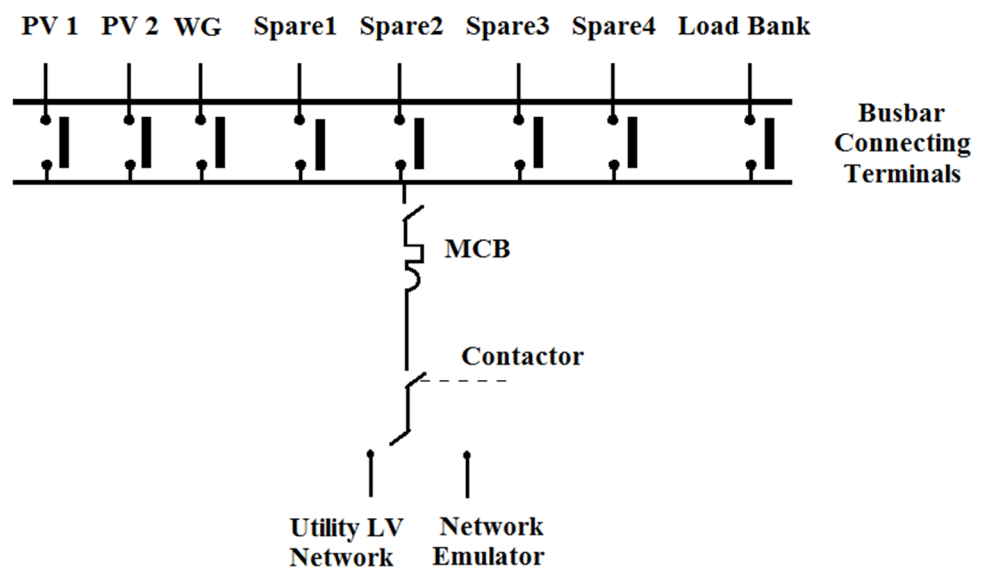


**Figure 3.9: Electrical layout of the low-voltage network panel**

### 3.4 Load Bank

A load bank is formed by a string of resistors controlled by solid-state relays (SSR). These SSR are switched using a NI 9403 digital input/output module. Figure 3.10 shows the power resistor and SSR used to construct the load bank.



**Figure 3.10: Power resistor and SSR**

Six power resistors rated at  $115.4 \Omega$ , 500 W are connected in parallel for each phase. The load can be varied in steps of 500 W up to 3 kW per phase and up to 9 kW for 3-phase. Each phase is connected to the MCB rated at 20 A for overcurrent protection. SSR is used as an electronic switch to connect and disconnect the power supply from the power resistors. The SSR is rated at 240 V, 25 A with a triggering signal range of 3 to 32 V DC. The per-phase electrical circuit of the load bank is shown in Figure 3.11. It can be seen that there are two power resistors connected in parallel to the last SSR. If the last SSR is activated, then two power resistors will be connected and the total load will become 1000 W.

CB - Circuit Breaker  
R - Power Resistor  
SSR - Solid-state Relay

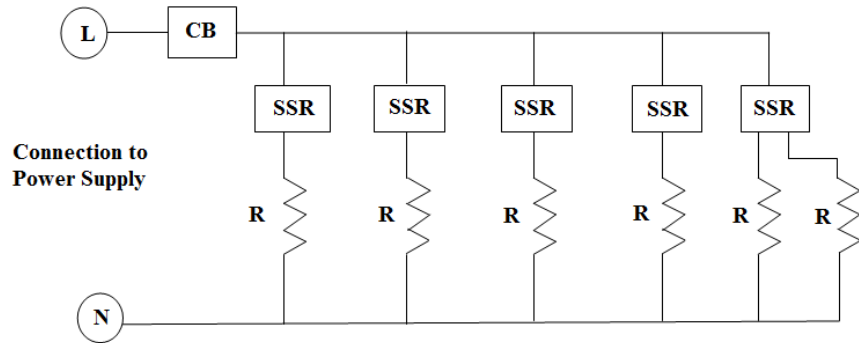


**Figure 3.11: Per-phase electrical circuit of the load bank**

Figure 3.12 illustrates the layout of the load bank. Two identical load bank have been constructed such that the total load that can be manipulated is 18 kW. Physical power resistors are encased in the net to prevent any possible physical contact with animals and human.



**Figure 3.12: Load bank encased in the net**

Figure 3.13 shows the configuration of the SSRs. The SSRs are placed inside a distribution board in order to prevent any unintentional physical contacts.



**Figure 3.13: Configuration of the SSRs**

A digital input/ output (I/O) module NI 9403 is used to send switching signals from the supervisory computer to SSRs. This digital I/O module has 32 digital channels as illustrated in Figure 3.14. Each channel is compatible with 5 V transistor-transistor-logic (TTL) signals and features 1,000 Vrms transient isolation between the I/O channels and the backplane. The transient isolation can physically and electrically separate the I/O channels and the backplane using the electromagnetic field coupling between the I/O channels and the backplane. This is the standard safety requirement for the measurement and control instruments. The isolation permits the two parts to have different voltage levels. When one part is subjected to a hazardous high voltage, the other part can still have a safe voltage level. The NI 9403 can also source up to 2 mA output current for each channel.



**Figure 3.14: NI 9403 32-channel digital I/O module**

The NI 9403 is slotted to a C-series compact data acquisition chassis, known as cDAQ-9174. The NI cDAQ-9174 has four slots that provide a connection for a custom analogue I/O, digital I/O, and counter measurement systems. The cDAQ-9174 has four 32-bit general-purpose counters that have an operating frequency range of 5 Hz to 500 Hz. The counters can store the number of times a particular event or process has occurred. The timing resolution of the NI cDAQ-9174 is 12.5 ns and the input first-in-first-out (FIFO) size is 127 samples per slot. Figure 3.15 shows the picture of the NI cDAQ-9174.

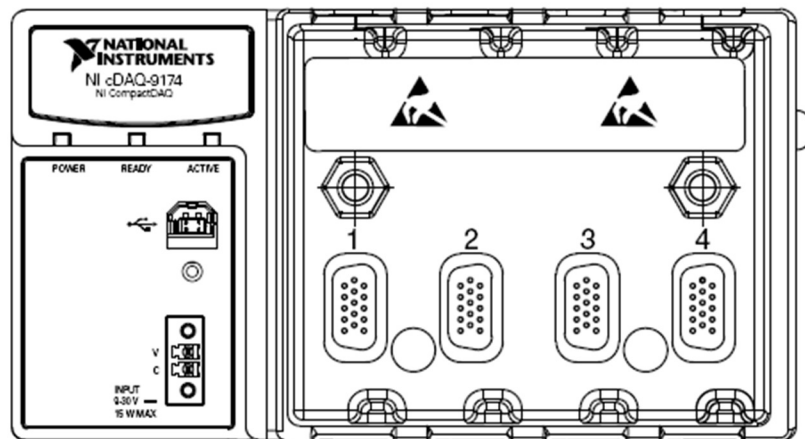


**Figure 3.15: NI cDAQ-9174 4-slot chassis**

### 3.5 Bi-directional Power Flow Converter

The bi-directional power flow converter chosen for this research is Sunny Island 5048 which is manufactured by SMA. This model of the converter is typically used in standalone power systems with renewable energy sources. However, it can also be used in the grid-tied electrical network to provide other services such as reactive power compensation and peak reduction. Table 3.1 shows the technical data of the Sunny Island 5048.

**Table 3.1: Technical data of the Sunny Island 5048**

Technical data	Nominal Values
DC	
Maximum DC voltage	63 V
Nominal output voltage	48 V
Operating temperature range	-25 °C– 50 °C
AC	
Nominal output voltage	230 V
Maximum continuous output current	21.7 A
Maximum input current	56 A
Maximum continuous output power	5000 W/25 °C 4000 W/45 °C
Efficiency	95 %

Sunny Island 5048 is a single-phase converter that has a power rating of 5 kVA. Sunny Island 5048 has three basic operating modes, namely the grid forming, grid-tied and droop mode operations. The grid forming mode forms a standalone grid and keeps the voltage and frequency of the grid at a constant level. The grid-tied mode enables the Sunny Island 5048 to be interconnected to the utility low-voltage network by meeting the grid's voltage magnitude, phase sequence, phase angle, and frequency. During the droop mode operation, the Sunny Island

5048 varies the frequency of the grid with changes in real power and varies the grid's voltage with changes in reactive power.

In addition, the Sunny Island 5048 also includes a load management and an intelligent battery management system. The load management will deactivate the loads connected to the Sunny Island 5048 automatically when the available energy in batteries drops below the limit set by users to prevent the batteries from over-discharged. The intelligent battery management system can precisely record the battery's state of charge and improve the utilization of the battery capacity. The battery management system has an intelligent charge control and reliable deep discharge protection to prevent the premature aging of batteries, caused by incorrect charging and frequent deep discharge. This helps to extend the batteries' life and performance. The overview of all control elements and connections of the Sunny Island 5048 are shown in Figure 3.16. The control keys are used to navigate the features and settings of the device.

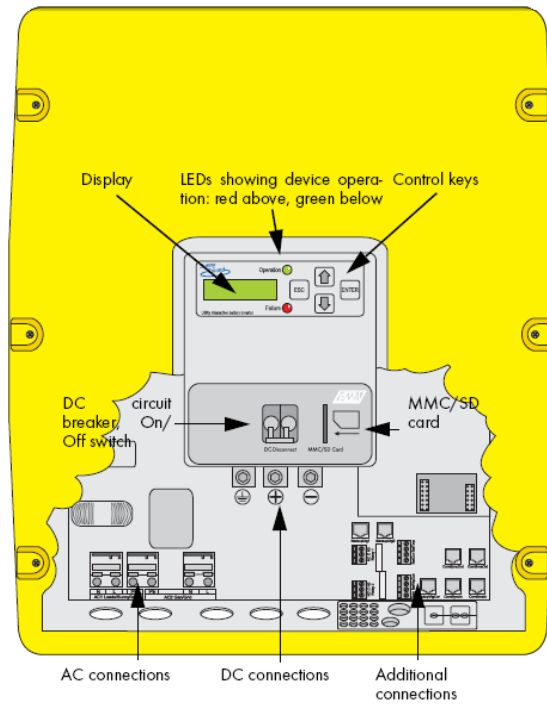


**Figure 3.16: Overview of all control elements and connections of the Sunny Island 5048**

Sunny Island 5048 allows users to store the firmware settings as well as the measured data in a multi-media card (MMC/SD card). The data saved on the MMC/SD can be processed with usual spreadsheet programs in the computer. The users can store and retrieve their designated settings by inserting the MMC/SD to the Sunny Island 5048. In addition, the Sunny Island 5048 can also save the measurement, events and failures report of the operations in the MMC/SD.



### 3.6 Battery Bank Configuration

Each Sunny Island 5048 is connected to a string of 16 valve-regulated lead-acid (VRLA) batteries. The battery model chosen for the battery bank is Hoppecke Solar bloc. The electrode design allows efficient charge current acceptance. Besides, the batteries are also integrated with backfire protection and central degassing system to improve the operational safety. Four batteries are connected in series to form a string of batteries in order to provide a 48 V DC supply to the Sunny Island 5048. There is a total of 4 strings of batteries connected in parallel as illustrated in Figure 3.17. The total capacity of the batteries is 21.32 kWh. The physical 3-phase ESS setup is illustrated in Figure 3.18. The total storage capacity of the ESS is 63.96 kWh.

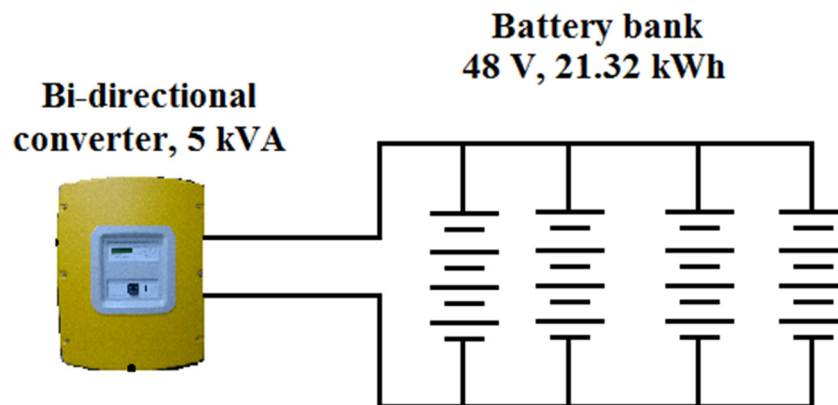


**Figure 3.17: Batteries connected to the Sunny Island 5048**



**Figure 3.18: Physical 3-phase ESS setup**

Figure 3.19 shows the number of cycle life of the batteries with respect to its depth of discharge. It can be seen that the number of cycle life is inversely proportional to the depth-of-discharge of batteries. The batteries' cycle life is 4000 cycle if it is discharged to 20 % depth of discharge while the batteries' cycle life becomes 750 cycles if it is discharged to 80 % depth of discharge. The depth-of-discharge of the batteries is limited to 50 % based on the recommendation of the battery manufacturer to prolong the cycle life of the batteries.

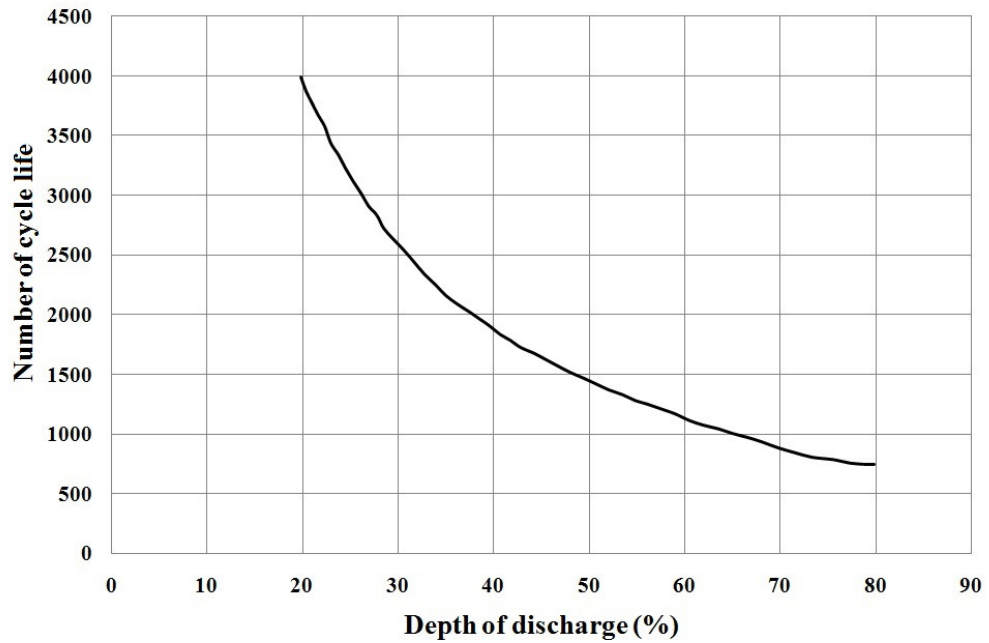


**Figure 3.19: Number of cycle life of the batteries with respect to its depth of discharge**

### 3.7 Configuration of Sunny Island 5048

For the first time of powering up the Sunny Island, a quick configuration guide (QCG) will prompt the user for initial configuration. The system configuration such as grid voltage, battery types, nominal voltage, charging current, and battery capacity need to be set in the QCG. Upon the completion of the configuration, users can proceed to the main menu. Initially, all parameters in the Sunny Island 5048 are set at default values. If users intend to change the settings, a security password is required. The password is the sum of digits of the operating hours illustrated on the screen. For instance, the password for the operating hours of 1036 is 10 ( $1 + 0 + 3 + 6$ ).

To enable power injection to the network, the parameter #23801 FedInEna must be set to enable mode. The parameter #23802 FedInMod is used to activate the communication between the converter and the computer. The parameter #23807 FedInCurAt can be set to absorb or deliver real power to the network while #23808 FedInCurRt can be configured to absorb or deliver reactive power to the network.

For the single-phase system, the Sunny Island 5048 can be cascaded with two or more units to increase the total output power. Figure 3.20 (a) shows the configuration of a single unit connection Figure 3.20 (b) shows the configuration of dual unit connection to the network. For connecting two or more unit, one of the converters must be assigned as a master unit while the others as slave units.

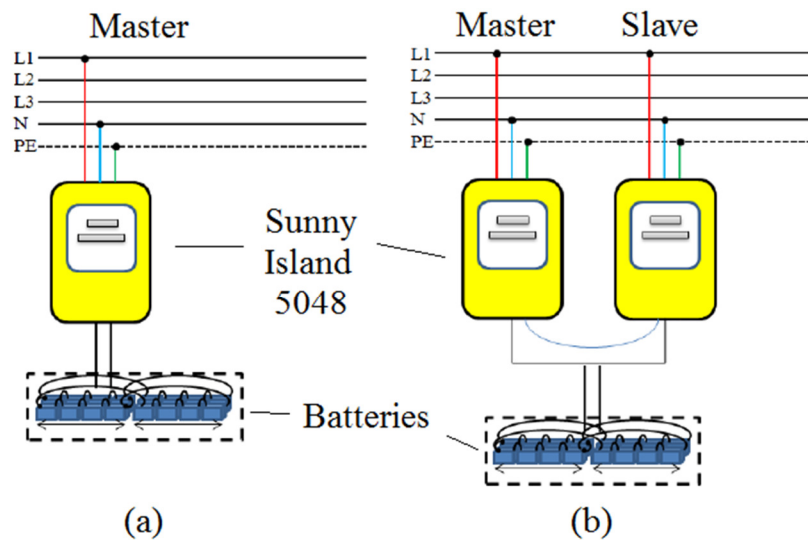


**Figure 3.20: (a) Single unit connection and (b) dual unit connection**

Figure 3.21 shows the interior master-slave configuration of the Sunny Island converters. The communications are established using Ethernet computer

network cable, known as RJ45. The port labelled as Com-Sync-Out at the master unit is connected to the port labelled as Com-Sync-In at the Slave 1 unit. A termination resistor is connected to the Com-Sync-In port at the master unit to provide an equal characteristic impedance of the network cable. The Com-Sync-Out port at the Slave 1 is connected to Com-Sync-In port at the Slave 2. A termination resistor is connected to the Com-Sync-Out port at the Slave 2 for the same purpose as mentioned above.

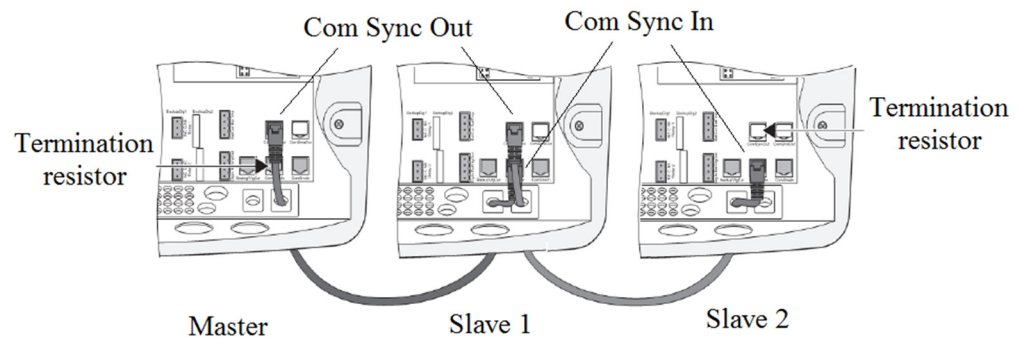


**Figure 3.21: The interior master-slave configuration of the Sunny Island converters**

To configure the 3-phase system, each Sunny Island 5048 is connected to each phase and is configured as the master unit as shown in Figure 3.22.

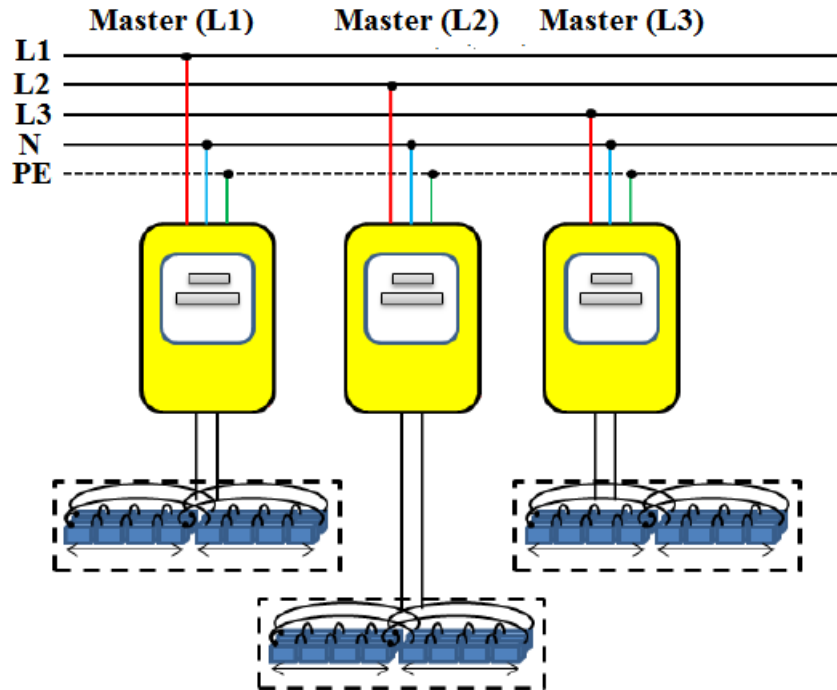


**Figure 3.22: Configuration of Sunny Island 5048 in a 3-phase system**

### 3.8 External Communication of Sunny Island 5048

The interface of Sunny Island 5048 with a computer can be established via a communication chipset, piggy back PB-485-G2. The chipset is a communication module inserted into position A of the converter as shown in Figure 3.23. The Com-Sma-Out port, as shown in position B, is connected to an external RS485/USB converter, namely ICP CON I-7563. A termination resistor is connected to the Com-Sma-In port as shown in position C.

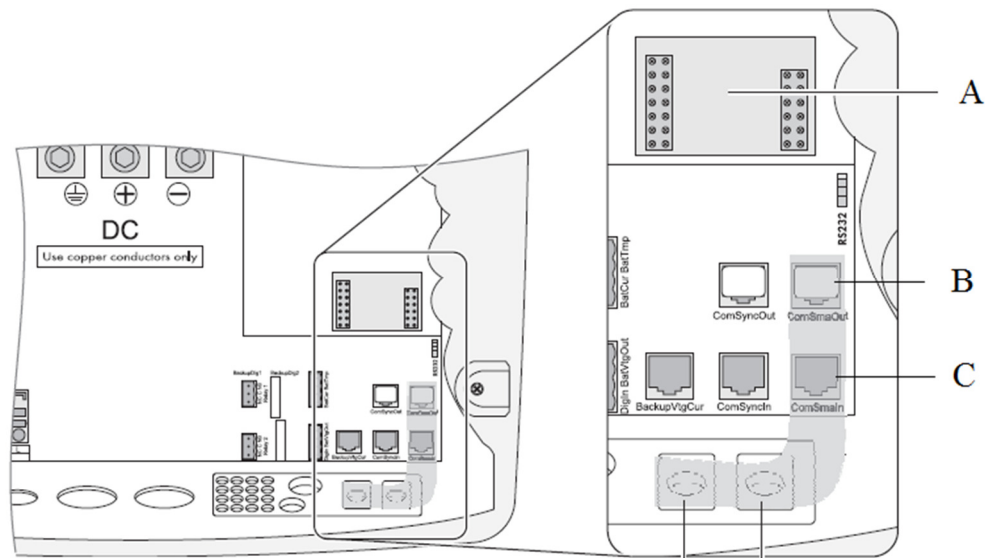


**Figure 3.23: Ports for external interface at Sunny Island 5048**

The external RS485/USB converter, ICP CON I-7563, is a communication module for transferring serial data to the supervisory computer over USB. The RS485/USB converter contains a self-tuner chip that can automatically tune the baud rate and data format to the RS485 network. The data transmission rate is 115.2 kb/s. Figure 3.24 shows the interface of the RS485/USB converter with the Sunny Island 5048.

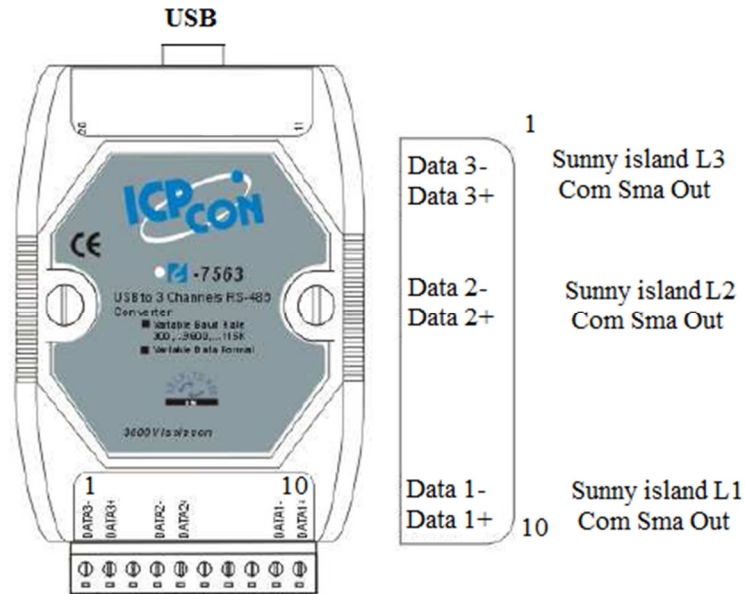


**Figure 3.24: Interface of the RS485/USB converter with the Sunny Island 5048**

### 3.9 Configuration of Sunny Island 5048 Communication System

The communication between Sunny Island 5048 and the supervisory computer is established using the RS485/USB converter. The topology of the communication system is illustrated in Figure 3.25.

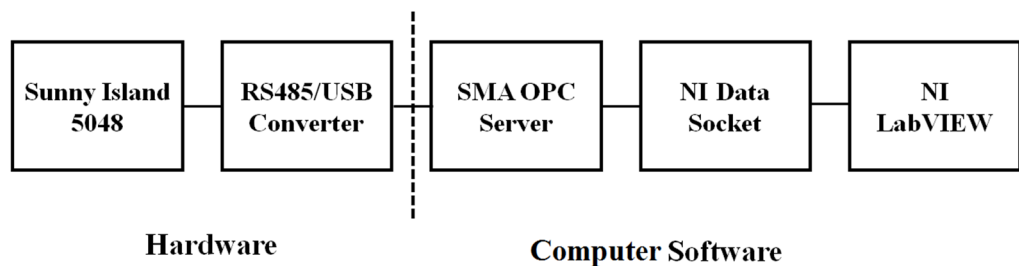


**Figure 3.25: Topology of the communication system between Sunny Island 5048 and the supervisory computer**



SMA OPC server is a server-based 32-bit application for data exchange between the SMA products and the computer using SMA data protocols via SunnyNet or SMANet. OPC is known as OLE process control while OLE is known as Object Linking and Embedding. The SMA OPC server can be configured in a file named “yasdi.ini”. The drive module is set to “yasdi\_drv\_serial.dll” and the media is set to RS232. The baud rate serial interface is set at 19200 and the transport protocol is SMANet. NI Data socket is a high-performance programming tool that is designed specifically to share and publish data in Laboratory Virtual Instrument Engineering Workbench (LabVIEW) programming environment. NI data socket is capable of interfacing with many protocols such as OPC, Hypertext Transfer Protocol (HTTP) and File Transfer Protocol (FTP).

### **3.10 Data Acquisition System**

Data acquisition (DAQ) is the process of measuring an electrical or physical phenomenon with a computer. A DAQ system comprises of sensors, measurement hardware, and a computer. Figure 3.26 illustrates the path of an analog signal in a LabVIEW DAQ application. The analog signals are converted into digital signals via Analog-Digital Converter (ADC) in the DAQ device. The signals are sent in the order of First-In-First-Out (FIFO) method.

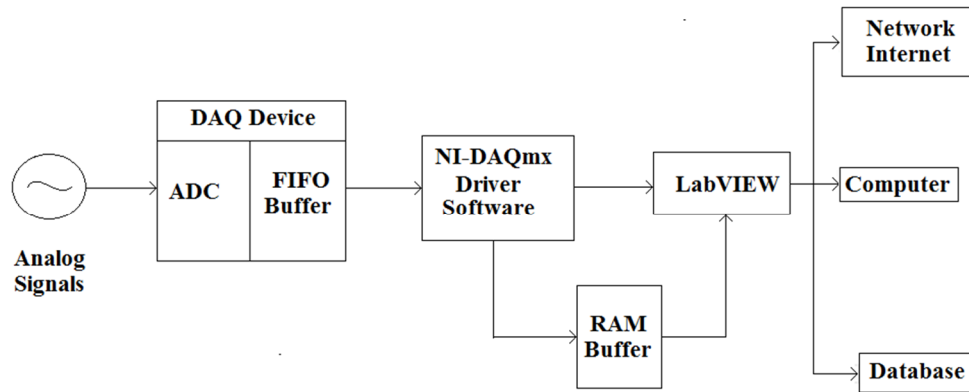


**Figure 3.26: Path of an analogue signal in a LabVIEW DAQ application**

The DAQ device sends the digital signals to the NI-DAQmx driver software that interfaces the device with a computer. NI-DAQmx is the newest data acquisition driver developed by NI. It incorporates an entirely new driver architecture and complete with new functions and development tools for controlling NI DAQ devices. NI-DAQmx instructs the hardware to initiate the I/O operation in the LabVIEW. The random-access memory (RAM) buffer is used as an intermediate place to store the data acquired if the LabVIEW program is busy. For instance, if a few thousand data samples are acquired in one second, it would be difficult to be displayed in the graph at the same second. The DAQ device can acquire the data into a memory buffer for temporary storage and later be retrieved for further analysis. Finally, the data acquired is displayed on the computer. The data can either be shared via network internet or stored into the database.

Figure 3.27 shows the logical organization of NI-DAQmx applications. The first step is to create a virtual channel and adds it to a task. The second step is to configure timing such as sample rate and timing source. The task can also be

configured to start or stop on a rising or falling edge of the digital or analogue data based on the predetermined triggering mode. Once the configuration is done, the task will be started. The main task of acquiring or generating data will be accomplished in the grey square block as illustrated in the figure. Once the codes in the grey square block are executed, the task will be stopped and cleared to release the resources occupied during the execution of the code.

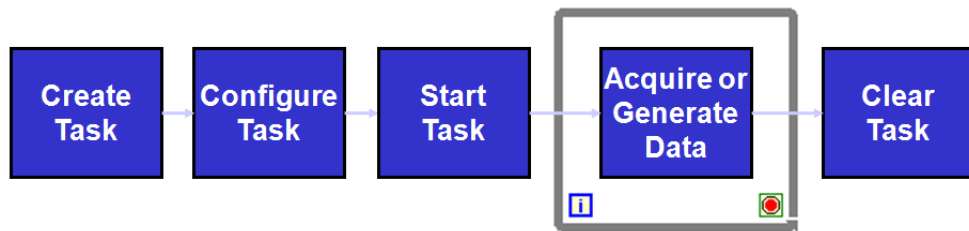


**Figure 3.27: Logical organization of NI-DAQmx applications**

The power flow of the electrical network is measured using the voltage and current measurement modules manufactured by National Instruments (NI). The voltage measurement module used is NI 9225 while the current measurement module used is NI 9227. The technical data of these two measurement modules are shown in Table 3.2.

**Table 3.2: Technical data of the voltage and current modules**

NI 9225 Voltage Module	NI 9227 Current Module
300 Vrms measurement range	5 Arms measurement (14A peak)
600 Vrms channel-to-channel isolation	250 Vrms channel-to-channel isolation
50 k sample/s/channel	50 k sample/s/channel
Built-in anti-alias filters	Built-in anti-alias filters

### 3.11 Installation of the Data Acquisition System

The ESS is installed in two different buildings in two different periods of time. The ESS was first installed in early 2012 at one of the campus buildings located at Setapak, namely SE block. The ESS was then moved to a building located at Sungai Long in 2015, namely KA block. In the Setapak campus, two DAQ systems were developed at SE block to measure the power flow of the ESS and load demand. Figure 3.28 shows the location of the DAQ systems installed at the SE block.

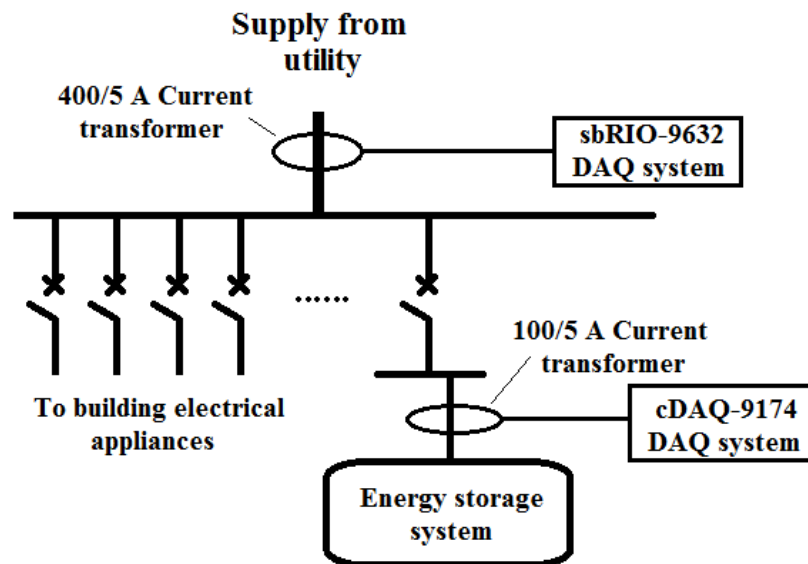


**Figure 3.28: Location of the DAQ systems installed at the SE block**

For the DAQ system installed at the research laboratory, a 4-slot C-series compact data acquisition controller, cDAQ-9174, is used to access the voltage and current modules. Figure 3.29 shows the DAQ system installed at the research laboratory for the ESS.

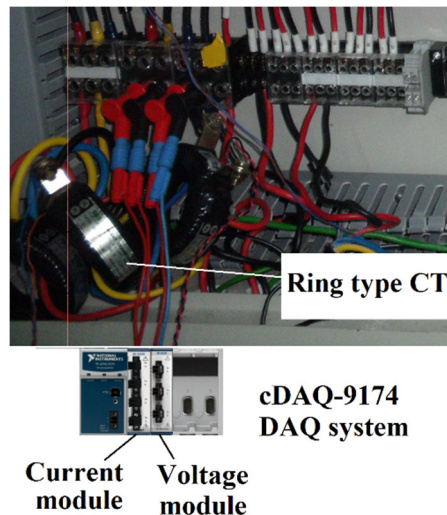


**Figure 3.29: DAQ system installed at the research laboratory for ESS**

Ring-type current transformers (CTs) with the ratio of 100/5 A and burden of 5VA as shown in Figure 3.30 are used for the DAQ system installed at the cables that are connected to the low-voltage network connection panel. The primary side of the ring-type current transformers is attached to the cables to step down the current flows in the low-voltage network connection panel while the secondary side of the CTs is connected to the NI 9227 current module. The ratio of 100/5 A implies the transformation ratio of the primary current to the secondary current. For example, a current transformer with the ratio of 100/5 A will step down a line current of 100 A at primary side to 5 A at the secondary side of the current transformer. Ring-type current transformers have relatively small physical size and the price is relatively cheap. The rating of the ring-type current transformer is suitable for current measurements in the experimental low-voltage network connection panel.



**Figure 3.30: Ring-type current transformer**

The DAQ system installed for measuring the power consumption of the whole building consists of a single board-RIO controller (sbRIO-9632), a voltage module, and a current module as illustrated in Figure 3.31.

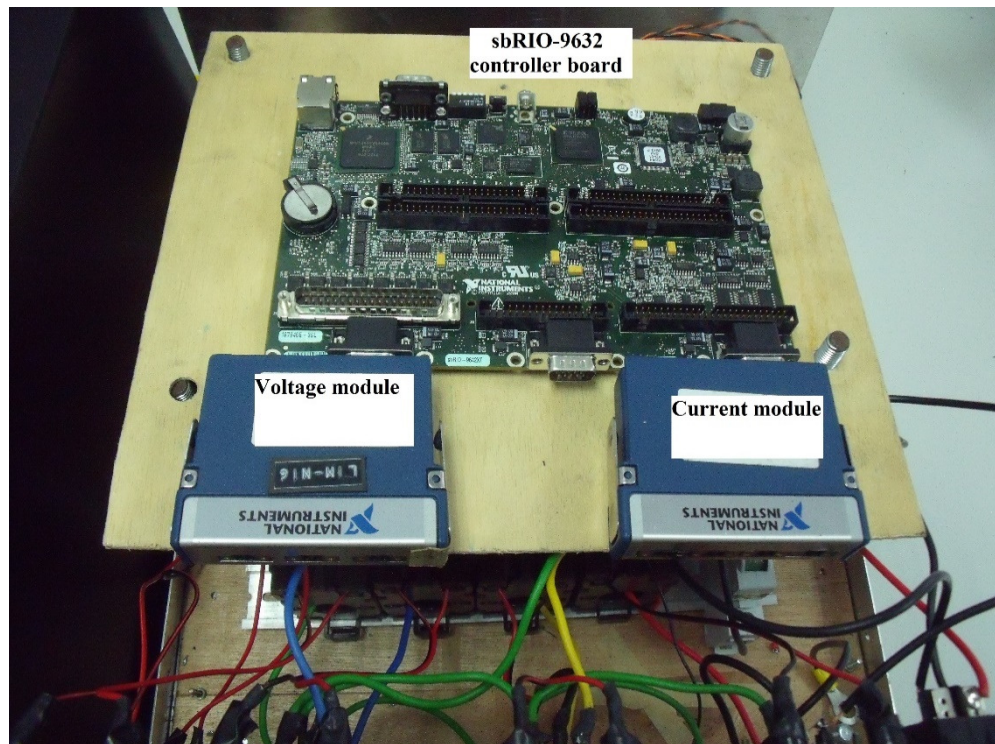


**Figure 3.31: The DAQ system for measuring the power consumption of the whole building**

The single board-RIO controller is an embedded control and acquisition device that is integrated with a 400 MHz real-time processor, a user-reconfigurable field-programmable gate array (FPGA), and 110 digital input/ output (I/O) on a single printed circuit board. Table 3.3 shows the specifications of the sbRIO-9632.

**Table 3.3: Specifications of the sbRIO-9632**

<b>Specification</b>	<b>Value</b>
Processor	400 MHz
Sample rate	250 k sample/ s
Maximum voltage range	-10 V to +10 V
Digital I/O	110 channels
Maximum clock rate	40 MHz

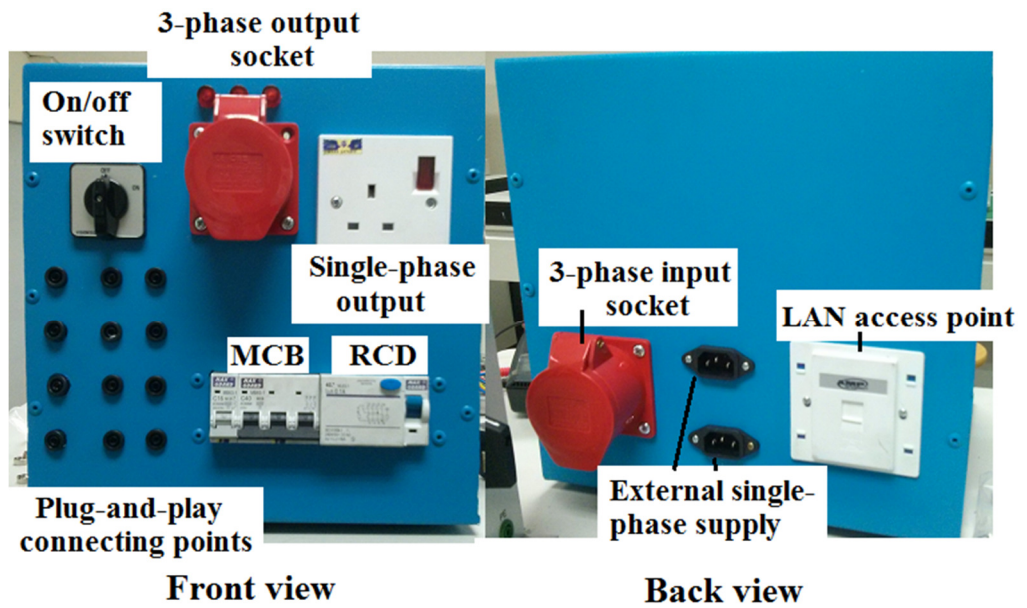
Split-core current transformers with the ratio of 400/5 A and burden of 5VA as shown in Figure 3.32 are used to step down the current measured for the building. The split-core current transformer has a core with a removable section that allows the transformer to be attached to the cable without disconnecting the line or interrupting the supply. The primary side of the split-core current transformers is clipped on the armored cables risen from underground to step down the current flows in the building while the secondary side of the current transformers is connected to the current module NI 9227.



**Figure 3.32: Split-core current transformer**

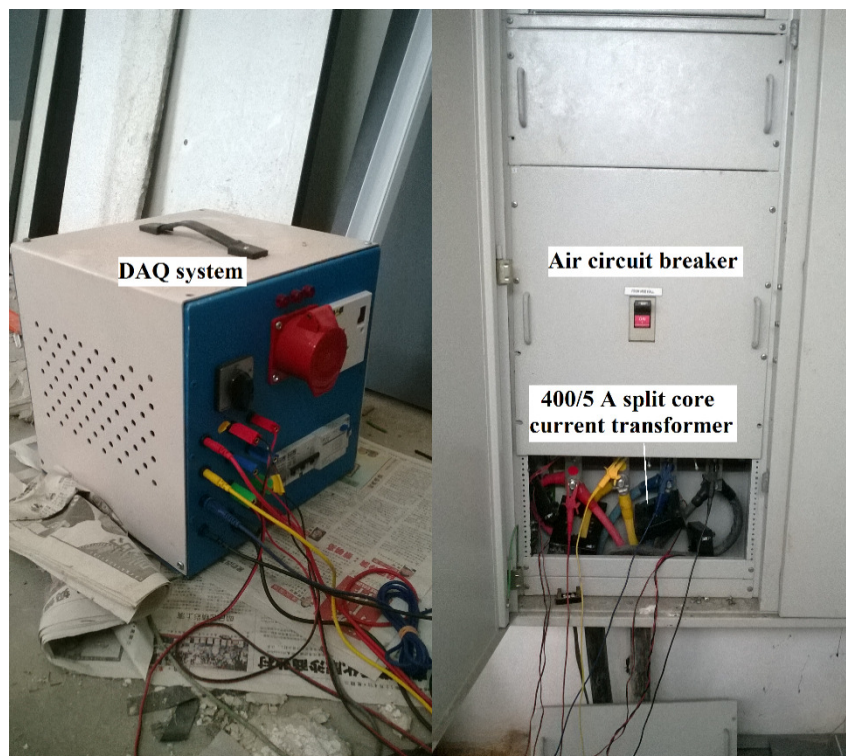
A portable enclosure is designed and developed to encase the DAQ system to prevent any possible physical contact with a human. A flexible plug-and-play connecting points are designed such that the measuring wires can be plugged and unplugged from the enclosure conveniently and safely. This design is important to ensure the safety of the users because the DAQ system needs to be connected to the three-phase network without interrupting the supply. The communication between the device and the computer is set up via a local area network (LAN). Figure 3.33 shows the front view and back view of the portable DAQ system.





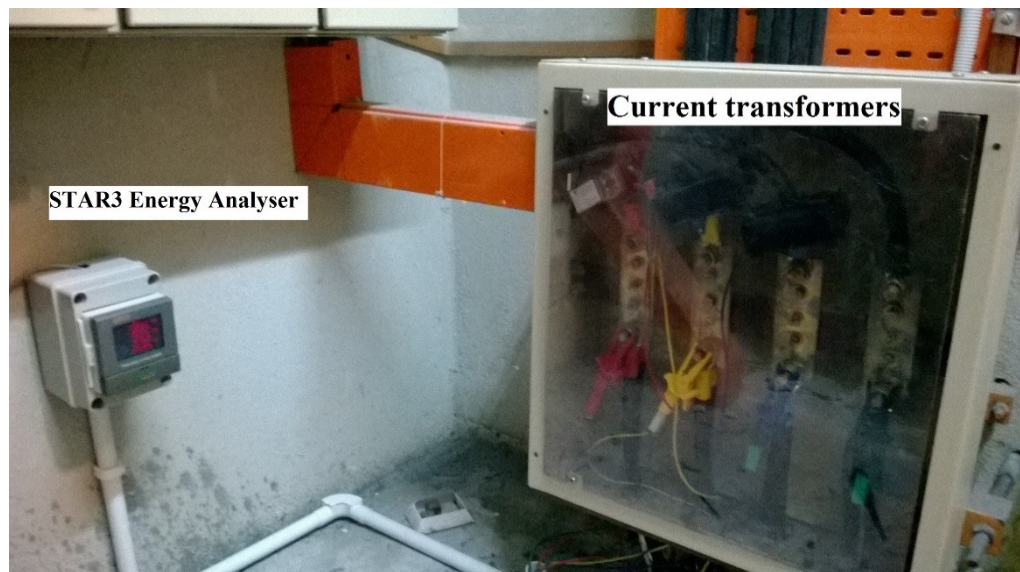
**Figure 3.33: Front view and back view of the portable DAQ system**

Figure 3.34 shows the portable DAQ system installed in the switch room. It can be seen that the 400/5 A split-core current transformers are installed on the armored cable risen from underground.



**Figure 3.34: DAQ system installed in the switch room**

For the KA building located at the Sungai Long campus, two power energy meters are installed to measure the power consumption of lower ground floor, ground floor, and the first floor in the building. The power energy meters used are STAR3 Energy Analyser. Figure 3.35 shows the installation of the STAR3 Energy Analyser on the three-phase power supply riser of the Sungai Long building.



**Figure 3.35: Installation of STAR3 Energy Analyser on the 3-phase power supply riser of the KA building**

### **3.12 Summary**

The experimental low-voltage distribution network and ESS have been developed to investigate the effectiveness of the ESS in reducing peak demand of a building. The setup consists of a network emulator, a LV network connection panel, two load banks, two PV systems, a wind turbine emulator, and an energy storage system. Experiments are conducted in two different

buildings of Universiti Tunku Abdul Rahman (UTAR) in two different time periods. Two data acquisition systems have been developed to monitor the power flows between the ESS and the grid. The data acquisition system for the building located at Setapak campus is established using sbRIO-9632 DAQ system and cDAQ-9174 DAQ system while the data acquisition system for the building located at Sungai Long campus is established using the STAR3 energy analysers.

## **CHAPTER 4**

# **CONTROL ALGORITHMS IN ENERGY STORAGE FOR PEAK REDUCTION**

### **4.1 Introduction**

This chapter elaborates the challenges in reducing the peak demands of a building. The problem formulation for reducing the peak demands and the implementation of the peak reduction algorithms are discussed in details. The energy storage system is installed in two different buildings, namely the SE block and KA block, to evaluate the effectiveness of the control algorithms in reducing peak demands under various load profiles. The load profiles of SE block are forecasted based on the scheduled activities while the load profiles of KA block are predicted based on the average load demands. The predicted daily load profile provides information on the amount of energy required to shave the peak demands.

### **4.2 Challenges in Reducing the Peak Demands**

Due to the limited energy in the batteries, it is therefore important to supply the power at the appropriate time during the peak demands hours in order to reduce the peak effectively. However, the actual peak demands is always different from

the predicted peak demands depending on the nature of the daily activities in the building. There are four possible scenarios that can cause the energy storage system to fail. The first scenario is that the actual peak demands is unexpectedly high. The energy storage system is not able to supply such a high power due to the limited rating of the inverters. The second is that the actual peak demands occurs for a much longer duration than that of the predicted one. The energy storage system does not have enough energy to sustain the delivery of its power over such a long duration. The third scenario is that the occurrence of the peak demands is much earlier or later than that of the predicted one. The energy storage system may fail to cut down the peak if it supplies power at the wrong time. The final one is the combination of any of the three scenarios described above. Therefore, appropriate control strategies have been developed and implemented into the power converters of the energy storage system so that the power can be supplied at the timely manner with the aid of the load prediction.

Considering the fluctuation in the actual load demand, any control strategies used for the energy storage system has to be assessed empirically. Three control algorithms, namely the fixed-threshold, adaptive-threshold, and fuzzy-based control algorithms, have been developed for the energy storage system to reduce the peak demands. The energy storage system will be charged during the off-peak hours and will be discharged during the peak demand hours. The performance of these strategies is evaluated under various load profiles. The magnitude of the peak reductions achieved by each control algorithm is recorded and compared with others in order to identify which control strategies can provide the maximum peak reduction. The control algorithms are developed

in the LabVIEW software to manipulate the charge and discharge of the energy storage system.

### **4.3 Load Prediction**

Load prediction plays an important role in peak demand reduction because it helps the users know the daily energy consumption pattern of the building. Without the information about the daily energy consumption pattern, the users are not able to determine the appropriate power thresholds for the energy storage system to absorb or deliver power to the load at the appropriate times. If the power thresholds are set at the inappropriate level, then the energy storage system may not be able to reduce the peak demands effectively.

In this study, the daily load profile of the building and the energy required to reduce the peak demands are predicted. The load profiles of the two buildings at two locations are quite different. The SE block is a three storey building that comprises of 6 small classrooms, 4 big classrooms, 3 computer laboratories, 2 electronic laboratories, 1 material laboratory, 1 thermodynamic laboratory, 3 offices, and 4 toilets. The KA block is made up of a basement car park, a lobby area, 1 cafeteria, 3 lecture halls, 4 toilets, and 5 administrative offices. Hence, two different load prediction methods are used to predict the load profiles of the respective buildings.

### 4.3.1 Load Prediction for KA Block at Sungai Long campus

The building at Sungai Long campus, namely KA block, is a nine-storey building that has an average maximum demand of 1000 kW. The peak reductions by the energy storage system for the whole building is not significant because the size of the existing energy storage system, 15 kW, is too small as compared to that of the building maximum demand. It is therefore decided to reduce the peak demands of the first three storeys of the building because the total maximum demand of these three storeys is approximately 100 kW. This can be achieved by connecting the energy storage system and power measuring devices to the respective electrical switchboards. Figure 4.1 shows the single-line diagram of the electrical network for the KA block. It is noticed that the lower ground floor and ground floor are connected to the same feeder. Three sets of power measuring devices are installed at A, B, and C as shown in the figure to measure the power flow of the loads and the energy storage system.

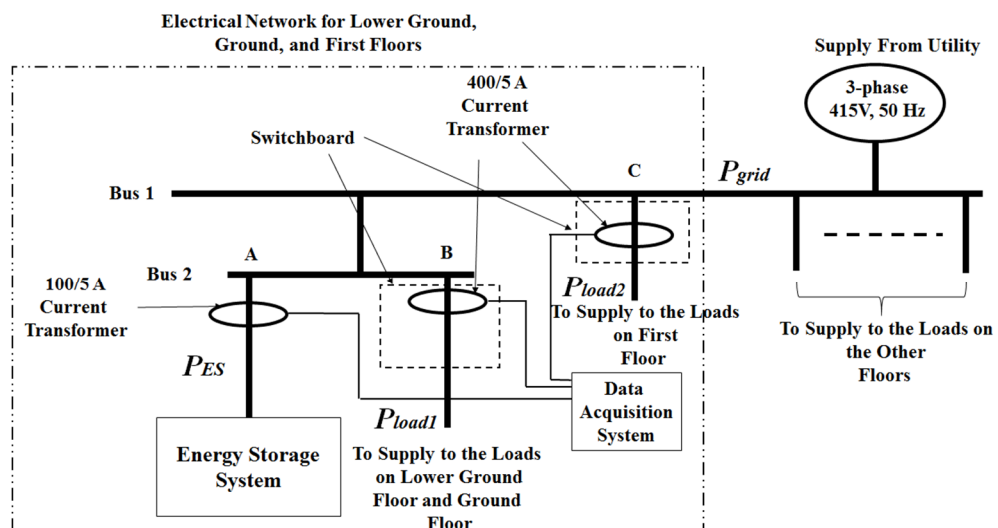


**Figure 4.1: Single-line diagram of the electrical network for the KA block**

The total load demands ( $P_{load}$ ) of the three storeys can be obtained by summing the load demands at B and C as follows:

$$P_{load} = P_{load1} + P_{load2} \quad (4.1)$$

where  $P_{load1}$  is the total load demands of the lower ground and ground floors while  $P_{load2}$  is the total load demands of the first floors. The energy storage system is connected to the bus 2 as shown in the figure. Hence, the power flows of the energy storage system and the loads connected to the lower ground, ground, and the first floors can be measured separately using the power measuring devices. The grid power ( $P_{grid}$ ) can be determined by summing the  $P_{load}$  and the power of the energy storage ( $P_{ES}$ ) as follows:

$$P_{grid} = P_{load} + P_{ES} \quad (4.2)$$

The load profiles of the building are collected by the data acquisition system installed at the respective electrical switchboards as shown in Figure 4.1. The average of the daily load profiles over a period of a week is used to predict the daily load profile because the daily load profiles of this building are quite similar. The accuracy of the predicted load profile is evaluated using the mean absolute percentage error (MAPE) criteria defined as follows:

$$MAPE = \frac{1}{n} \sum_{t=1}^n \left| \frac{A_t - F_t}{A_t} \right| \times 100\% \quad (4.3)$$

where  $A_t$  and  $F_t$  are the actual and predicted load demands at time  $t$ , respectively, and  $n$  is the number of observations. Figure 4.2 shows the historical load profiles of KA block over a period of five days, from Monday to Friday and its average load profile. It is found that the MAPE of the predicted load profile is 7.66 %. The proposed load prediction has an acceptable MAPE of 7.66 % as compared



to other load predicting methods whose MAPE values within 10 % (Efendi et al., 2015; Hong et al., 2015; Song et al., 2005).

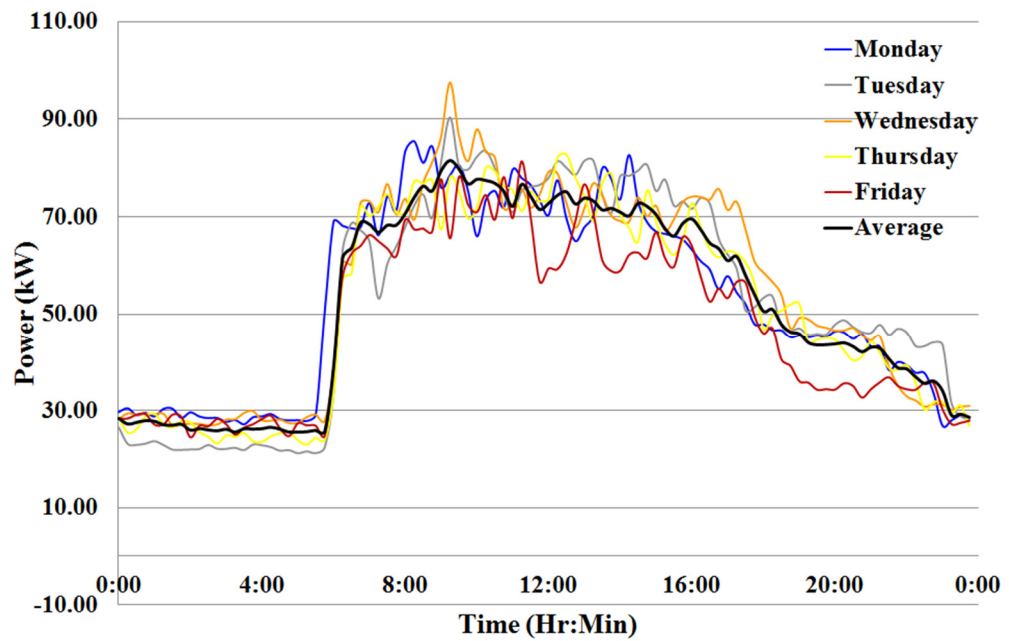


**Figure 4.2: Historical load profiles of KA block from Monday to Friday and its average load profile**

#### **4.3.2 Load Prediction for SE Block in Setapak campus**

One of the buildings located at Setapak campus, namely SE block, is chosen to evaluate the performance of the energy storage system. Figure 4.3 shows the single-line diagram of the electrical network for the SE block.

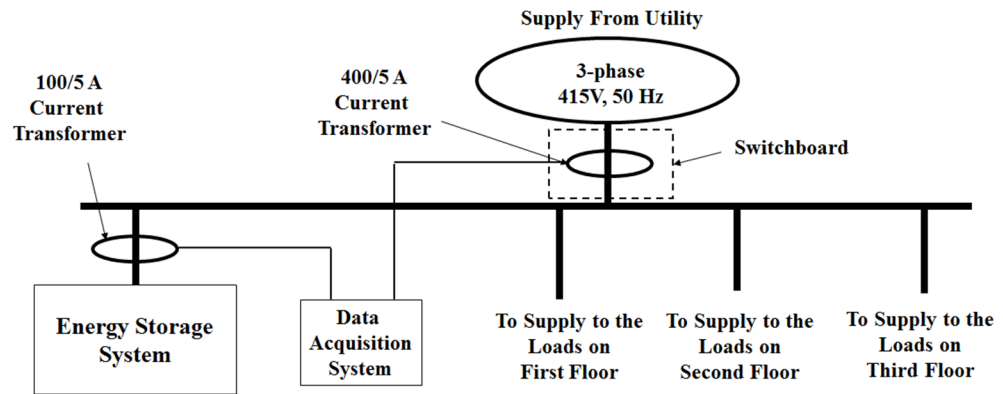


**Figure 4.3: Single-line diagram of the electrical network for the SE block**

Figure 4.4 shows the historical load profiles of the building over a period of five days, from Monday to Friday, and its average load profile. It is calculated that the MAPE of the predicted load profile is 24.7 %. The load profiles of this building have a higher fluctuation as compared to the load profiles of KA block. This is due to the fact that the power consumption is highly dependent on the occupancy of the laboratories. Hence, the average historical load profile approach is not suitable for predicting the load profile of this building which will result in a higher MAPE.

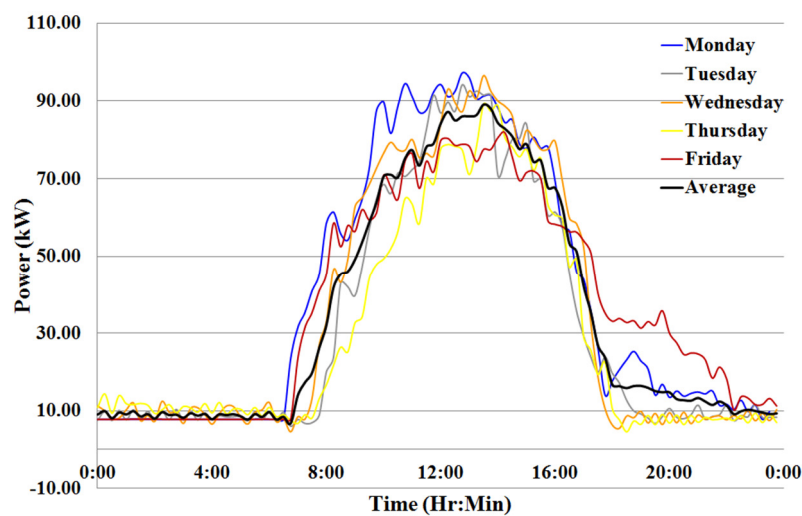


**Figure 4.4: Historical load profiles of SE block from Monday to Friday and its average load profile**

An alternative method is proposed to predict the load profile of this building. It is found that the occupancy of the venues can reflect the power consumption of the building. The power consumption of each venue ( $P_v$ ) can be expressed as follows:

$$P_v = \sum_{i=1}^n N_i A_i \quad (4.4)$$

where  $n$  is the number of venues,  $A$  is the power consumption of the electrical appliances and  $N$  is the number of the appliances. The total power consumption of each venue ( $P_{Tot}$ ) can be estimated by summing up the power consumed by all the electrical appliances in that venue as follows:

$$P_{Tot} = \sum_{i=1}^n P_{vi} \quad (4.5)$$

Table 4.1 shows the power consumption of each venue according to the power consumption of the electrical appliances. The load profile of SE block can be predicted by calculating the total power consumed by each venue based on the teaching schedule on a particular day.

**Table 4.1: Power consumption of each venue according to the power consumption of the electrical appliances**

Venue	Number of Electrical Appliances							Total (kW)
	A	B	C	D	E	F	G	
Small class room	2	0	12	2	1	1	0	5.15
Big class room	0	2	24	3	1	1	0	7.66
Computer laboratory	0	2	18	2	1	20	0	12.50
Electronic laboratory	0	4	30	0	0	15	3	20.13
Material laboratory	0	0	48	8	0	6	5	8.95
Thermodynamic laboratory	0	0	24	4	0	4	5	7.24
Office	2	0	12	0	0	1	0	4.70
Toilet	0	0	24	0	0	0	0	0.86
Corridor	0	0	78	0	0	0	0	2.81

Footnotes:

- A- Small air-con rated at 2 kW
- B- Big air-con rated at 3 kW
- C- Light rated at 0.036 kW
- D- Fan rated at 0.075 kW
- E- Projector rated at 0.3 kW
- F- Computer rated at 0.27 kW
- G- Miscellaneous rated at 1 kW

Figure 4.5 shows the actual daily load profile and predicted load profile of the building on 16<sup>th</sup> October 2014. It can be seen that the predicted load profile is very close to the actual profile.

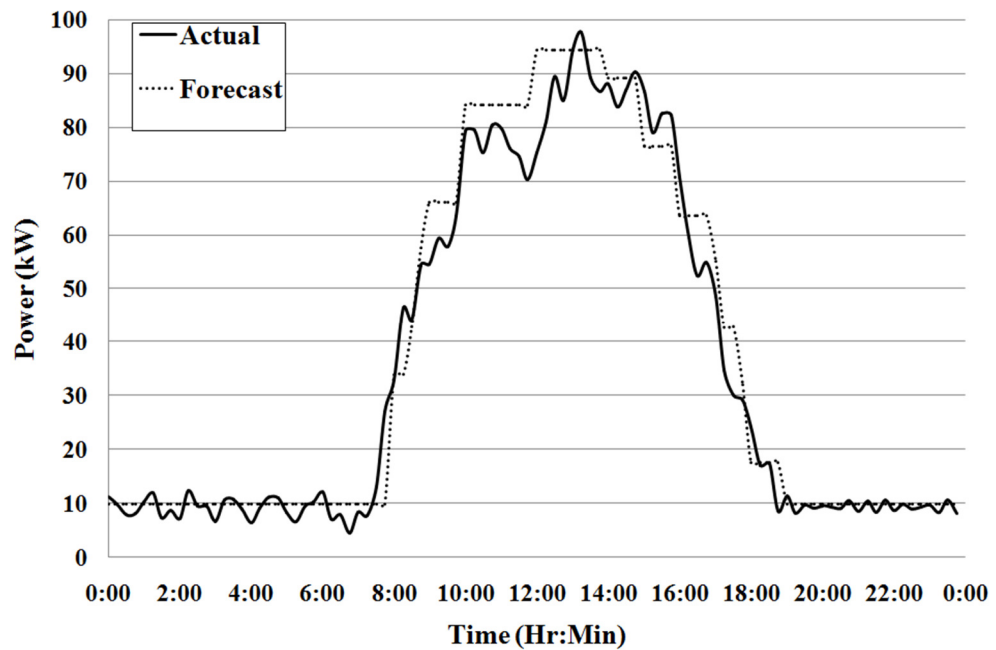


**Figure 4.5: Actual daily load profile and predicted load profile on 16<sup>th</sup> October 2014**

Figure 4.6 shows the absolute percentage errors (APE) of the predicted load profiles over a period of 40 days. It is found that the MAPE of the predicted load profile is 16.8%. This load prediction method is more accurate than the averaging the historical load profiles. Nevertheless, the performance of the load

prediction can be further improved by intelligent approaches which are beyond the scope of this research project.

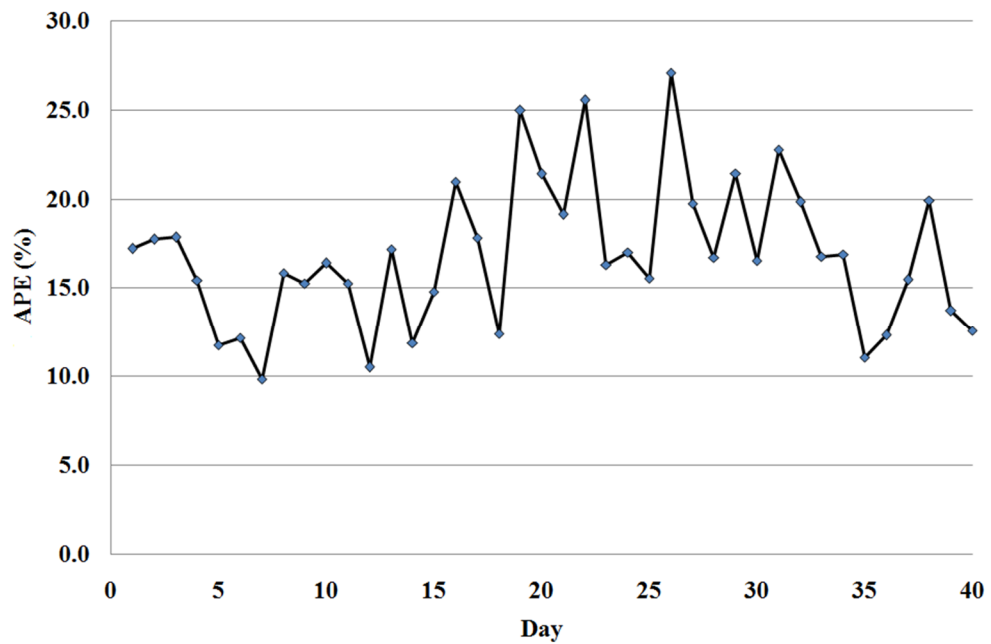


**Figure 4.6: APE of the predicted load demands**

#### 4.4 Fixed-threshold Control Algorithm

Fixed-threshold control algorithm is the most basic control strategy developed to control the energy storage system for peak reduction. The lower power threshold ( $P_{LTh}$ ) and upper-power thresholds ( $P_{UTh}$ ) are defined in the algorithm to control the operation of the energy storage system. As suggested by the name, the value of the upper power threshold is fixed using the forecasted load profiles for each day before the operation of the energy storage system. This control strategy is simple and easy to be implemented. Also, the response of the energy storage system to any incoming instruction is very fast. However, the success

of this controller for any peak reduction is very dependent on the accuracy of the forecasted load profiles.

Figure 4.7 shows an example of a daily load profile. The daily load profile can be categorised into three sections to reflect 3 different possible operations of the energy storage system, namely the charging, discharging and idle modes.

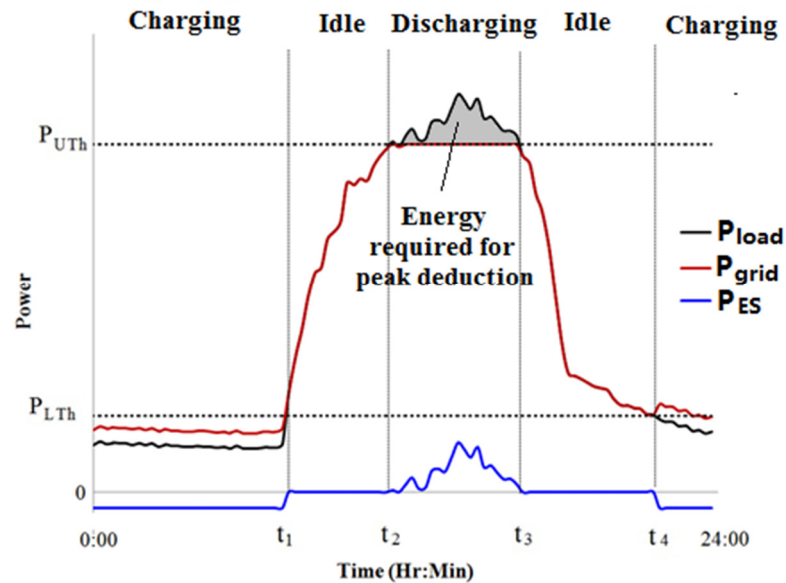


**Figure 4.7: Daily load profile and the desired response of the energy storage system**

The lower power threshold ( $P_{LTh}$ ) and an upper power threshold ( $P_{UTh}$ ) are set such that the energy storage system operates when the load demand falls within a certain range of the thresholds. During the period from 0:00 to  $t_1$  and  $t_4$  to 24:00,  $P_{load}(t)$  is lower than  $P_{LTh}$ . The energy storage system charges the batteries if it is not fully charged or stays in the idle mode if the batteries are fully charged. During the period from  $t_1$  to  $t_2$  and from  $t_3$  to  $t_4$ , the energy storage system stays idle because  $P_{load}(t)$  is in between  $P_{LTh}$  and  $P_{UTh}$ . During the period from  $t_2$  to  $t_3$ , the energy storage system delivers power to the load because

$P_{load}(t)$  is greater than  $P_{UTh}$ . The energy required to reduce the peak demands for each day can be determined by calculating the area under the graph between the load demand and  $P_{UTh}$  as illustrated in Figure 4.7.

During the discharging mode, the load demand is greater than  $P_{UTh}$ . The energy storage system begins to supply power to the load if the SOC is greater than 50%. This SOC value is the recommendation from the lead-acid batteries manufacturer to prevent the over-charging of the batteries in order to prolong the service life of the batteries. If the difference between  $P_{load}(t)$  and  $P_{UTh}$  is less than the rated power of the energy storage system ( $P_{ESmax}$ ), then the energy storage system will inject power with the magnitude being the same as  $P_{load}(t)$  minus  $P_{UTh}$  as shown in the following equation:

$$P_{ES}(t) = P_{load}(t) - P_{UTh} \quad (4.6)$$

If the difference between  $P_{load}(t)$  and  $P_{UTh}$  is greater than the rating  $P_{ESmax}$ , then the energy storage system will inject its nominal power to the load as follows:

$$P_{ES}(t) = P_{ESmax} \quad (4.7)$$

If the SOC is equal to or less than 50%, then the power converter will stop injecting power to the load.

During the charging mode, the energy storage system starts to charge the batteries when the actual load demand is lower than  $P_{LTh}$  in order to restore the batteries' energy for the next day of peak reductions. If the state-of-charge (SOC) of the batteries is less than 90%, then the batteries will be charged at moderate rate of 6 kW. If the SOC is greater than or equal to 90 %, then the battery is charged at a low rate of  $3*[0.7 \ln(t) - 2]$  kW. These charging rate

expressions are chosen from the battery converter handbook with a view to prevent the overcharging of the batteries and to prolong the service life of the batteries.

In the idle mode, there is no power flow between the load and the power converters because the energy storage system should output zero power as follows:

$$P_{ES}(t) = 0 \quad (4.8)$$

The flow chart of the fixed-threshold control algorithm is illustrated in Figure 4.8.

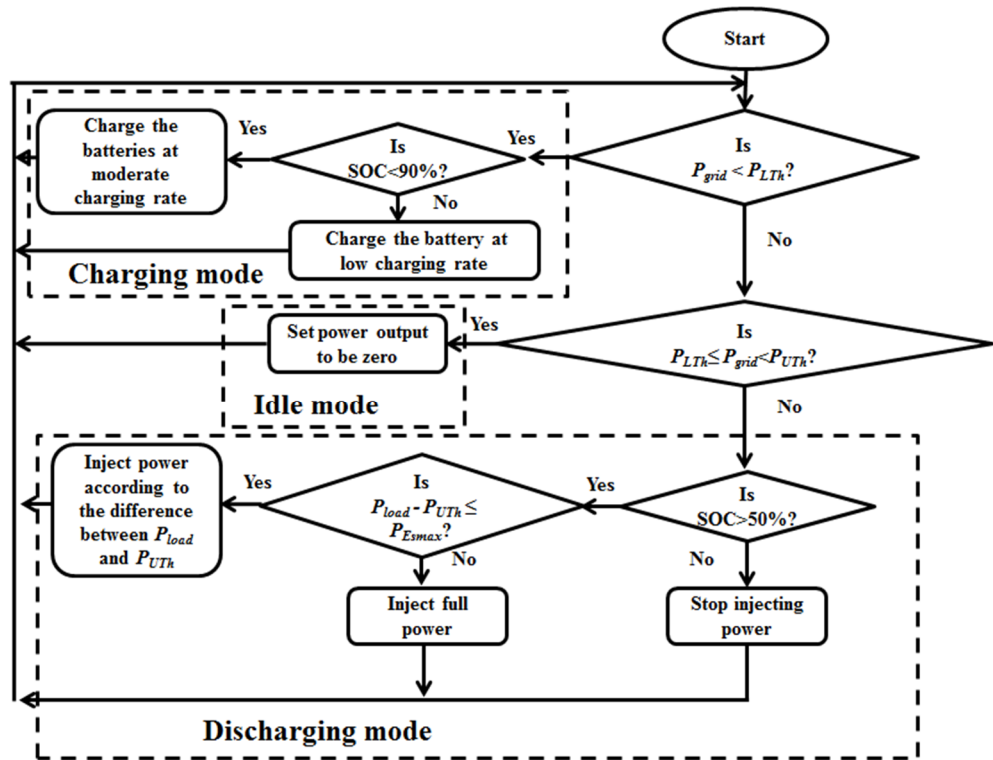


Figure 4.8: Flow chart of the fixed-threshold control algorithm



## 4.5 Adaptive-threshold Control Algorithm

Adaptive-threshold controller is an improved version of the fixed-threshold controller because the output power of the energy storage system can be reduced to preserve the energy of the batteries when the actual peak demands occur for an extended period of time. The operation of the charging and idle modes of the adaptive-threshold control algorithm are the same as that of the fixed-threshold control algorithm except for the operation of the discharging mode.

During the discharging mode, if the difference between  $P_{load}(t)$  and  $P_{UTh}$  is greater than  $P_{ESmax}$  within a specific duration of time ( $N$ ) in minutes, then the high load demand is considered as temporary. The energy storage system will inject its nominal power of  $P_{ESmax}$ . When the difference between  $P_{load}(t)$  and  $P_{UTh}$  is greater than  $P_{ESmax}$  for more than  $N$  minutes, the high load demands is no longer temporary. Hence, the new upper threshold ( $P_{UTh'}$ ) will be moved to a new value based on the following equation:

$$P_{UTh'} = P_{load}(t) - P_{ESmax} \quad (4.9)$$

The adaptive feature enables the ESS to deliver power to the load over the longest possible period. The flow chart of the adaptive-threshold control algorithm for peak reductions is illustrated in Figure 4.9.

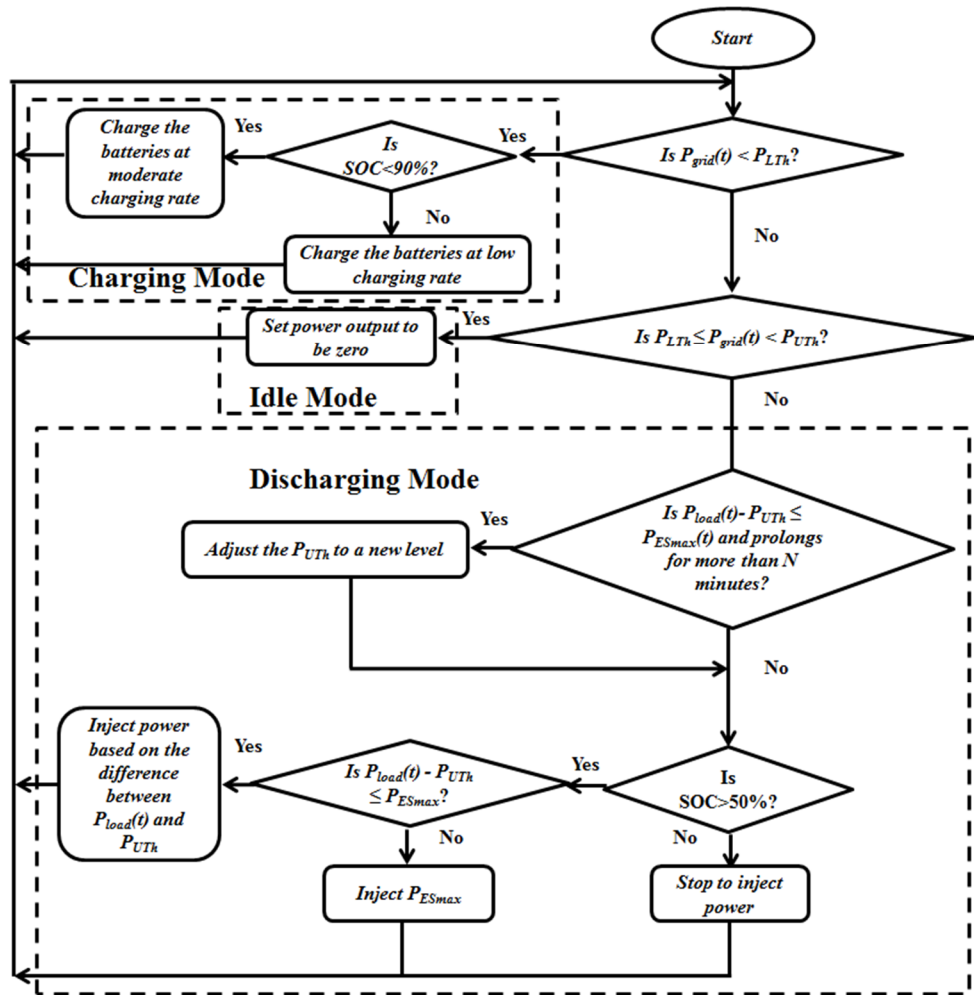


Figure 4.9: Flow chart of the adaptive-threshold control algorithm

#### 4.6 Software Implementation

The measurements and control of the energy storage system are implemented using LabVIEW software. Two project explorers are established in LabVIEW for each building under investigation because there is some deviation in data acquisition system for the two buildings.

#### **4.6.1 Introduction to LabVIEW**

LabVIEW (Laboratory Virtual Instrumentation Engineering Workbench) is a development platform for a visual programming language from National Instruments. LabVIEW offers unrivalled integration with many hardware devices and provides hundreds of built-in libraries for advanced analysis and data visualization. In general-purpose programming languages, the code is as much of a concern as the application. The users must pay close attention to the syntax such as commas, periods, semicolons, square brackets, curly brackets, and round brackets. In contrast, LabVIEW uses icons to represent functions, and the users can wire them together to determine the flow of data through a program, similar to creating flowcharts. The programming language used in LabVIEW is a data flow programming language. The execution of the code is determined by the structure of a graphical block diagram on which the different function nodes are connected by drawing wires. These wires propagate variables and any node can be executed immediately when it receives the input data. The users can easily divide measurement and automation application into three main parts: acquisition, analysis, and presentation of data.

LabVIEW provides a platform to acquire data, perform necessary analysis on that data, and present the information in a chosen format. Each program in LabVIEW is called a virtual instrument (VI). The VI serves as the primary building block of a LabVIEW, and the programming code can be modularized into a subVI for efficient design, concise documentation, and simplified

maintenance. Each LabVIEW VI is made up of three main components, namely the front panel, block diagram, icon and connector pane as shown in Figure 4.10.

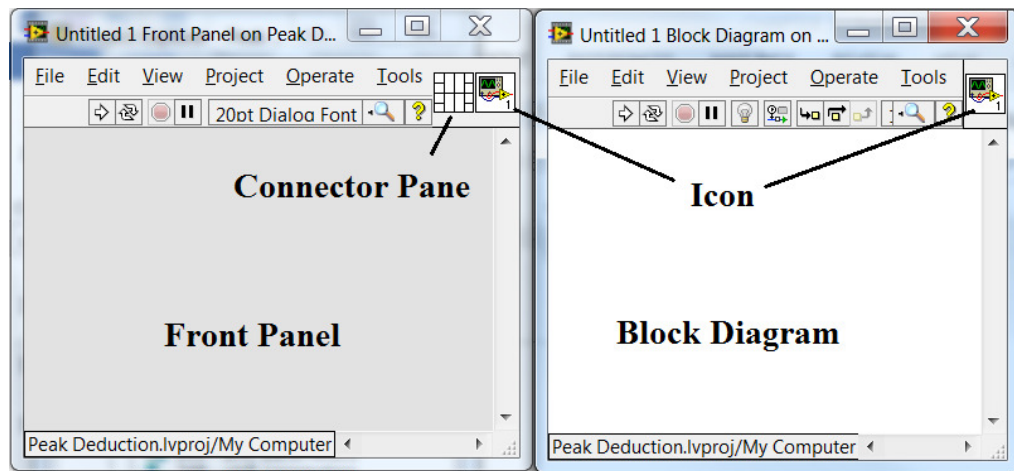


**Figure 4.10: Front panel, block diagram, icon and connector pane in a VI**

The front panel is a platform for the users to interact with the VI. The users can add code using graphical representations of functions such as switches, push buttons, and charts to control and monitor the front panel objects. The front panel provides a platform for the users to control the program, change inputs, and see data updated in real time. Every front panel control or indicator has a corresponding terminal on the block diagram. When a VI is executed, values from front panel controls flow through the block diagram, where they are used in the functions on the diagram, and the results are passed to other functions or indicators through wires.

Block diagram contains codes that control the program. In some way, the block diagram resembles a flowchart of the program. The block diagram toolbar is very similar to the front panel with a few extra features such as highlight execution, clean up feature, function palette, and terminal. Highlight Execution

allows the users to slow down code execution and displays beads on the wires as data flows through them. Output values are also displayed in small boxes. The users can use highlight execution for debugging the codes. Function palette is available only on the block diagram. It contains the VIs and functions that can perform mathematical operations, signal processing, and interface with other instruments. Terminals are the connection between the block diagram and front panel objects.

Icon and connector pane provide a path for connecting a VI to other VIs and the graphical representation of the VI. Icon and connector pane correspond to function prototype in text-based programming languages. VI can be used as a subVI by building a connection in the icon and connector pane. A VI icon is a graphical representation of a VI that contains text, images, or a combination of both. The connector pane is a set of terminals that corresponds to the controls and indicators of the VI. The connector pane defines the inputs and outputs that can be wired to receive data at its input terminals and passes the data to the block diagram code through the front panel controls and receives the results at its output terminals from the front panel indicators.

#### **4.6.2 Project Explorer for the Energy Storage System in SE Block**

A project explorer is created in LabVIEW for the energy storage system that is installed at the SE block. The project explorer provides a tree-driven list of VI and libraries to keep the project organized. It allows the users to create an

executable application where the target doesn't need to have LabVIEW installed on their computers. The project explorer also allows the users to create a web service or a shared library such that it can be accessed via the internet. Figure 4.11 shows the organization of the project explorer for the energy storage system at SE block. The VIs are categorized into data acquisition and control group under NI-sbRIO9632. There are 3 VIs for data acquisition, 4 VIs for control, and 2 are the custom control files. The custom control files are saved in the format "ctl" to define the similar control on different VIs. It enables the users to change the control when it is necessary and maintain consistency between different control instances.

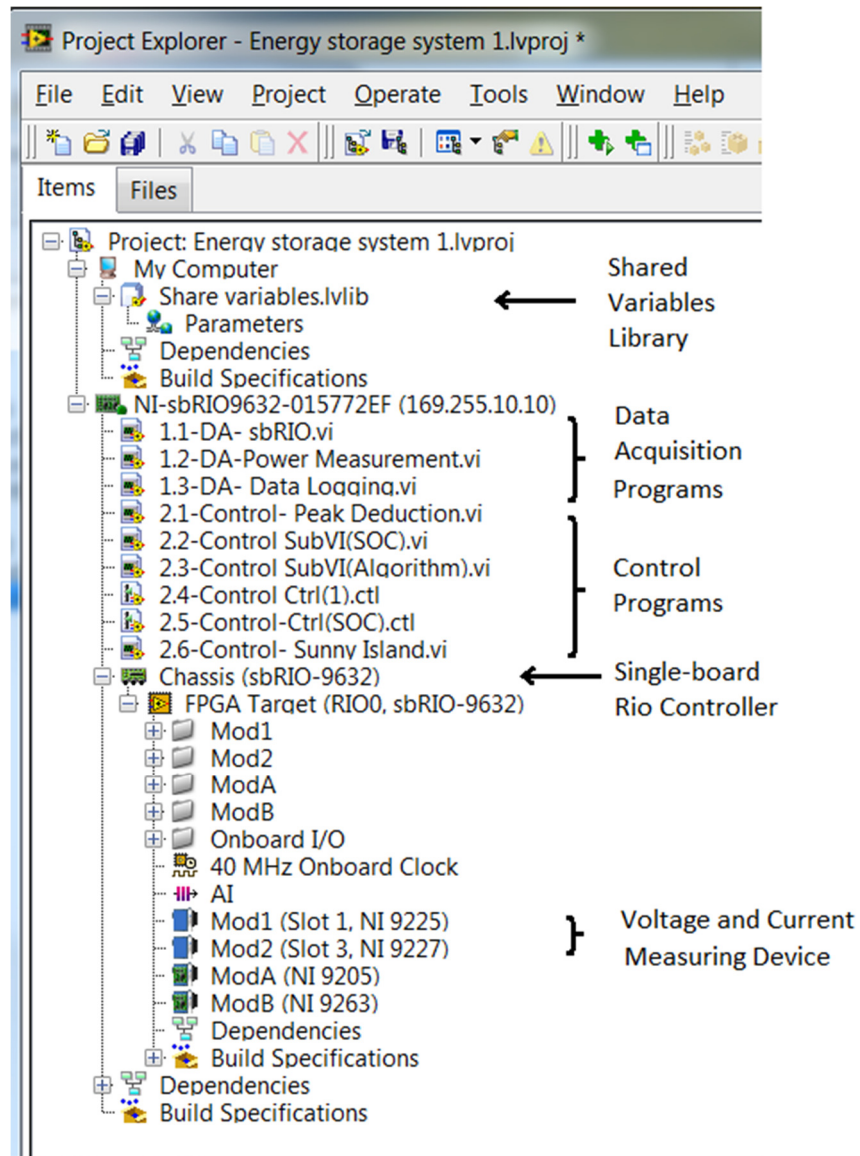
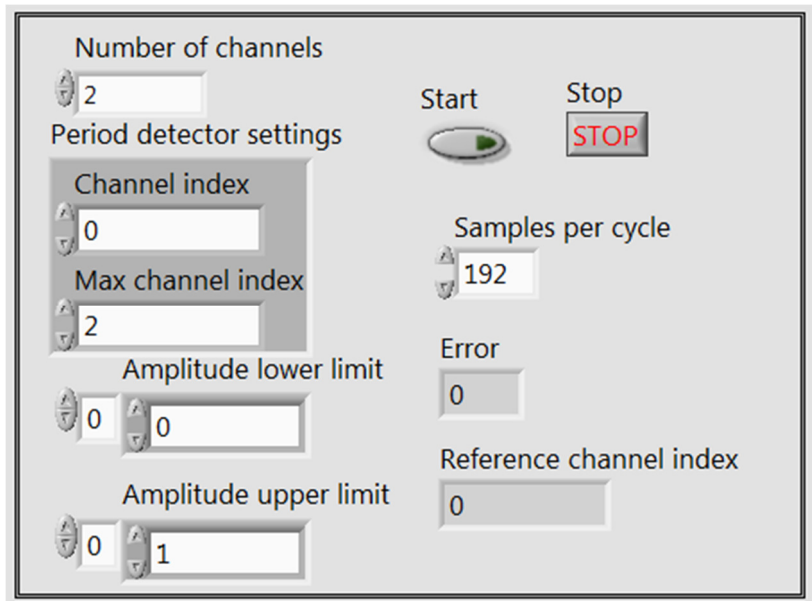


**Figure 4.11: Organization of project explorer for the energy storage system at SE block**

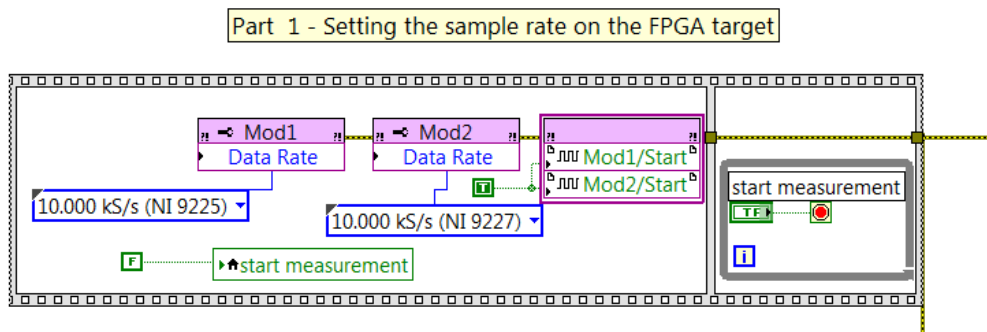
### 4.6.3 Data Acquisition Programs

There is a total of 3 VIs created for the data acquisition system. The VI entitled ‘1.1- DA- sbRIO.vi’ is established to set up the fundamental parameters for data acquisition from the single-board RIO controller. Figure 4.12 (a) shows the front

panel of '1.1- DA- sbRIO.vi' while Figure 4.12 (b), (c) and (d) show the block diagram of '1.1- DA- sbRIO.vi'. The block diagram of the '1.1- DA- sbRIO.vi' is categorised into 4 parts. Part 1 is used to set the sampling rate of the FPGA target. The data rate for voltage module (NI9225) and current module (NI9227) is set at 10 kilo-sample (kS) per second. Part 2 functions to acquire signals from the designated address for the voltage and current modules. Part 3 reads and samples the designated signals according to the sampling rate. Part 4 writes the sampled signals into the FPGA target and allows the users to retrieve the signals from other VIs.



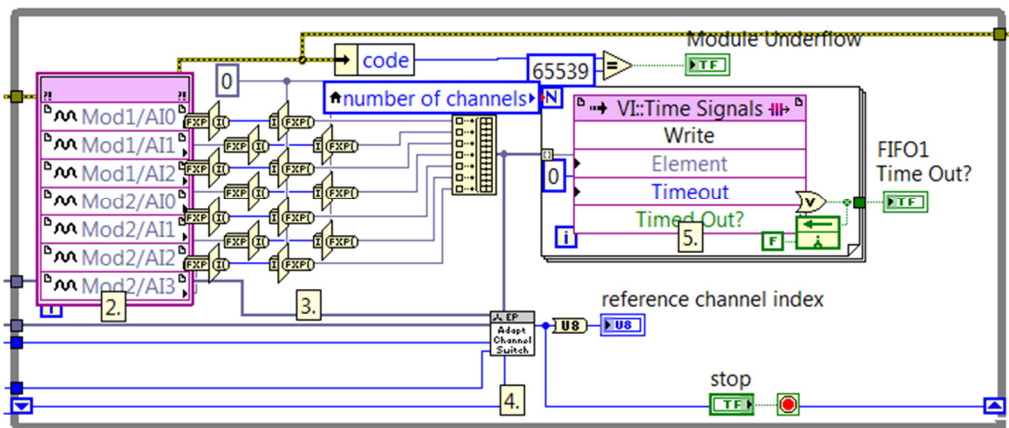
(a)



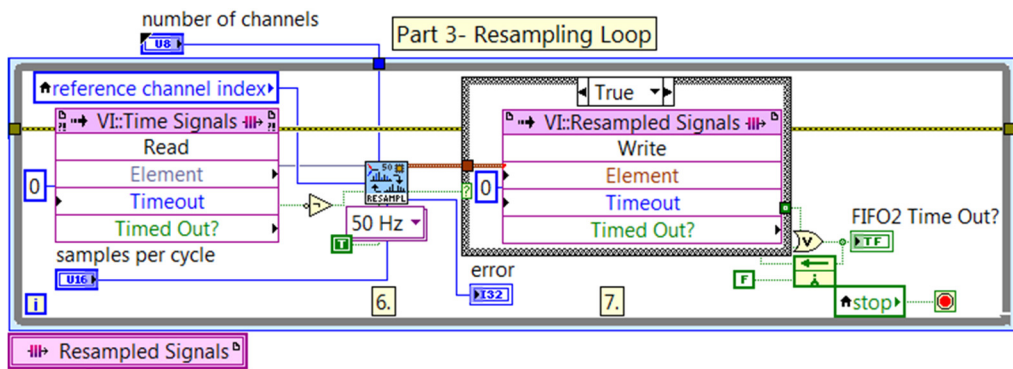
(b)



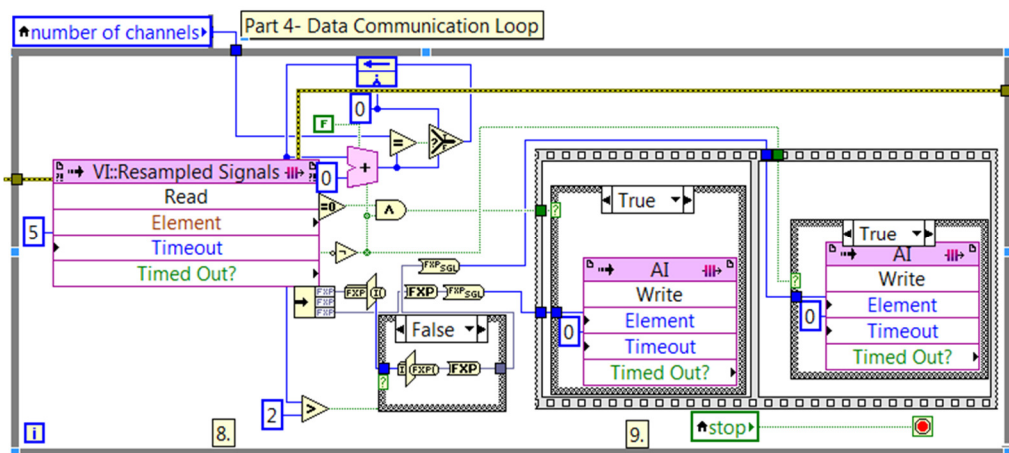
Part 2 - Data Acquisition



(c)



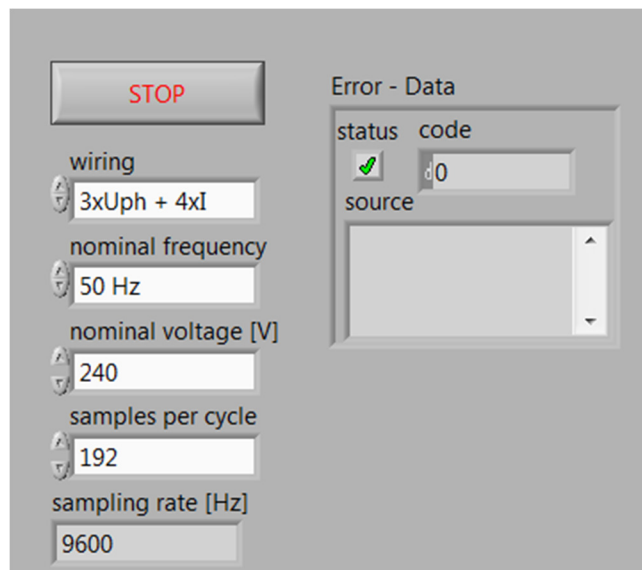
(d)



(e)

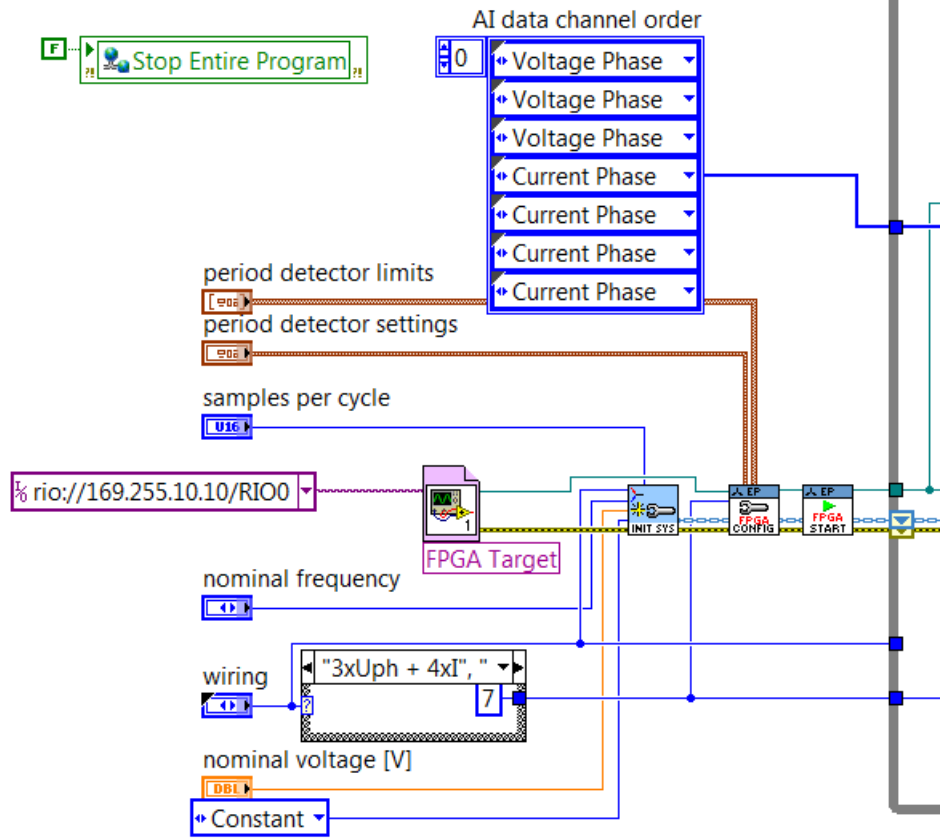
Figure 4.12: '1.1- DA- sbRIO.vi' (a) Front panel (b) part 1 (c) part 2 (d) part 3 and (e) part 4 of the block diagram

The VI entitled '1.2- DA- Power measurement.vi' is developed to acquire the basic electrical parameters such as voltage, current, frequency, and power. Figure 4.13 (a) shows the front panel of '1.2- DA- Power measurement.vi'. Figure 4.13 (b), (c), and (d) show the block diagram of '1.2- DA- Power measurement.vi'. The block diagram is categorised into 2 parts, namely the initialization and the acquisition of fundamental power parameters.

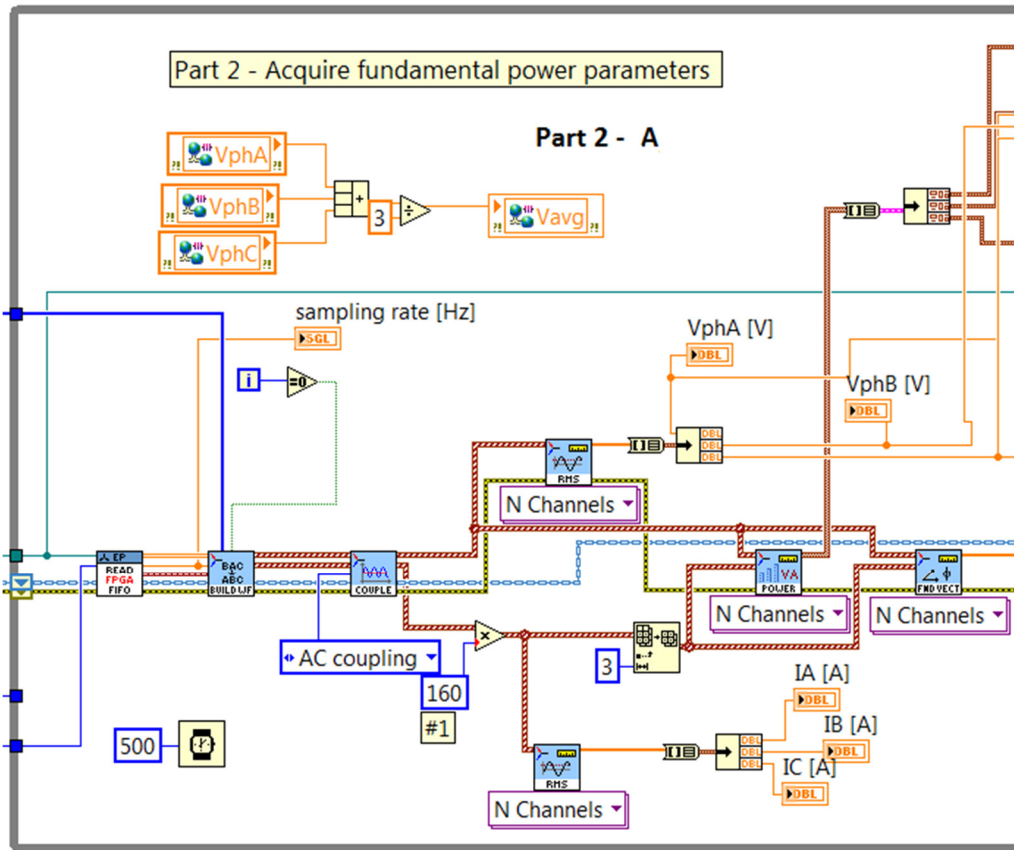


(a)

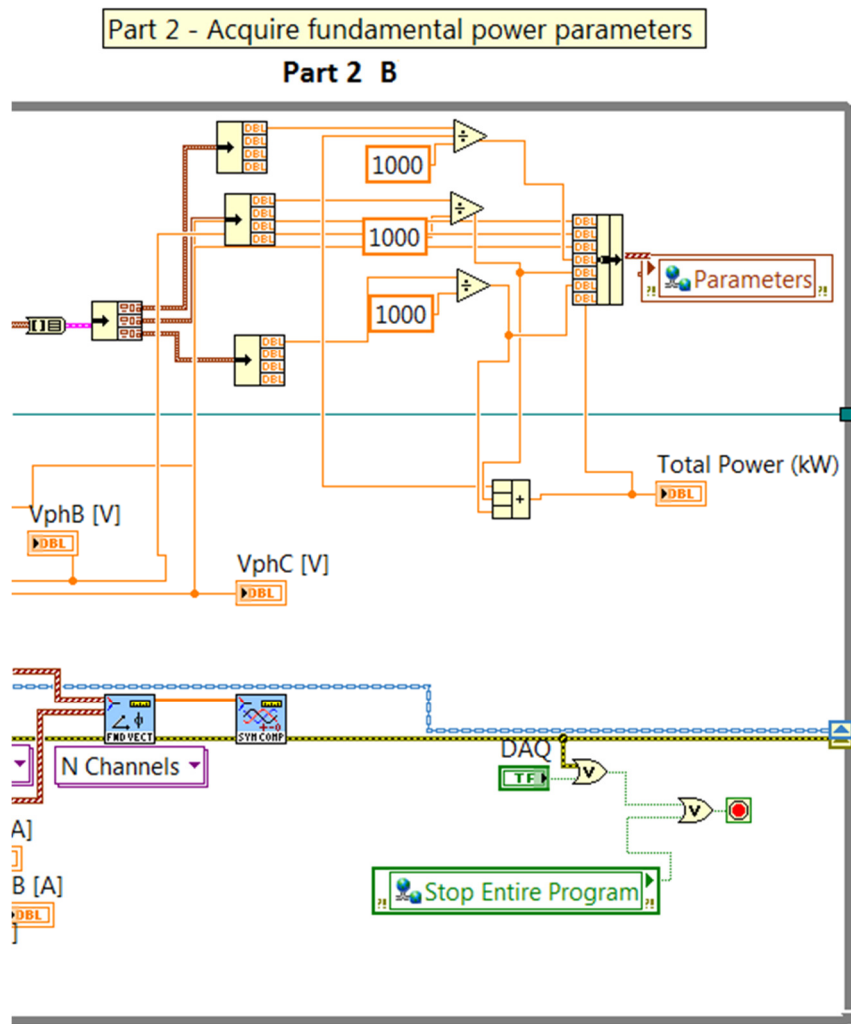
Part 1 - Initialization



(b)



(c)



(d)

**Figure 4.13: ‘1.2- DA- Power measurement.vi’ (a) Front panel (b) initialization (c) acquisition of fundamental power parameters (part 2A), and (d) acquisition of fundamental power parameters (part 2B)**

Part 1 represents an initialization to initialize the data channel, period detector settings, sample per cycle, nominal frequency, wiring topology, and nominal voltage. After the initialization, the data enters the main loop in part 2. Part 2 functions to acquire the fundamental electrical parameters such as voltage, current, frequency, active power, reactive power, and apparent power. All the parameters are bundled together as “Parameters” and shared in the library

established in the project explorer so that these parameters can be used for other VIs.

The VI entitled '1.3-DA- Data Logging.vi' is developed to create a database to store the data collected from the power meters and Sunny Island converters. Figure 4.14 shows the block diagram of '1.3-DA- Data Logging.vi'. There are three main parts in this VI to create a folders and a daily file. The codes are created in the flat sequence structure so that the execution of the codes will always begin by creating a daily file. In part 1, a daily file is created in the designated file's name of 'day/month/year' that is represented by '%d%b%y'. Part 1.1 allows the users to decide the interval of the data to be recorded. The users can choose to record the data in the interval of 30 seconds, 1 minute, 5 minutes, 10 minutes, 15 minutes, and 30 minutes. Part 2 allows the users to categorise the daily data by the dates and locate these data into a monthly folder. Part 3 allows the users to create a data file in TDMS format. TDMS stands for Test Data Exchange Stream that organizes data in a three-level hierarchy of objects. The top level consists of a single object that contains file-specific information such as author or title. The second level consists of the path object that includes the name of the object and the name of its owner in the TDMS hierarchy. The third level consists of a file object that contains the measured data.

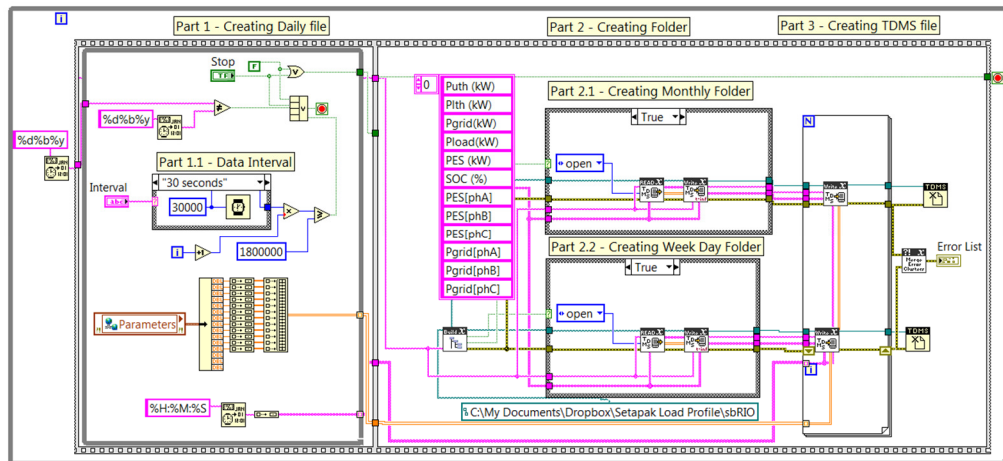
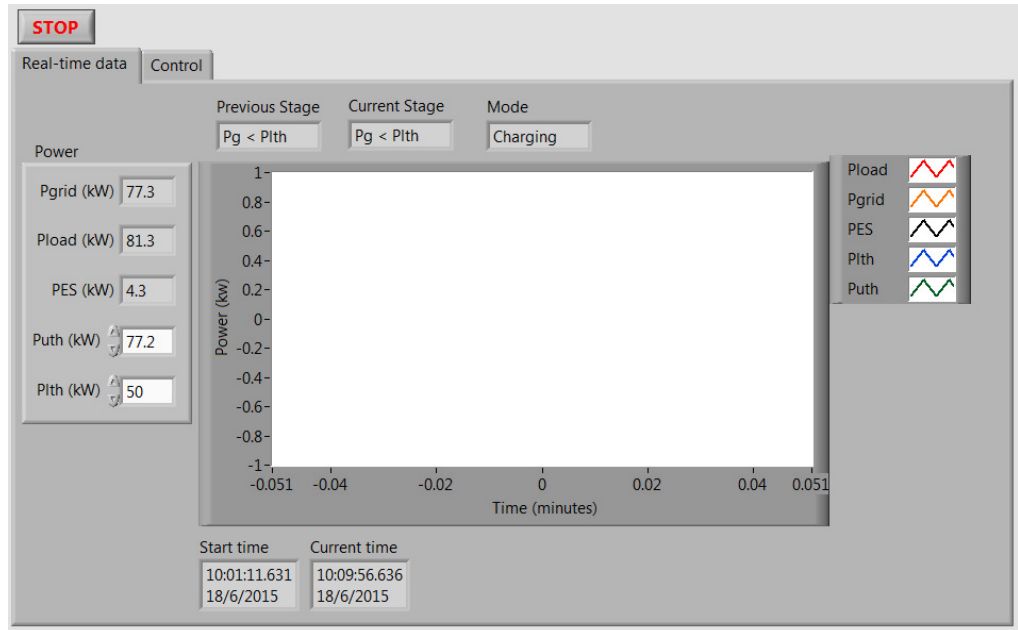


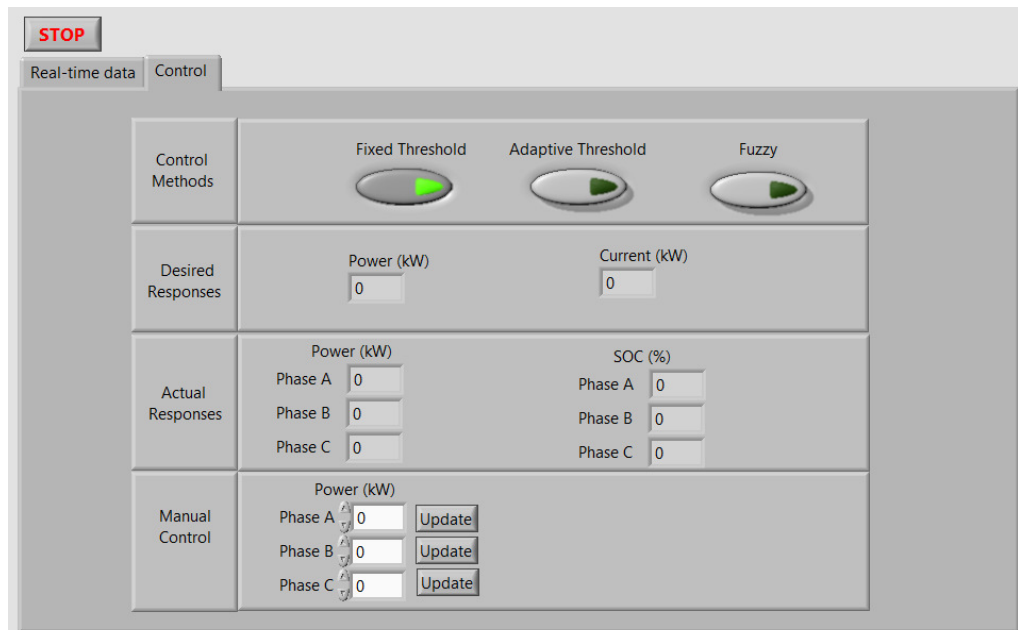
**Figure 4.14: Block diagram of ‘1.3-DA- Data Logging.vi’**

#### **4.6.4 Implementation of the Control Algorithms**

There are 4 VIs and 2 custom control files developed for the control algorithms of the energy storage system. The VI entitled ‘2.1-Control- Peak Reduction.vi’ is developed to mitigate the peak demands. Figure 4.15 (a) shows the real-time data tab and Figure 4.15 (b) shows the control tab for the front panel of ‘2.1-Control- Peak Reduction.vi’. The two tabs are created to keep the user interface tidy and easy to read.



(a)



(b)

**Figure 4.15: Front panel of '2.1-Control- Peak Reduction.vi' (a) Real-time data tab and (b) control tab**

In the real-time data tab, the power parameters are displayed in both values and charts. The previous and current stage indicate the operating stage of the energy



storage system. There are four parts in the control tab, namely the control methods, desired responses, actual responses, and manual control. There are three control algorithms, namely the fixed-threshold, adaptive-threshold, and fuzzy-based control algorithms. The desired responses of the energy storage system are determined based on the control method chosen. The actual power and SOC of the energy storage system are shown in actual responses tab. The manual control allows the users to manually control the power flow of the Sunny Island converters.

The control strategies are developed in the block diagram of the VI entitled ‘2.1-Control- Peak Reduction.vi’. The first part is the data acquisition as shown in Figure 4.16. The data collected from the meters and converters are sorted using the functional block 1 and block 2 to obtain the designated parameters.

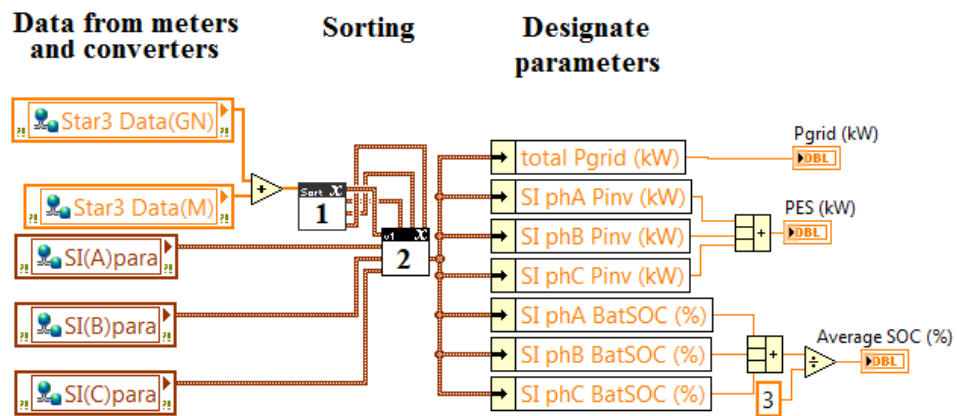


**Figure 4.16: Block diagram of ‘2.1-Control- Peak Reduction.vi’**

The control strategies are developed in the control subVI entitled ‘2.3-Control-SubVI (Algorithm).vi’. The connection of the subVI is shown in Figure 4.17. There are 12 inputs and 7 outputs that are linked to the main VI.

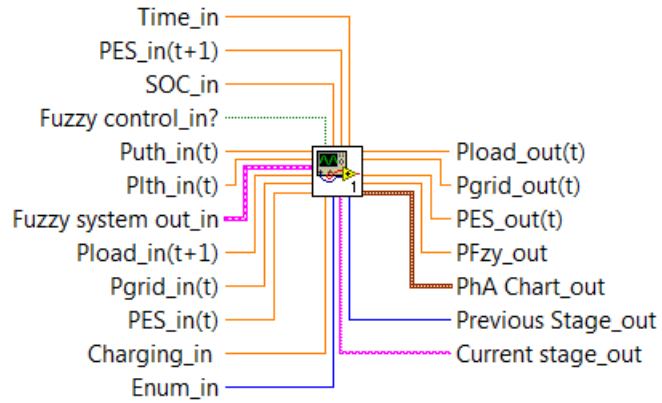
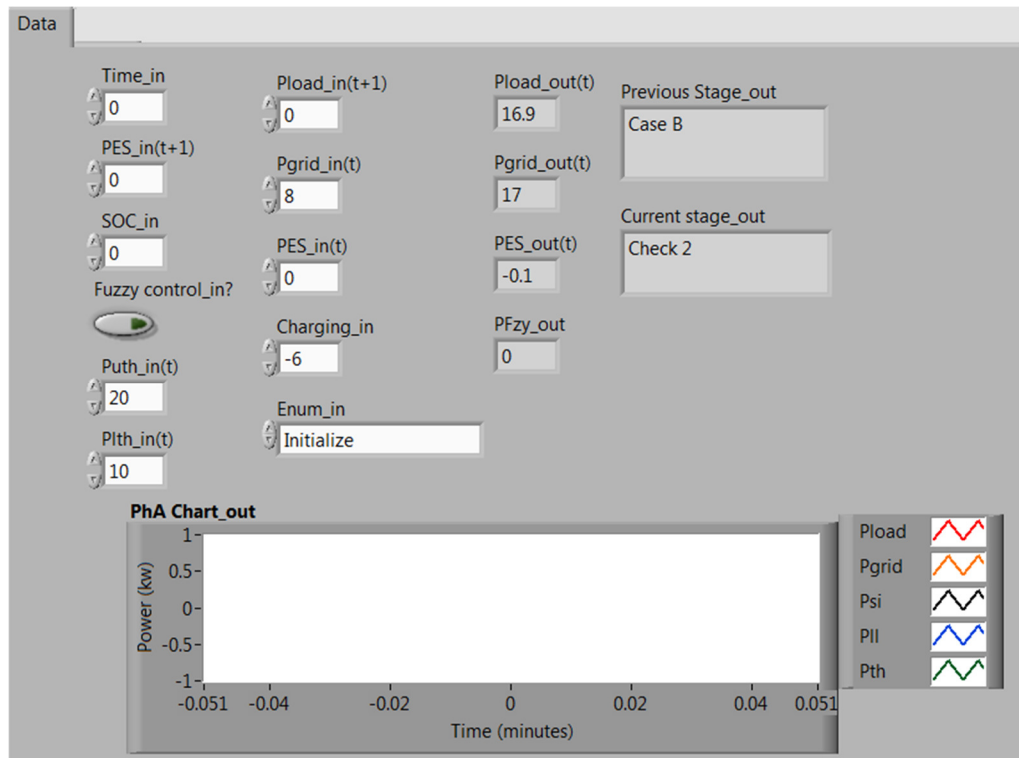
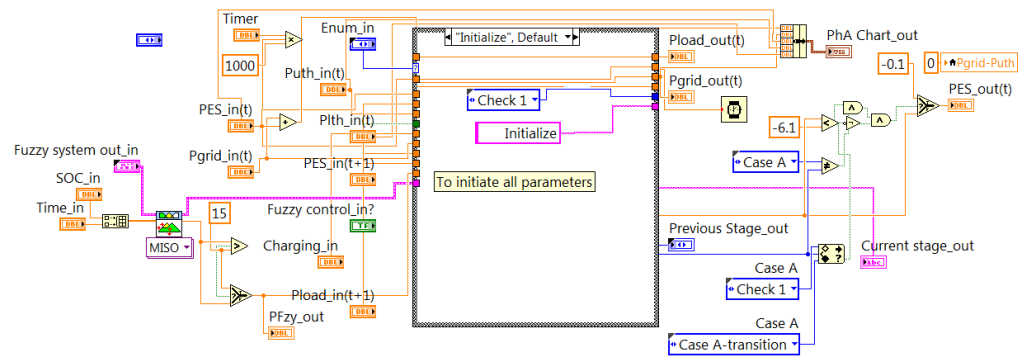


**Figure 4.17: Connection of ‘2.3-Control- SubVI (Algorithm).vi’**

The state machine architecture is chosen to establish the control algorithm. The state machine architecture is formed by a while loop and case structure. The while loop is the main program loop that executes the codes until the conditions stated by the users are met. The case structure is a method of executing conditional loop. In ‘2.3-Control- SubVI (Algorithm).vi’, there are 13 cases created in the state machine. Figure 4.18 (a) and (b) show the front panel and block diagram of the control ‘2.3-Control- SubVI (Algorithm).vi’. The program begins with Initialize case to initialize all the input parameters.



(a)

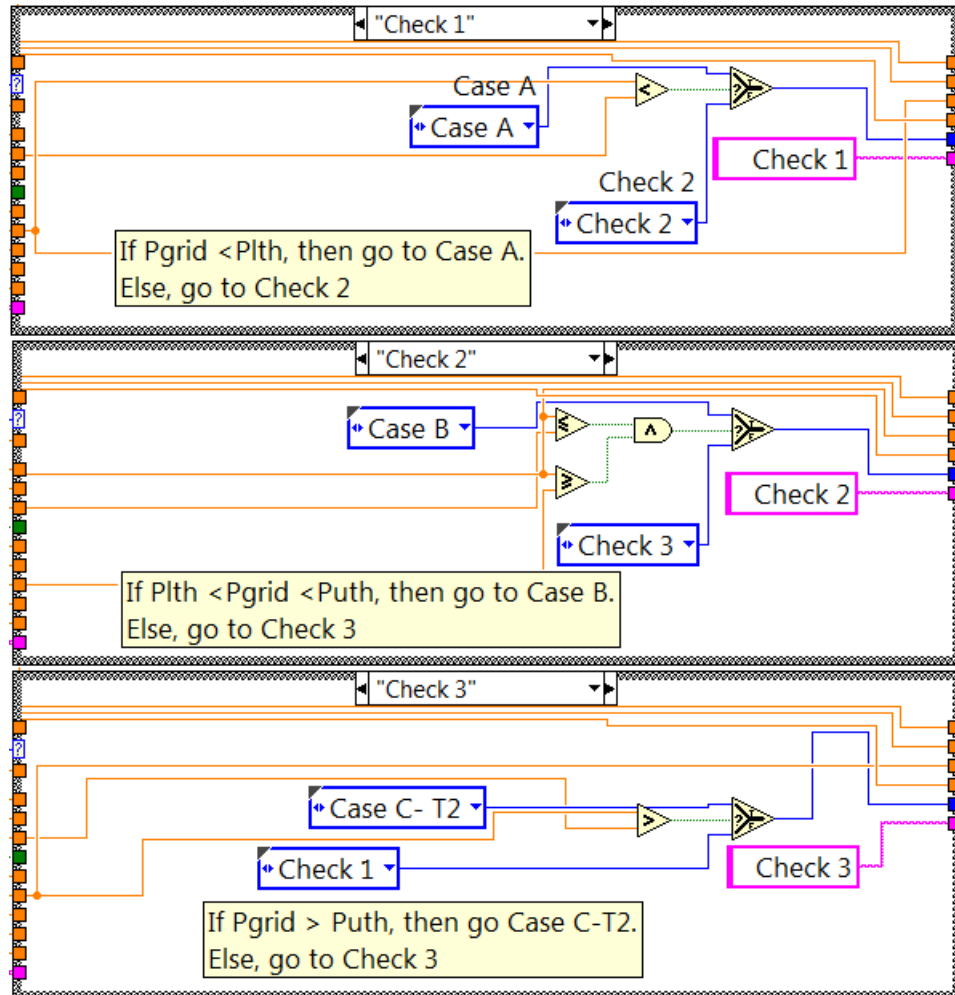


(b)

**Figure 4.18: ‘2.3-Control- SubVI (Algorithm).vi’ (a) Front panel and (b) block diagram**

After the execution of Initialize case, the program moves to the case entitled Check 1. In Check 1, the  $P_{grid}$  is compared with  $P_{LTh}$ . If  $P_{grid}$  is less than  $P_{LTh}$ , then the program will move on to Case A. Otherwise, it will go to Check 2. In Check 2, the  $P_{grid}$  is compared with the  $P_{LTh}$  and  $P_{UTh}$ . If  $P_{LTh} \leq P_{grid} < P_{UTh}$ ,

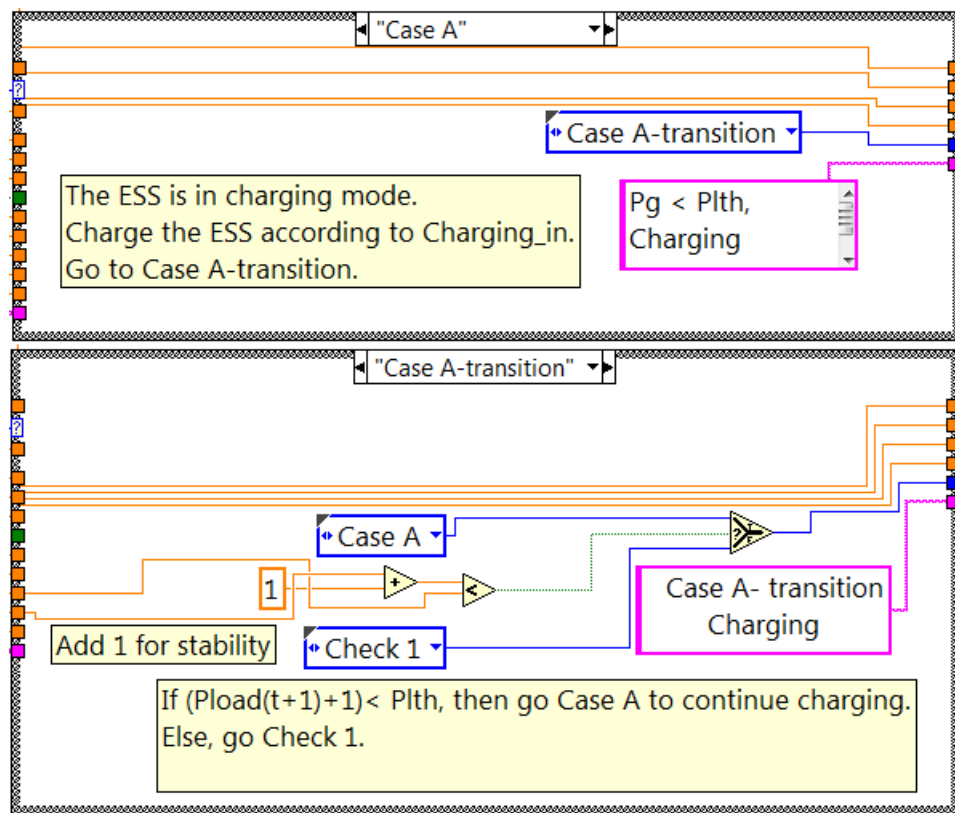
then it will move on to Case B. Otherwise, it will move on to Check 3. In Check 3,  $P_{grid}$  is compared with  $P_{UTh}$ . If  $P_{grid}$  is greater than  $P_{UTh}$ , then the program will move on to Case C-T2. Otherwise, it will move on to Check 1. Figure 4.19 shows the block diagram of Check 1, Check 2, and Check 3.



**Figure 4.19: Block diagram of Check 1, Check 2, and Check 3**

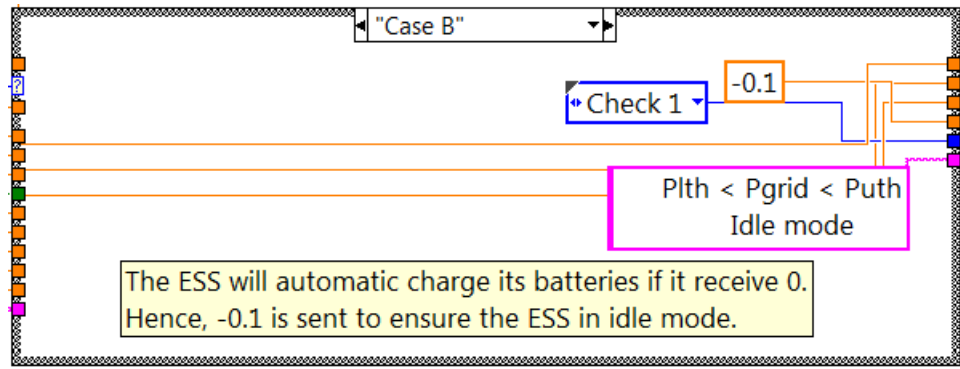
Case A represents the charging operation of the energy storage system. In this case, the energy storage system is charged according to the designated value from the Charging\_in input. The program continues to move on to Case A-transition. In Case A-transition, if  $(P_{Load}(t+1) + 1)$  is less than  $P_{LTh}(t)$ , then the program will move on to Case A to continue the charging process. Otherwise,

it will go to Check 1 and repeat the checking process. Figure 4.20 shows the block diagram of Case A and Case A-transition.



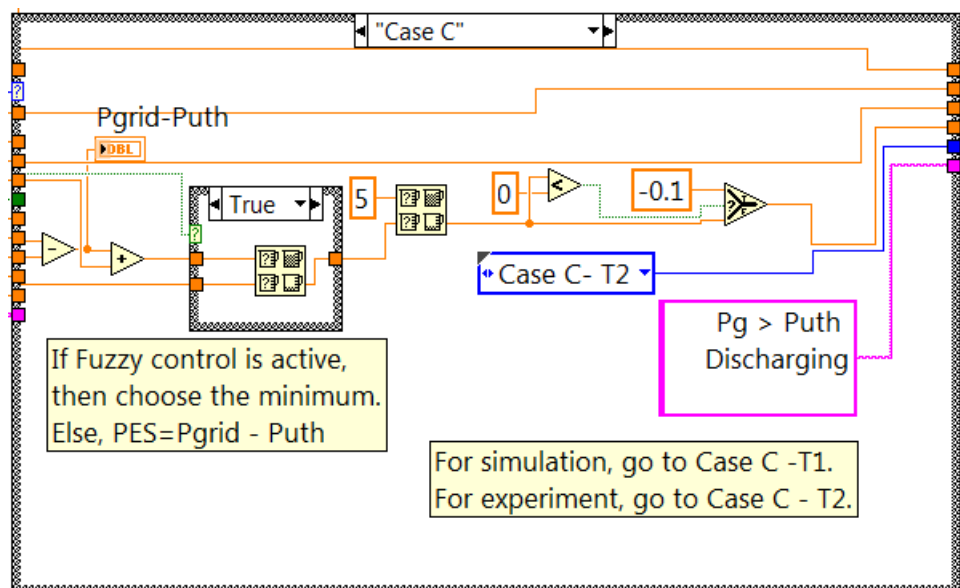
**Figure 4.20: Block diagram of Case A and Case A-transition**

In Case B, the energy storage system is in the idle mode where  $P_{LTh} \leq P_{grid} < P_{UTh}$ . In this case, the output power designated for the energy storage system is -0.1 kW. This is due to the fact that by default the energy storage system will automatically charge the batteries when it receives zero value. The output power of -0.1 kW is to ensure that the energy storage system is charged at a very low rate and does not charge its batteries based on the default value. The program continues to proceed to Check 1 and repeats the checking process. Figure 4.21 shows the block diagram of Case B.



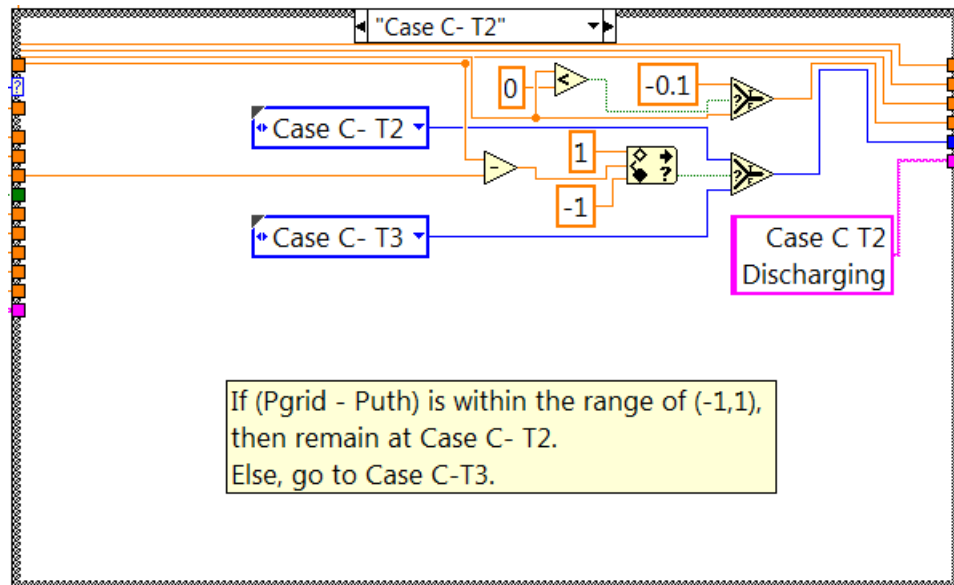
**Figure 4.21: Block diagram of Case B**

In Case C,  $P_{grid}$  is greater or equal to  $P_{UTh}$ . Firstly, the status of the Fuzzy control\_in input will be checked. If the status is active, then it means that the fuzzy-based control algorithm is chosen and the  $P_{ES}$  will be determined based on the lowest value between  $(P_{grid} - P_{UTh})$  and  $P_{Fzy\_out}$ . This is due to the fact the fuzzy-based control algorithm may reduce the power injection according to the available energy in the batteries. Hence, the value of the  $P_{ES}$  could be lower than  $(P_{grid} - P_{UTh})$ . If the Fuzzy control\_in is inactive, then the  $P_{ES}$  will be based on the value of  $(P_{grid} - P_{UTh})$ . Figure 4.22 shows the block diagram of Case C.



**Figure 4.22: Block diagram of Case C**

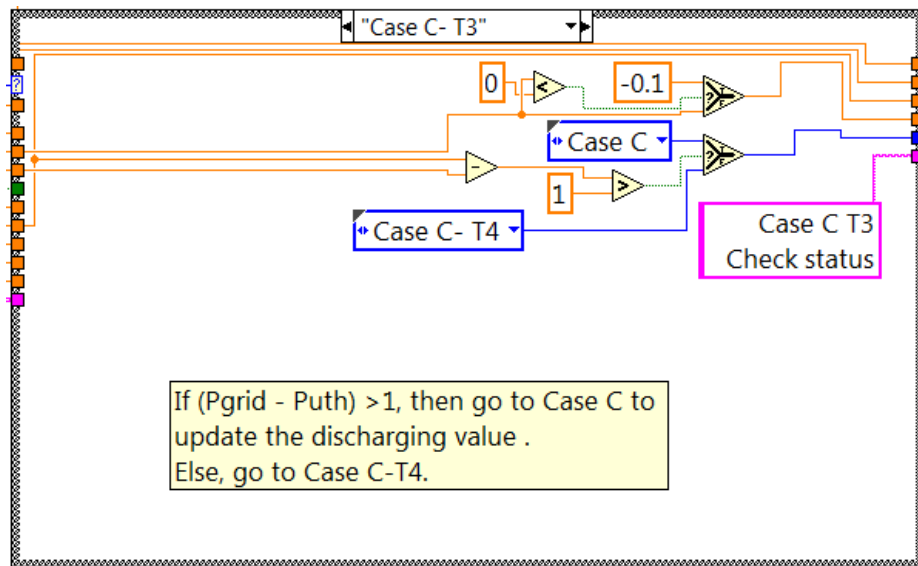
After the execution of Case C, the program will move on to Case C-T2. In Case C-T2, if  $(P_{grid} - P_{UTh})$  is within the range of -1 kW to 1 kW, then the program will continue to loop Case C-T2. If  $(P_{grid} - P_{UTh})$  is not within the range of -1 kW to 1 kW, then it will move on to Case C-T3. The range of -1 kW to 1 kW is set to accommodate the small load fluctuation within 1 kW and to ensure the stability of the energy storage system operation. If the range is set to zero, the energy storage system will continue to vary their power output from time to time because the load demand is fluctuating at all time. As long as the magnitude of  $(P_{grid} - P_{UTh})$  is within 1 kW, the energy storage system will continue to deliver the same amount of power to the load. Figure 4.23 shows the block diagram of the Case C-T2.



**Figure 4.23: Block diagram of Case C-T2**

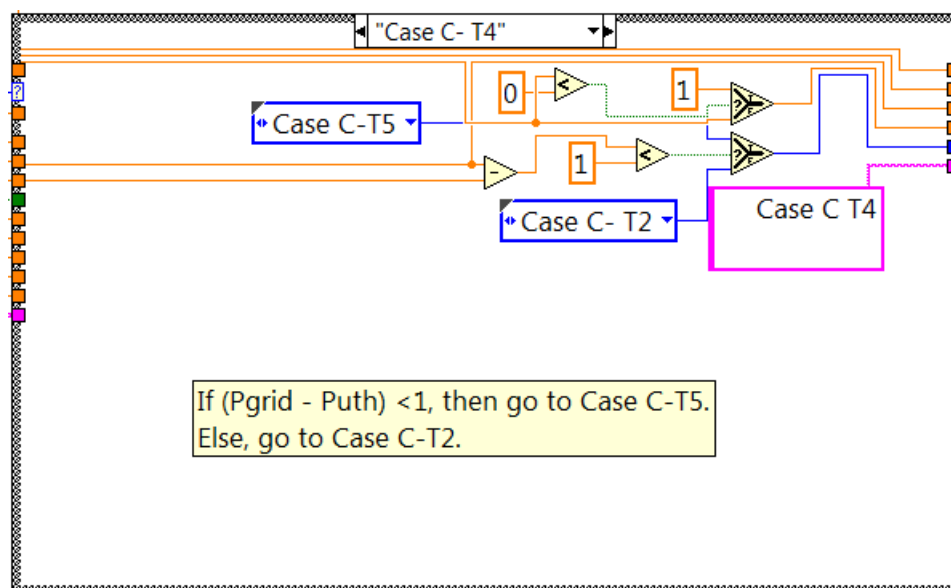
In Case C-T3, if  $(P_{grid} - P_{UTh})$  is greater than 1 kW, then the program will proceed to the Case C to update the new discharging value because the load has increased and more power is required from the energy storage system to

suppress the grid power. If  $(P_{grid} - P_{Uth})$  is less than 1kW, then it will go to Case C-T4. Figure 4.24 shows the block diagram of the Case C-T3.



**Figure 4.24: Block diagram of Case C-T3**

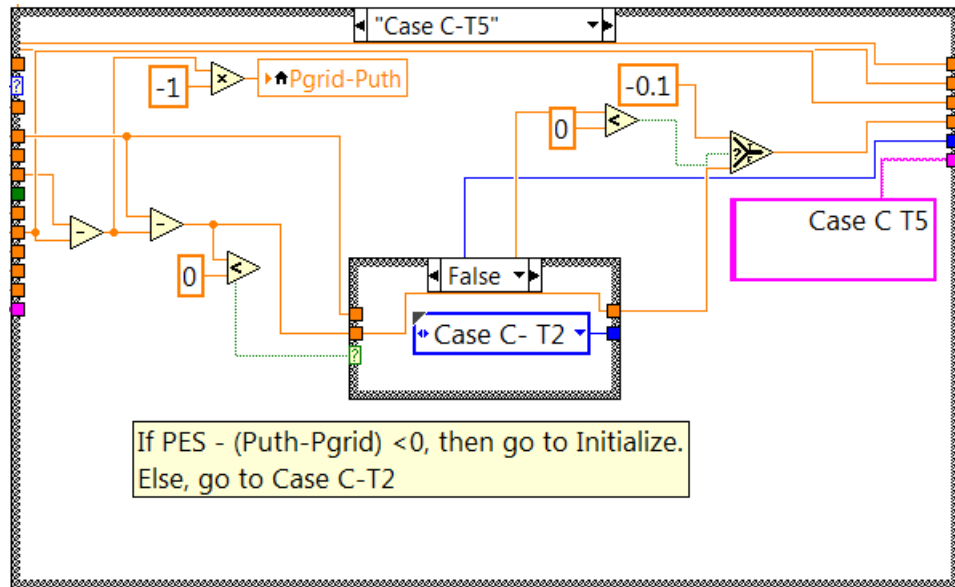
Case C-T4 is to ensure that the energy storage system continuously output the same amount of power based on the previous condition. If  $(P_{grid} - P_{Uth})$  is less than 1 kW, then it will proceed to Case C-T5, otherwise, it will proceed to Case C-T2. Figure 4.25 shows the block diagram of the Case C-T4.



**Figure 4.25: Block diagram of Case C-T4**

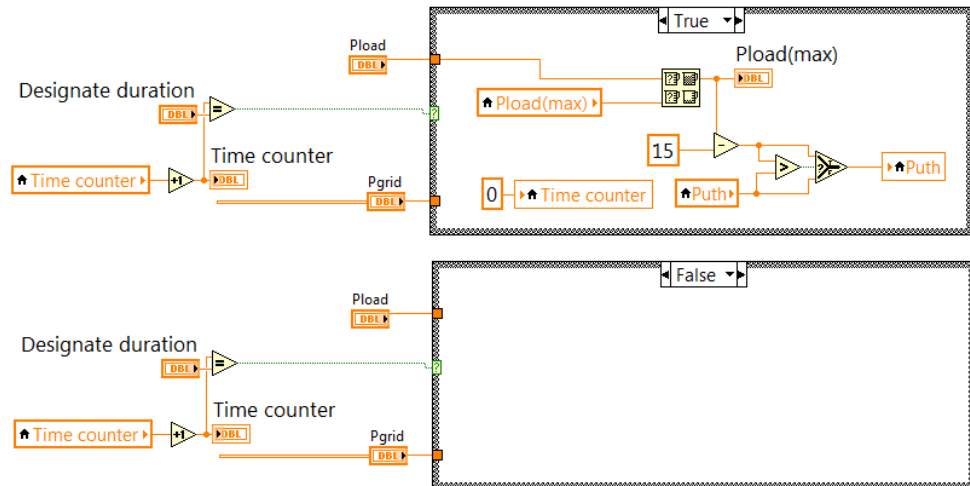


Case C-T5 is to check whether the load demand has dropped below the  $P_{UTh}$  or not. If  $P_{ES} - (P_{UTh} - P_{grid})$  is less than zero, then the program will proceed to Initialize. Otherwise, it will proceed to Case C-T2. Figure 4.26 shows the block diagram of Case C-T5.



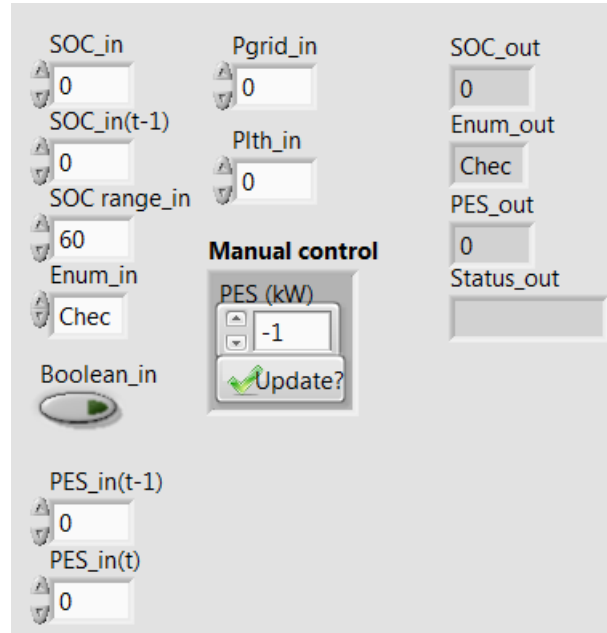
**Figure 4.26: Block diagram of Case C-T5**

For the adaptive-threshold control strategy, the  $P_{UTh}$  will be changed if the difference between  $P_{load}$  and  $P_{UTh}$  is greater than 15 kW and prolongs for more than the designated duration. The new value of the  $P_{UTh}$  is equal to  $(P_{load} - 15 \text{ kW})$ . Figure 4.27 shows the block diagram of the adaptive-threshold control strategy for the true and false cases.



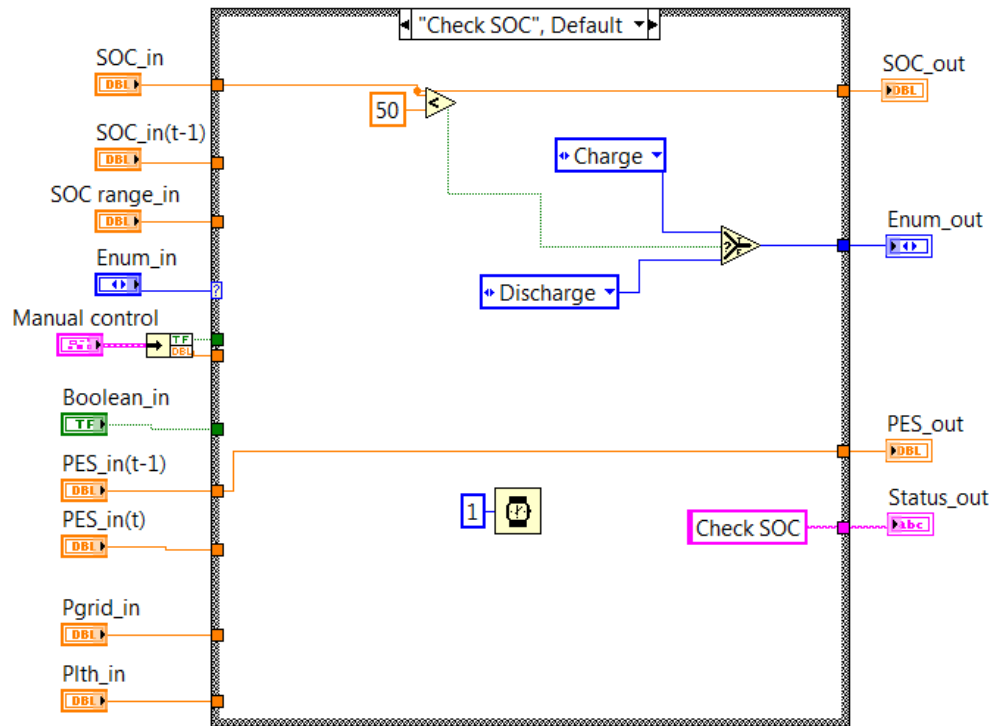
**Figure 4.27: Block diagram of the adaptive-threshold control strategy**

The VI entitled ‘2.2-Control SubVI (SOC).vi’ serves the function to ensure that the charging and discharging of the energy storage system is in stable condition when the SOC is altered. The front panel of this VI is shown in Figure 4.28.



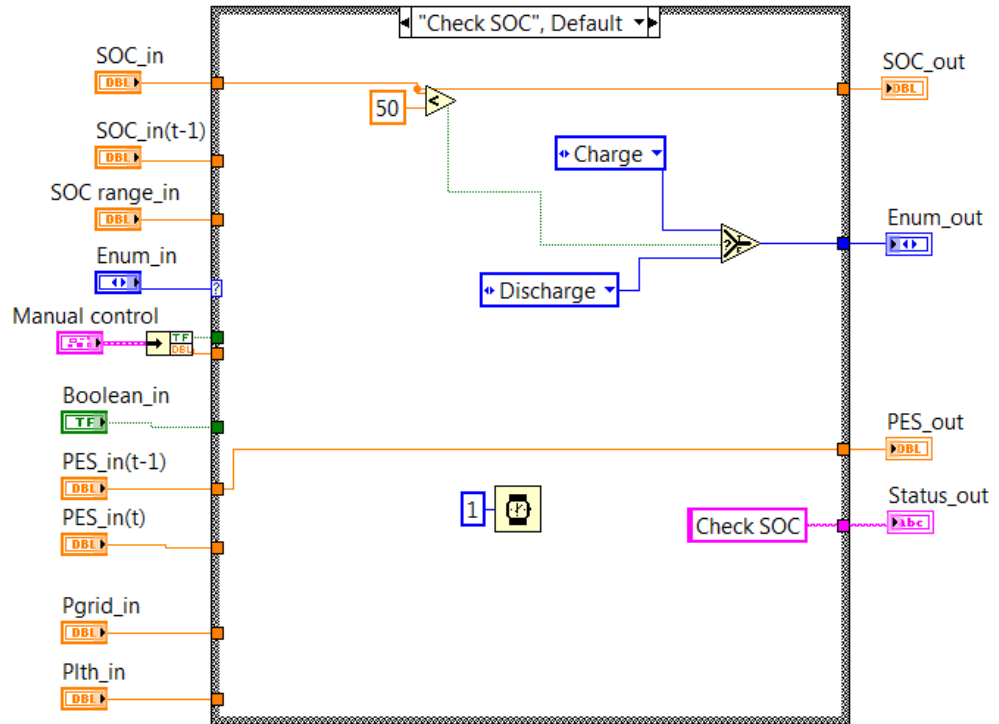
**Figure 4.28: Front panel of ‘2.2-Control SubVI (SOC).vi’**

The block diagram of '2.2-Control SubVI (SOC).vi' consists of 4 cases in the case structure. The first case is to check the SOC level of the batteries. If the SOC is lower than 50%, then it will proceed to the Charge case. Otherwise, it will proceed to the Discharge case. Figure 4.29 shows the block diagram of the Check SOC case.



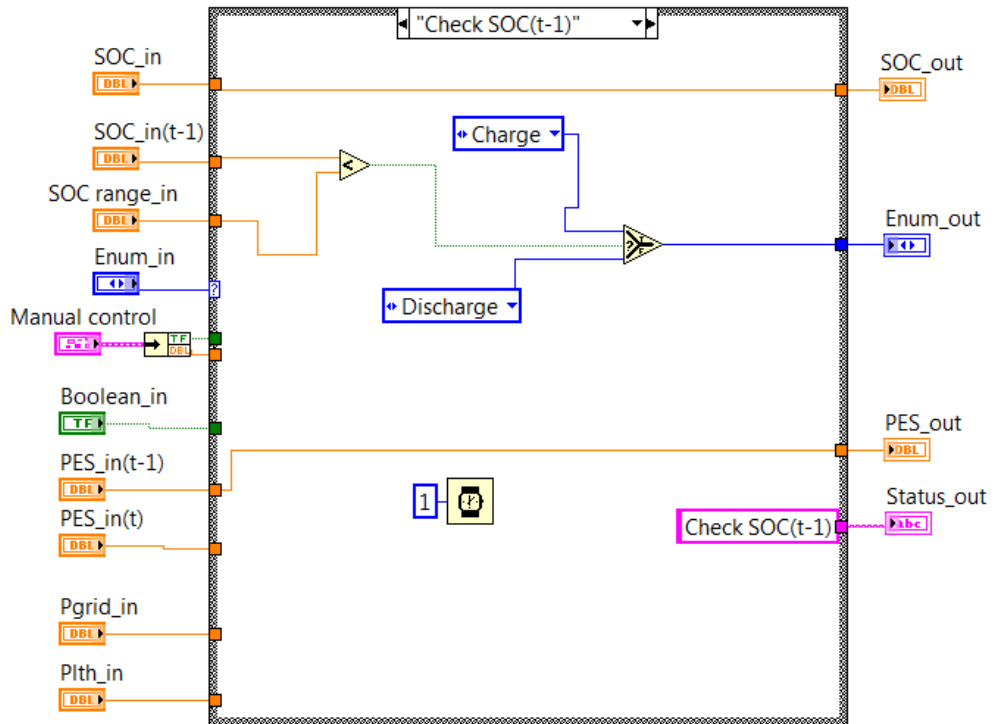
**Figure 4.29: Block diagram of the Check SOC case**

In the Charge case, if the  $P_{grid}$  is greater than the  $P_{LTh}$ , then the energy storage system will be charged at -0.1 kW. Otherwise, it will retain the current  $P_{ES}$  value. Then, the program will proceed to the Check SOC(t-1) case. Figure 4.30 shows the block diagram of the Charge case.



**Figure 4.30: Block diagram of the Charge case**

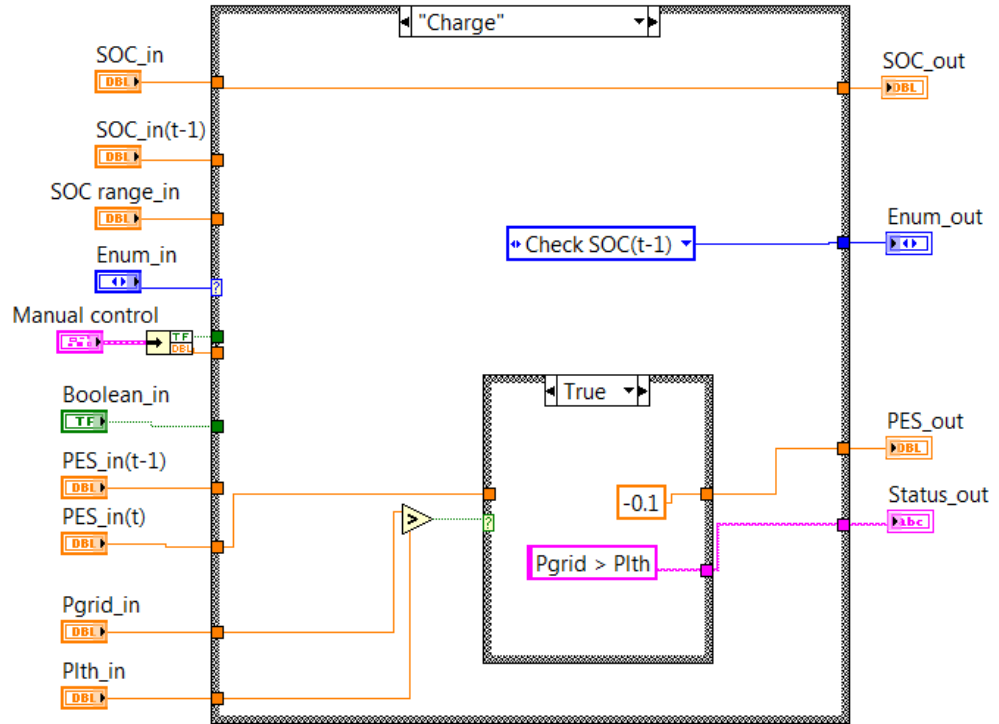
In the Check SOC(t-1) case, if the SOC\_in (t-1) is less than the designated SOC range, then the energy storage system will continue to charge the batteries. If the SOC\_in (t-1) is equal or more than the designated SOC range, then the energy storage system will proceed to the Discharge case. Figure 4.31 shows the block diagram of the Check SOC(t-1) case.



**Figure 4.31: Block diagram of the Check SOC(t-1) case**

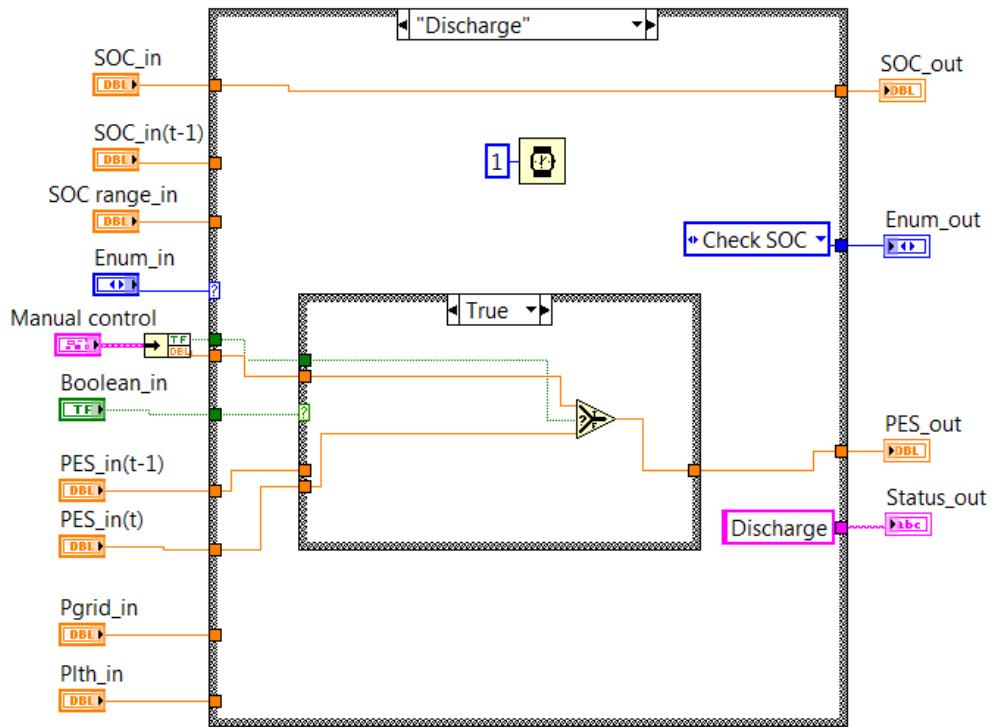
In the Charge case, if  $P_{grid}$  is greater than  $P_{LTh}$ , the output power designated to the energy storage system is -0.1 kW. Otherwise, it will follow the designated values from  $P_{ES\_in}$ . After that, the program will proceed to Check SOC(t-1).

Figure 4.32 shows the block diagram of the Charge case.



**Figure 4.32: Block diagram of the Charge case**

A manual control option is included in the Discharge case to enable the users to change the output power of the energy storage system manually when it is necessary. If the manual control is activated, then the energy storage system will operate according to the value specified by the input of the manual control. Otherwise, the energy storage system will operate based on the value of  $P_{ES\_in}$ . Figure 4.33 shows the block diagram of the Discharge case.



**Figure 4.33: Block diagram of the Discharge case**

The VI entitled '2.6-Control- Sunny Island.vi' serves the function to control the Sunny Island converters. There are 5 parts in this VI. Part 1 shows the current time and starts time of the Sunny Island converters, and two control buttons to activate the Sunny Island converters and to stop the program. Part 2 provides manual control option to the users to manually control the current flow of the converters. The update button is used to update the manual control current to the converters. The indicator notifies the users when the values have been updated. Part 3 shows the instructions sent from the '2.2-Control-Peak reduction.vi'. Part 4 shows the average value of the SOC. The users can update the converters automatically by specifying the update duration in part 4. Part 5 illustrates the fundamental parameters of the converters. Figure 4.34 shows the front panel of '2.6-Control- Sunny Island.vi'.

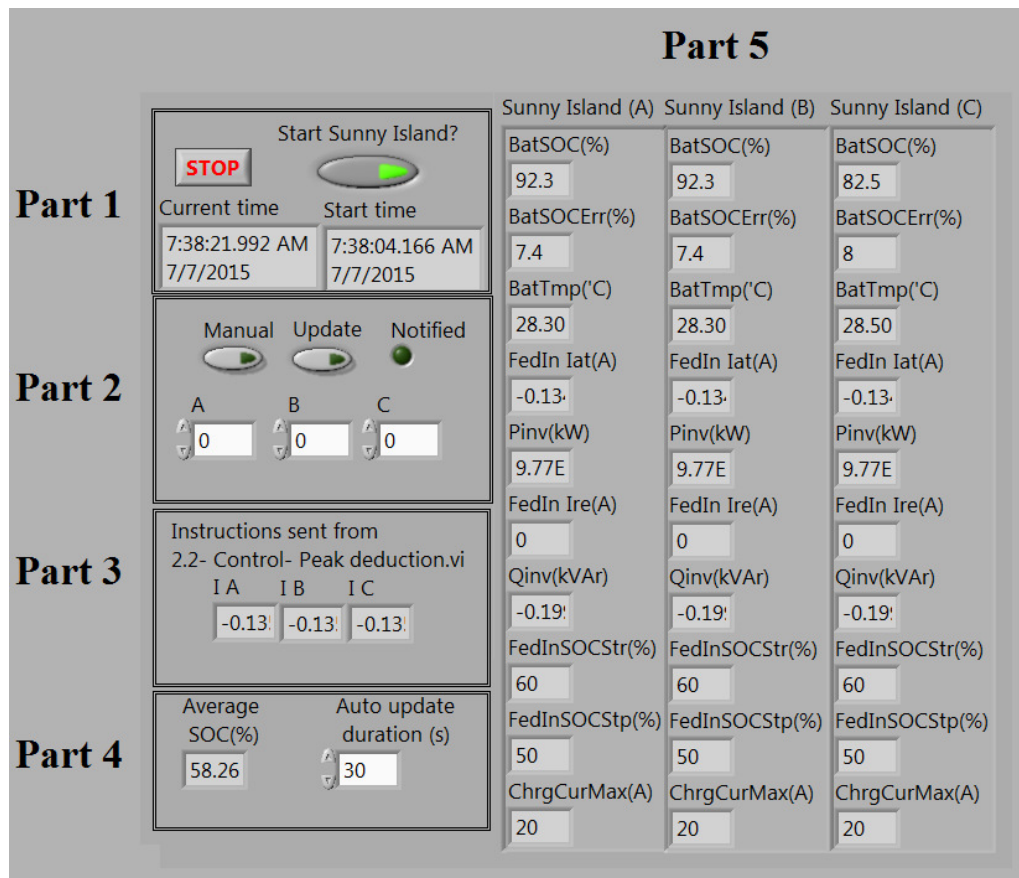


**Figure 4.34: Front panel of '2.6-Control- Sunny Island.vi'**

There are three parts in the block diagram of '2.2-Control-Peak reduction.vi'. Part 1 opens the data sources from the designated Sunny Island converter. Part 2 serves the functions of reading and writing the data to the designated variables. Part 3 closes the opened task so that the tasks are terminated and closed correctly. To ease the reading of the block diagram, it is split into the upper portion and the lower portion. Figure 4.35 shows the upper portion of the block diagram of '2.2-Control-Peak reduction.vi'. The codes shown in this portion are to create variables that store data in the library and share data between VIs in the project.



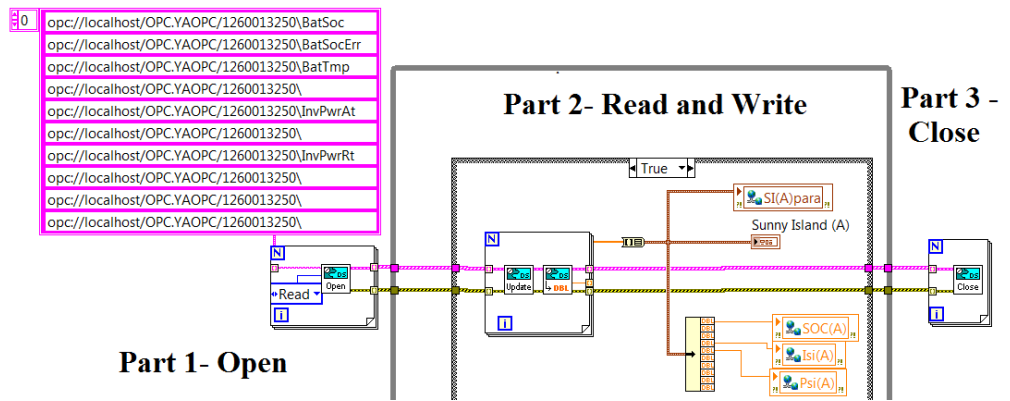


**Figure 4.35: The upper portion of block diagram of ‘2.2-Control-Peak reduction.vi’**

Figure 4.36 shows the lower portion of the block diagram of ‘2.2-Control- Peak reduction.vi’. This portion allows the users to choose the control mode, either in manual or centre control mode. For manual control, the users can key in the desired power as shown in the diagram. For centre control, the instructions are sent from ‘2.2-Control- Peak reduction.vi’.

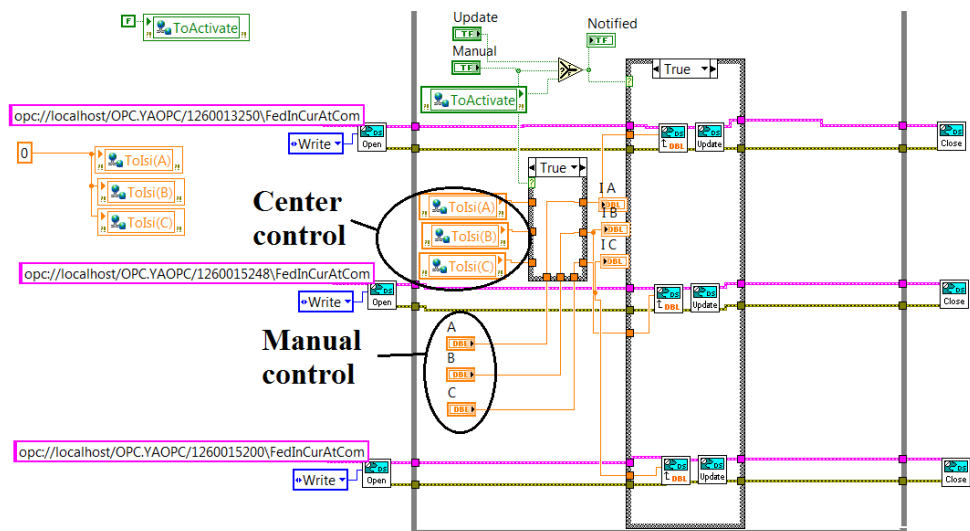


**Figure 4.36: The lower portion of the block diagram of ‘2.2-Control- Peak reduction.vi’**

#### 4.6.5 Project Explorer of the Energy Storage System for KA Block

The control VIs of the energy storage system are the same for SE block and KA block. However, the data acquisition of the two buildings is different. Figure 4.37 shows the project explorer of the energy storage system installed at KA block. Three VIs are developed for the data acquisition system, 4 VIs are developed to control the energy storage system, and 2 custom control files are designed to standardize the setting of the control input.

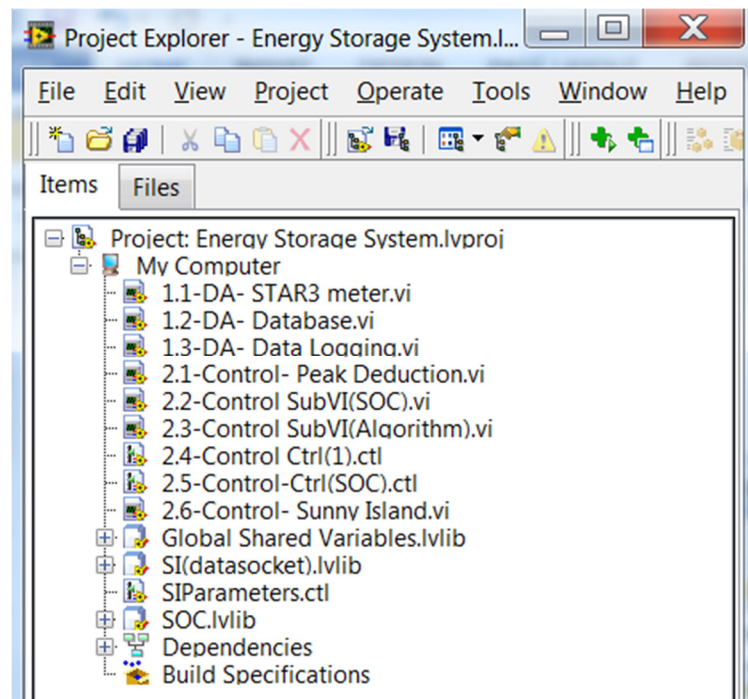


**Figure 4.37: Organization of project explorer for the energy storage system in KA block**

The VI entitled '1.1-DA- STAR3 meter.vi' is developed to establish the communication between the power energy meters. Figure 4.38 shows the front panel and block diagram of the VI. There are three main parts in the block diagram, namely the initialization, read, and close. The initialization part

establish the communication with the targeted power energy meters and number of parameters to be read. The read part acquires the data from the meters and sends the data to library in the project explorer. The close part terminates all the opened resources. The error cluster will alert the users when there is an error during the execution of the code.

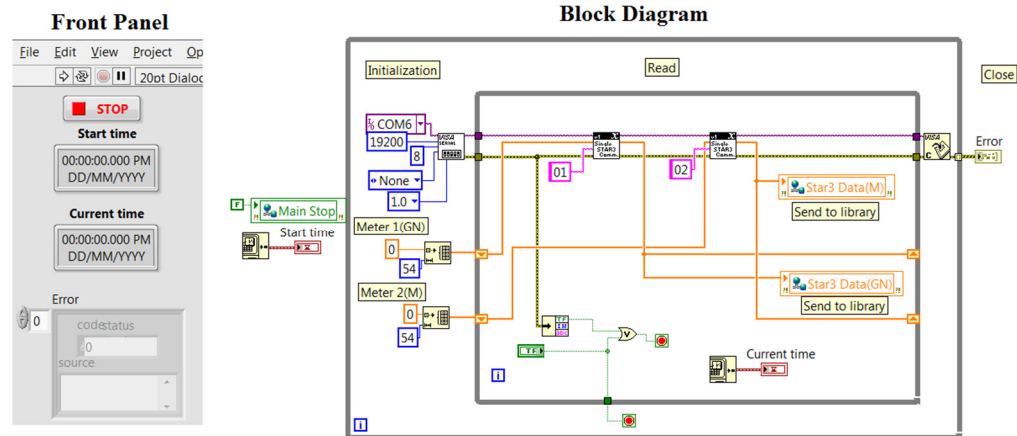


**Figure 4.38: Front panel and block diagram of ‘1.1-DA- STAR3 meter.vi’**

The VI entitled ‘1.2-DA- Database.vi’ serves the function to collect data from the power meters and the Sunny Island converters. Figure 4.39 shows the block diagram of the VI. There are two parts in this VI. Part 1 organizes the parameters obtained from the power energy meters and the Sunny Island converters. Part 2 sorts the parameters in the desired order.

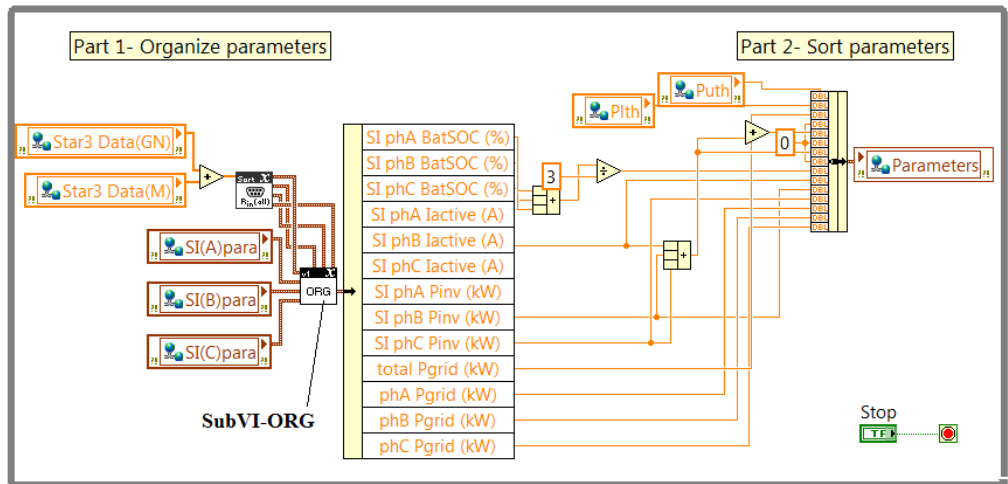
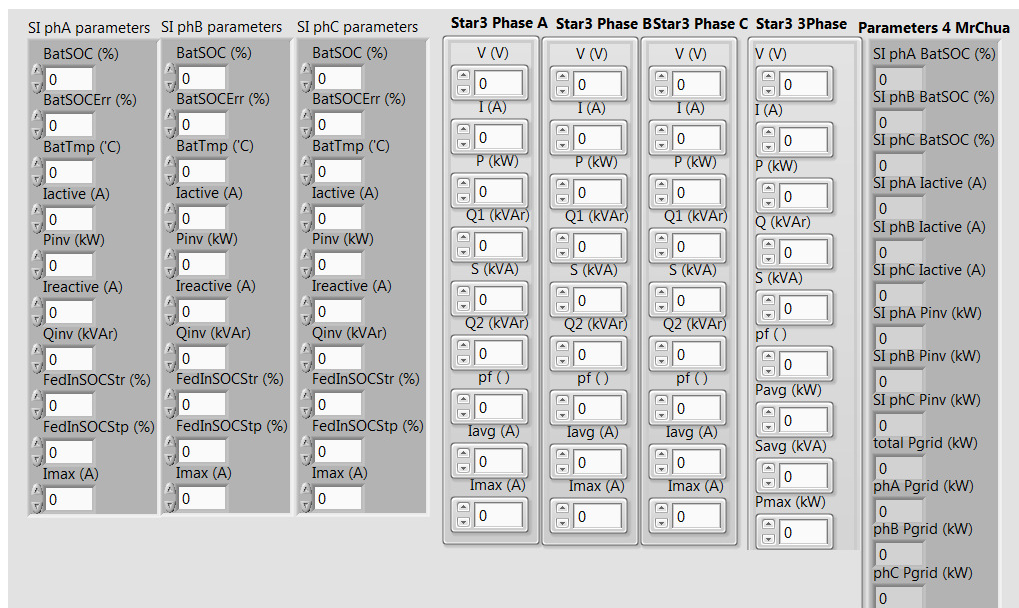


**Figure 4.39: Block diagram of '1.2-DA- Database.vi'**

The VI entitled 'subVI-ORG.vi' serves the functions to organize the parameters from the power meters and converters in the designated order. Figure 4.40 (a) and (b) show the front panel and block diagram of 'subVI-ORG.vi'.



**(a)**

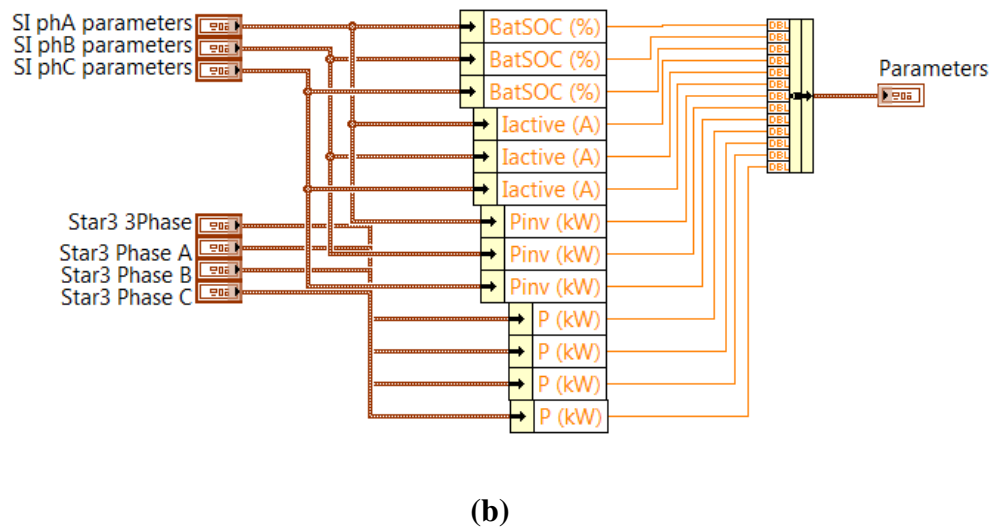


**Figure 4.40: 'subVI-ORG.vi' (a) Front panel and (b) block diagram**

#### 4.7 Summary

Fixed-threshold and adaptive-threshold control algorithms have been developed and were presented in this chapter. The fixed-threshold controller is a basic control strategy that will fix the upper power threshold using the forecasted load profiles for each day before the operation of the energy storage system. However, the success of this controller relies on the accuracy of the forecasted load profiles. Adaptive-threshold controller is an improved version of the fixed-threshold controller where it can reduce the output power of the energy storage system to preserve the energy of the batteries when the actual peak demands occur for an extended period of time. The performances of these two controllers are evaluated in Chapter 5.

## CHAPTER 5

### EVALUATION OF THE FIXED-THRESHOLD AND ADAPTIVE-THRESHOLD CONTROL ALGORITHMS FOR PEAK REDUCTION

#### 5.1 Introduction

In the previous chapter, the development and implementation of the fixed-threshold and adaptive-threshold control algorithms have been elaborated in details. This chapter discusses the performances of these two control algorithms for the peak reduction at two different buildings, namely the SE block and KA block. A single-phase energy storage system is set up to describe the operation of the energy storage system on the single-phase distribution network before it is extended to the three-phase distribution network. Thereafter experiments are carried out at the three-phase distribution network to evaluate the performance of the fixed-threshold and adaptive-threshold control algorithms.

#### 5.2 Single-phase Energy Storage with Fixed-threshold Control Strategy

A single-phase energy storage system is set up to illustrate the operation of a bi-directional power converter with the fixed-threshold control strategy. A single-phase energy storage system formed by a 5 kVA bi-directional power converter and a battery bank is connected to the experimental low-voltage distribution

network and a load bank. The load bank acts as a load emulator that can be varied in steps of 500 W up to 9 kW. Four batteries are connected in series to form a string of batteries to provide a 48 V DC supply to the bi-directional converter. Figure 5.1 shows the experimental setup of the single-phase energy storage system.

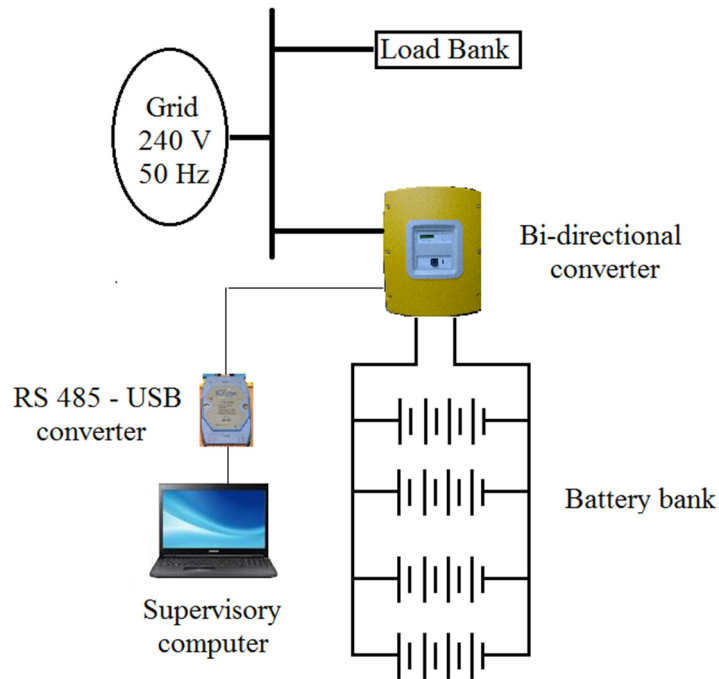


**Figure 5.1: Experimental setup of the single-phase energy storage system**

The load bank is controlled in such a way that its demand increases from 0 kW to 5 kW and then decreases from 5 kW to 0 kW in steps of 500 W for every 3 minutes. The bi-directional power converter is set to the idle mode if the load ( $P_{load}$ ) is below the designated threshold ( $P_{Th}$ ). The bi-directional power converter delivers power ( $P_{ES}$ ) to the distribution network when the  $P_{load}$  has exceeded the value of  $P_{Th}$ . Figure 5.2 shows the responses of the single-phase energy storage system with the threshold setting of 1 kW. It can be seen that when the load is below the threshold of 1 kW, the energy storage system absorbs

the little power of 0.1 kW. When the load has exceeded 1 kW and reached 1.45 kW at the sixth minute, the energy storage system begins to deliver 0.45 kW to the load. The net effect is that the power demand as seen by the grid ( $P_{grid}$ ) is maintained within the range of  $1 \pm 0.1$  kW. It is also noticed that the energy storage system took about 5 to 10 seconds to respond when it receives the control instruction, hence creating a number of spikes on the  $P_{grid}$  graph. However, the duration of the spikes is negligible because it is relatively short as compared to the duration used to determine the maximum demand which is 30 minutes.

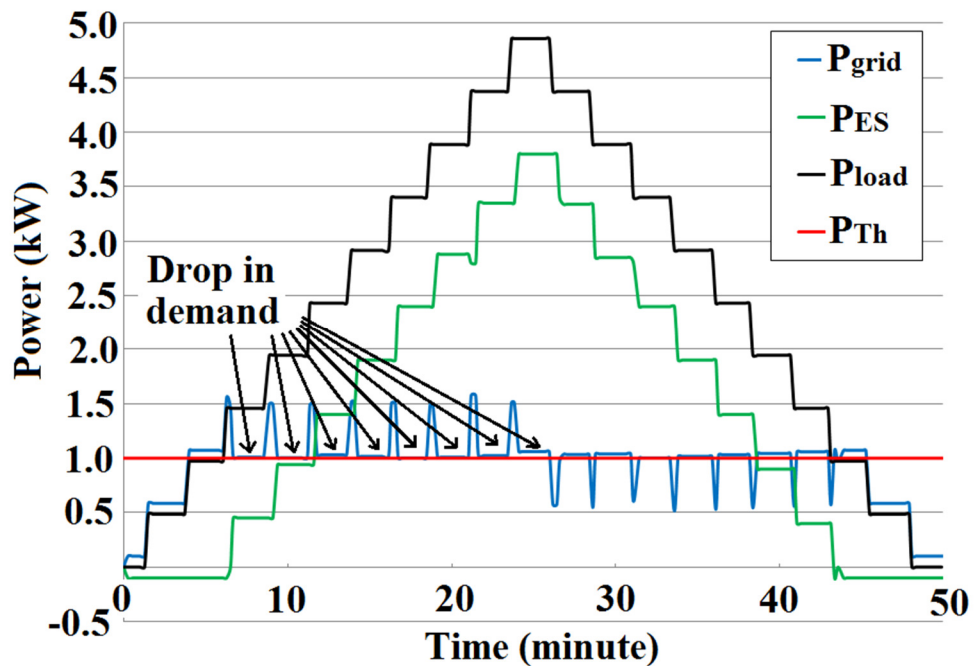


Figure 5.2: Reduction of the grid demand with the threshold setting of 1

kW



### **5.3 Evaluation of the Fixed-threshold and Adaptive-threshold Control Algorithms in Three-Phase Energy Storage**

Several case studies have been carried out to evaluate the fixed-threshold and adaptive-threshold control algorithms in three-phase energy storage to reduce the peak demands for the SE and KA blocks. Case study 1 to case study 4 is carried out to evaluate the performance of the fixed-threshold control algorithm while case study 5 to case study 9 are carried out to evaluate the performance of the adaptive-threshold control algorithm.

#### **5.3.1 Performance Evaluation of the Fixed-threshold Control Algorithm**

Case study 1 investigates the performance of the fixed-threshold control algorithm conducted at the SE block for the scenario where the load demand is higher than the predicted value and the actual peak occurs for a much longer duration than the predicted duration. The actual peak demands are unexpectedly higher than the predicted value where its maximum demand is 97.21 kW while the predicted maximum demand is 95 kW. Initially,  $P_{UTh}$  and the  $P_{LTh}$  are set at 80 kW and 30 kW, respectively according to the predicted value. Figure 5.3 shows the results of the peak reduction using the fixed-threshold control algorithm for the case study 1. It can be seen that when the load has exceeded 80 kW at 10:00, the energy storage system begins to deliver power to the load based on the difference between the  $P_{load}$  and  $P_{UTh}$ . The SOC of the batteries has declined to 50 % at 13:00, triggering the energy storage system to stop

delivering power to the load. As a result, the energy storage system fails to reduce the peak after 13:00. The energy storage system begins to charge the batteries when the demand falls below the lower threshold of 30 kW at 17:45. In this case study, the energy storage system is not able to cut down the peak demand due to the limited rating of the power converters. It is also found that the actual peak occurs for a much longer duration than the predicted one. Hence, the energy storage system does not have enough energy to sustain the delivery of its power over such a long duration.

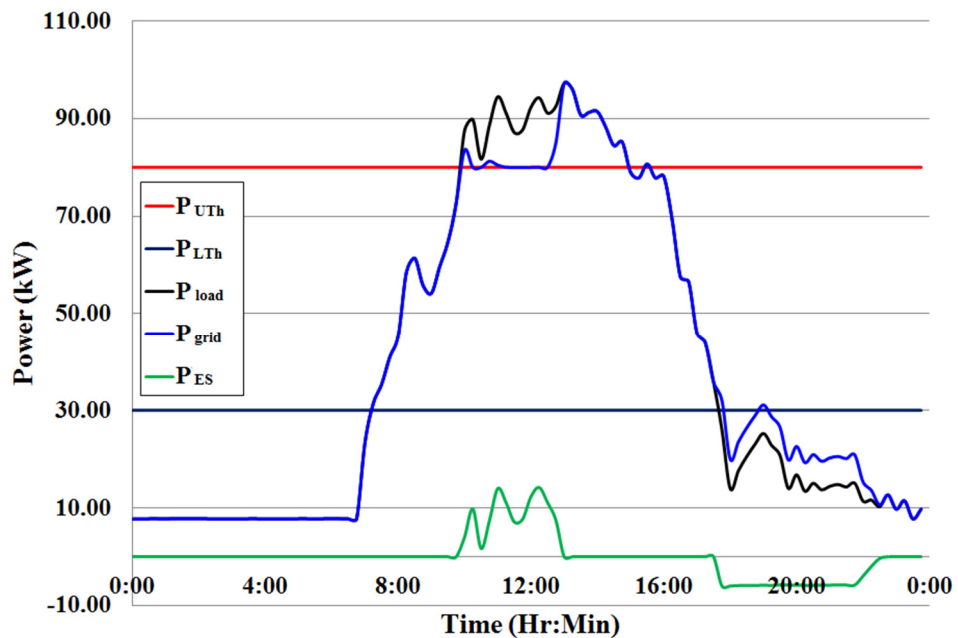


**Figure 5.3: The peak reduction using the fixed-threshold control algorithm for case study 1**

In the case study 2, the load demand is lower than that of the predicted load demand. The maximum demand is 97.82 kW while the predicted maximum demand is 105 kW. Initially, the  $P_{UTH}$  is set at 90 kW while the  $P_{LTh}$  is set at 30 kW. Figure 5.4 shows the results of the peak reduction using the fixed-threshold control algorithm for the case study 2. It can be seen that when the load has

exceeded 90 kW at 13:00, the energy storage system begins to deliver power to the load based on the difference between the  $P_{load}$  and  $P_{UTh}$ . The peak demand has been reduced from 97.8 kW to 91.4 kW. It is found that the peak shaved is 6.44 kW. In this case study, the capacity of the energy storage system is under-utilized.

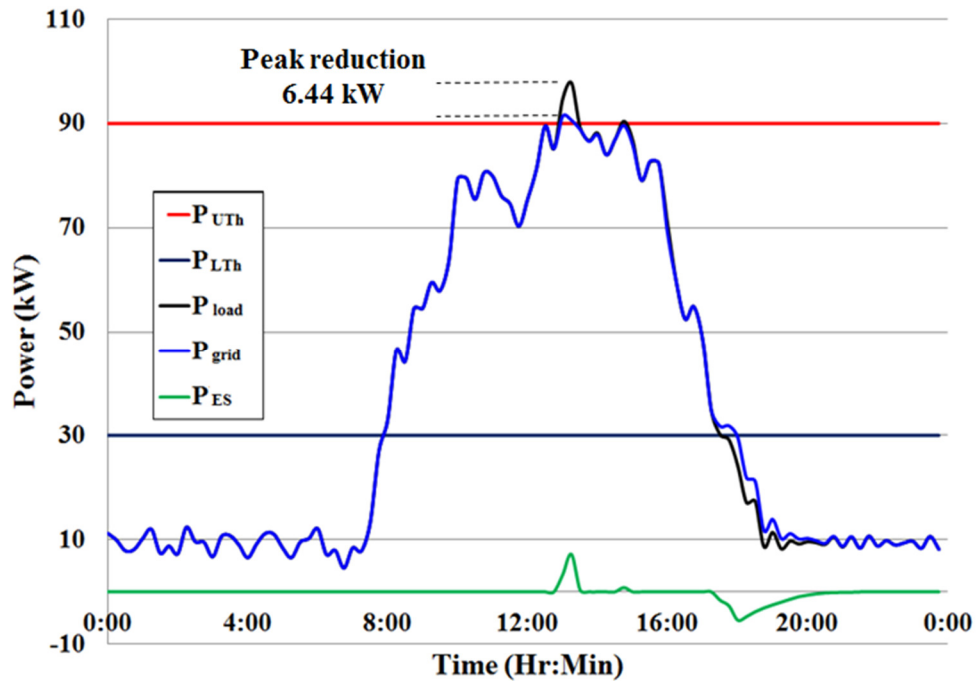


**Figure 5.4: The peak reduction using the fixed-threshold control algorithm for the case study 2**

Case studies 3 and 4 investigate the performance of the fixed-threshold control algorithm conducted at KA block. In the case study 3,  $P_{UTh}$  is set at 71 kW according to the predicted value while the  $P_{LTh}$  is set at 50 kW. Figure 5.5 shows the results of the peak reduction. It is found that the peak demand above the  $P_{UTh}$  at 12:45 is 18 kW. This value is higher than the rating of the energy storage system. Hence, the peak demand as seen by the grid is 77.46 kW. In this case, the peak shaved is 11.41 kW. The idea reduction is 15 kW. However, the fixed-

threshold controller can only reduce the peak by 11.41 kW. This is due to the fact that the  $P_{UTh}$  is set at the inappropriate level based on the predicted load demand.

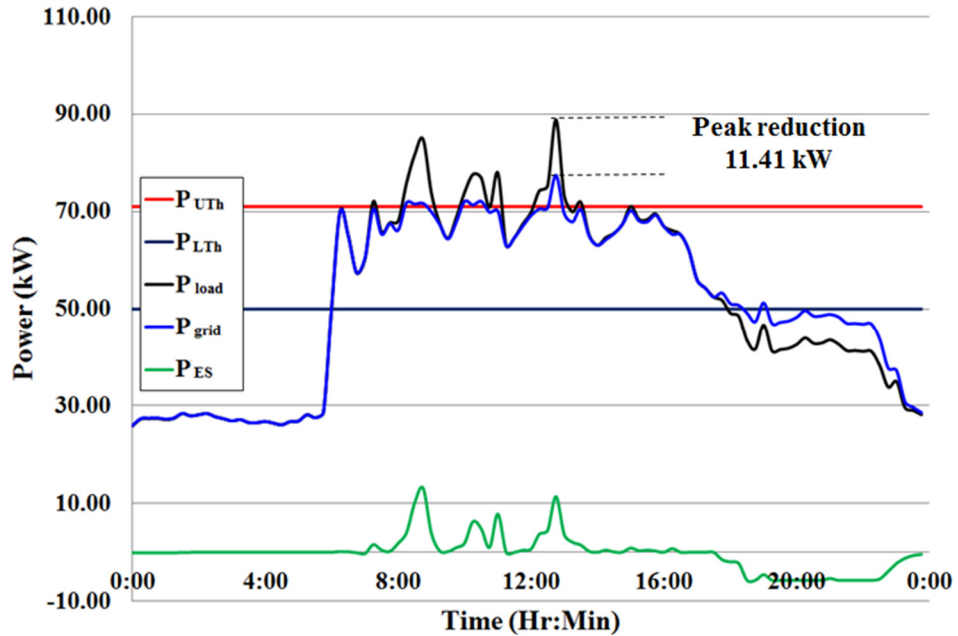


**Figure 5.5: The peak reduction using the fixed-threshold control algorithm for the case study 3**

In the case study 4, the  $P_{UTh}$  is set at 70 kW according to the predicted value while the  $P_{LTh}$  is set at 50 kW. Figure 5.6 shows the results of the peak reduction. It can be seen that when the load has exceeded 70 kW at 7:45, the energy storage system begins to deliver power to the load based on the difference between the  $P_{load}$  and  $P_{UTh}$ . The peak demand has been reduced from 78.4 kW to 70.9 kW. It is found that the peak reduction in this case study is 7.5 kW. The peak reduction is relatively low because the  $P_{UTh}$  is set at relatively high level.

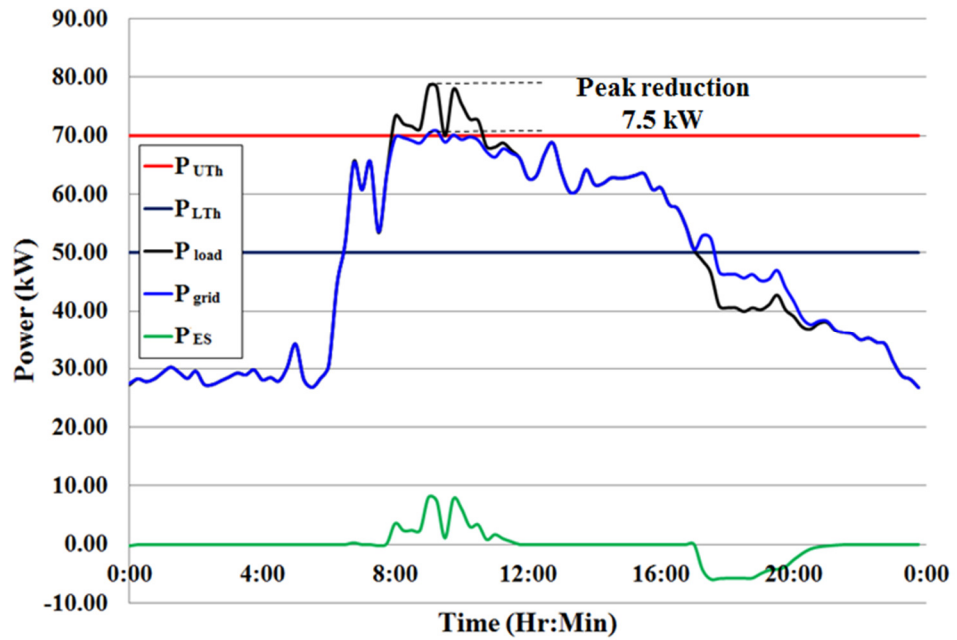


**Figure 5.6: The peak reduction using the fixed-threshold control algorithm for the case study 4**

### 5.3.2 Performance Evaluation of the Adaptive-threshold Control Algorithm

Case study 5 investigates the performance of the adaptive-threshold control algorithm conducted at SE block. This case study illustrates the scenario where the actual peak is unexpectedly higher than the predicted value. Figure 5.7 shows the results of the peak reduction using the adaptive-threshold control algorithm for the case study 5. It is found that the maximum demand is 90.2 kW while the predicted maximum demand is 86 kW. Initially, the  $P_{UTH}$  is set at 71 kW according to the predicted value while the  $P_{LTh}$  is set at 30 kW. It can be seen that when the load demand has exceeded 71 kW at 12:00, the energy storage system begins to deliver power to the load. At 13:30,  $P_{load}$  has increased

to 89.2 kW and prolonged for more than 10 minutes. The corrective mechanism in the adaptive-threshold algorithm adjusts the  $P_{UTh}$  to 74.5 kW at 13:45. At 14:00,  $P_{load}$  has increased to 90.2 kW and prolonged for more than 10 minutes and the  $P_{UTh}$  is adjusted to 77.3 kW at 14:15. The energy storage system begins to restore its energy at 17:00. The peak demand has been reduced from 90.2 kW to 78.5 kW. In this case, the peak shaved is 11.7 kW.

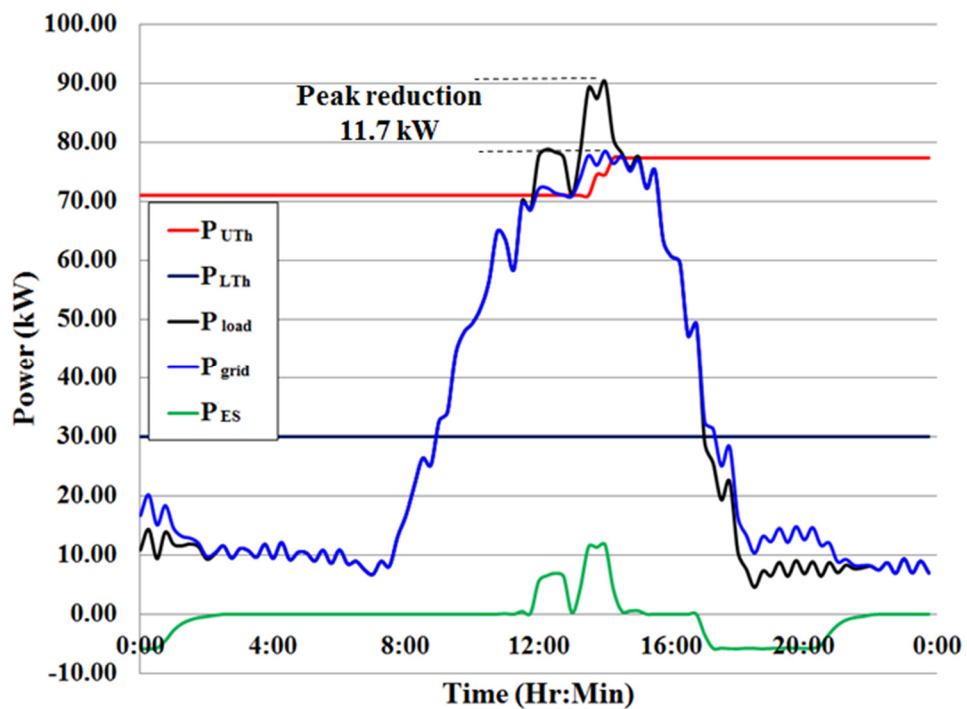


**Figure 5.7: The peak reduction using the adaptive-threshold control algorithm for the case study 5**

In the case study 6, the  $P_{UTh}$  is set at 70 kW according to the predicted value while the  $P_{LTh}$  is set at 30 kW. Figure 5.8 shows the results of the peak reduction. It can be seen that when the  $P_{load}$  has increased to 84.9 kW and prolonged for more than 10 minutes at 14:15, the  $P_{UTh}$  has adopted to a new value of 75 kW at 14:30. The peak demand has been reduced from 84.9 kW to 75.7 kW. It is found that the peak shaved in this case study is 9.2 kW. The peak reduction is

considered moderate because the adaptive-threshold controller has adjusted to  $P_{UTh}$  preserve the energy storage.

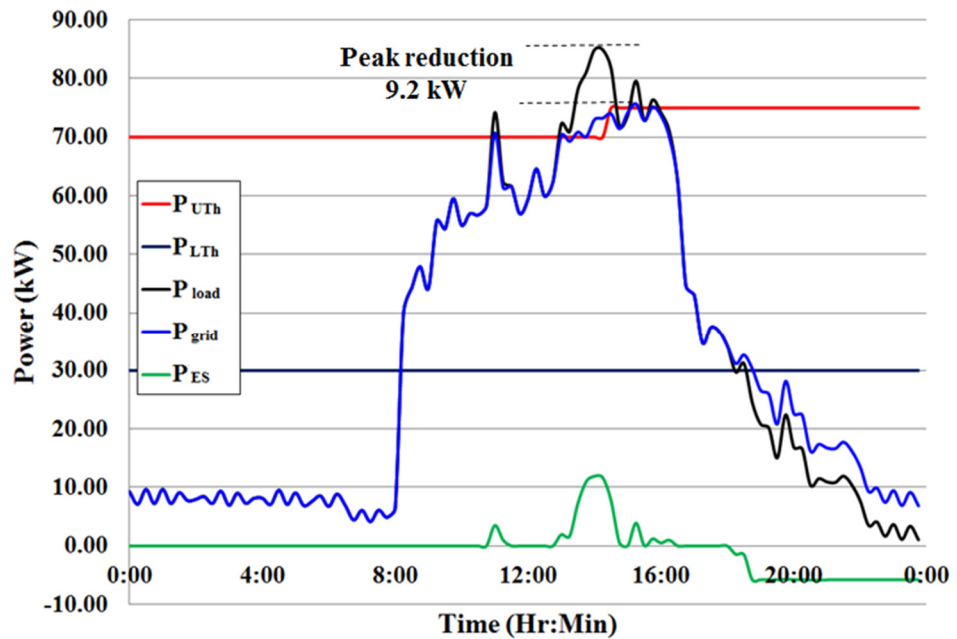


**Figure 5.8: The peak reduction using the adaptive-threshold control algorithm for the case study 6**

In the case study 7, the  $P_{UTh}$  is set at 68 kW according to the predicted value while the  $P_{LTh}$  is set at 50 kW. It can be seen in Figure 5.9 that when the  $P_{load}$  has increased to 89.5 kW and prolonged for more than 10 minutes at 9:45, the  $P_{UTh}$  has adopted to a new value of 78.2 kW. The peak demand has been reduced from 90 kW to 80.3 kW. It is found that the peak shaved in this case is 9.7 kW. It is noticed that the peak begins to drop after 9:45. It can be seen that the increment and decrement of peak demand are very drastic. Consequently, the adaptive-threshold controller is not able to respond immediately to the dramatic changes due to its delayed setting of 10 minutes.

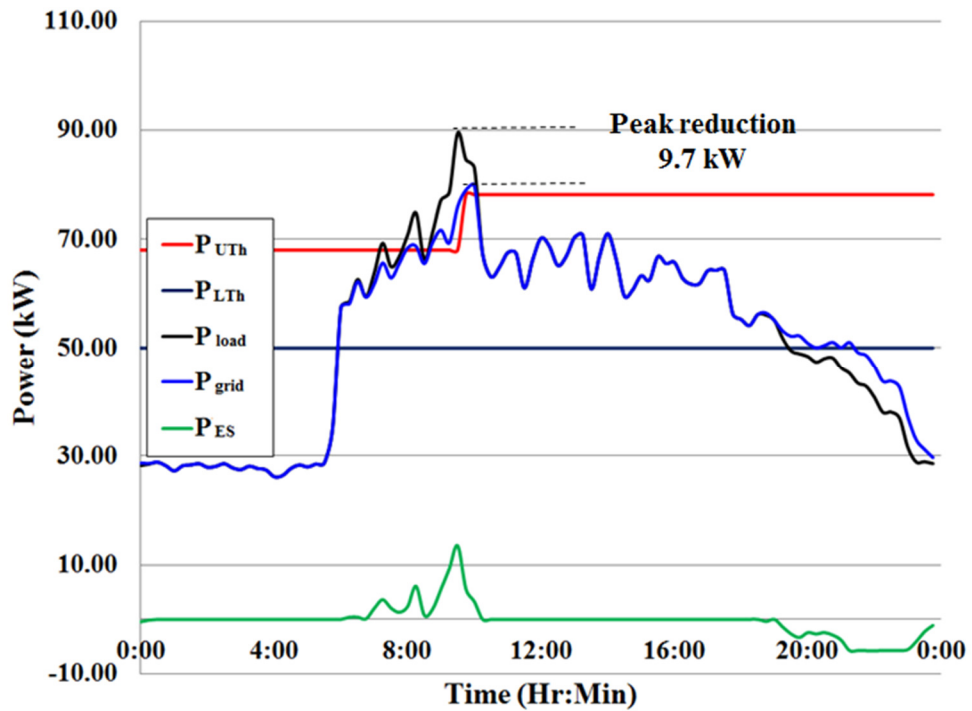


**Figure 5.9: The peak reduction using the adaptive-threshold control algorithm for the case study 7**

In the case study 8, the  $P_{Th}$  is set at 70 kW according to the predicted value while the  $P_{LTh}$  is set at 50 kW. It can be seen in Figure 5.10 that when the  $P_{load}$  has increased to 88.1 kW and prolonged for more than 10 minutes, the  $P_{Th}$  has adopted to a new value of 75.5 kW at 9:30. The peak demand has been reduced from 88.1 kW to 76.2 kW. It is found that the peak shaved in this case study is 11.9 kW. In this case, the peak reduction is satisfactory.



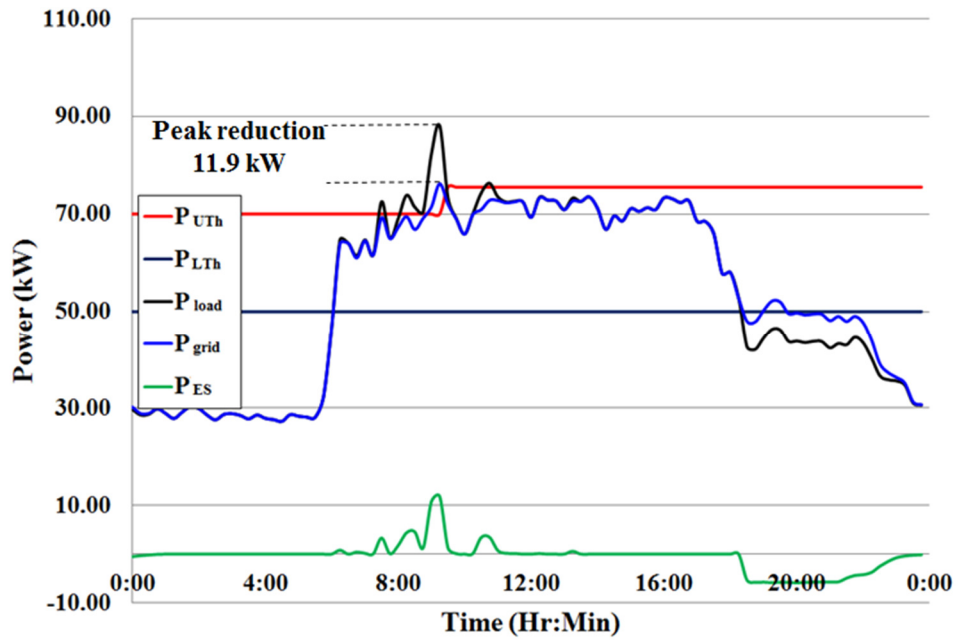


**Figure 5.10: The peak reduction using the adaptive-threshold control algorithm for the case study 8**

In the case 9, the  $P_{UTh}$  is set at 68 kW according to the predicted value while the  $P_{LTh}$  is set at 50 kW. Figure 5.11 shows the results of the peak reduction. The peak demand is 82.78 kW while the predicted  $P_{UTh}$  is 83 kW. It can be seen that the energy storage system starts to deliver power to the load at 7:15 when the  $P_{load}$  is greater than the  $P_{UTh}$ . At 12:15, the SOC of the energy storage system has dropped to 50%. Consequently, the energy storage system stops to deliver power to the load. As a result, the energy storage system failed to reduce the peak demand when the load has increased to 82.78 kW at 12:30. This case study shows that when the actual peak occurs for a much longer duration than the predicted one, the energy storage system fails to deliver power to the load because it does not have enough energy to sustain the delivery of its power over such a long duration.

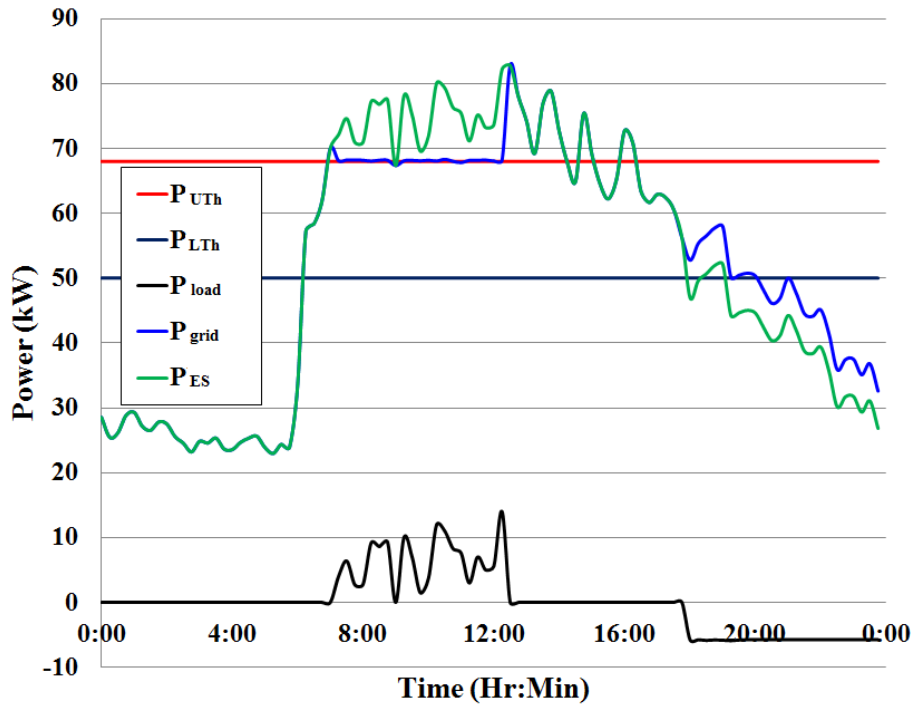


**Figure 5.11: The peak reduction using the adaptive-threshold control algorithm for the case study 9**

Table 5. 1 shows the summary of the electricity bill saving for the fixed-threshold and adaptive-threshold control algorithms. The tariff used to calculate the bill saving is based on the medium voltage general commercial tariff (C1) where the maximum demand charge is RM 45.1/ kW.

**Table 5. 1: Summary of the electricity bill saving**

Control method	Case study	Peak reduction (kW)	Bill saving (RM)	Bill saving (%)
Fixed-threshold	1	0	0	0
	2	6.44	290.4	6.6
	3	11.41	514.6	12.8
	4	7.5	338.3	9.6
Adaptive-threshold	5	11.7	527.7	13
	6	9.2	414.9	10.8
	7	9.7	437.5	10.8
	8	11.9	536.7	13.5
	9	0	0	0

## 5.4 Summary

One of the challenges of using energy storage system for peak reduction in a building is that the cost of the batteries is high. The energy storage system should supply the appropriate amount of power at the right timing with its limited energy and power rating in order to reduce the peak effectively. However, the actual peak demand can be higher than that of the predicted peak demand. As a result, the energy storage system may fail to reduce the peak demand effectively. In this chapter, the fixed-threshold and adaptive-threshold control algorithms have been evaluated experimentally at two buildings. These two buildings illustrated different load characteristics where the load profile of the SE block has a relatively sharp and narrow peak demand while the peak demand of the KA block occurs in the wider time frame and the load demand is relatively flat.

The case study 1 illustrates the scenario where the load demand is higher than the predicted load demand and the actual peak demand occurs for a much longer duration than the predicted duration. The fixed-threshold control algorithm failed to reduce the peak demand due to the limited energy stored in the batteries. There are two major drawbacks to using the fixed-threshold control algorithm. Firstly, when the actual peak occurs for a much longer duration than the predicted duration, the energy storage system may fail to reduce the peak demand because it does not have enough energy to sustain the delivery of its power over such a long duration. Secondly, when the actual peak demand is

unexpectedly high, the energy storage system is not able to supply such a high power due to the limited power rating of the power converters.

The adaptive-threshold control algorithm is capable of adjusting the output power of the energy storage system when the actual peak demand is unexpectedly high to preserve the energy of the batteries when the actual peak demand happens for the extended period of time. The adaptive-threshold control algorithm resolves the problem of unexpected high peak demands where the energy storage system may not be able to deliver such a high power due to the limited rating of the power converters. However, the adaptive-threshold control algorithm may fail to reduce the peak demand when the actual peak demand occurs for a much longer duration than the predicted peak demand. This can be seen in the case study 9 where the energy storage system does not have enough energy to sustain the delivery of its power over such a long duration and results in failure to reduce the peak demand.

The fixed-threshold and adaptive-threshold control algorithms have limitations to cut down the peak demand for the scenarios as discussed above. In order to cope with these problems, a fuzzy-based control algorithm is developed. The development and evaluation of the fuzzy-based control algorithm are elaborated in Chapter 6.

## CHAPTER 6

### FUZZY-BASED CONTROL ALGORITHM AND EXPERIMENTAL EVALUATION

#### 6.1 Introduction

In chapter 5, the experimental results showed that the fixed-threshold control algorithm failed to reduce the peak demands in the case where the actual peak demand is unexpectedly high and happens for a much longer duration than the predicted duration because the energy storage system does not have enough energy to sustain the delivery of its power over such a long duration. The adaptive-threshold control algorithm can cope with the problem of unexpectedly high peak demands by adjusting the  $P_{UTh}$  when the energy storage system is not able to deliver such a high power due to the limited rating of the power converters. However, the adaptive-threshold control algorithm may fail to reduce the peak demand if the actual peak demand occurs for a much longer duration than the predicted peak demand because the adaptive-threshold control algorithm does not take into account the state of charge (SOC) of the lead-acid batteries. The SOC of the lead-acid batteries is varied in the range of 50 % to 100 % so that the batteries can sustain their lifespan.

In this chapter, a novel fuzzy-based control algorithm is developed taking into account the SOC or the useable energy of the batteries. The fuzzy-based control

algorithm can adjust its output power based on the time of operation and SOC of the batteries.

The overview of the fuzzy logic theory and its applications in energy storage system are discussed. The fuzzy-based control algorithm is developed using the Fuzzy System Designer Toolbox in LabVIEW software. Experiments are carried out to evaluate the performance of the fuzzy-based control algorithms. The performance of the fuzzy-based control algorithm is compared with the performance of the fixed-threshold and adaptive-threshold control algorithms using the performance evaluation index, namely the peak reduction factor.

## **6.2 Overview of Fuzzy Logic and Its Applications in Energy Storage Systems**

Fuzzy logic is first introduced by Dr. Lotfi Zadeh in 1965 to solve a complex control system without a complicated mathematical model (Perry, 1995). Fuzzy control has been widely adopted in industrial process control since the 1900s because it does not rely upon an accurate mathematical model of the controlled object. The conventional controllers have poor performance in dealing with nonlinear plants because the nonlinear models have complex stability problems (Gaurav and Amrit, 2012). It is difficult to obtain an accurate plant model due to the uncertainty and lack of perfect knowledge on all dependencies that may affect the operation of the plant. Fuzzy controllers are more robust as compared to PID controllers because they have a wider range of operating conditions and

can tolerate with noise and disturbances (Coleman and Godbole, 1994). Fuzzy control is suitable for the system where its mathematical model is difficult to be derived and its dynamic characteristics are not easy to be quantified. Datta and Senjyu (2013) have proposed a fuzzy control strategy for energy storage systems to address the frequency fluctuation problem introduced by the large penetration of PV power and sudden load variation. The proposed method is evaluated under various insolation and load variations where its mathematical expressions are difficult to be obtained. A fuzzy droop control loop adjustment has been proposed to investigate the performance of energy storage system in smoothing the variations at the prime energy generator in AC microgrid (Diaz et al., 2015). The proposed fuzzy control method weights the action of conventional droop control loops for energy storage system in order to balance their stored energy. A decentralized fuzzy-based strategy has been proposed for a low voltage DC microgrid with energy storage system to balance and prevent the deep discharge of energy storage units (Diaz et al., 2014). The proposed strategy takes into account the different stages required for charging and discharging the energy storage to assure good energy balance and low voltage deviation. Although there are many fuzzy control algorithms developed for the emerging energy storage system, there are a handful of studies carried out in fuzzy control for peak demand reduction. The advantages of the fuzzy logic control are summarized as follows (Guanrong and Trung Tat, 2001; Pedro and Antonio, 1998):

- Fuzzy logic describes plants in terms of a combination of numeric and linguistics. This has advantages over pure mathematical approaches or pure symbolic approaches because the system knowledge is usually

available in such a combination.

- Fuzzy logic algorithms are easier to be understood than the mathematical descriptions because it use the intuitive linguistic description.
- The end-user is able to interpret the parameters effectively because the control and supervision use the language that can be easily understood.
- Fuzzy logic can tackle the control problems where its exact mathematic model is difficult to be derived or is only available for very restricted conditions.
- The fuzzy logic controller is more robust as compared to the conventional PID controller because it is insusceptible to changing environments.
- The fuzzy logic controller can incorporate a conventional PID and fine-tune it to certain plant nonlinearities due to its capabilities of universal approximation.
- Fuzzy logic algorithms have shorter development time as compared to that of the conventional methods.
- Fuzzy logic algorithms can be described with little data and require relatively less memory.
- The reasoning process is often simple as compared to that of the mathematically precise systems. Hence, the fuzzy logic controller occupies less computing power.

Although fuzzy logic controller has many advantages over the conventional PID control, it does not fit every problem. The drawbacks of the fuzzy logic controller are as follows:



- Fuzzy logic algorithms are suitable only for the trivial problems that do not require high accuracy. For example, the highly damped low-level systems.
- In areas that have profound mathematical models, the performance of the conventional controllers is better than that of the fuzzy logic controllers.
- The characteristics of fuzzy inference system are difficult to be proved in most cases because of lacking mathematical descriptions.
- Thousands of different fuzzy system configurations can be formulated depending on conjunction, disjunction, implication, and defuzzification choices. This increase the complexity in determining the optimal fuzzy inference system.
- Fuzzy logic controllers are more suitable for use on higher levels of system control such as decision-making process. It is not an alternative for the lower level controls such as speed and position controllers.

### **6.3 Fuzzy Inference System**

The classical set theory is established on the fundamental concept of ‘set’ which an individual is either a member or non-member. It is not allowed to have an element that is in a set and not in the set at the same time in the classical set theory. On the contrary, fuzzy set theory accepts partial memberships. Fuzzy sets are a set whose elements have the degrees of membership. The set

membership values can range between 0 and 1 and is not restricted to the two truth values, namely the true or false values.

Generally, fuzzy inference system has three main developing processes, namely fuzzification, inference, and defuzzification. Fuzzification is a process of converting the crisp quantity into the grades of membership for the linguistic terms of fuzzy sets. Fuzzy statements in the antecedent are resolved into a degree of membership between zero and one. Fuzzy inference is a method of deductive reasoning that incorporates human expert's knowledge about the system. The 'If-Then' rules are established for each fuzzy set. The fuzzy output set is converted into a crisp number in defuzzification process before it is output to the system. The general fuzzy inference system is illustrated in Figure 6.1.

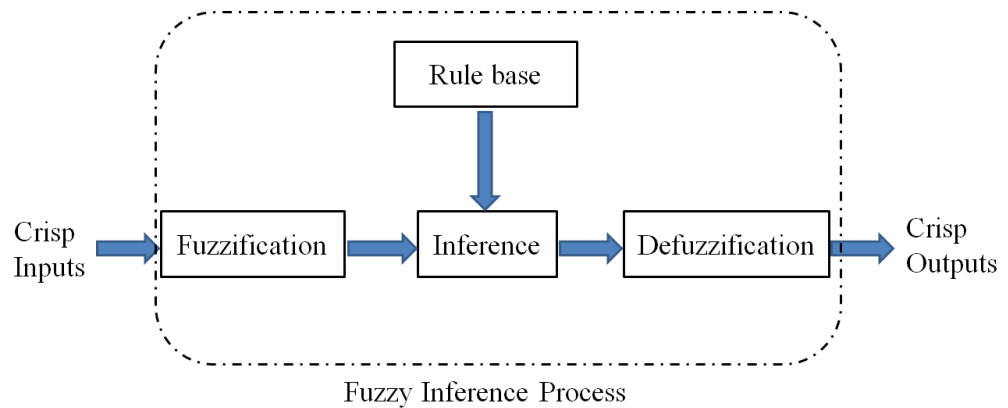


**Figure 6.1: General fuzzy inference system**

## 6.4 Fuzzy-based Control Algorithm

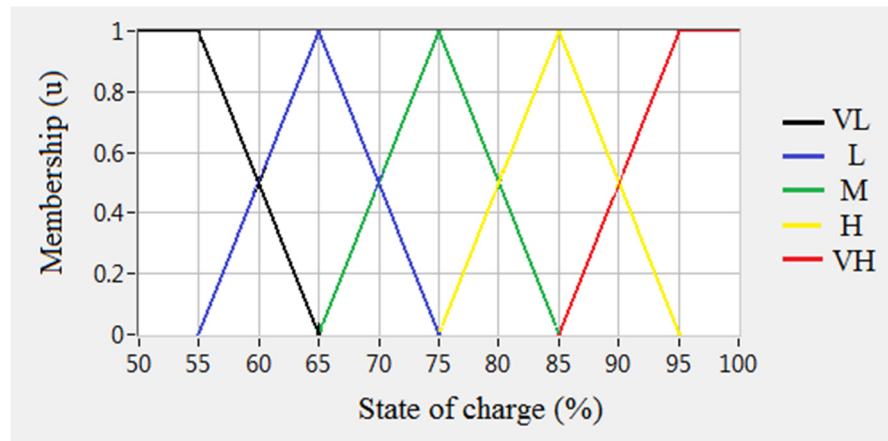
### 6.4.1 Fuzzy Sets and Membership Functions for the Energy Storage System

The fuzzy-based control algorithm developed for peak reduction takes into account the SOC or useable energy ( $E_U$ ) during the time of operation ( $t_{op}$ ) to determine the amount of power to be delivered to the grid during the peak shaving process. The  $t_{op}$  is defined as the time where the energy storage begins to supply its power. When the  $E_U$  has declined at the certain time, the power injection from the energy storage system is also decreased to ensure that the  $E_U$  can be sustained until the end of the peak shaving process. The input variables for the fuzzy-based controller are the SOC of the batteries and the  $t_{op}$  while the output variable is the power injection of the energy storage system ( $P_{ES}$ ). The crisp inputs and output are fuzzificated into fuzzy sets that can be characterized by membership functions. Instead of denoting the inputs and output with values, the fuzzy sets express the inputs and output with a vague description. Table 6.1 shows the definition of the fuzzy sets of the SOC,  $t_{op}$ , and  $P_{ES}$  in linguistic terms. There are five membership functions for both the SOC and the  $P_{ES}$  while there are seven membership functions for the  $t_{op}$ .

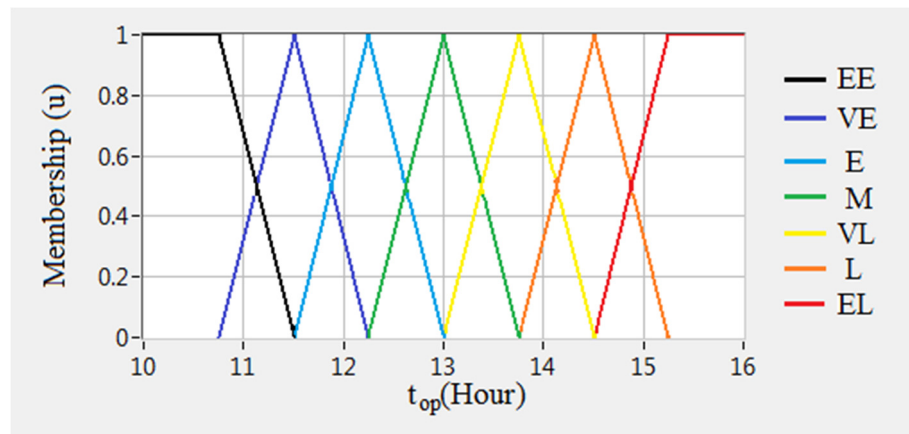
**Table 6.1: Definition of the fuzzy sets of the SOC,  $t_{op}$  and  $P_{ES}$  in linguistic variables**

SOC	Time of Operation ( $t_{op}$ )	$P_{ES}$
VL – Very Low	EE – Extremely Early	VL – Very Low
L – Low	VE – Very Early	L – Low
M – Middle	E – Early	M – Middle
H – High	M – Middle	H – High
VH – Very High	L – Late	VH – Very High
	VL – Very Late	
	EL – Extremely Late	

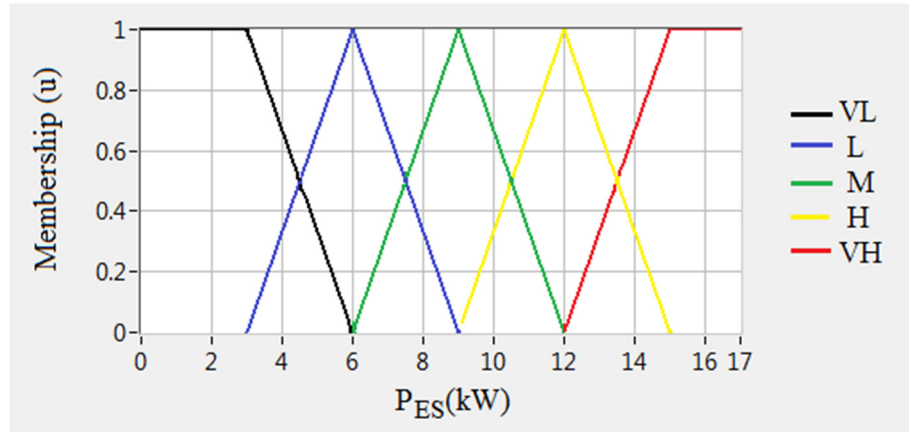
The fuzzy inference system is developed using the Fuzzy System Designer Toolbox in LabVIEW™. There are two basic fuzzy system inference method, namely Mamdani and Takagi-Sugeno inference method. In this study, a Mamdani’s fuzzy inference method is adopted because it is the most commonly used fuzzy methodology in control systems. The SOC is set in the range of 50 % to 95 % while the  $t_{op}$  is set in the range of 10:00 to 15:15. The range of  $P_{ES}$  is set in the range of 0 kW to 15 kW. The membership functions of the SOC,  $t_{op}$  and  $P_{ES}$  are illustrated in Figure 6.2.



(a)



(b)



(c)

**Figure 6.2: Membership functions of (a) SOC, (b)  $t_{op}$ , and (c)  $P_{ES}$**

#### 6.4.2 Fuzzy Inference Rules for the Energy Storage System

The rules in the fuzzy inference system are derived from the desired responses of the energy storage system based on the predicted load demands. An algorithm is developed to obtain the fuzzy inference rules based on the desired responses of the energy storage system at the specific  $t_{op}$  for a specific SOC. Figure 6.3 shows the flow chart of the algorithm developed to optimize the  $P_{ES}$  of the energy storage system.

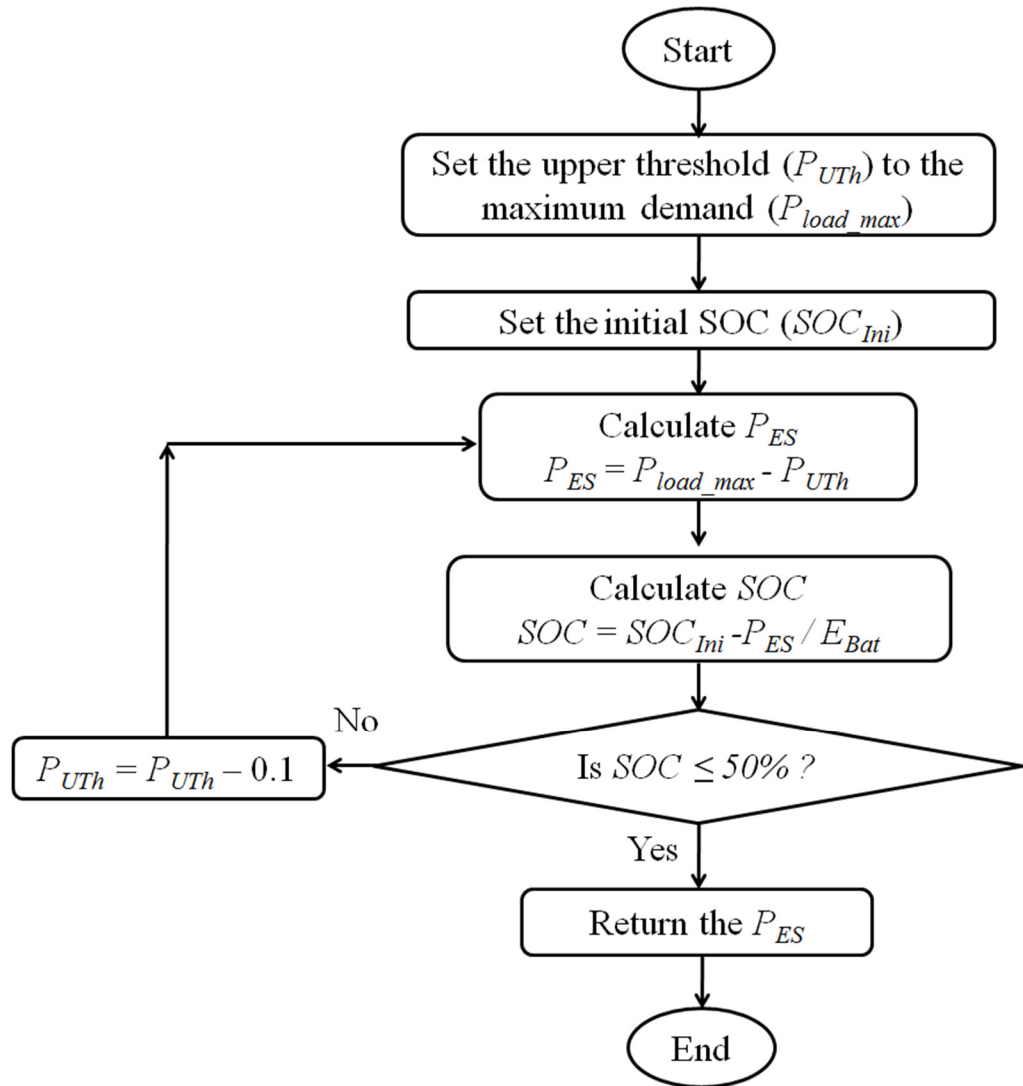


**Figure 6.3: Flow chart of the algorithm developed to optimize the  $P_{ES}$  of the energy storage system**

There are five fuzzy sets for the SOC, namely the VL, L, M, H, and VH. Hence, it is required to execute the algorithm for five times using five initial SOC ( $SOC_{Ini}$ ), namely 55 %, 65 %, 75 %, 85 %, and 95 %, which is corresponding to the SOC fuzzy sets of VL, L, M, H, and VH, respectively. The  $SOC_{Ini}$  is set at 55 % for the first execution of the algorithm. The  $P_{UTH}$  is set to the forecasted maximum demand ( $P_{load\_max}$ ). The  $P_{ES}$  is determined using the equation as follows:

$$P_{ES} = P_{load\_max} - P_{UTh} \quad (6.1)$$

Initially, the value of the  $P_{ES}$  is zero because the value of the  $P_{UTh}$  is same as  $P_{load\_max}$ . Then, the SOC of the battery is calculated using the following equation:

$$SOC = SOC_{Ini} - \frac{P_{ES}}{E_{Bat}} \quad (6.2)$$

where  $E_{Bat}$  is the total capacity of the battery bank. If the SOC is greater than 50 %, then the  $P_{UTh}$  is subtracted by 0.1 kW. This is to deduct the  $P_{UTh}$  iteratively from its initial value to the desired value. Then, the  $P_{ES}$  and the SOC are re-calculated. The process is repeated until the SOC is equal to or less than 50 %. Finally, the  $P_{ES}$  is obtained. The algorithm is then executed for different  $SOC_{Ini}$ . Table 6.2 shows the values of the fuzzificated SOC,  $t_{op}$ , and the corresponding  $P_{ES}$  of the fuzzy controller.

**Table 6.2: The fuzzificated SOC,  $t_{op}$  and the corresponding  $P_{ES}$  of the fuzzy controller**

<b>SOC</b> <i>t<sub>op</sub></i>	VL	L	M	H	VH
EE	VL	VL	VL	VL	VL
VE	VL	VL	VL	VL	VL
E	VL	L	L	M	M
M	VL	L	M	M	H
L	L	M	H	VH	VH
VL	M	H	VH	VH	VH
EL	M	H	VH	VH	VH

The fuzzy inference rules are keyed into the Fuzzy System Designer Toolbox as shown in Figure 6.4. The defuzzification method chosen for this study is the center of area (COA). The AND antecedent with minimum consequent implication is chosen.

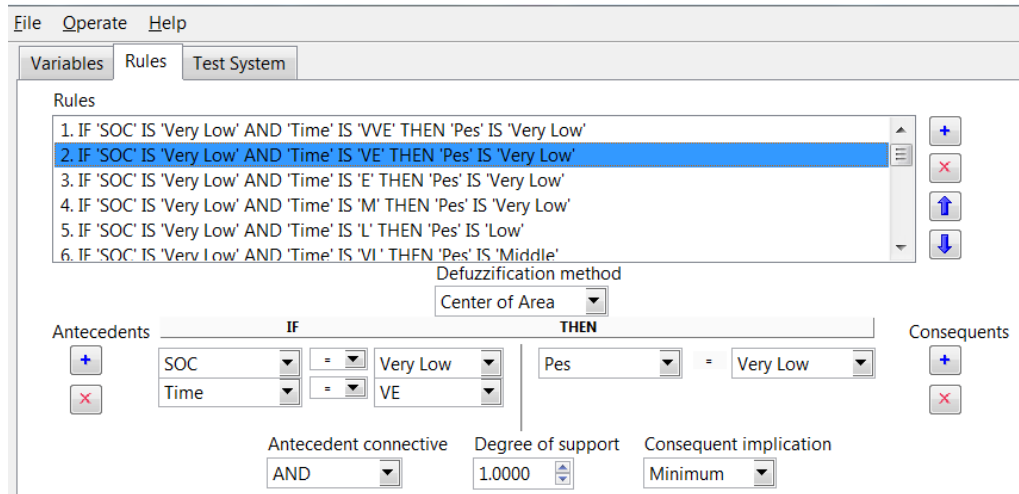


**Figure 6.4: Fuzzy inference rules in the Fuzzy System Designer Toolbox**

A surface chart as shown in Figure 6.5 shows a three-dimensional surface of the SOC,  $t_{op}$  and  $P_{ES}$  plotted from the surface viewer in the Fuzzy System Designer toolbox. The surface chart indicates the optimal  $P_{ES}$  to be delivered by the energy storage system based on SOC and  $t_{op}$ . For example, if the time is 14:00 and the SOC is 100 %, then the  $P_{ES}$  to be delivered by the energy storage system is 15 kW.

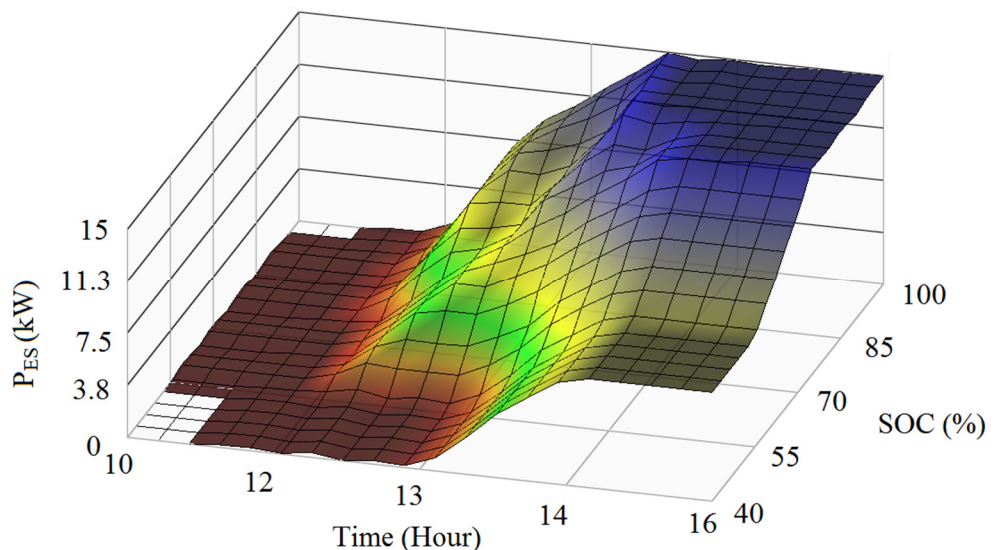


**Figure 6.5: Surface chart of the SOC,  $t_{op}$  and  $P_{ES}$  plotted using the surface viewer in the LabVIEW Fuzzy System Designer toolbox**



## 6.5 Experimental Results

Experiments are carried out at the SE block and KA block. Case study 1, case study 2, and case study 3 are the results obtained from the experiments carried out at SE block while case study 4 and case study 5 are the result obtained from the experiments carried out at KA block. Case study 1 shows the peak reduction when the predicted peak demand is close to its actual value. Case study 2 illustrates the scenario where the peak demand is unexpectedly high. Case study 3 demonstrates the scenario where the actual peak demand occurs for a much longer duration than the expected duration. Case study 4 and case study 5 show the scenario where the peak demand is much earlier than the expectation.

### 6.5.1 Case study 1: Predicted Peak Demand is Close to Actual Value

In the case study 1, the  $P_{UTh}$  and  $P_{LTh}$  are set at 81 kW and 30 kW, respectively. The predicted peak demand is 95 kW while the actual peak demand is 93.8 kW. It can be seen that at 12:45,  $P_{load}$  is greater than  $P_{UTh}$  and the energy storage system begins to deliver power to the grid such that  $P_{grid}$  is not higher than  $P_{UTh}$ . Figure 6.6 shows the experimental results for the case study 1. The peak demand has been reduced from 93.8 kW to 82.7 kW. The peak demand reduction for this case is 11.1 kW.

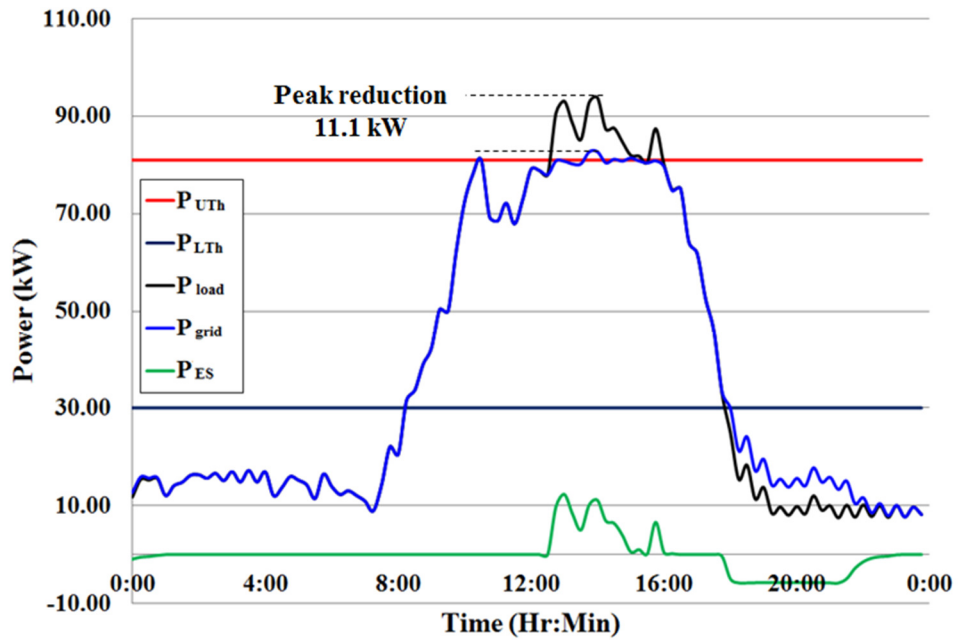


**Figure 6.6: The peak reduction using the fuzzy-based control algorithm for the case study 1**

### 6.5.2 Case Study 2: Peak Demand is Unexpectedly High

In this case, the  $P_{UTh}$  and  $P_{LTh}$  are set at 80 kW and 30 kW, respectively. The estimated peak demand is 95 kW. At 10:30,  $P_{load}$  is greater than  $P_{UTh}$  and the energy storage system begins to deliver power to the grid such that  $P_{grid}$  is not higher than  $P_{UTh}$ . It can be seen that at 13:45,  $P_{load}$  has reached 100.5 kW and it is higher than the estimated peak demand. The fuzzy-based controller delivers up to 12.1 kW instead of its full capacity of 15 kW to preserve energy so that the remaining energy is sufficient to shave the peak for the rest of time. Figure 6.7 shows the experimental results for the case study 2. The peak demand has been reduced from 100.5 kW to 88.4 kW. The peak demand reduction for this case is 12.1 kW.

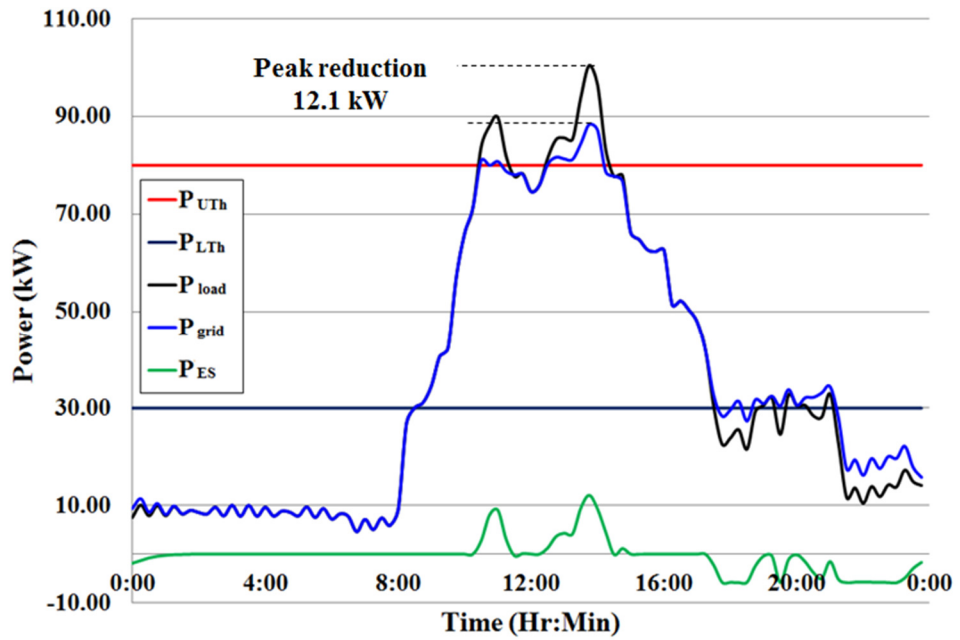


**Figure 6.7: The peak reduction using the fuzzy-based control algorithm for the case study 2**

### 6.5.3 Case Study 3: Actual Peak Demand Occurs for a Much Longer Duration

In this case,  $P_{UTh}$  and  $P_{LTh}$  are set at 70.1 kW and 30 kW, respectively. The energy storage system begins to deliver power to the grid at 10:45 when  $P_{load}$  is greater than  $P_{UTh}$ . It can be seen that at 13:15, the fuzzy-based controller begins to restrict the power delivered to the load because the useable energy in the batteries has decreased and the energy storage system may not have enough energy to sustain the delivery of its power over the rest of the time. Figure 6.8 shows the experimental results for the case study 3. The peak demand has been reduced from 81.8 kW to 75.6 kW. The peak demand shaved for this case is 6.2 kW.

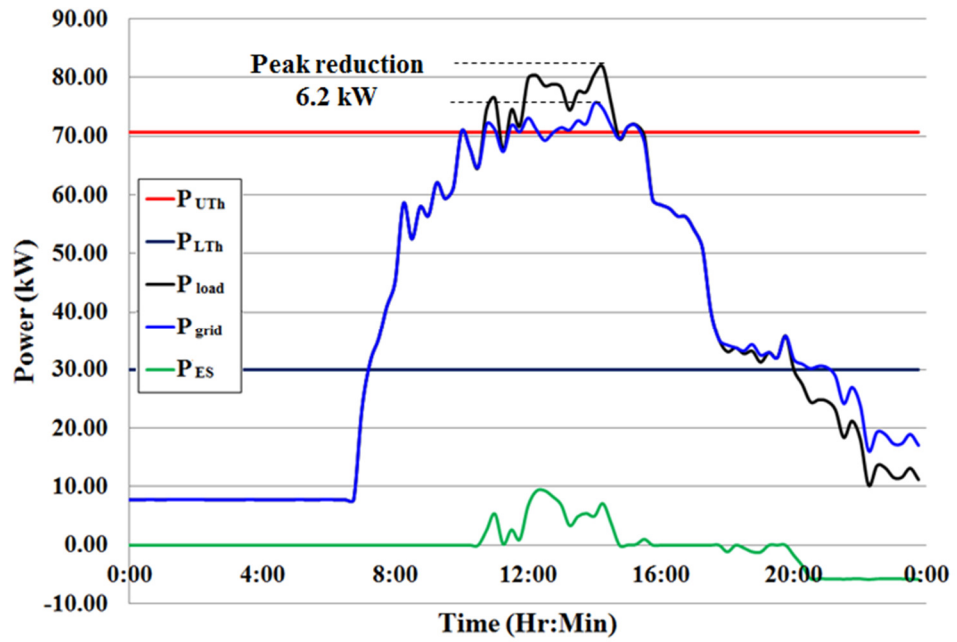


**Figure 6.8: The peak reduction using the fuzzy-based control algorithm for the case study 3**

#### **6.5.4 Case Studies 4 & 5: Peak Demand Occurs Much Earlier Than the Predicted Time of Occurrence**

In the case study 4,  $P_{UTh}$  and  $P_{LTh}$  are set at 70 kW and 50 kW, respectively. The peak demand occurs earlier than the predicted time of occurrence at 6:45. It can be seen that at 9:30 when  $P_{load}$  is 80 kW, the energy storage system restricts the power injection to only 5.9 kW in order to preserve energy for the rest of the time. Figure 6.9 shows the experimental results for the case study 4. The peak demand has been reduced from 82.2 kW to 74 kW. The peak demand shaved for this case is 8.2 kW.

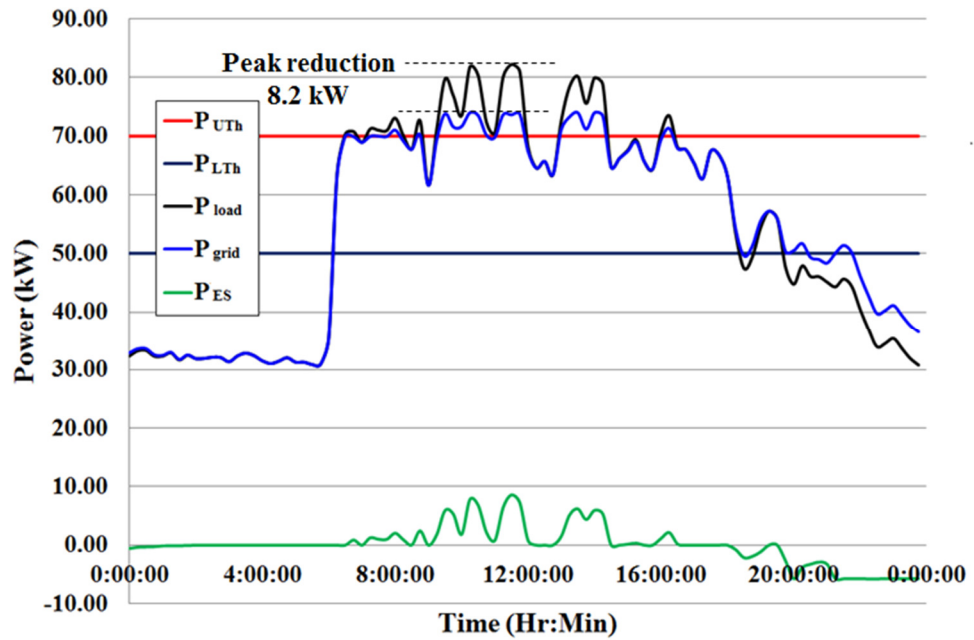


**Figure 6.9: The peak reduction using the fuzzy-based control algorithm for the case study 4**

In the case study 5,  $P_{UTh}$  and  $P_{LTh}$  are set at 72 kW and 50 kW, respectively. The peak demand occurs earlier than the predicted time of occurrence at 6:45. It can be seen that at 6:30 when  $P_{load}$  has exceeded 72 kW, the energy storage system begins to deliver power to the load. At 6:45, the energy storage system restricts the power injection to only 5.2 kW when  $P_{load}$  has reached 81.1 kW in order to preserve energy for the rest of the time. Figure 6.10 shows the experimental results for the case study 5. The peak demand has been reduced from 89.4 kW to 80 kW. The peak demand shaved for this case is 9.4 kW.

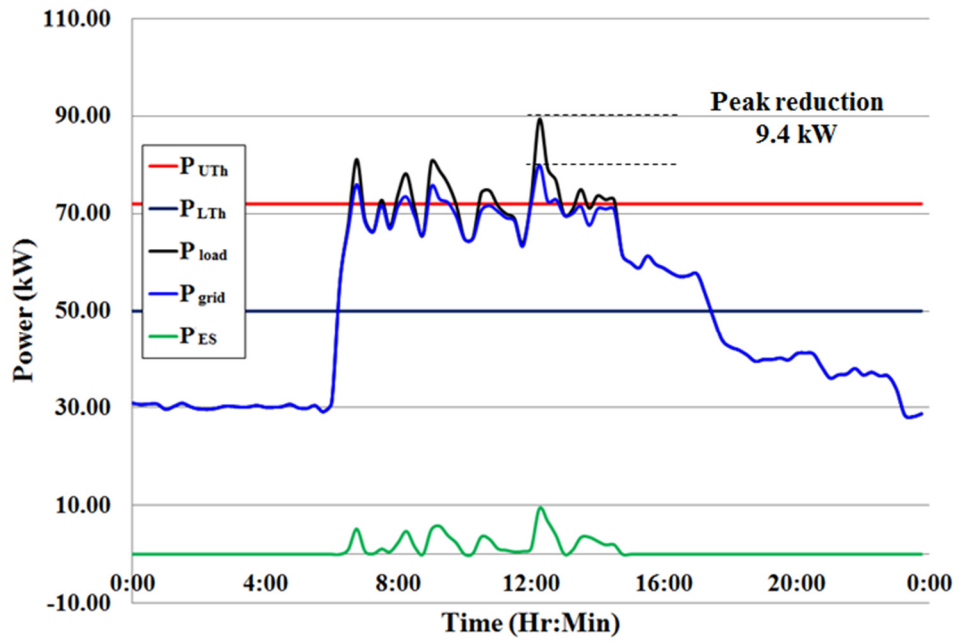


**Figure 6.10: The peak reduction using the fuzzy-based control algorithm for the case study 5**

Table 6. 3 shows the summary of the electricity bill savings using fuzzy-based control algorithm. The tariff used to calculate the bill saving is based on the medium voltage general commercial tariff (C1) where the maximum demand charge is RM 45.1/ kW.

**Table 6. 3: Summary of the electricity bill saving using fuzzy-based control algorithm**

Case study	Peak reduction (kW)	Bill saving (RM)	Bill saving (%)
1	11.1	500.6	11.8
2	12.1	545.7	12.0
3	6.2	279.6	7.6
4	8.2	369.8	10.0
5	9.4	423.9	10.5

## 6.6 Performance Comparisons of the Three Control Algorithms

The performance of the fuzzy-based control algorithm is compared with the performance of the fixed-threshold and adaptive-threshold control algorithms obtained in chapter 5. A performance evaluation index, peak reduction factor, is introduced to assess the performance of different control algorithms for energy storage system in peak reduction. The peak reduction factor ( $K_{PS}$ ) is defined as a ratio of the peak power reduction ( $P_{shaved}$ ) to the maximum achievable peak reduction ( $P_{maxshave}$ ) as shown in the following equation:

$$K_{PS} = \frac{P_{shaved}}{P_{maxshave}} \quad (6.3)$$

A high  $K_{PS}$  shows that the power capacity of the energy storage system has been effectively used for peak reduction while a low  $K_{PS}$  implies that the power capacity of the energy storage system is under-utilized and the energy storage system is not operated at its optimal level. The performance of the three control algorithms for SE block and KA block are summarized in Table 6.4. It can be seen that the fuzzy-based controller has the highest peak reduction factor as compared to that of the fixed-threshold and adaptive-threshold controllers.

**Table 6.4: Performances summary of the fixed-threshold, adaptive-threshold and fuzzy-based control algorithms**

Building	Case	Peak reduction factor		
		Fixed-threshold	Adaptive-threshold	Fuzzy-based
SE block	1	0.43	0.40	0.60
	2	0.51	0.78	0.81
	3	0.47	0.40	0.82
	4	0.45	0.63	0.47
	5	0.42	0.65	0.61

	6	0.49	0.79	0.63
KA	7	0.76	0.80	0.66
block	8	0.63	0.41	0.59
Average		0.52	0.61	0.65

## 6.7 Summary

It is not economically viable to install a large energy storage system for the purpose of shaving the peak demand of a building because the cost of the batteries is high. The energy storage system needs an appropriate controller to deliver an appropriate amount of power at the right timing with its limited energy as well as power rating in order to achieve the optimal peak reduction. This chapter presents a novel fuzzy-based control algorithm to reduce the peak demand of the building effectively. The fuzzy-based control algorithm has overcome the problem arise due to the high peak demand as well as the actual peak demand occurs for a much longer duration than the predicted duration. By estimating the useable energy from the batteries using their SOC level and incorporating it into the fuzzy inference rules, the fuzzy-based control algorithm can determine the appropriate output power to be delivered to the load in order to prevent insufficient energy supply from the batteries. The fuzzy-based control algorithm is capable of incorporating a priori qualitative knowledge and expertise about the load characteristic of the buildings as well as the useable energy of the energy storage in peak demand reduction. The experimental results show that the fuzzy-based control algorithm has achieved the highest performance in peak reduction as compared to that of the fixed-threshold and adaptive-threshold control algorithms.



## CHAPTER 7

### COST-BENEFIT ASSESSMENT OF ENERGY STORAGE FOR UTILITY AND CUSTOMERS

#### 7.1 Introduction

Under the existing commercial framework of electricity in Malaysia, commercial and industrial customers are required to pay their peak power demand charge every month. Usually, the peak demand charge can contribute to about 30 % of their electricity bills due to the use of open-cycle gas power plants that deliver expensive electricity to the customers. Therefore, alternative means are sought after in order to reduce the peak demand of the customers. Distributed small-scaled energy storage can offer a good option to reduce the peak demand for commercial and industrial customers.

In this chapter, the financial benefits of using energy storage to reduce peak demand are evaluated. An energy dispatch model is developed in Hybrid Optimization Model for Electric Renewables (HOMER) software to determine the cost of electricity (COE) for the system with and without energy storage. The model considers the heat rates of power plants in calculating the COE under different regulatory frameworks of natural gas with various prices of battery components. Apart from that, the cost-benefit for the customers under various electric tariff structures is also evaluated. Four battery storage technologies,

namely lead acid, vanadium redox flow, zinc-bromine, and lithium-ion are considered in this research work. The tariffs that are currently applied to the commercial and industrial sectors are chosen for the evaluations. The COE obtained from the simulations for the cases with gas subsidy and without gas subsidy are compared. The deferral cost of reinforcement of the T&D infrastructure and the reduction of CO<sub>2</sub> emission cost are also evaluated.

## 7.2 Power Demand and Generation in Malaysia

The growth of Gross Domestic Product (GDP) is an important indicator for the power demand growth worldwide (Borozan, 2013; Coers and Sanders, 2013). In Malaysia, GDP is one of the key elements in determining future demand growth. Table 7.1 shows the comparison of periodical average growth rates of GDP with electricity sales, generation, and peak demand during the period between 2012 and 2030. The predicted peak demand growth increases the pressure and challenges to the utility to build more power plants as well as reinforce the existing transmission and distribution (T&D) infrastructure.

**Table 7.1: Comparison of periodical average growth rates of GDP with electricity sales, generation, and peak demand during the period between 2012 and 2030**

Period	Average period growth rates (% p.a.)			
	GDP <sup>a</sup>	Electricity Sales <sup>a</sup>	Generation <sup>a</sup>	Peak Demand <sup>a</sup>
2012 - 2015	5.7	4.2	3.7	3.6
2016 - 2020	5.9	3.6	3.4	3.3
2021 - 2030	6.2	1.9	1.7	1.6

Footnotes:

Data collected from (Energy Commission, 2013)

The operation of the electric power system is carried out by committing and dispatching various types of generators in order to meet the varying power demand. The dispatch of power plants is aided by using simulation software taking into account many constraints imposed by different generators, such as ramp rates, minimum loading, and heat rate. Generally, power plants are classified into base load power plants, intermediate power plants and peak load power plants to meet the fluctuating power demand. Figure 7.1 shows the typical mixture of generation in Malaysia on 1 July 2013. It can be seen that the coal-fired power plants are used as base load power plants whose power output are consistent throughout the day. Combined-cycle gas turbines (CCGT) are used as intermediate power plants. The peak power generations are formed by open-cycle gas turbine (OCGT), co-generation (Co-Gen), hydro, oil steam turbine (ST-Oil) gas steam turbine (ST-Gas), and interconnection with Thailand and Singapore. The generation fleet offers the grid operator the flexibility to achieve economic dispatch of power plants while maintaining the stability and reliability of the power supply.

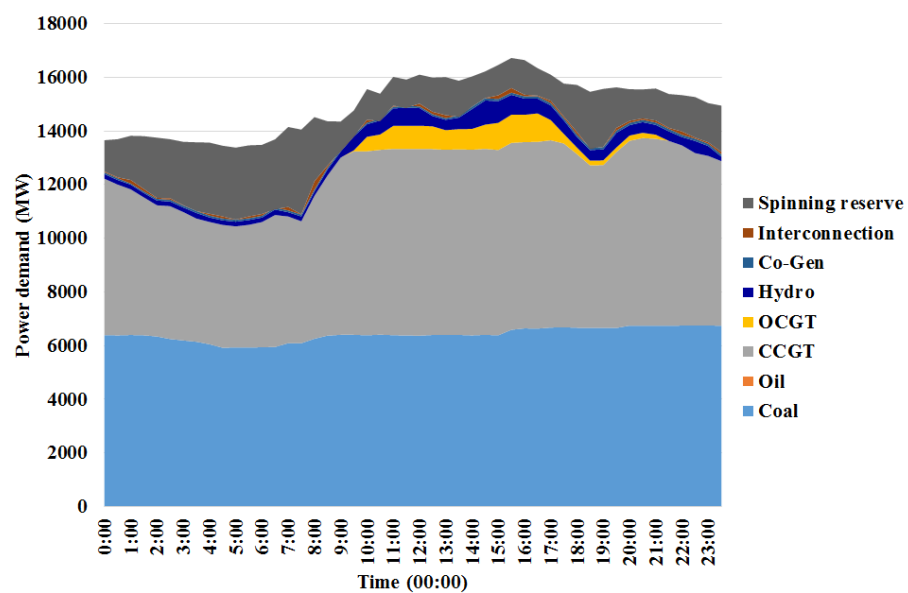


**Figure 7.1: Generation profile of Malaysia on 1 July 2013**

Figure 7.2 shows the electricity generation portfolios of Malaysia in 2013. The OCGT are dedicated as peak power generating units because they are capable of being interconnected with the grid within 5 to 10 minutes from initiation to synchronization. It can be seen that the OCGT contributes to 11 % to the overall installed capacity (Suruhanjaya Tenaga Malaysia, 2013).

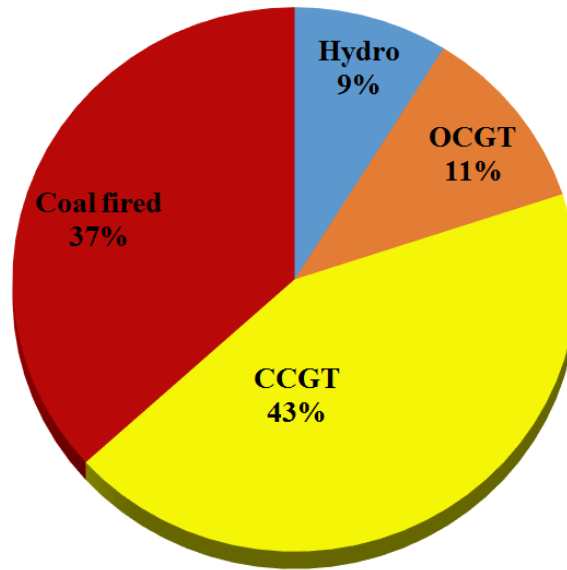


**Figure 7.2: Electricity generation portfolios of Malaysia in 2013**

In Malaysia, the tariffs for the commercial and industrial consumers are still one of the lowest among the ASEAN countries because the natural gas supply for the electricity sector is heavily subsidized by the government. However, the Malaysian government has set out a schedule of subsidy reductions for gas via Subsidy Rationalization Program (SRP) to increase the gas price for power and industrial sectors by RM3/ mmbtu every six months from 2010 to 2014 (IISD, 2013). However, the actual implementation is behind the proposed schedule. As of November 2014, the gas price for power sector is RM15.2/ mmbtu while the market price was around RM35/ mmbtu to RM44/ mmbtu. In this research

work, the sensitivity analysis is carried out for cases with and without gas subsidy (Malaysian Gas Association, 2014).

### **7.3 Methodology**

A system with ESS and without ESS systems are modelled in HOMER. HOMER performs three main tasks, namely simulation, optimization and sensitivity analysis. In the optimization analysis, HOMER calculates the optimal system configurations with the minimum total net present cost to meet the constraints defined by users. In the sensitivity analysis, various possible system configurations and factors that have the greatest impact on the design and operation of the system can be evaluated. The optimization and sensitivity analysis provide solutions to the challenges arising from the large number of design options and the variability of parameters, such as future fuel prices, load growth, and increment of operation and maintenance cost.

#### **7.3.1 Introduction to HOMER**

Hybrid energy systems that incorporate renewable energy resources and energy storage have been widely utilized for supplying power in urban and rural areas. Due to the complexities of design and operations, the hybrid energy systems require a sophisticated analytical tool to perform techno-economic analyses. There are various software available for hybrid energy system analysis such as

HOMER, SOMES, Hybrid2, ARES, INSEL, iHOGA, etc (Sinha and Chandel, 2014). In this research work, HOMER is chosen for cost-benefit analysis because the software enables users to carry out feasibility study, optimization, and sensitivity analysis for various system configurations. It is developed by the National Renewable Energy Laboratory (NREL) of the United States to simplify the design evaluation of both off-grid and grid-connected power systems. HOMER facilitates the design process by taking into account various parameters such as the size of components, technology options and its costs, fuel costs, availability of energy resources, and many possible system configurations.

Users can develop their model in single-line schematic easily using HOMER. Various technology options and component costs can be used to simulate different system configurations or combinations of components, and generates results that can be viewed as a list of feasible configurations according to the sorting preference. The results can also be displayed in a wide variety of tables and graphs to ease the comparisons and evaluations. These tables and graphs can also be exported to Microsoft Excel as data or to web browser as reports. HOMER provides users options to explore the effect that changes and changing factors such as resource availability as well as economic conditions using sensitivity analyses.

There are three main operating tasks in HOMER, namely simulation, optimization, and sensitivity analysis. HOMER simulates the operation of a system based on the energy balance calculations in each time step of the year.

For the system that comprises of energy storage or fuel-powered generators, the operation of these components is decided by HOMER based on the built in optimal energy dispatch algorithm. All the possible system configurations are simulated and sorted by net present cost for users to compare the system design options. The sensitivity analysis can be carried out to identify the factors that have the greatest impact on the design and operation of the power system. Figure 7.3 shows the user interface of the HOMER software. A power system can be modelled by adding components to the schematic.

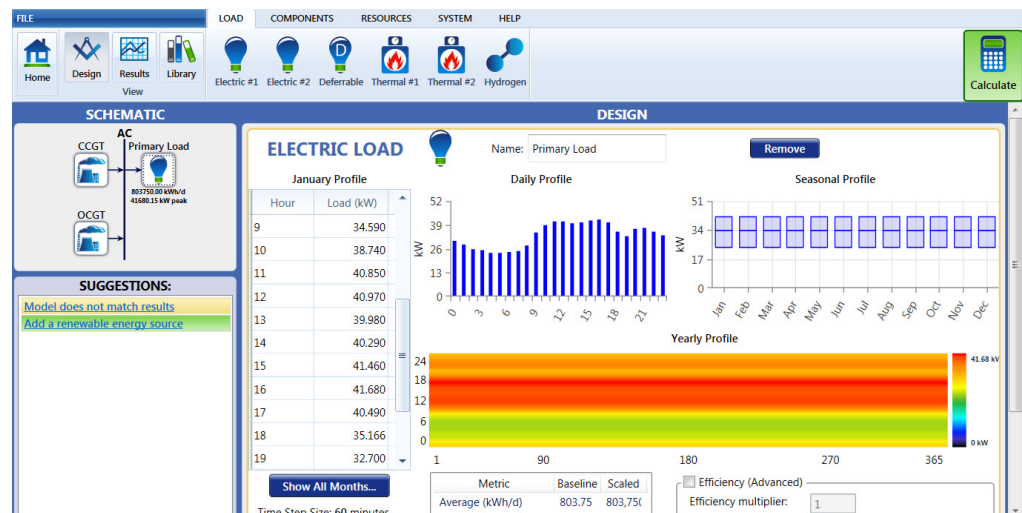


**Figure 7.3: User interface of the HOMER software**

### 7.3.2 Electrical System Configuration

The power system with ESS and without ESS are modelled in HOMER as illustrated in Figure 7.4. The system without ESS is formed by a CCGT, an OCGT, and an electrical load. The CCGT acts as the grid and OCGT acts as the peaking power plant. In the second model, the same CCGT and load are used but the OCGT is replaced by ESS in order to study the effect of replacing the

OCGT on the COE and CO<sub>2</sub> emission. If the grid block-set is used instead of the CCGT and OCGT block-sets, then the grid will supply all the power including the peak power throughout the time and therefore be impossible to study the effect of replacing the OCGT.

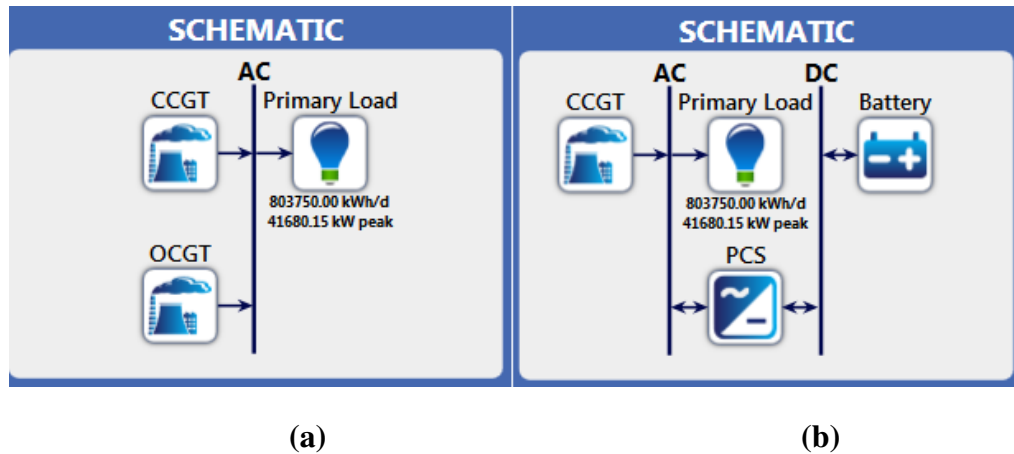


**Figure 7.4: Schematic of electrical system in HOMER for (a) System without ESS and (b) System with ESS**

The economic inputs such as discount rate, inflation rate, and project lifetime can be set in the project set up in HOMER. There are 4 tabs under the project set up, namely economics, system control, emissions, and constraints. Figure 7.5 shows the parameters under the economics tab. The discount rate and inflation rate are set at 6 % and 2 %, respectively (Anna and Lucky, 2014; Siong Lee et al., 2011). The project lifetime is set at 20 years based on the lifetime of OCGT and CCGT.



## PROJECT SET UP



Economics	System Control	Emissions	Constraints
Discount rate (%):	6.00	{..}	
Expected inflation rate (%):	2.00	{..}	
Project lifetime (years):	20.00	{..}	
System fixed capital cost (RM):	0.00	{..}	
System fixed O&M cost (RM/yr)	0.00	{..}	
Capacity shortage penalty (RM/kWh)	0.00	{..}	

**Figure 7.5: Parameters under the economics tab**

HOMER allows users to model two dispatch strategies, namely the load following and cycle charging strategy. If the load following strategy is chosen, then the generator will only produce enough power to meet the demand. Battery storage system will be charged only by renewable energy source connected to the system. Load following strategy tends to be optimal in systems with high penetration of renewable energy in which the renewable power output exceeds the load demand. Under the cycle charging strategy, the generator is operated at its full capacity with the surplus power being stored in the battery bank. Cycle charging tends to be optimal in systems with low or no renewable energy penetration. If both strategies are selected, HOMER will simulate each system using both dispatch strategies for comparison. In this research work, the cycle charging dispatch strategy is selected for the system with CCGT and ESS. Under this strategy, the generator operates at full capacity with the surplus

power charging the ESS. Under the system control tab, the economic minimization is chosen for the optimization option as illustrated in Figure 7.6. Under the advanced option, multiple generators are allowed to operate simultaneously in the system. The time step chosen for the simulation is 60 minutes and the total number of steps per year is 8760.

**PROJECT SET UP**

Economics System Control Emissions Constraints

Engine Extension: [Dropdown]

Economic minimization  
 Fuel minimization  
 Weight minimization

Dispatch Strategy

Load following  
 Cycle charging  
 Apply setpoint state of charge (%): 80.00 [Reset]  
 Allow diesel-off operation

Advanced


Allow systems with multiple generators.  
 Allow generators to operate simultaneously.  
 Allow systems with two types of wind turbines.  
 Limit excess thermal output (% of load): 10  
 Issue a warning if an off-grid system has:  
 maximum renewable penetration greater than 55%  
 battery autonomy of less than 2 hrs  
 Allow systems with generator capacity less than peak load

Simulation













Minutes per time step: 60 [Dropdown]  
 Number of time steps per year: 8,760

**Figure 7.6: Parameters under the system control tab**

Users can define the emission penalties for greenhouse gas emissions under the emissions tab as illustrated in Figure 7.7. The emission penalties in this case study is set to zero.


**PROJECT SET UP** 

Economics System Control Emissions Constraints







Emissions Penalties	Limits on Emissions
Carbon dioxide (RM/t): 0.00 	<input type="checkbox"/> Carbon dioxide (kg/yr): 0.00 
Carbon monoxide (RM/t): 0.00 	<input type="checkbox"/> Carbon monoxide (kg/yr): 0.00 
Unburned hydrocarbons (RM/t): 0.00 	<input type="checkbox"/> Unburned hydrocarbons (kg/yr): 0.00 
Particulate matter (RM/t): 0.00 	<input type="checkbox"/> Particulate matter (kg/yr): 0.00 
Sulfur dioxide (RM/t): 0.00 	<input type="checkbox"/> Sulfur dioxide (kg/yr): 0.00 
Nitrogen oxides (RM/t): 0.00 	<input type="checkbox"/> Nitrogen oxides (kg/yr): 0.00 

**Figure 7.7: Parameters in the emissions tab**

Under the constraints tab, users can set the maximum annual capacity shortage, minimum renewable fraction, and operating reserve as shown in Figure 7.8. The operating reserve can be defined either as a percentage of load or as a percentage of renewable output.

**PROJECT SET UP** 

Economics System Control Emissions Constraints

Maximum annual capacity shortage (%):	100.00 
Minimum renewable fraction (%):	0.00 
<b>Operating Reserve</b>	
As a percentage of load	
Load in current time step (%):	0.00 
Annual peak load (%):	0.00 
As a percentage renewable output	
Solar power output (%):	0.00 
Wind power output (%):	0.00 

**Figure 7.8: Parameters in the constraints tab**

### 7.3.3 Electric Load Profile

The generation profile of the CCGT and OCGT on 1 July 2013 is chosen as the electrical load profile for the investigation because it exhibits the generic daily generation profile in Malaysia. Due to the constraints of HOMER, the actual load profile is scaled down from the peak of 7959 MW to 41.68 MW. The total daily energy consumption is 803.75MWh. The daily electrical load profile is shown in Figure 7.9.

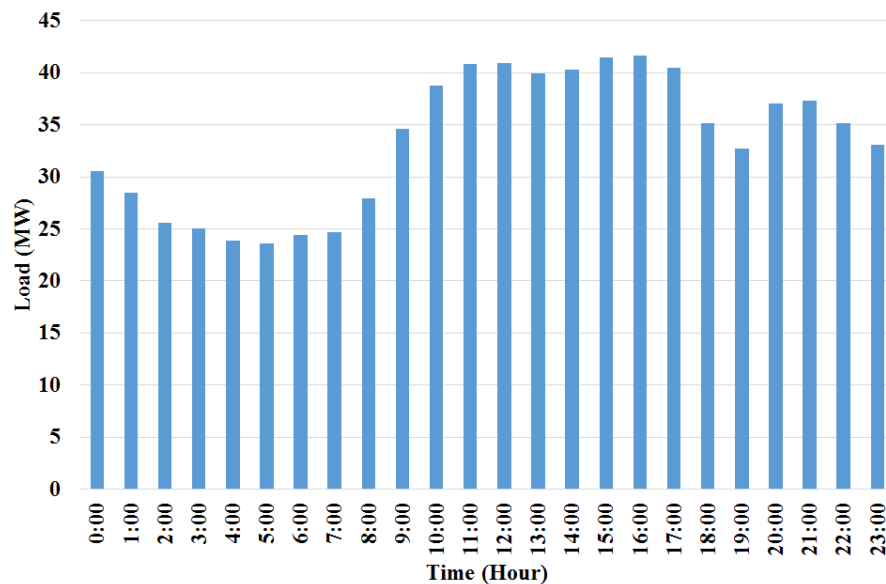


**Figure 7.9: Daily electrical load profile**

### 7.3.4 System without ESS

The scaled down generation profile of the CCGT and OCGT is illustrated in Figure 7.10. It can be seen that the CCGT is operated at the part load during the periods 0:00 to 10:00, 17:00 to 20:00, and 21:00 to 23:00. The CCGT is operated

near its full load during the periods 10:00 to 17:00 and 20:00 to 21:00. The OCGT begins to operate during the period 10:00 to 21:00.

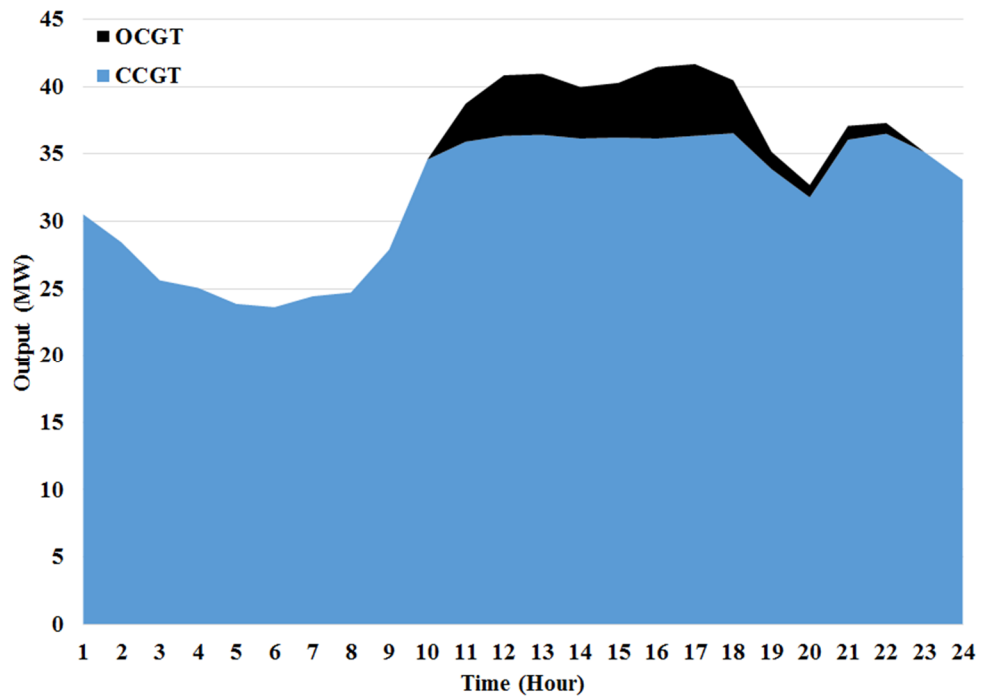


**Figure 7.10: The scaled down generation profile of the CCGT and OCGT**

The generators operating at part load requires additional fuel due to the reduced output power of the plants. In addition, non-steady state operation can increase operation and maintenance cost (Kumar et al., 2012). Heat rate is frequently used to indicate the fuel consumption rate for specific levels of power plant output. It is defined as the amount of energy used by generator to generate 1 kilowatt-hour (kWh) of electricity. In HOMER, user can input the fuel consumption rate to generate the electrical efficiency curve. HOMER assumes that the fuel curve ( $F$ ) given by Equation (1) is a linear line as follows:

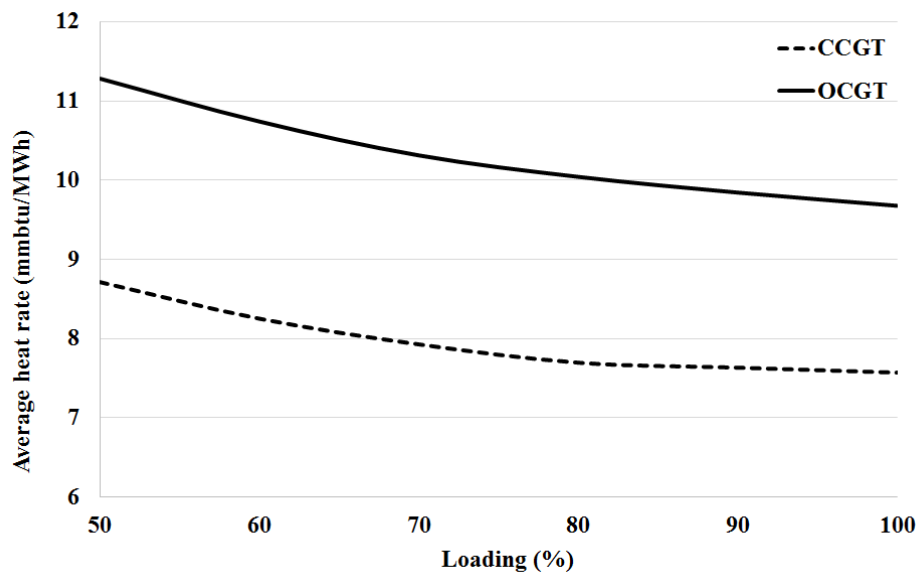
$$F = F_0 Y_{gen} + F_1 P_{gen} \quad (1)$$

where  $F_0$  is the fuel curve intercept coefficient in units/ hour/ kW,  $F_1$  is the fuel curve slope in units/ hour/ kW,  $Y_{gen}$  is the rated capacity of the generator in kW,

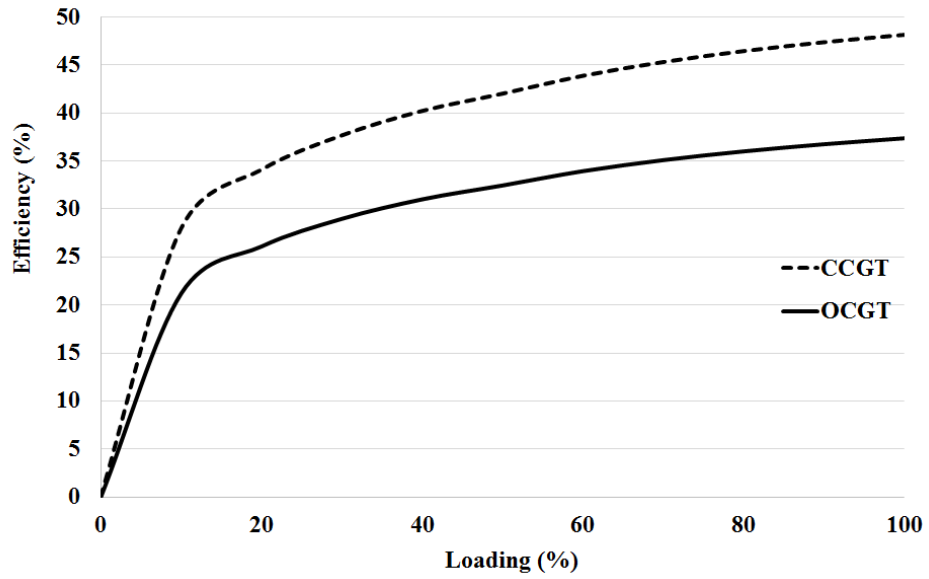
and  $P_{gen}$  is the electrical output of the generator in kW. The generator's electrical efficiency ( $\eta_{gen}$ ) is defined as the electrical energy output divided by the chemical energy of the input fuel as follows:

$$\eta_{gen} = \frac{3.6 P_{gen}}{m_{fuel} LHV_{fuel}} \quad (2)$$

where  $m_{fuel}$  is the mass flow rate of the fuel in kg/ hour and  $LHV_{fuel}$  is the lower heating value of the fuel in MJ/kg. The factor of 3.6 arises because 1 kWh is equal to 3.6 MJ. Figure 7.11 shows the heat rate and the electrical efficiency curve of the CCGT and OCGT with respect to its loading conditions (Greg et al., 2012).



(a)



(b)

**Figure 7.11: (a) Heat rate and (b) Electrical efficiency curve of CCGT and OCGT with respect to its loading conditions**

Operation and maintenance(O&M) expenses consist of fixed operation and maintenance (FOM) as well as variable operation and maintenance (VOM) (Jose, 1999). FOM includes wage, monthly fees under pertinent operating agreements, plant support equipment, routine preventive maintenance, general and administrative expenses, etc. VOM consists of air filter replacements, water treatment expenses, catalyst replacements, major overhaul maintenance, etc. The capital costs are the investments in equipment and plant to provide physical infrastructure, generation hardware, and plant auxiliary services. On the other hand, fuel costs are variable costs that include purchase, transportation and storage of the source of energy. The key parameters of CCGT and OCGT for cost analysis are summarized in Table 7.2.

**Table 7.2: Key parameters of CCGT and OCGT**

Technology	CCGT	OCGT
Plant life time (year)	20 <sup>a</sup>	20 <sup>a</sup>
Efficiency (%)	42-48 <sup>b</sup>	32-37 <sup>b</sup>
Capital cost (RM/ kW) <sup>c</sup>	7752 <sup>b</sup>	3600 <sup>b</sup>
FOM (RM/ kW-year) <sup>c</sup>	117.623 <sup>b</sup>	27.158 <sup>b</sup>
VOM (RM/ MWh) <sup>c</sup>	25.086 <sup>b</sup>	57.165 <sup>b</sup>
Capacity (MW)	36.5	5.18
Capital(RM million) <sup>c</sup>	283	19
O&M (RM/ hour) <sup>c</sup>	1,406	328

Footnotes:


a- Data is collected from (Koh et al. 2011)

b- Data is collected from (U.S. Energy Information Administration, 2013)

c- The conversion rate of USD to RM is 1:3.7

Figure 7.12 shows the user interface of the CCGT setup in HOMER. The desired power rating of the CCGT is entered under the search space column. Users can define the fuel resource and its price under the fuel resource tab. The fuel price for cases with subsidy and without subsidy are entered for sensitivity analysis. The fuel price with subsidy is RM0.543 while the fuel price without subsidy is RM1.571.



**GENERATOR**  Name: CCGT Abbreviation: CCGT Remove Copy To Library

**Properties**  
 Name: CCGT  
 Abbreviation: CCGT  
 Manufacturer: Innovus Power  
 Website: [www.innovus-power.com](http://www.innovus-power.com)

**Costs**

Capacity (kW)	Capital (RM)	Replacement (RM)	O&M (RM/hr)
100000	RM754,000,000	RM754,000,000.00	RM3,747.000

Click here to add new item

Multiplier: [.] [.] [.]

**Site Specific Input**

Minimum Load Ratio (%): 0.00 [.] Heat Recovery Ratio (%): 0.00 [.]  
 Lifetime (Hours): 175,200.00 [.] Minimum Runtime (Minutes): 0.00 [.]

Electrical Bus:  AC  DC

Fuel Resource: Fuel Curve Biogas Emissions Maintenance Schedule

Natural Gas

**PROPERTIES**

Lower Heating Value (MJ/kg): 45  
 Density (kg/m3): 0.790  
 Carbon Content (%): 67  
 Sulfur Content (%): 0.33

Natural Gas Fuel Price (RM/m<sup>3</sup>): 0.54 [2]  Limit Consumption (m<sup>3</sup>): 5,000.00 [.]

**Figure 7.12: User interface of the CCGT setup in HOMER**

The fuel consumption in m<sup>3</sup>/hr is keyed in under the fuel curve tab. Figure 7.13 shows the fuel flow and fuel efficiency of the CCGT. The efficiency of the CCGT at 100 % loading is 48 %.

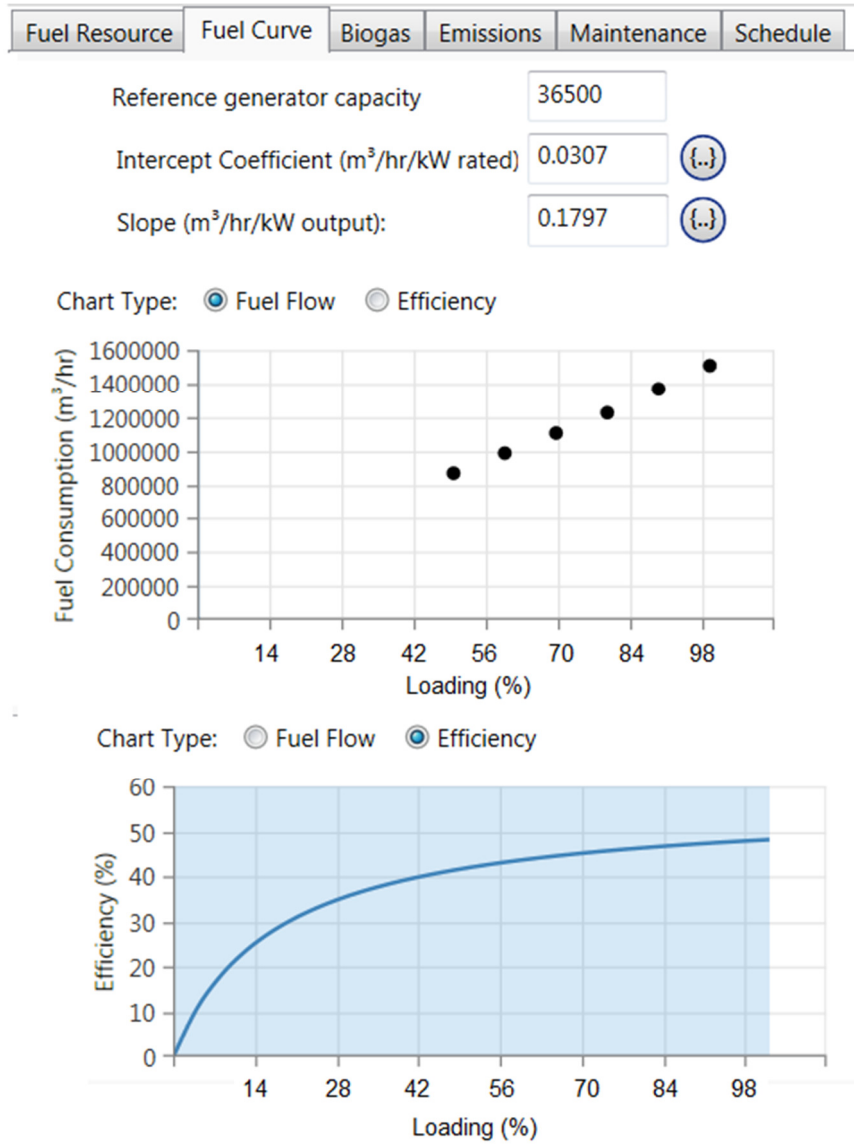


**Figure 7.13: Fuel flow and fuel efficiency of the CCGT**

Figure 7.14 shows the fuel flow and fuel efficiency of the OCGT. The efficiency of the OCGT at 100 % loading is 37 %.

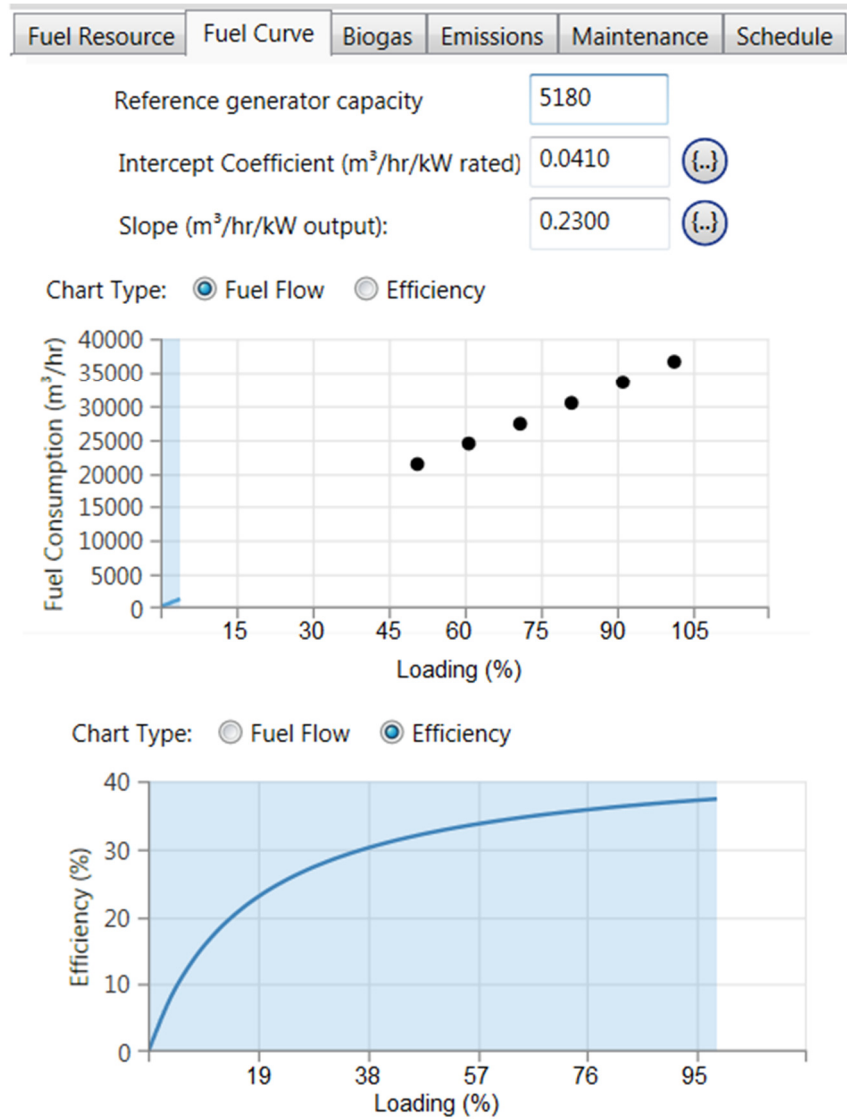


**Figure 7.14: Fuel flow and fuel efficiency of the OCGT**

### 7.3.5 System with ESS

The system with ESS consists of a CCGT, electric load profile, and the ESS that is formed by a converter and batteries. Once the OCGT is replaced by the energy storage, the heat rate of OCGT and the fuel cost are not considered in this system. However, the parameters required for this model are the depth of

discharge (DOD), the efficiency, the cycle life and the cost of energy of the energy storage system. The converter is formed by an inverter and a rectifier for the conversion of alternating current (AC) to direct current (DC) or vice versa. Batteries will be charged and discharged according to the dispatch strategy in HOMER via the converter. The price range of the converter falls between RM740 to RM5550 with a lifetime of 20 years and efficiency of 90 % (Poullikkas, 2013).

Four battery technologies are chosen for the investigation of system with ESS, namely lead acid (LA), vanadium redox flow (VRB), zinc-bromine flow (ZnBr), and lithium-ion (Li-ion) battery. The key parameters for these batteries are summarized in Table 7.3.

**Table 7.3: Key parameters for LA, VRB, ZnBr and Li-ion.**

Battery	DOD (%)	Efficiency (%)	Cycle Life		Cost of Energy (RM/kWh)	
			Low	High	Low	High
Lead acid	50 <sup>a</sup>	85 <sup>b</sup>	500 <sup>c</sup>	2800 <sup>d</sup>	185 <sup>b</sup>	1147 <sup>b</sup>
VRB	100 <sup>a</sup>	85 <sup>b</sup>	12000 <sup>c</sup>	13342 <sup>c</sup>	647.5 <sup>b</sup>	3700 <sup>b</sup>
ZnBr	100 <sup>a</sup>	75 <sup>b</sup>	1500 <sup>c</sup>	2000 <sup>c</sup>	740 <sup>b</sup>	2220 <sup>b</sup>
Li-ion	85 <sup>a</sup>	90 <sup>b</sup>	1000 <sup>c</sup>	10000 <sup>c</sup>	2220 <sup>b</sup>	9250 <sup>b</sup>

Footnotes:


a- Data is collected from (Abbas et al., 2015)

b- Data is collected from (Poullikkas, 2013)

c- Data is collected from (Luo et al., 2015)

d- Data is collected from (Hoppecke, 2014)

Figure 7.15 shows the user interface for batteries in HOMER. Users can specify the number of batteries to be connected in a string, initial SOC, minimum SOC, and lifetime throughput.

**BATTERY**  Name:  Abbreviation:

**Properties**

Name: Lead Acid(Cycle life 500) Copy  
 Abbreviation: Battery  
 Manufacturer: Trojan Battery Company  
 Nominal Voltage (V): 2  
 Nominal Capacity (Ah): 1849  
 Nominal Capacity (kWh): 3.70  
 Round Trip Efficiency (%): 85  
 Float Life (years): 20  
 Maximum Capacity (Ah): 2,461.652  
 Capacity Ratio, c: 0.495  
 Rate Constant, k: 0.125  
 Suggested Life Throughput (kWh): 6199.847  
 Max. Charge Rate (A/Ah): 1  
 Max. Charge Current (A): 310  
 Max. Discharge Current (A): 276.5

**Costs**

Quantity	Capital (RM)	Replacement (RM)	O&M (RM/year)
1	RM684.50	RM684.50	RM0.00

Multiplier:

**Site Specific Input**

Batteries per string:  (24 V bus)

Initial State of Charge (%):

Minimum State of Charge (%):

Lifetime Throughput (kWh):

Enforce minimum battery life?

Minimum battery life (yr)

**Search Space**

Strings  
6756

**Figure 7.15: User interface for batteries in HOMER**

Figure 7.16 shows the lead acid capacity curve under the storage tab. This capacity curve is obtained from one of the commercial available battery model in the HOMER library.

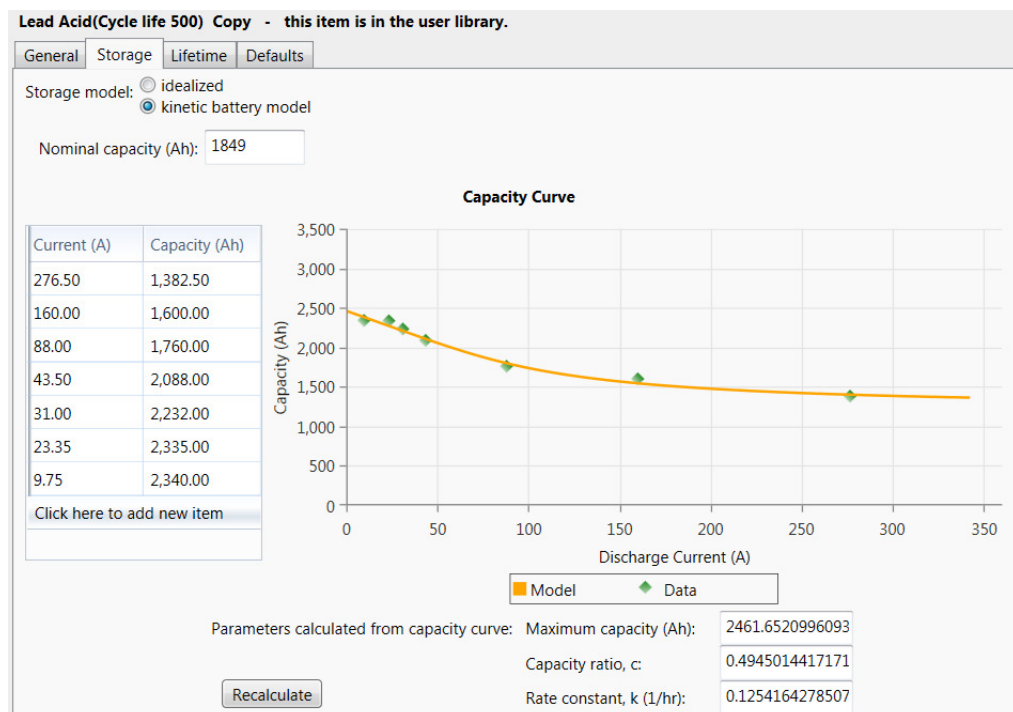


**Figure 7.16: Lead acid capacity curve under the storage tab**

### **7.3.6 Carbon Dioxide Emissions**

Various carbon emission trading schemes have been introduced throughout the world to combat climate change. For example, the European Union Emissions Trading Scheme (EU ETS) has been established on 1 January 2005 to reduce greenhouse gas emissions cost-effectively. The EU ETS covers more than 11,000 power stations and industrial plants across 31 countries and introduces emission allowances which can be traded as needed. Hence, power producers have to include this cost to their marginal production cost and increase the electricity price in wholesale power markets (Jouvet and Solier, 2013). The carbon dioxide (CO<sub>2</sub>) emission price between schemes differ from each other over a significant range, from US\$ 1/ tons CO<sub>2</sub> in the Mexican carbon tax up to US\$168/ tons CO<sub>2</sub> in the Swedish carbon tax. The prices in emission trading schemes is clustered under US\$ 12/ tons CO<sub>2</sub> (World Bank, 2014). Although Malaysia doesn't have any carbon emissions trading scheme at this moment, it is expected to be implemented in the future. In this research work, the carbon price of US\$ 12/ tons CO<sub>2</sub> is adopted for the assessment.

### **7.3.7 Deferral of Transmission and Distribution Reinforcement**

Utilities are required to enhance the T&D facility when the electricity demand approaches its capacity. The reinforcement of the T&D infrastructure depends on the growth of demand and peak demand, aging of infrastructure and the upgrade with new technology. Installation of ESS at distribution level or

customer-end could result in deferral of T&D reinforcement. During peak demand periods, the ESS can deliver power to consumers and hence reduce the power to be transmitted by the transmission lines. This can defer the need for high investment costs in new T&D facilities such as substations, transformers, protective equipment, capacitors, cables, and line support towers. In addition, the T&D facilities' life could be extended because these facilities are operated at a lower temperature (Tom, 2011). T&D upgrade deferral is estimated based on the peak demand projection, the assumption of 5 % ESS penetration rate, and 5 % ESS growth rate from 2015 to 2030. The growth projection of the peak demand and ESS from 1990 till 2030 is shown in Figure 7.17 (Energy Commission, 2013). With the assumed growth rate for the ESS, it is expected to achieve 7.4 % of reduction in overall peak demand growth by 2030.

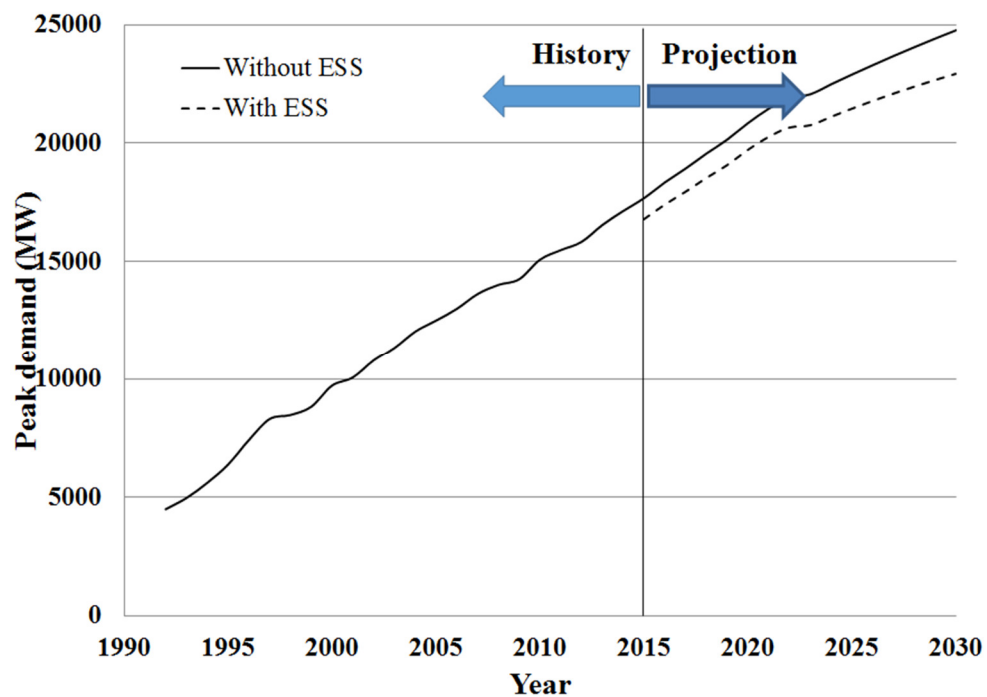


**Figure 7.17: Growth projection of the peak demand and ESS from 1990 till 2030**

The T&D avoided cost values can be estimated based on either the historical annual marginal T&D investment or the future T&D investment at specific sites. Based on the US experience, the typical values for annual T&D upgrade deferral fall within the range of USD55/ kW to USD120/ kW (Chris and Rich, 2012). In this research work, annual T&D upgrade deferral is assumed to be in the range of RM203/ kW to RM444/ kW.

### 7.3.8 Cost-benefit to Industrial and Commercial Customers

ESS installed at end-users' premises can provide significant benefits such as reduction of the peak demand surcharge, avoidance of financial losses due to power outage, and improvement of power quality. In this research work, the reduction of the peak demand surcharge is investigated. In Malaysia, commercial and industrial sectors were the largest electricity consumers, which consumed 78 % of total electricity generated in the year 2012 (Suruhanjaya Tenaga Malaysia, 2012). These two sectors are the main contributors to the economy as well as peak demand. The installation of ESS for peak demand mitigation on these sectors has significant advantages compared to that of other sectors. The financial analysis focuses on the four tariff categories for commercial and industrial customers (Tenaga Nasional Berhad, 2014). Table 7.4 shows the tariff rate for the four categories, namely C1, C2, E1 and E2.

**Table 7.4: Tariff rates for different categories of commercial and industrial customers**

Tariff	C1 <sup>a</sup>	C2 <sup>b</sup>	E1 <sup>c</sup>	E2 <sup>d</sup>
Peak (RM/kWh)	-	0.365	-	0.365



Off-peak (RM/kWh)	-	0.224	-	0.219
Energy (RM/kWh)	0.365	-	0.337	-
MD <sup>e</sup> (RM/kW)	30.3	45.1	29.6	37.0

Footnotes:

- a- C1 represents the Medium Voltage General Commercial
- b- C2 represents the Medium Voltage Peak/Off-Peak Commercial
- c- E1 represents the Medium Voltage General Industrial
- d- E2 represents the Medium Voltage Peak/Off-Peak Industrial
- e- MD is the abbreviation of maximum demand

Maximum demand is computed based on the highest energy used in kilowatt-hours within any consecutive period of 30 minutes in a month, and this highest energy is multiplied by two to get the maximum demand. This duration of time is defined as the Demand Evaluation Period (DEP). The electricity bill ( $C_{Bill}$ ) for commercial and industrial customers is calculated as follows:

$$C_{Bill} = \int_{t_{start}}^{t_{end}} P(t) \cdot C_{EU} \cdot dt + \int_{t_A}^{t_B} 2P(t) \cdot C_{MD} \cdot dt \quad (3)$$

where  $t_{start}$  and  $t_{end}$  are the periods of time during the billing cycle in a month,  $P(t)$  is the power demand during the time interval,  $t_A$  and  $t_B$  are the DEP in the same month,  $C_{EU}$  is the charge of the energy usage, and  $C_{MD}$  is the maximum demand charge. Commercial and industrial consumers can use ESS to shave the maximum demand during peak period to reduce their electricity cost. For the consumers with tariff rates of C1 and E1, the monthly savings ( $S_{mth}$ ) can be calculated as follows:

$$S_{mth} = (P_{shave} \times C_{MD}) - (E_{ES} \times (1 - \eta_{bat}) \times C_{EU}) \quad (4)$$

where  $P_{shave}$  is the peak shaved by the distributed energy storage system,  $E_{ES}$  is the energy used for peak shaving, and  $\eta_{bat}$  is the round trip efficiency of the batteries. For the consumers with tariff rate of C2 and E2, there are two different rates for peak and off-peak periods. Hence, the monthly savings ( $S_{mth}$ ) can be calculated as follows:

$$S_{mth} = (P_{shave} \times C_{MD}) + (E_{ES} \times C_P) - (E_{ES} \times (2 - \eta_{bat}) \times C_{OP}) \quad (5)$$

where  $C_P$  and  $C_{OP}$  are the charge of energy usage during peak and off-peak periods, respectively.

The two most important components to be considered in achieving the cost-benefit of the ESS in peak shaving are the size of battery bank and the power converter. Improper sizing of the battery bank and power converter may incur additional cost to the ESS. The optimal size of the ESS can be obtained from the comparisons of the cost of ESS and the electricity bills. Firstly, a typical daily load profile of a commercial building is analyzed. Figure 7.18 illustrates a typical daily load profile for one of the buildings at Universiti Tunku Abdul Rahman (UTAR), Malaysia. It is found that the peak demand is 1084 kW and the daily energy consumption is 13.5MWh.

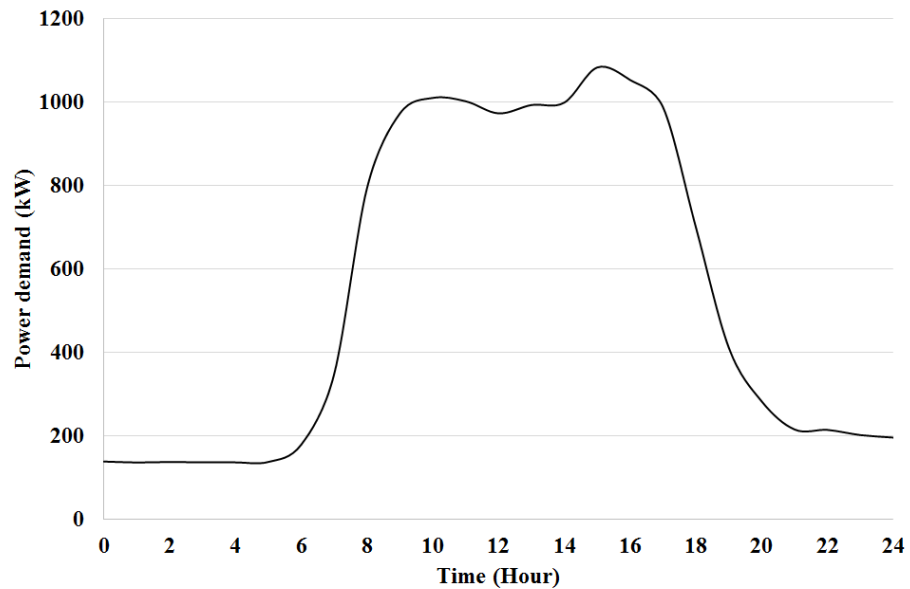


**Figure 7.18: Typical daily load profile for one of the buildings at UTAR**

Lead acid battery is chosen for the cost-benefit analysis because it is the most economic and viable storage technology. It is assumed that the batteries are charged and discharged one cycle per day during Monday to Friday, throughout a year. By taking into account the Malaysian national holidays of 13 days, the ESS will operate 248 days in a year. The key assumptions for the ESS are summarized in Table 7.5.

**Table 7.5: Key assumptions for the lead acid-based ESS**

Cost of converter (RM/ kW)	740
Cost of battery (RM/ kWh)	185
Round-trip Efficiency (%)	90
Efficiency of the converter (%)	85
Depth of discharge	50
Cycle life	2800
Battery life span	11.3

Round trip efficiency and cycle life of the ESS are important parameters to be considered in the cost-benefit analysis because it affects the overall cost of the system. The ratio of energy discharged from the storage system to the energy charged into the storage system is known as round trip efficiency. Cycle life of the batteries is an important cost driver that indicates the number of discharges before the replacement of the batteries. The battery DOD has a significant impact on batteries' cycle life. The relation between the cycle life and the DOD appears to be logarithmic in which the cycle life goes up exponentially with decrement of the DOD. The cost of batteries ( $C_{Bat}$ ) can be calculated by as follows:

$$C_{Bat}(\$) = U_{Bat}(\$/kWh) \times E_R(kWh) \times \frac{DOD}{\eta_{bat}} \quad (6)$$

where  $U_{Bat}$  is the unit cost of the batteries in kWh,  $E_R$  is the rated capacity of the batteries,  $\eta_{Bat}$  is the round trip efficiency of the battery. The cost of power conversion units ( $C_{conv}$ ) is calculated as follows:

$$C_{Conv}(\$) = U_{Conv}(\$/kW) \times P_R(kW) \quad (7)$$

where  $U_{Conv}$  is the unit cost of the power conversion units in kW, and  $P_R$  is the power rating of the converter. The cost of the ESS ( $C_{ES}$ ) is determined as follows:

$$C_{ES} = C_{Bat} + C_{Conv} \quad (8)$$

#### 7.4 Results and discussion

This section presents the results of the analysis carried out using HOMER. The cost-benefit of using ESS for utility is evaluated based on the generation cost, deferral cost of reinforcement of the T&D infrastructure, and the reduction of CO<sub>2</sub> emissions cost. The analysis also compares the cost of energy for the cases with gas subsidy and without gas subsidy. For commercial and industrial customers, the economic viability of using ESS to reduce peak demand is evaluated via the electricity bill savings as well as payback periods.

#### 7.4.1 System without ESS

HOMER performs the simulation for the system with and without ESS. HOMER simulates the operation of these systems using the energy balance calculations for each year to meet the requirements under the designated conditions, and estimates the cost of installing and operating the systems over the lifetime of the project. Based on the inputs such as the technology options, component costs, resource availability, and the constraints defined by users, HOMER simulates all the possible system configurations and ranks the results in ascending order of levelized COE in RM/ kWh. Sensitivity analysis is carried out to investigate the impact of the sensitive variables on the levelized COE such as price of batteries and generators, and fuel prices. The levelized COE is used to measure the overall competitiveness of the two systems. The levelized COE is calculated as follows:

$$COE = \frac{\sum_{i=1}^n \frac{C_i + O_i + F_i}{(1+r)^i}}{\sum_{i=1}^n \frac{E_i}{(1+r)^i}} \quad (9)$$

where  $C_i$  is the investment expenditure in the year  $i$ ,  $O_i$  is the operations and maintenance expenditure in the year  $i$ ,  $F_i$  is the fuel expenditure in the year  $i$ ,  $E_i$  is the electricity generation in the year  $i$ ,  $n$  is the expected lifetime of the system, and  $r$  is the discount rate. Optimization and sensitivity analyses are carried out across all the cost parameters and system constraints, and provide the results in ascending order of COE in RM/ kWh as illustrated in Figure 7.19.

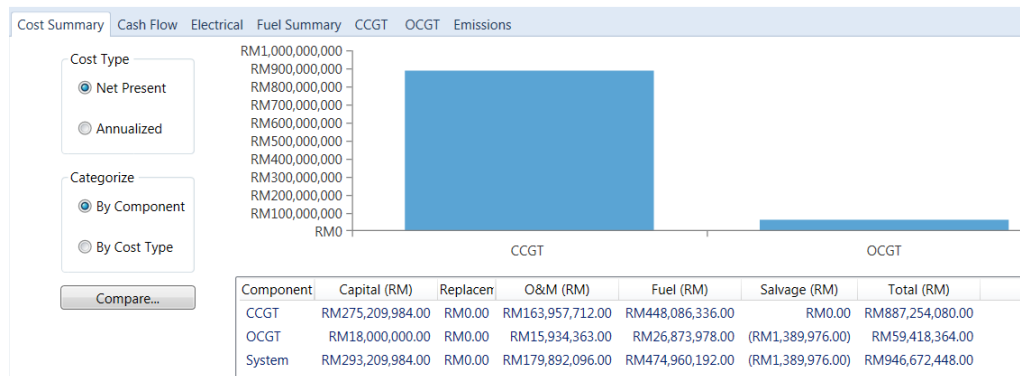
RESULTS													
Sensitivity Cases: Left Click on sensitivity case to see optimization cases.													
Sensitivity	Architecture				Cost				System	CCGT		OCGT	
Natural Gas Fuel Price (RM/L)	CCGT (kW)	OCGT (kW)	Dispatch	COE (RM)	NPC (RM)	Operating cost (RM)	Initial capital (RM)	Ren. Frac (%)	Fuel (m <sup>3</sup> )	Hours	Fuel (m <sup>3</sup> )	Hours	
0.54	36,500	5,180	CC	RM0.236	RM946,672,400	RM47,749,560	RM293,210,000	0	60,310,170	8,760	3,617,103	3,650	
1.57	36,500	5,180	CC	RM0.460	RM1,846,463,000	RM113,498,800	RM293,210,000	0	60,310,170	8,760	3,617,103	3,650	

Optimization Cases: Left Double Click on simulation to examine details.												
Architecture				Cost				System	CCGT		OCGT	
CCGT (kW)	OCGT (kW)	Dispatch	COE (RM)	NPC (RM)	Operating cost (RM)	Initial capital (RM)	Ren. Frac (%)	Fuel (m <sup>3</sup> )	Hours	Fuel (m <sup>3</sup> )	Hours	
36,500	5,180	CC	RM0.236	RM946,672,400	RM47,749,560	RM293,210,000	0	60,310,170	8,760	3,617,103	3,650	

**Figure 7.19: Results in ascending order of COE**

In each case, the simulated results are organized into cost summary, cash flow, electricity consumption, fuel summary, components detail, and emissions. The cost summary of the system without ESS is illustrated in Figure 7.20.



**Figure 7.20: Cost summary of the system without ESS**

The annual electricity production of CCGT and OCGT and consumption of electricity are shown in Figure 7.21. It can be seen that the annual electricity production of CCGT and OCGT are 95.79 % and 4.21 %, respectively.

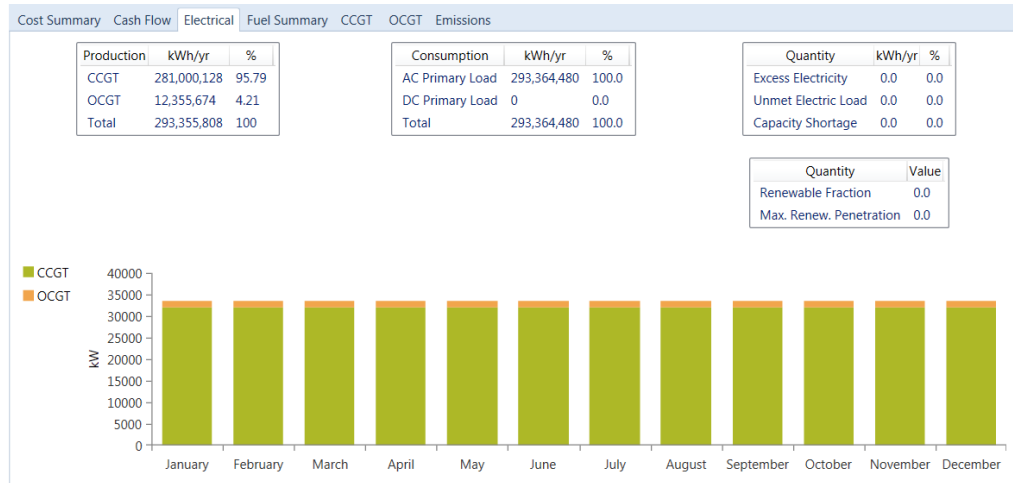


**Figure 7.21: Annual electricity production of CCGT and OCGT and consumption of electricity**

The annual fuel consumption of the system without ESS is illustrated in Figure 7.22. It is found that the total annual fuel consumption is 63.9 million m<sup>3</sup>.

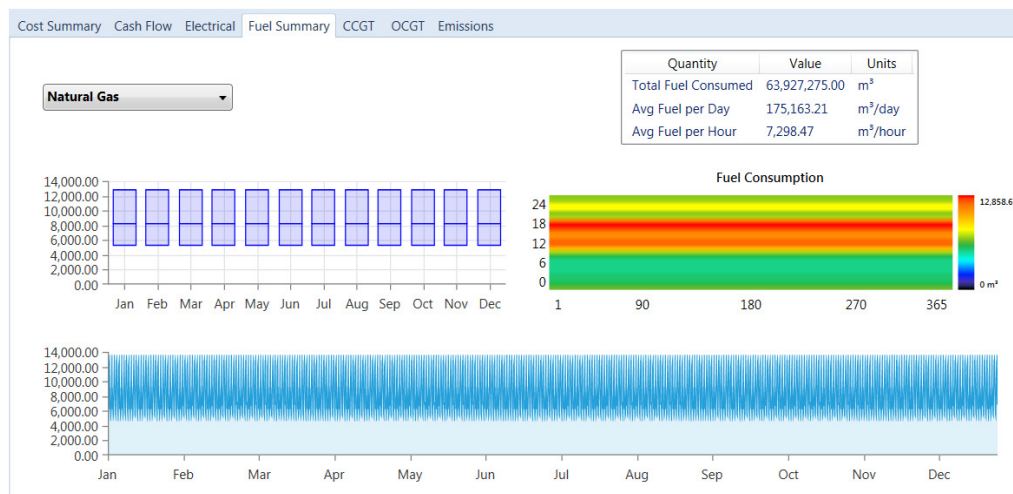


**Figure 7.22: Annual fuel consumption of the system without ESS**

The operating parameters of the system without ESS are summarized in Table 7.6. The capacity factor of CCGT and OCGT are 87.9 % and 27.2 %, respectively.

**Table 7.6: The operating parameters of the system without ESS**

Items	CCGT	OCGT
Energy production (GW/year)	281	1.85
Percentage of energy (%)	95.8	4.2
Hours of operation	8,760	3,650
Capacity factor (%)	87.9	27.2

Table 7.7 shows the comparison of cost components for the system without ESS for cases with and without subsidy. It can be seen that the levelized COE for the case without subsidy is about two times more expensive than that of the case with subsidy.

**Table 7.7: Comparison of cost components for the system without ESS for cases of with and without subsidy**

Items	With Subsidy	Without subsidy
Net present cost (RM million)	947	1,846
Capital (RM million)	293	293
O&M cost (RM million)	180	180
Fuel cost (RM million)	475	1,375
Salvage (RM million)	-1.4	-1.4
Levelized COE (RM/ kWh)	0.236	0.46



### 7.4.2 System with ESS

The sensitivity analysis is carried out for a number of prospective design configurations, namely the cycle life, PCS costs, battery price, and gas price. Table 7.8 shows the COE for the four battery technologies with gas subsidy. It can be seen that the COE of the lead acid batteries with high cycle life, low PCS and low battery cost in the case of with subsidy is lower than that of the system without ESS. The VRB batteries with low and high cycle life, low PCS and low battery cost in the case with subsidy is also lower than that of the system without ESS. The ZnBr batteries with low PCS and low battery cost for low and high cycle life has the same COE as that of the system without ESS.

**Table 7.8: Cost of energy for the four battery technologies with subsidy**

				COE with subsidy (RM/ kWh)	
				Low battery cost	High battery cost
LA	Low cycle life	PCS	Low	0.253	0.383
			High	0.259	0.389
	High cycle life	PCS	Low	0.233	0.262
			High	0.240	0.268
VRB	Low cycle life	PCS	Low	0.234	0.265
			High	0.241	0.271
	High cycle life	PCS	Low	0.234	0.265
			High	0.241	0.271
ZnBr	Low cycle life	PCS	Low	0.236	0.252
			High	0.243	0.258
	High cycle life	PCS	Low	0.236	0.252
			High	0.243	0.258
Li-ion	Low cycle life	PCS	Low	0.346	0.722
			High	0.353	0.728
	High cycle life	PCS	Low	0.259	0.357
			High	0.265	0.363

Table 7.9 shows the COE for the four battery technologies without gas subsidy. It can be seen that the COE without subsidy is much higher than that of the system with subsidy. The COE of the lead acid batteries and VRB batteries with high cycle life, low PCS and low battery cost in the case with subsidy are lower than that of the system without ESS. The ZnBr batteries with low PCS and low battery cost for low and high cycle life has the same COE as that of the system without ESS.

**Table 7.9: Cost of energy for the four battery technologies without subsidy**

				COE without subsidy (RM/ kWh)	
				Low battery cost	High battery cost
LA	Low cycle life	PCS	Low	0.476	0.605
			High	0.482	0.612
	High cycle life	PCS	Low	0.456	0.484
			High	0.462	0.491
VRB	Low cycle life	PCS	Low	0.457	0.487
			High	0.463	0.494
	High cycle life	PCS	Low	0.457	0.487
			High	0.463	0.494
ZnBr	Low cycle life	PCS	Low	0.461	0.476
			High	0.467	0.483
	High cycle life	PCS	Low	0.461	0.476
			High	0.467	0.483
Li-ion	Low cycle life	PCS	Low	0.568	0.944
			High	0.575	0.951
	High cycle life	PCS	Low	0.481	0.579
			High	0.488	0.586

Figure 7.23 shows the range of COE for the highest and lowest battery cost with low PCS and high cycle life. It can be seen that lead acid and VRB batteries

have COE lower than that of the system without ESS while ZnBr battery has the same COE as that of the system without ESS. With the current technology price, these three battery technologies are the economically viable candidates to replace the OCGT.

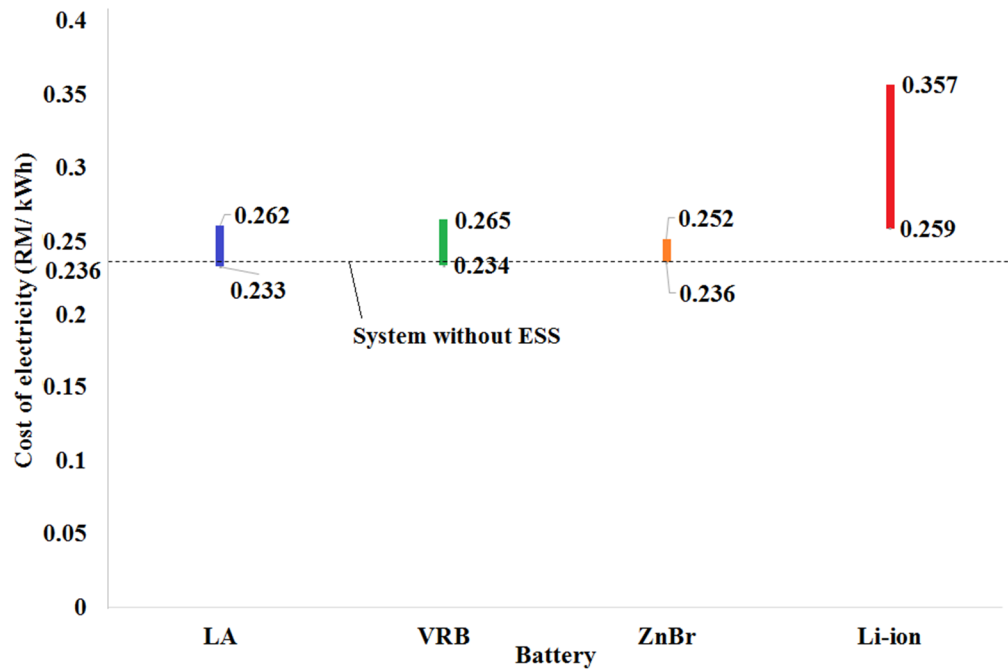
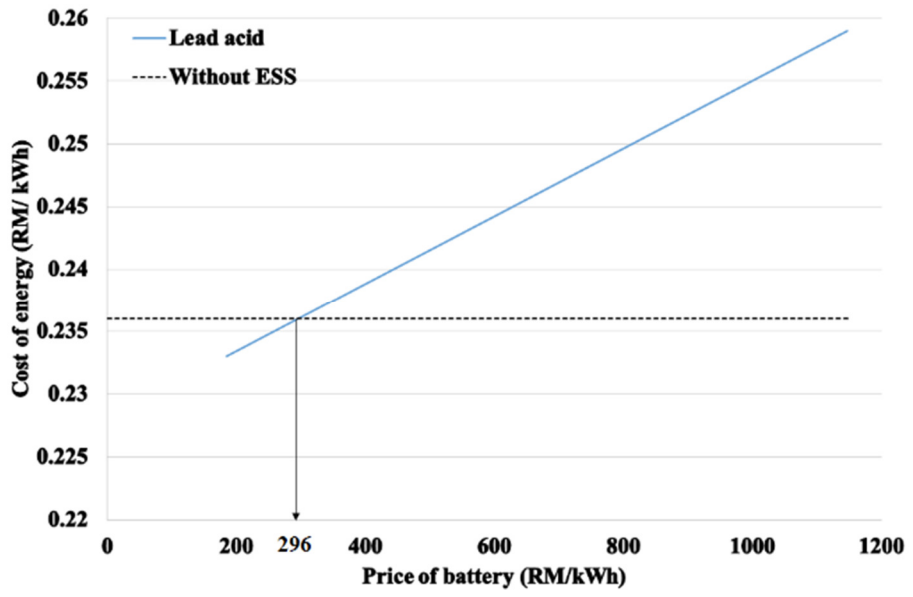
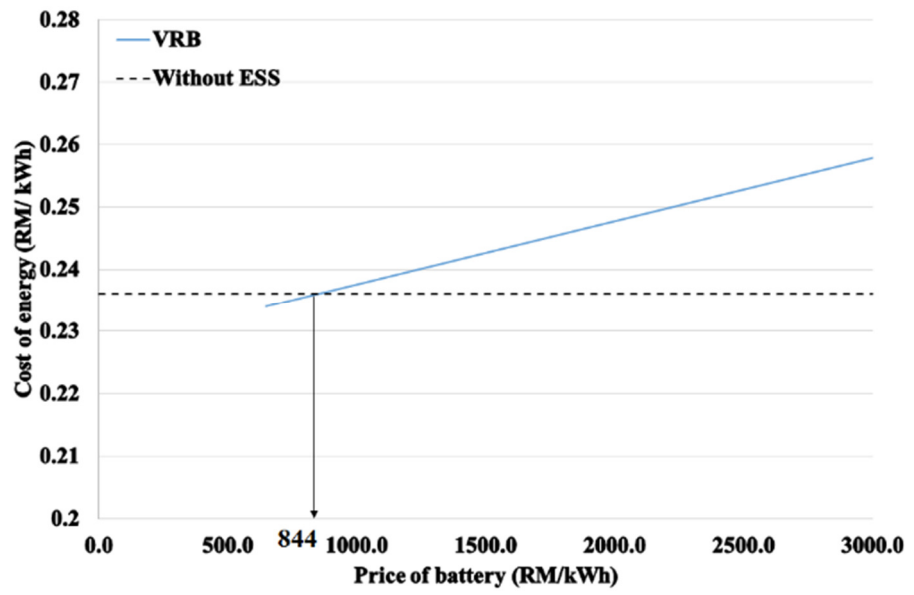


**Figure 7.23: Range of COE for the highest and lowest battery cost**

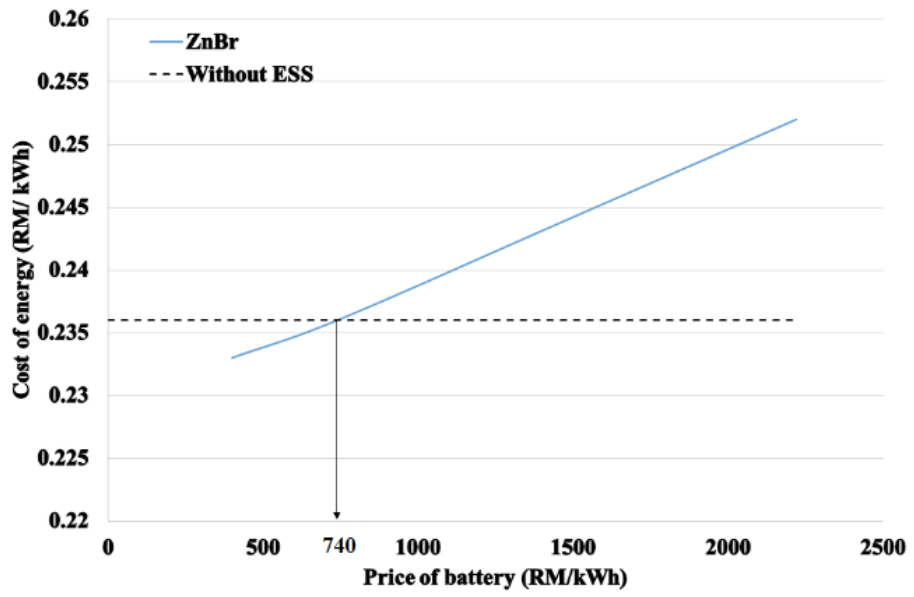
The break-even price of these four battery technologies are investigated. Figure 7.24 shows the break-even price of LA, VRB, ZnBr, and Li-ion batteries. It can be seen that the break-even price for LA, VRB, ZnBr, and Li-ion batteries are RM296, RM844, RM740, and RM610, respectively.



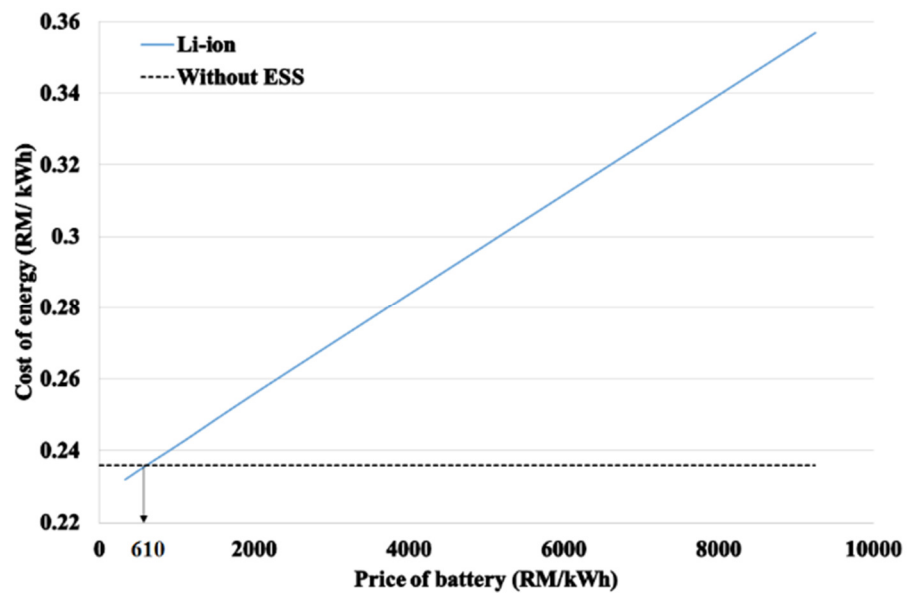
(a)



(b)



(c)



(d)

Figure 7.24: Break-even price of (a) Lead acid (b) VRB (c) ZnBr and (d) Li-ion

### 7.4.3 Reduction in Carbon Dioxide Emissions

In this research work, the cost of CO<sub>2</sub> emissions is investigated for the system with and without ESS. The carbon price of US\$ 12/ tons CO<sub>2</sub> is adopted. The total power generation of CCGT and OCGT of Malaysia in a year is considered for the system without ESS. It is assumed that the OCGT can be completely replaced by ESS for the system with ESS. Table 7.10 shows the summary of the reduction of CO<sub>2</sub> emissions for the system with ESS. It can be seen that there is a potential to reduce the CO<sub>2</sub> emissions by 140,000 tons every year. The assessment found that the CO<sub>2</sub> emission factor for the system with ESS is 2.5 % less than that of the system without ESS.

**Table 7.10: Summary of the reduction of CO<sub>2</sub> emissions cost for the system with ESS**

System	With ESS
Reduction of CO <sub>2</sub> emission (tons/year)	140,000
CO <sub>2</sub> emission factor (kg/ kWh)	0.407
Saving in the Cost of CO <sub>2</sub> (RM million)	9.0

### 7.4.4 Deferral of T&D Reinforcement

The T&D upgrade deferral cost for the power system with ESS is evaluated based on the low and high cost from the range of RM203/ kW (USD55/ kW) to RM444/ kW (USD120/ kW). Figure 7.25 shows the projection of the T&D upgrade deferral based on the low upgrade deferral cost and high upgrade

deferral cost. It can be seen that the T&D upgrade deferral in 2030 is in the range of RM385 million (USD104 million) to RM 840 million (USD227 million).

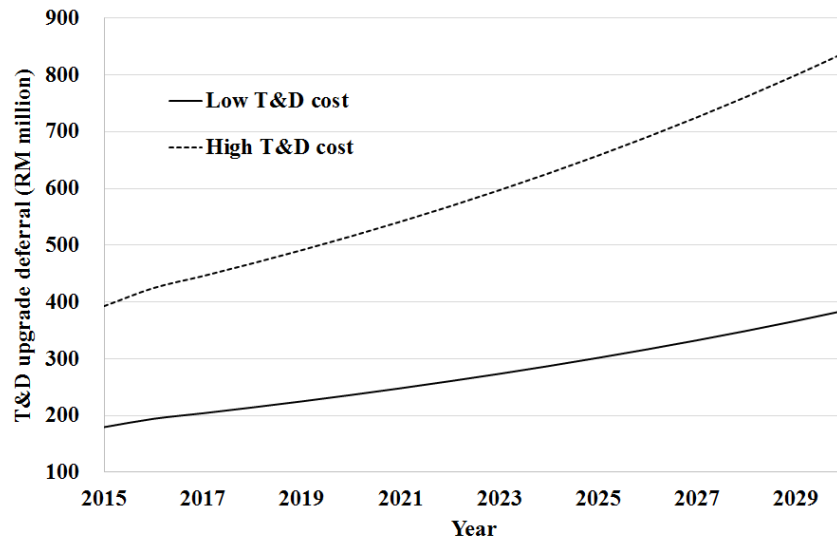


**Figure 7.25: Projection of T&D upgrade deferral from 2015 to 2030**

#### **7.4.5 Cost-benefit Analysis of Peak Shaving for Commercial and Industrial Consumers**

The objective of this section is to evaluate the costs and potential savings of energy storage in peak shaving for commercial and industrial consumers. Intuitively it can be said that as the increment of the ESS capacity reduces the electricity bills. However, the ESS increases the investment cost. An optimum cost of ESS can be obtained by summing up the cost of ESS with the electricity bill. The electricity bill throughout the life span of ESS is estimated. Figure 7.26 shows the electricity bill and the cost of ESS. It is found that the total cost

exhibits a minimum that defines the optimal size of the converter. The optimal size of the converter is 110 kW and the corresponding battery size is 395 kWh.

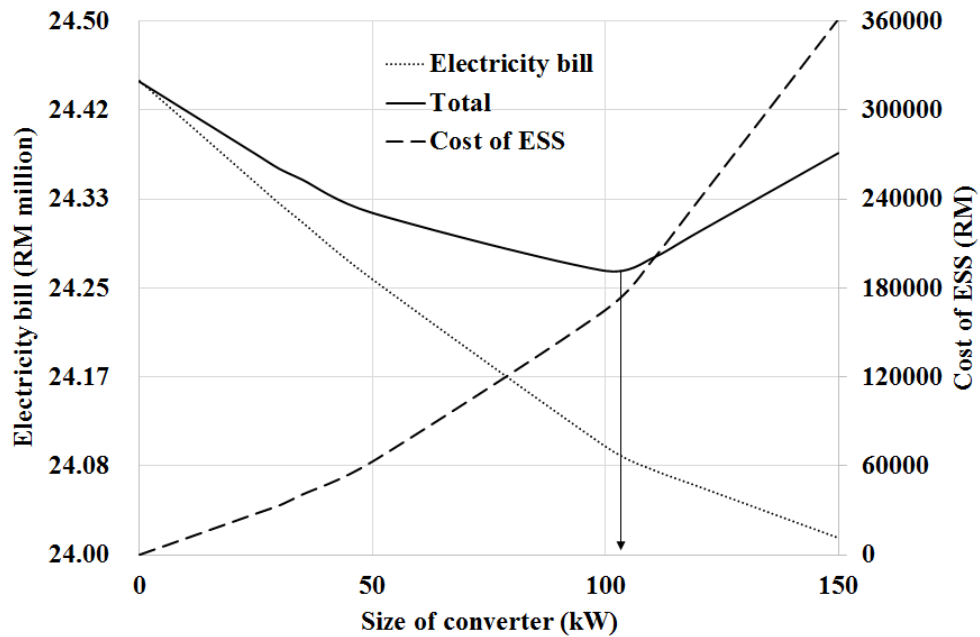


**Figure 7.26: Electricity bill and the cost of the ESS**

Commercial and industrial customers can manage their electric energy cost by storing inexpensive energy in the ESS and discharging the ESS during peak periods to reduce the maximum demand. Table 7.11 shows the monthly electricity bills for the system with and without ESS for the four categories of tariffs. Tariff C2 shows the greatest potential savings for the system with ESS, followed by E2, C1, and E1. The simple payback period for tariff C2 is the shortest, namely 2.8 years.

**Table 7.11: Monthly electricity bill for the system with and without ESS**

Cost		Energy (RM)	Maximum demand (RM)	Monthly bill (RM)	Payback period (year)	Savings (RM)
Without ESS	C1	147,420	32,845	180,265	-	-
	C2	132,498	48,888	181,386	-	-
	E1	136,111	32,086	168,197	-	-



	E2	128,988	40,108	169,096	-	-
	C1	147,939	29,512	177,451	5.9	2,814
With	C2	131,480	43,927	175,407	2.8	5,979
ESS	E1	136,590	28,830	165,421	6.0	2,777
	E2	128,010	36,038	164,048	3.3	5,048

## 7.5 Summary

Energy storage is profoundly important in power systems due to its multifaceted functionality such as increasing deployment of renewable integration, reducing peak demands, and enhancing electric grid reliability. The evaluations show that the cost of energy for the electrical system with lead acid batteries is lower than that of the system without ESS. For the ESS installed near the customer-ends, the reinforcement of T&D infrastructure can be deferred since the energy storage can reduce or delay the need for additional T&D capacity. The electricity cost savings using lead acid battery storage system to reduce the maximum demand is economically viable for commercial and industrial customers. The payback periods of the ESS range from 2.8 years to 6 years. It is expected that the price of batteries may drop due to the increase of manufacturing scale, lower component prices, and advancement of manufacturing technology. It is foreseen that the price of Li-ion batteries could drop to one-third of its current price from about USD 600/ kWh to USD200/ kWh by 2020. This will provide a great opportunity for energy storage to be adopted in mitigating the peak demand. Although some lead compounds are very toxic, the lead recycling is a well-established industry and hence the potential risk to the environment and human health are low. This research work

is essential to the regulatory body, the utility companies and the customers in Malaysia which intends to reduce the electricity price for the effective growth of economics in the country.

## CHAPTER 8

### CONCLUSIONS AND FUTURE WORK

#### 8.1 Conclusions

Energy storage is a very important component in the future electricity infrastructure due to its multifaceted functionality in reducing peak demands, increasing deployment of renewable integration, and enhancing electric grid security and reliability. Recent improvements in energy storage technologies and the decline in the cost of the battery can imply that the energy storage is a financially viable solution for peak reduction one day. There are numerous potential benefits associated with energy storage that could lead to value propositions such as the improvement of power supply reliability. The cost-benefit and value propositions of energy storage presented in this research work provide an important information for the utility companies as well as the customers to use energy storage for the peak reduction.

The objectives of this thesis are defined in Chapter 1 and its outcomes are listed as follows:

1. *To design and develop a laboratory-scale low-voltage distribution network with energy storage system.*

A laboratory-scale low-voltage distribution network with the energy storage system has been developed to investigate the peak reduction for buildings. The experimental setup consists of a network emulator, a low-voltage network connection panel, two load banks, and an energy storage system. The energy storage system is formed by three bi-directional power converters and 48 pieces of lead-acid batteries. Data acquisition systems have been developed to measure the power flows between the energy storage and the connected network.

2. *To develop suitable control algorithms for energy storage system to cut down the peak demand of a commercial building.*

The problem formulation for reducing the peak demand is derived and three control algorithms have been developed and implemented on the energy storage system to reduce the peak demand of a building. The three control algorithms are fixed-threshold, adaptive-threshold, and fuzzy-based control algorithms. The control algorithms are implemented using LabVIEW software. The developed control algorithms are evaluated at two different buildings, namely the SE block at Setapak UTAR campus and KA block at Sungai Long UTAR campus. The load profiles of SE block are forecasted based on the scheduled activities while the load profiles of KA block are predicted based on the average load demands. The predicted daily load profile provides information on the amount of energy required to shave the peak demands.

3. *To evaluate the performance of the proposed energy storage system and control algorithms in mitigating the peak demand of the commercial building.*

A single-phase energy storage system is set up to describe the operation of the energy storage system on the single-phase distribution network before it is extended to the three-phase distribution network. Thereafter experiments are carried out at the three-phase distribution network to evaluate the performance of the fixed-threshold, adaptive-threshold, and fuzzy-based control algorithms. Several case studies are carried out at these two buildings for the purpose of evaluating the performance of these control algorithms under various load characteristics.

The fixed-threshold control algorithm is simple and easy to be implemented. Under this control algorithm, the response of the energy storage system to any incoming instruction is very fast. However, the success of this control algorithm for any peak reduction is dependent on the accuracy of the forecasted load profiles. If the actual peak occurs for a much longer duration than the predicted one or the actual peak demand is unexpectedly high, then the fixed-threshold control algorithm may fail to reduce the peak demand. The adaptive-threshold control algorithm is an improved version of the fixed-threshold control algorithm where it can reduce the output power of the energy storage system to preserve the energy of the batteries when the actual peak demands occur for an extended period of time. However, the adaptive-threshold control algorithm may fail to reduce the peak demand if the actual peak demand occurs for a much longer duration than the predicted peak demand. The fuzzy-based control algorithm has eliminated the problem of unexpectedly high peak demand and the problem associated with actual peak demand occurs for a much longer duration than the predicted duration. The fuzzy-based control algorithm can

estimate the appropriate output power to be delivered to the load by estimating the useable energy from batteries using their SOC level and incorporates it into the fuzzy inference rules to improve the performance of the energy storage system. The fuzzy-based control algorithm is capable of incorporating a priori qualitative knowledge and expertise about the load characteristic of the buildings and the useable energy of the energy storage to reduce the peak demand. The experimental results showed that the fuzzy-based control algorithm has achieved the highest performance in peak shaving as compared to that of the fixed-threshold and adaptive-threshold control algorithms.

4. *To investigate the socioeconomic benefits of using energy storage in peak reduction for utility companies and customers.*

This research work has developed an energy dispatch model with energy storage to assess the socioeconomic benefits of energy storage. The energy dispatch model is simulated in HOMER to determine the cost of electricity for the system with- and without the energy storage system. The models take into account the heat rates of power plants in calculating the cost of electricity under different regulatory frameworks of natural gas and various prices of batteries. Apart from that, the cost-benefit for the customers under various electric tariff structures is also evaluated. Four battery storage technologies, namely the lead-acid, vanadium redox flow, zinc-bromine, and lithium-ion are considered in the evaluations. The simulation results reveal that the generation cost for the power system with energy storage is lower than that without energy storage.

Besides, the power system coupled with the energy storage has lower greenhouse gas emissions than that without energy storage. According to International Energy Agency (IEA) report, the Malaysian CO<sub>2</sub> emission factor is 0.669 kg/ kWh (International Energy Agency, 2013). The system with the energy storage system is 0.407 kg/ kWh. The simulation results show that the CO<sub>2</sub> emission factor for the system with energy storage is 2.5 % less than that of the system without energy storage.

The deferment of the reinforcement of transmission and distribution infrastructure can be achieved with the installation of energy storage system at distribution network. Based on the assumed annual growth rate of 5 % for the energy storage, it is expected to achieve 7.4 % of the reduction in overall peak demand growth by 2030. The transmission and distribution upgrade deferral are in the range of RM 385 million to RM 840 million in 2030.

The evaluations also found that the cost of electricity for the electrical system with lead-acid batteries is more cost-effective than that with other battery technologies. The electricity cost savings using lead-acid battery storage system to reduce the maximum demand is economically viable for commercial and industrial customers. The payback periods of the energy storage system fall within 2.8 years to 6 years.

## **8.2 Limitations and Opportunities for Future Improvement**

There are several limitations found throughout this research work. The existing size of the power converters is too small as compared to the building load demand. If the fluctuation of the load is greater than that of the rating of the power converters, then the effect of peak reduction is insignificant. Furthermore, the existing capacity of the batteries is too small and can only last for one and a half hour if the power converters are delivering power at its full capacity. The future work should consider increasing the size of the power converters and the capacity of the batteries so that the peak reduction for a large building can be achieved.

Accurate load profile prediction plays an important role in determining the effectiveness of peak reduction. The load predicting methods used in this research work is rather simpler and have relatively high mean absolute percentage error. This has reduced the effectiveness of the ESS in reducing the peak demand. Nevertheless, the sophisticated load predicting methods is beyond the scope of this research work. The future work can introduce a sophisticated load predicting method to accurately predict the load profile and its corresponding energy requirement for the peak reduction.

Currently, the lead-acid batteries are chosen for the energy storage system. However, due to its low energy density, the existing battery bank occupies a large space in the laboratory. In addition, the lead-acid batteries can only be discharged up to 50% of its full capacity to prolong its lifespan. This has



contributed to the large space occupation. The future work can replace the lead-acid batteries with Li-ion batteries because Li-ion batteries have many advantages over the lead-acid batteries such as high energy density, high cycle life, and depth-of-discharge up to 20% of its full capacity. However, the cost competitiveness of Li-ion batteries is still high and to some extent shows safety issues. Although the current price of Li-ion batteries is high, it is anticipated that the price could drop to one-third of its current price, which is the current price of USD 600 /kWh to USD 200 /kWh by 2020 in line with the fast-growing electric vehicular technology that will trigger a mass production in the near future. This will make Li-ion batteries an economically viable solution for peak reduction.

## LIST OF REFERENCES

Abbas, A.A., Georgianne, H., Aileen, B.C., Benjamin, C.K., Dan, M.R., 2015. DOE/EPRI Electricity Storage Handbook in Collaboration with NRECA.

Abbas, A.A., Georgianne, H., Aileen, B.C., Benjamin, C.K., Dan, M.R., Stella, C., Andrew, L.C., T. Bradshaw Dale, William, D.G., 2013. DOE/EPRI 2013 Electricity Storage Handbook in Collaboration with NRECA. Sandia National Laboratories.

Amodeo, S.J., Chiacchiarini, H.G., Solsona, J.A., Busada, C.A., 2009. High-performance sensorless nonlinear power control of a flywheel energy storage system. *Energy Convers. Manag.* 50, 1722–1729. doi:10.1016/j.enconman.2009.03.024

Andreas, O., 2012. Energy Storage Technologies & Their Role in Renewable Integration. Research Associate, Global Energy Network Institute.

Anna, B., Lucky, L., 2014. Lessons Learned: Malaysia's 2013 Fuel Subsidy Reform. The International Institute for Sustainable Development.

Ardizzon, G., Cavazzini, G., Pavesi, G., 2014. A new generation of small hydro and pumped-hydro power plants: Advances and future challenges. *Renew. Sustain. Energy Rev.* 31, 746–761. doi:10.1016/j.rser.2013.12.043

Berg, S.V., Savvides, A., 1983. The theory of maximum kW demand charges for electricity. *Energy Econ.* 5, 258–266. doi:10.1016/0140-9883(83)90030-0

Blanke, H., Bohlen, O., Buller, S., De Doncker, R.W., Fricke, B., Hammouche, A., Linzen, D., Thele, M., Sauer, D.U., 2005. Impedance measurements on lead–acid batteries for state-of-charge, state-of-health and cranking capability prognosis in electric and hybrid electric vehicles. *J. Power Sources*, Selected papers from the Ninth European Lead Battery Conference Ninth European Lead Battery Conference 144, 418–425. doi:10.1016/j.jpowsour.2004.10.028

Borozan, D., 2013. Exploring the relationship between energy consumption and GDP: Evidence from Croatia. *Energy Policy* 59, 373–381. doi:10.1016/j.enpol.2013.03.061

Bradley, P., Leach, M., Torriti, J., 2013. A review of the costs and benefits of demand response for electricity in the UK. *Energy Policy*, Special Section: Transition Pathways to a Low Carbon Economy 52, 312–327. doi:10.1016/j.enpol.2012.09.039

Cappers, P., MacDonald, J., Goldman, C., Ma, O., 2013. An assessment of market and policy barriers for demand response providing ancillary services in U.S. electricity markets. *Energy Policy* 62, 1031–1039. doi:10.1016/j.enpol.2013.08.003

Castillo, A., Gayme, D.F., 2014. Grid-scale energy storage applications in renewable energy integration: A survey. *Energy Convers. Manag.* 87, 885–894. doi:10.1016/j.enconman.2014.07.063

Chen, J., Garcia, H.E., 2016. Economic optimization of operations for hybrid energy systems under variable markets. *Appl. Energy* 177, 11–24. doi:10.1016/j.apenergy.2016.05.056

Chen, X.Y., Jin, J.X., 2013. Application prospects of integrated SMES technology for future smart grids, in: 2013 IEEE International Conference on Applied Superconductivity and Electromagnetic Devices (ASEMD). Presented at the 2013 IEEE International Conference on Applied Superconductivity and Electromagnetic Devices (ASEMD), pp. 517–518. doi:10.1109/ASEMD.2013.6780834

Chris, N., Rich, S., 2012. US Experience with Efficiency As a Transmission and Distribution System Resource.

Chua, K.H., Lim, Y.S., Morris, S., 2015. Cost-benefit assessment of energy storage for utility and customers: A case study in Malaysia. *Energy Convers. Manag.* 106, 1071–1081. doi:10.1016/j.enconman.2015.10.041

Chua, K.H., Lim, Y.S., Taylor, P., Morris, S., Wong, J., 2012. Energy Storage System for Mitigating Voltage Unbalance on Low-Voltage Networks With Photovoltaic Systems. *IEEE Trans. Power Deliv.* 27, 1783–1790. doi:10.1109/TPWRD.2012.2195035

Coers, R., Sanders, M., 2013. The energy–GDP nexus; addressing an old question with new methods. *Energy Econ.* 36, 708–715. doi:10.1016/j.eneco.2012.11.015

Coleman, C.P., Godbole, D., 1994. A comparison of robustness: fuzzy logic, PID, and sliding mode control, in: , Proceedings of the Third IEEE Conference on Fuzzy Systems, 1994. IEEE World Congress on Computational Intelligence. Presented at the , Proceedings of the Third IEEE Conference on Fuzzy Systems, 1994. IEEE World Congress on Computational Intelligence, pp. 1654–1659 vol.3. doi:10.1109/FUZZY.1994.343945

Coleman, M., Hurley, W.G., Lee, C.K., 2008. An Improved Battery Characterization Method Using a Two-Pulse Load Test. *IEEE Trans. Energy Convers.* 23, 708–713. doi:10.1109/TEC.2007.914329

Datta, M., Senjyu, T., 2013. Fuzzy Control of Distributed PV Inverters/Energy Storage Systems/Electric Vehicles for Frequency Regulation in a Large Power System. *IEEE Trans. Smart Grid* 4, 479–488. doi:10.1109/TSG.2012.2237044

Diaz, N.L., Dragicevic, T., Vasquez, J.C., Guerrero, J.M., 2014. Intelligent Distributed Generation and Storage Units for DC Microgrids #x2014;A New Concept on Cooperative Control Without Communications Beyond Droop

Control. *IEEE Trans. Smart Grid* 5, 2476–2485.  
doi:10.1109/TSG.2014.2341740

Diaz, N.L., Wu, D., Dragicevic, T., Vasquez, J.C., Guerrero, J.M., 2015. Fuzzy droop control loops adjustment for stored energy balance in distributed energy storage system, in: 2015 9th International Conference on Power Electronics and ECCE Asia (ICPE-ECCE Asia). Presented at the 2015 9th International Conference on Power Electronics and ECCE Asia (ICPE-ECCE Asia), pp. 728–735. doi:10.1109/ICPE.2015.7167864

Efendi, R., Ismail, Z., Deris, M.M., 2015. A new linguistic out-sample approach of fuzzy time series for daily forecasting of Malaysian electricity load demand. *Appl. Soft Comput.* 28, 422–430.  
doi:10.1016/j.asoc.2014.11.043

EIA, U.E.I.A., 2015. Levelized Cost and Levelized Avoided Cost of New Generation Resources in the Annual Energy Outlook 2015.

EIA, U.E.I.A., 2013. Updated Capital Cost Estimates for Utility Scale Electricity Generating Plants.

Energy Commission, 2014. Peninsular Malaysia Electricity Supply Industry Outlook 2014. Putrajaya.

Energy Commission, 2013. Peninsular Malaysia Electricity Supply Industry Outlook 2013.

Energy Information Administration, 2008. International Energy Statistics - Pumped Storage. United States Department of Energy.

European Commission, 2012. Study on the state of play of energy efficiency of heat and electricity production technologies.

Garcia, H.E., Chen, J., Kim, J.S., Vilim, R.B., Binder, W.R., Bragg Sitton, S.M., Boardman, R.D., McKellar, M.G., Paredis, C.J.J., 2016. Dynamic performance analysis of two regional Nuclear Hybrid Energy Systems. *Energy* 107, 234–258. doi:10.1016/j.energy.2016.03.128

Gareth, K., Akeel, A.S., Frank, C.W., 2011. Development of the all-vanadium redox flow battery for energy storage: a review of technological, financial and policy aspects. *Int. J. Energy Res.* 36, 1105–1120.

Gaurav, Amrit, K., 2012. Comparison between Conventional PID and Fuzzy Logic Controller for Liquid Flow Control: Performance Evaluation of Fuzzy Logic and PID Controller by using MATLAB/Simulink. *Int. J. Innov. Technol. Explor. Eng.* 1, 2278–3075.

Greg, B., Debra, L., Paul, D., 2012. Impacts of Renewable Generation on Fossil Fuel Unit Cycling: Costs and Emissions (No. NREL/PR-6A20-55828).

Guanrong, C., Trung Tat, P., 2001. Introduction to Fuzzy Sets, Fuzzy Logic, and Fuzzy Control Systems. CRC Press, USA.

H. A., K., 2003. Battery Technology Handbook, Second. ed. CRC Press.

Hong, T., Wang, P., White, L., 2015. Weather station selection for electric load forecasting. *Int. J. Forecast.* 31, 286–295.  
doi:10.1016/j.ijforecast.2014.07.001

Hoppecke, 2014. Installation, Commissioning and Operating Instructions for Vented Stationary Lead-Acid Batteries.

IEC, 2011. Electrical Energy Storage White Paper. International Electrotechnical Commission, Switzerland.

IISD, 2013. A Citizens' Guide to Energy Subsidies in Malaysia. International Institute for Sustainable Development.

Imre, P.G., 2003. EPRI-DOE Handbook of Energy Storage for Transmission & Distribution Applications.

International Energy Agency, 2013. CO2 Emissions from Fuel Combustion Highlights.

IRENA, 2015. From Baseload to Peak: Renewables Provide a Reliable Solution. International Renewable Energy Agency.

Johnson, M.P., Bar-Noy, A., Liu, O., Feng, Y., 2011. Energy peak shaving with local storage. *Sustain. Comput. Inform. Syst., Theoretical aspects of Sustainable Computing* 1, 177–188. doi:10.1016/j.suscom.2011.05.001

Jose, F.P., 1999. The Value of Reliability in Power Systems - Pricing Operating Reserves. Massachusetts Institute of Technology.

Joseph, A., Shahidehpour, M., 2006. Battery storage systems in electric power systems, in: IEEE Power Engineering Society General Meeting, 2006. Presented at the IEEE Power Engineering Society General Meeting, 2006, p. 8 pp.-pp. doi:10.1109/PES.2006.1709235

Jouvet, P.-A., Solier, B., 2013. An overview of CO2 cost pass-through to electricity prices in Europe. *Energy Policy* 61, 1370–1376.  
doi:10.1016/j.enpol.2013.05.090

Kashem, M.A., Ledwich, G., 2007. Energy requirement for distributed energy resources with battery energy storage for voltage support in three-phase distribution lines. *Electr. Power Syst. Res.* 77, 10–23.  
doi:10.1016/j.epsr.2006.01.008

Koh, S.L., Lim, Y.S., Morris, S., 2011. Cost Effective Options for Greenhouse Gas (GHG) Emission Reduction in the Power Sector for Developing Economies — A Case Study in Sabah, Malaysia. *Energies* 4, 780–803. doi:10.3390/en4050780

Koller, M., Borsche, T., Ulbig, A., Andersson, G., 2015. Review of grid applications with the Zurich 1 MW battery energy storage system. *Electr. Power Syst. Res., Smart Grids: World's Actual Implementations* 120, 128–135. doi:10.1016/j.epsr.2014.06.023

Kumar, N., Besuner, P.M., Lefton, S.A., Agan, D.D., Hilleman, D.D., 2012. *Power Plant Cycling Costs*. National Renewable Energy Laboratory.

Kundur, P., Paserba, J., Ajarapu, V., Andersson, G., Bose, A., Canizares, C., Hatziargyriou, N., Hill, D., Stankovic, A., Taylor, C., Cutsem, T.V., Vittal, V., 2004. Definition and classification of power system stability IEEE/CIGRE joint task force on stability terms and definitions. *IEEE Trans. Power Syst.* 19, 1387–1401. doi:10.1109/TPWRS.2004.825981

Leadbetter, J., Swan, L., 2012a. Battery storage system for residential electricity peak demand shaving. *Cool Roofs Cool Pavements Cool Cities Cool World* 55, 685–692. doi:10.1016/j.enbuild.2012.09.035

Leadbetter, J., Swan, L., 2012b. Battery storage system for residential electricity peak demand shaving. *Energy Build., Cool Roofs, Cool Pavements, Cool Cities, and Cool World* 55, 685–692. doi:10.1016/j.enbuild.2012.09.035

Levron, Y., Shmilovitz, D., 2012. Power systems' optimal peak-shaving applying secondary storage. *Electr. Power Syst. Res.* 89, 80–84. doi:10.1016/j.epsr.2012.02.007

Li, N., Hedman, K.W., 2015. Economic Assessment of Energy Storage in Systems With High Levels of Renewable Resources. *IEEE Trans. Sustain. Energy* 6, 1103–1111. doi:10.1109/TSTE.2014.2329881

Liu, H., Jiang, J., 2007. Flywheel energy storage—An upswing technology for energy sustainability. *Energy Build.* 39, 599–604. doi:10.1016/j.enbuild.2006.10.001

Lu, C., Xu, H., Pan, X., Song, J., 2014. Optimal Sizing and Control of Battery Energy Storage System for Peak Load Shaving. *Energies* 7, 8396–8410. doi:10.3390/en7128396

Luo, X., Wang, J., Dooner, M., Clarke, J., 2015. Overview of current development in electrical energy storage technologies and the application potential in power system operation. *Appl. Energy* 137, 511–536. doi:10.1016/j.apenergy.2014.09.081

Malaysian Gas Association, 2014. *Malaysia: Natural Gas Industry Annual Review - 2014 Edition*.

- Masoum, A.S., Deilami, S., Moses, P.S., Masoum, M.A.S., Abu-Siada, A., 2011. Smart load management of plug-in electric vehicles in distribution and residential networks with charging stations for peak shaving and loss minimisation considering voltage regulation. *IET Gener. Transm. Distrib.* 5, 877–888. doi:10.1049/iet-gtd.2010.0574
- Nair, N.-K.C., Garimella, N., 2010. Battery energy storage systems: Assessment for small-scale renewable energy integration. *Energy Build.* 42, 2124–2130. doi:10.1016/j.enbuild.2010.07.002
- Nasiri, A., 2011. 24 - Uninterruptible Power Supplies, in: Rashid, M.H. (Ed.), *Power Electronics Handbook (Third Edition)*. Butterworth-Heinemann, Boston, pp. 627–641.
- Ngamroo, I., 2011. An optimization of robust SMES with specified structure  $H_{\infty}$  controller for power system stabilization considering superconducting magnetic coil size. *Energy Convers. Manag.* 52, 648–651. doi:10.1016/j.enconman.2010.07.042
- Oudalov, A., Cherkaoui, R., Beguin, A., 2007a. Sizing and Optimal Operation of Battery Energy Storage System for Peak Shaving Application, in: *Power Tech, 2007 IEEE Lausanne*. Presented at the Power Tech, 2007 IEEE Lausanne, pp. 621–625. doi:10.1109/PCT.2007.4538388
- Oudalov, A., Cherkaoui, R., Beguin, A., 2007b. Sizing and Optimal Operation of Battery Energy Storage System for Peak Shaving Application, in: *Power Tech, 2007 IEEE Lausanne*. Presented at the Power Tech, 2007 IEEE Lausanne, pp. 621–625. doi:10.1109/PCT.2007.4538388
- Papic, I., 2006. Simulation model for discharging a lead-acid battery energy storage system for load leveling. *IEEE Trans. Energy Convers.* 21, 608–615. doi:10.1109/TEC.2005.853746
- Pedro, A., Antonio, S., 1998. Fuzzy Logic Controllers. Advantages and Drawbacks. VIII Congr. Control Autom.
- Perry, T.S., 1995. Lotfi A. Zadeh [fuzzy logic inventor biography]. *IEEE Spectr.* 32, 32–35. doi:10.1109/6.387136
- Peter, L., 2012. Demonstration of ZBB Energy Storage Systems.
- Piller, S., Perrin, M., Jossen, A., 2001. Methods for state-of-charge determination and their applications. *J. Power Sources*, Proceedings of the 22nd International Power Sources Symposium 96, 113–120. doi:10.1016/S0378-7753(01)00560-2
- Poullikkas, A., 2013. A comparative overview of large-scale battery systems for electricity storage. *Renew. Sustain. Energy Rev.* 27, 778–788. doi:10.1016/j.rser.2013.07.017

- Pudjianto, D., Aunedi, M., Djapic, P., Strbac, G., 2014. Whole-Systems Assessment of the Value of Energy Storage in Low-Carbon Electricity Systems. *IEEE Trans. Smart Grid* 5, 1098–1109. doi:10.1109/TSG.2013.2282039
- Purvins, A., Papaioannou, I.T., Debarberis, L., 2013. Application of battery-based storage systems in household-demand smoothening in electricity-distribution grids. *Energy Convers. Manag.*, Global Conference on Renewable energy and Energy Efficiency for Desert Regions 2011 “GCREEDER 2011” 65, 272–284. doi:10.1016/j.enconman.2012.07.018
- Rahimi, A., Zarghami, M., Vaziri, M., Vadhva, S., 2013. A simple and effective approach for peak load shaving using Battery Storage Systems, in: North American Power Symposium (NAPS), 2013. Presented at the North American Power Symposium (NAPS), 2013, pp. 1–5. doi:10.1109/NAPS.2013.6666824
- Reddy, S.S., Panigrahi, B.K., Kundu, R., Mukherjee, R., Debchoudhury, S., 2013. Energy and spinning reserve scheduling for a wind-thermal power system using CMA-ES with mean learning technique. *Int. J. Electr. Power Energy Syst.* 53, 113–122. doi:10.1016/j.ijepes.2013.03.032
- Rufer, A., Barrade, P., 2002. A supercapacitor-based energy-storage system for elevators with soft commutated interface. *IEEE Trans. Ind. Appl.* 38, 1151–1159. doi:10.1109/TIA.2002.803021
- Rüther, R., Knob, P.J., da Silva Jardim, C., Rebechi, S.H., 2008. Potential of building integrated photovoltaic solar energy generators in assisting daytime peaking feeders in urban areas in Brazil. *Energy Convers. Manag.* 49, 1074–1079. doi:10.1016/j.enconman.2007.09.020
- Serban, I., Marinescu, C., 2014. Battery energy storage system for frequency support in microgrids and with enhanced control features for uninterruptible supply of local loads. *Int. J. Electr. Power Energy Syst.* 54, 432–441. doi:10.1016/j.ijepes.2013.07.004
- Sharma, P., Bhatti, T.S., 2010. A review on electrochemical double-layer capacitors. *Energy Convers. Manag.* 51, 2901–2912. doi:10.1016/j.enconman.2010.06.031
- Sigrist, L., Lobato, E., Rouco, L., 2013. Energy storage systems providing primary reserve and peak shaving in small isolated power systems: An economic assessment. *Int. J. Electr. Power Energy Syst.* 53, 675–683. doi:10.1016/j.ijepes.2013.05.046
- Sinha, S., Chandel, S.S., 2014. Review of software tools for hybrid renewable energy systems. *Renew. Sustain. Energy Rev.* 32, 192–205. doi:10.1016/j.rser.2014.01.035



- Siong Lee, K., Yun Seng, L., Stella, M., 2011. Cost Effective Options for Greenhouse Gas (GHG) Emission Reduction in the Power Sector for Developing Economies - A Case Study in Sabah, Malaysia. *Energies* 4, 780–803.
- Song, K.-B., Baek, Y.-S., Hong, D.H., Jang, G., 2005. Short-term load forecasting for the holidays using fuzzy linear regression method. *IEEE Trans. Power Syst.* 20, 96–101. doi:10.1109/TPWRS.2004.835632
- Stan, K., 2008. *Power Plants: Characteristics and Costs*.
- Sun, Y., Wang, S., Xiao, F., Gao, D., 2013. Peak load shifting control using different cold thermal energy storage facilities in commercial buildings: A review. *Energy Convers. Manag.* 71, 101–114. doi:10.1016/j.enconman.2013.03.026
- Suruhanjaya Tenaga Malaysia, 2013. *Electricity Supply Industry in Malaysia: Performance and Statistic Information*.
- Suruhanjaya Tenaga Malaysia, 2012. *Electricity Supply Industry in Malaysia: Performance and Statistical Information*.
- Taylor, J.A., Callaway, D.S., Poolla, K., 2013. Competitive energy storage in the presence of renewables. *IEEE Trans. Power Syst.* 28, 985–996. doi:10.1109/TPWRS.2012.2210573
- Tenaga Nasional Berhad, 2016. *Maximum Demand*.
- Tenaga Nasional Berhad, 2014. *Electricity Tariff Schedule*.
- Thomas, B.R., 2011. *Linden's Handbook of Batteries*, 4th ed.
- Thomas, B.R., 2010a. Batteries for Electrical Energy Storage Applications, in: *Linden's Handbook of Batteries*. McGraw-Hill, United States, p. 1.3.
- Thomas, B.R., 2010b. Basic concepts, in: *Linden's Handbook of Batteries*. McGraw-Hill, United States, p. 1.3.
- Tom, B., 2011. *Development of Distributed Generation for Grid Support and Distribution System Infrastructure: A Summary Analysis of DG Benefits and Case Studies*.
- United Nations, 2015. *Adoption of the Paris Agreement*. Paris.
- Upshaw, C.R., Rhodes, J.D., Webber, M.E., 2015. Modeling peak load reduction and energy consumption enabled by an integrated thermal energy and water storage system for residential air conditioning systems in Austin, Texas. *Energy Build.* 97, 21–32. doi:10.1016/j.enbuild.2015.03.050
- U.S. Energy Information Administration, 2013. *Updated Capital Cost Estimates for Utility Scale Electricity Generating Plants*.

- Venu, C., Riffonneau, Y., Bacha, S., Baghzouz, Y., 2009. Battery Storage System sizing in distribution feeders with distributed photovoltaic systems, in: PowerTech, 2009 IEEE Bucharest. Presented at the PowerTech, 2009 IEEE Bucharest, pp. 1–5. doi:10.1109/PTC.2009.5282093
- Walawalkar, R., Apt, J., Mancini, R., 2007. Economics of electric energy storage for energy arbitrage and regulation in New York. *Energy Policy* 35, 2558–2568. doi:10.1016/j.enpol.2006.09.005
- Wang, X., Teichgraber, H., Palazoglu, A., El-Farra, N.H., 2014. An economic receding horizon optimization approach for energy management in the chlor-alkali process with hybrid renewable energy generation. *J. Process Control, Economic nonlinear model predictive control* 24, 1318–1327. doi:10.1016/j.jprocont.2014.04.017
- World Bank, 2014. State and Trends of Carbon Pricing 2014. Washington, DC.
- Wu, B., Wang, L., 2014. Energy and Exergy Analysis of China's Distributed Combined Heating and Power with Heat-Pump Heating for Peak Shaving. *J. Energy Eng.* 0, 5014003. doi:10.1061/(ASCE)EY.1943-7897.0000221
- Yan, X., Zhang, X., Chen, H., Xu, Y., Tan, C., 2014. Techno-economic and social analysis of energy storage for commercial buildings. *Energy Convers. Manag.* 78, 125–136. doi:10.1016/j.enconman.2013.10.014
- Yang, H., Zhang, Y., 2013. Analysis of Supercapacitor Energy Loss for Power Management in Environmentally Powered Wireless Sensor Nodes. *IEEE Trans. Power Electron.* 28, 5391–5403. doi:10.1109/TPEL.2013.2238683
- Yang, Y., Li, H., Aichhorn, A., Zheng, J., Greenleaf, M., 2014. Sizing Strategy of Distributed Battery Storage System With High Penetration of Photovoltaic for Voltage Regulation and Peak Load Shaving. *IEEE Trans. Smart Grid* 5, 982–991. doi:10.1109/TSG.2013.2282504
- Zhang, L., Xiang, J., 2014. The performance of a grid-tied microgrid with hydrogen storage and a hydrogen fuel cell stack. *Energy Convers. Manag.* 87, 421–427. doi:10.1016/j.enconman.2014.07.045
- Zhao, P., Wang, J., Dai, Y., 2015. Thermodynamic analysis of an integrated energy system based on compressed air energy storage (CAES) system and Kalina cycle. *Energy Convers. Manag.* 98, 161–172. doi:10.1016/j.enconman.2015.03.094

## **APPENDIX A: Precautions for Installing Current Transformers**

The procedure of installing the current transformers is important because dangerous voltages are likely to be presented in the vicinity of current transformers. The secondary circuit of a current transformer is not allowed to be opened circuited when current is flowing in the primary circuit because the voltage generated in the primary winding is stepped up by the turns-ratio of the current transformer. For instance, the current ratio of 400/5 A steps down the primary current by 80 times at the secondary circuit. At the mean time the voltage in the primary winding can reach several thousand volts in a fraction of a second if the secondary windings are open-circuited while current is flowing in the primary circuit. The high voltages can be dangerous to personnel and can cause serious damage to the transformer or equipment connected to it. Hence,

during the installation of current transformers, it is recommended that the secondary windings are grounded in order to provide protection against static voltages. This can be achieved by connecting a wire across the secondary leads labelled as S1 and S2, and connecting it to the ground.

## **APPENDIX B: SMA YAOPC server**

The communication between Sunny Island 5048 and the supervisory computer is established via SMA YAOPC server. The SMA OPC server is a server-based 32-bit application for standardized data exchange with devices from SMA. The initialisation program entitled “Yasdi.ini” is required to establish the communication. Yasdi is the data protocol developed by SMA to communicate with SMA devices. The “Yasdi.ini” program is as follows:

```
[DriverModules] //This is to indicate the specific driver module used
Drive0=yasdi_drv_serial.dll
[COM3] // This is to indicate the communication port used in the supervisory
computer
Device=COM3
Media=RS232 // The standard serial communication chosen is RS232
```

```
Baudrate=19200 // The available baudrate are 4800, 9600, and 19200
Protocol=SMANet // The available options are SunnyNet and SMANet
[Master]
ReadTestChannels=0
ReadParamChanTimeout=4
ReadParamChanRetry=3
WriteParamChanTimeout=4
WriteParamChanRetry=3
ReadSpotChanTimeout=4
ReadSpotChanRetry=3
AutoReadOnlineChannels=1
```

### **APPENDIX C: Calculation of the desired $P_{UTh}$ using ‘What-If Analysis – Goal Seek’ function in Microsoft Excel**

The ‘What-If Analysis – Goal Seek’ function in Microsoft Excel is used to calculate the desirable  $P_{UTh}$  based on the available energy from the ESS. The ‘What-If Analysis – Goal Seek’ function allows the user to use a formula to find the desired input based on the given output. This function is used because the available energy (given output) from the ESS is known but the desired input value,  $P_{UTh}$ , is an unknown. Figure A shows the example of ‘What-If Analysis – Goal Seek’ function.

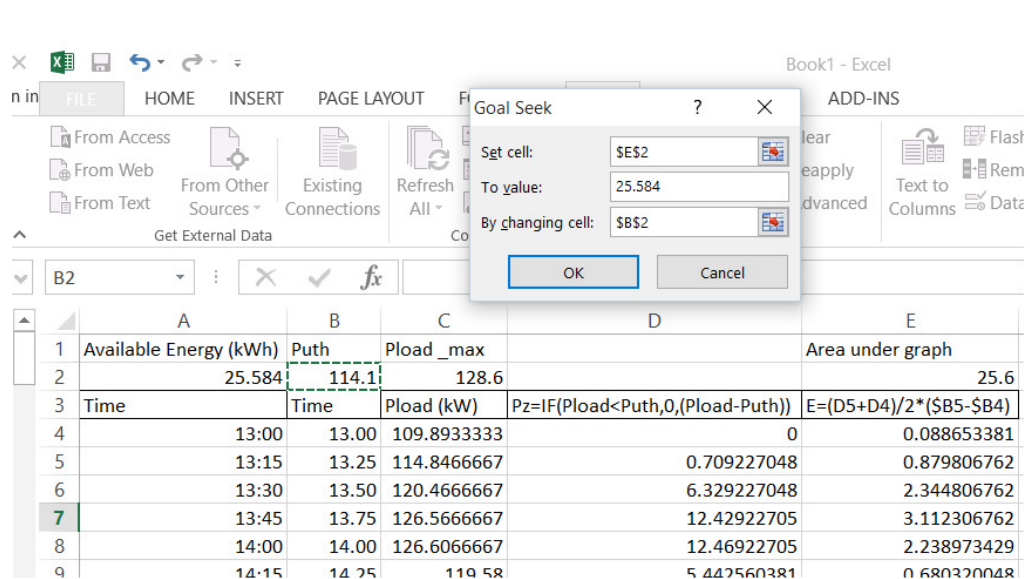


**Figure A: Example of ‘What-If Analysis – Goal Seek’ function**

Firstly,  $P_{UTh}$  at column B row 2 is set to the maximum value of the load, 128.6 kW. The load power that is higher than  $P_{UTh}$ , namely  $P_z$ , is identified from time to time. If the value of the load power is lower than  $P_{UTh}$ , then the zero value is returned to column D at the corresponding row. If the load power is higher than  $P_{UTh}$ , then the difference between the load power and  $P_{UTh}$  is returned in column D at the corresponding row. Secondly, the energy consumed by the load that is higher than  $P_{UTh}$  is calculated. The area under the graph between  $P_{UTh}$  and  $P_{load}$  can be calculated by summing up the energy consumed. Thirdly, the ‘What-If Analysis – Goal Seek’ function under ‘DATA’ tab in Microsoft Excel is selected. A cell E2 is chosen to allocate the result. The desired energy from the energy storage, namely 25.584 kWh, is set at ‘To value’ row. The cell B2 is selected as ‘By changing cell’ such that  $P_{UTh}$  is manipulated to obtain the desired energy from the energy storage. Finally, the desired energy from the energy storage is displayed at cell E2.

